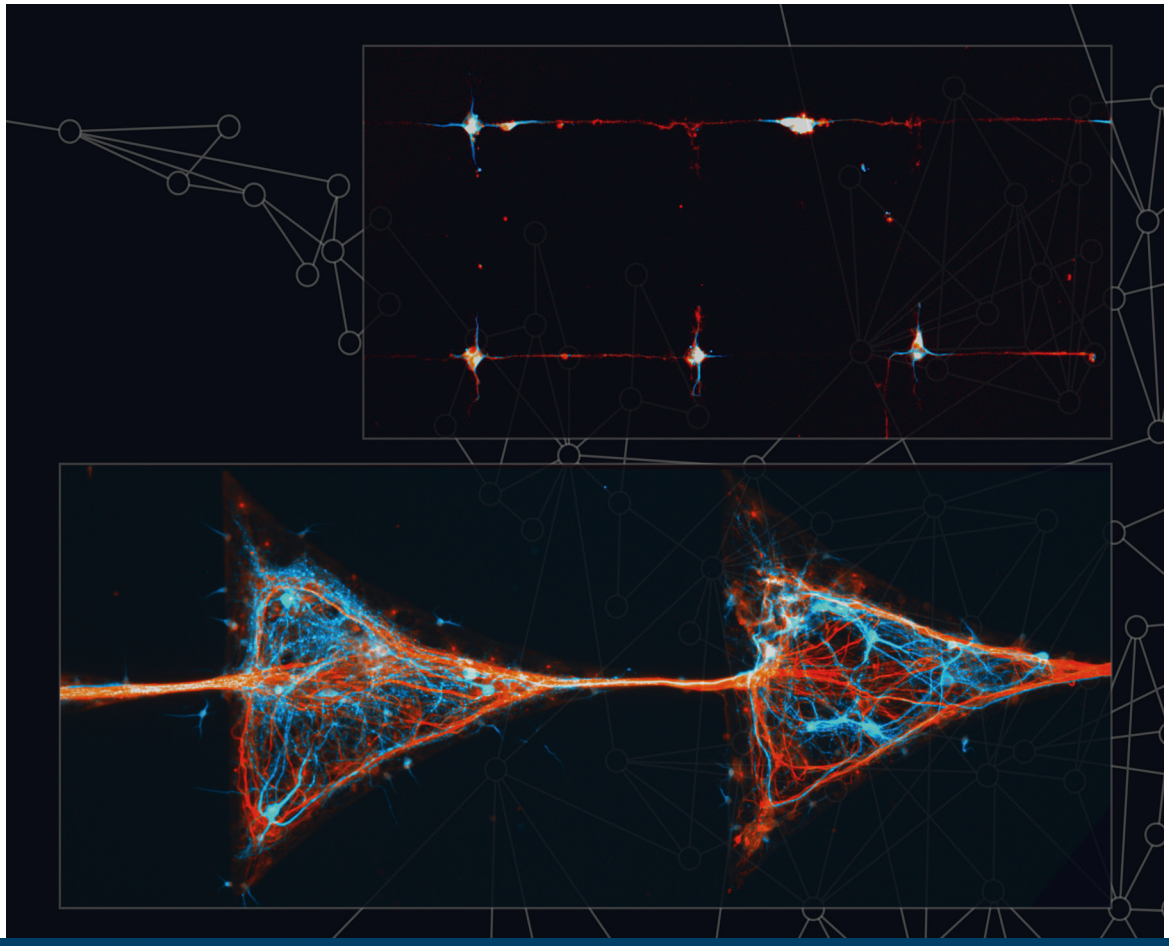

# Engineering neuronal networks in vitro: From single cells to population connectivity

Irina Tihaa

Information
Band / Volume 78
ISBN 978-3-95806-597-0

Mitglied der Helmholtz-Gemeinschaft

JÜLICH
Forschungszentrum

Schriften des Forschungszentrums Jülich
Reihe Information / Information Band / Volume 78

Forschungszentrum Jülich GmbH
Institute of Biological Information Processing
Bioelectronics (IBI-3)

# Engineering neuronal networks in vitro: From single cells to population connectivity

Irina Tihaa

Schriften des Forschungszentrums Jülich
Reihe Information / Information Band / Volume 78

ISSN 1866-1777 ISBN 978-3-95806-597-0

Bibliografische Information der Deutschen Nationalbibliothek.
Die Deutsche Nationalbibliothek verzeichnet diese Publikation in der
Deutschen Nationalbibliografie; detaillierte Bibliografische Daten
sind im Internet über http://dnb.d-nb.de abrufbar.

| | |
|---|---|
| Herausgeber und Vertrieb: | Forschungszentrum Jülich GmbH<br>Zentralbibliothek, Verlag<br>52425 Jülich<br>Tel.: +49 2461 61-5368<br>Fax: +49 2461 61-6103<br>zb-publikation@fz-juelich.de<br>www.fz-juelich.de/zb |
| Umschlaggestaltung: | Grafische Medien, Forschungszentrum Jülich GmbH |
| Druck: | Grafische Medien, Forschungszentrum Jülich GmbH |
| Copyright: | Forschungszentrum Jülich 2021 |

Schriften des Forschungszentrums Jülich
Reihe Information / Information, Band / Volume 78

D 82 (Diss. RWTH Aachen University, 2021)

ISSN 1866-1777
ISBN 978-3-95806-597-0

Vollständig frei verfügbar über das Publikationsportal des Forschungszentrums Jülich (JuSER)
unter www.fz-juelich.de/zb/openaccess.

# Abstract

The mammalian brain shows multiple levels of organisation ranging from single cell to regional organisation level. Structure and function are dependent on each other. The aim of this thesis is to incorporate the essential feature of organisation into cultured neuronal networks via microcontact printing (μCP). We do so to better understand the impact of pattern geometry onto network architecture, extend the *in vitro* models and provide more relevant systems.

The first part of this thesis considers single cell connectivity. Grid and star pattern designs featuring nodes and lines are utilized to control soma position and neurite elongation. Morphological analysis via immunofluorescence and live cell imaging revealed a high dependence of soma position and axon guiding efficiency on the patterns. For soma position itself the shape, dimensions and proportions of the pattern features are of great importance. Calcium imaging and electrical recordings with multi-electrode arrays (MEAs) proved functional connectivity of the created single cell networks.

In the second part, triangular shaped structures were used to create modular neuronal networks with differently sized populations. Immunofluorescence analysis revealed a highly directional structural connectivity between the populations. Calcium imaging analyses demonstrated a high intra-population and a weaker inter-population interconnectedness, a typical feature of modularly organised networks. Moreover, synchrony was observed to decrease with increasing population size indicating a rise in architectural complexity.

Overall, this thesis illustrates the potential of μCP for designing *in vitro* neuronal networks with micro- to mesoscale level of organisation. Here, the pattern design is crucial for the network architecture. A deeper understanding of the impact of pattern geometry onto network formation might contribute to a greater use of defined networks for neurobiological experiments by enhancing efficiency and predictability of patterned cultures. In combination with electrical and optical methods it provides a toolbox enabling a multi-

faceted communication analysis of neurons in various network designs. With that, the fundamentals of the brain structure and function can be evaluated in a bottom-up approach. Engineered *in vitro* systems can be used as a surrogate for *in vivo* experiments. Moreover, the discoveries can contribute to advances in neuronal tissue engineering.

# Zusammenfassung

Das Gehirn von Säugern zeigt einen hierarchischen Aufbau mit verschiedenen Leveln der Konnektivität, von einzelnen Zellen bis hin zu ganzen Hirnregionen. Dabei ist die Organisation des Gehirns unmittelbar mit dessen Funktion verbunden. Um das wesentliche Merkmal der Organisation *in vitro* abzubilden, wurden geometrische Proteinmuster mittels des Microcontact Printing Verfahrens (μCP) auf Substrate aufgetragen. Dadurch wurden neuronale Netzwerke mit spezifischer Konnektivität auf Einzelzell- und Populationsebene geschaffen. Die Auswirkungen der Proteinmuster auf die Netzwerkorganisation und -funktionalität wurden untersucht.

Der erste Teil dieser Dissertation beschäftigt sich mit der Konnektivität auf Einzelzellebene. Dabei wurden Gitter- und Sternstrukturen verwendet, um die Position des Somas und die Elongation der Neuriten zu beeinflussen. Die Morphologie der Netzwerke wurde mittels Immunofluoreszenz und Live-Cell-Imaging untersucht. Die Ergebnisse zeigen eine Abhängigkeit zwischen der Somaposition auf dem Proteinmuster und der Wachstumsrichtung der Neuriten. Die Position des Somas hingegen hängt von der Geometrie, der Dimension und der Proportionen der Muster-Bestandteile ab. Die funktionale Konnektivität der Einzelzellnetzwerke wurde mittels Calcium-Imagings und elektrischer Messungen mit MEAs nachgewiesen.

Im zweiten Teil wurden Dreiecke verwendet um modulare neuronale Netzwerke mit unterschiedlich großen Populationen zu erzeugen. Es konnte eine Direktionalität der Verbindungen zwischen den Populationen gezeigt werden. Die Funktionalität wurde mit Calcium-Imaging untersucht, wobei ein höherer Grad an Vernetzung innerhalb der Populationen beobachtet wurde. Dies ist eine typische Eigenschaft modular organisierter Netzwerke. Zusätzlich wurde eine abnehmende Synchronität mit zunehmender Populationsgröße beobachtet, was auf eine erhöhte architektonische Komplexität hinweist.

Diese Arbeit verdeutlicht das Potential des μCP, organisierte, neuronale *in vitro* Netzwerke im Mikro- bis Mesobereich zu entwickeln. Die Architek-

tur des Zellnetzwerks wird maßgeblich durch das Design des Proteinmusters bestimmt. Ein besseres Verständnis der Designparameter steigert die Effektivität und die Planbarkeit von neurobiologischen Experimenten mit µCP. Zusammen mit optischen und elektrischen Methoden bildet es ein Baukastensystem zur Kommunikationsanalyse von Nervenzellen in Netzwerken unterschiedlicher Ausprägung. Damit können die Grundlagen der Gehirnstruktur und -funktionalität in einer Bottom-up Methode untersucht werden. Organisierte *in vitro* Modelle sind potentielle Stellvertreter für *in vivo* Experimente. Darüber hinaus können die Erkenntnisse zu Fortschritten auf dem Gebiet der Gewebezüchtung beitragen.

# Contents

# Acronyms

| | |
|---|---|
| **µCP** | microcontact printing |
| **$A^-$** | organic ion |
| **AAV** | adeno-associated virus |
| **AIS** | AP initiation segment |
| **AP** | action potential |
| **$Ca^{2+}$** | calcium ion |
| **$Cl^-$** | chloride ion |
| **CP** | cortical plate |
| **DIV** | days in vitro |
| **E** | embrionic day |
| **EPSP** | excitatory postsynaptic potential |
| **ER** | endoplasmic reticulum |
| **GECI** | genetically encoded calcium indicator |
| **HSV** | herpes simplex virus |
| **IF** | Immunofluorescence |
| **IPSP** | inhibitory postsynaptic potential |
| **IZ** | intermediate zone |
| **$K^+$** | potassium ion |
| **MEA** | multi-electrode array |
| **MZ** | marginal zone |
| **$Na^+$** | sodium ion |
| **ncMEA** | nanocavity MEA |

| | |
|---|---|
| **NF** | neurofilaments |
| **OD** | ocular dominance |
| **PDMS** | Polydimethylsiloxane |
| **PI** | polyimid |
| **POP** | Polyolefin plastomer |
| **PSP** | postsynaptic potential |
| **rAAV** | recombinant adeno-associated virus |
| **SNR** | signal-to-noise ratio |
| **SVZ** | subvebtricular zone |
| **VGPC** | voltage-gated $K^+$ channels |
| **VGSC** | voltage-gated $Na^+$ channels |
| **VZ** | ventricular zone |

# Chapter 1

# Introduction

The human brain is one of the most complex objects that we know of. Emerson Pugh, a leading research scientist at IMB once said, *"If the human brain were so simple that we could understand it, we would be so simple that we couldn't."* It was exactly this complexity, problem-solving prowess and creative ability of the human brain, that fascinated many scientists ever since. Researches stained brain slices(Franz Nissl, Santiago RamÃ³n y Cajal and Camillo Golgi), delineated brain maps (Brodmann,[19] Economo and Koskinas[47]), elucidated deficits and their manifestations in neurological conditions.[129] Several novel methods were discovered to unveil cellular characteristics, signalling capabilities and organisation of the brain including the Nissl stain, Golgi stain, Patch clamp by Neher and Sakmann, discoveries of structure and function of the visual cortex by Hubel and Wiesel, just to name a few.[58,108]

Shedding light on the nervous system became one of the greatest intellectual challenges. Yet, humanity is only at the beginning of understanding the organ of mind. There is still no full explanation of epilepsy, dementia, addiction, schizophrenia, attention deficits or memory disorders or any other afflictions linked to the brain neither is there a cure. Many mechanisms and processes need do be discovered and unravelled.

The 80 billion neurons and at least ten times more glial cells are organised in a complex manner and certain areas are known to be responsible for specific

functions of the human body, such as motor actions, vision or memory. It is understood that structure and function are two sides of the same coin, dependent on each other.[79]

The brain, like all biological structures, operates at multiple levels, from molecules to whole brain regions. Its architecture is characterised by a hierarchical organisation of individual cells to cell assemblies into micro- to macrocircuits.[79] In order to understand the fundamentals of these circuits and the underlying mechanisms of neuronal communication a variety of experiments were and are still performed *in vivo*, *in vitro*, and *in silico* to tackle different questions: *How do neurons behave and communicate? How do neurons behave and communicate in a network? How is the signal propagated between single cells within a interconnected network? How do these interconnection patterns evolve in perception, behaviour and mind? In vitro* experiments with random neuronal cultures are widely spread and revealed many important discoveries in neuroscience. However, these cultures suffer from the randomness of connectivity. In order to meet the organised architecture of the brain, the incorporation of structurally organised cultures becomes essential at some point. Engineering networks *in vitro* can help unravel structural and functional principles of the *in vivo* state in a controlled and simplified environment. Furthermore, these networks can bridge experimental approaches to theoretical modeling systems, which also deal with controlled and simplified conditions. On the micro- and mesoscale level this means that a defined connectivity between individual neurons or groups of neurons has to be recreated.

Lithography is a powerful tool from microelectronics that was proven useful to create patterns on substrates and control cellular growth. Soft lithography methods like µCP, enables creation of custom neuronal networks with defined architecture.[156] In this work, different pattern geometries were introduced in order to shape the architecture of neuronal networks. Here, the focus was on controlling single cells as well as groups of neurons. Effects of geometric constraints on the morphology as well as functionality of neurons

and networks were investigated.

This thesis starts with providing some theoretic concepts and fundamentals in chapter 2. First, the mammalian brain and its organisational structure are outlined, followed by methodological basics for recreation of brain connectivity *in vitro* and analysis methods. Chapter 3 describes the materials and methods employed for the experiments presented in this thesis. Chapter 4 to chapter 7 present the results of this work. Here, the focus is placed on defining and analysing single cell (chapter 4, chapter 5) and population connectivity (chapter 6, chapter 7).

Several research groups focused on controlling individual neurons and their discoveries have been inspiration for the patterns presented in Part I.[163] However, in many publications neurons are chosen for analysis if they grow on a specific intended pattern position.[167,162] This selective approach is suitable to investigate questions concerning cellular mechanisms of individual cells such as neurite formation. Yet, for analysis of the behaviour of individual cells within a network this approach neglects differences in pattern efficiency. Here, all cells in the created single cell networks are considered and neuron morphology as well as pattern efficiency are evaluated in a holistic approach (chapter 4). Chapter 5 aims to show the statistical spectrum of individual neuronal activity, which was mainly analysed via calcium imaging.

Part II is devoted to the population connectivity. Here, reported studies used differently sized neuronal clusters and illuminated the impact of size onto network properties. However, the populations were characterised by random connectivities. The focus of this work is to address the randomness and incorporate structural connectivity by creating directional neuronal networks comprised of differently sized populations. Here too, previous studies gave inspiration for the chosen pattern design.[3] In chapter 6 and chapter 7 the impact of triangular pattern geometry and size on population architecture and functionality within networks is analysed. As for single cell functionality, neuronal activity is mainly analysed via calcium imaging and the whole spectrum of transients and activity patterns is presented.

Chapter 8 provides general conclusions on the presented work and give perspectives on engineered neuronal networks.

# Chapter 2

# Theory and fundamentals

This chapter provides the theoretical background for the thesis. First, fundamental concepts of the brain, its cells, development and architecture are described followed by a methodology part where technologies for creation and analysis of neuronal networks *in vitro* are presented.

## 2.1 The mammalian brain

The central nervous system enables a precise control of the whole body and organism. The command room of our body sits within our head: the brain. The mammalian brain is a stunning organ capable of multiple tasks: starting from functions for survival such as heart beating, breathing, looking for food, etcetera going to complex analysis and understanding of things, learning, pattern recognition, social behaviour and other challenging tasks, such as working and writing on this thesis.

### 2.1.1 Single unit: Neurons and glial cells

The single units of this highly complex organ capable of maintaining all the functions are two cell types - neuronal and glial cells. Neurons are traditionally seen as the single unit of our complex neuronal communication and the glial cells are believed to play an important role in e.g. maintaining and supporting the neuronal cells.[79] Figure 2.1 shows dissociated neuronal (blue) and glial cells (red), that were cultured for 24 days.

#### Neuron

**Neuronal morphology** The neuron is the smallest unit in the chain of signal processing in our brain. A typical neuron is depicted in Figure 2.2 and shows morphologically defined regions: soma, dendrites, and an axon. The soma or cell body contains the nucleus with the genetic information, the endoplasmic reticulum for protein synthesis and many other organelles necessary for maintaining the metabolic functions of a cell (not depicted in Figure 2.2). Two types of processes arise from the soma of a neuron: dendrites as main signal receiving structures and the axon that transmits neuronal signals over a distance to subsequent neurons. Typically, neurons have multiple dendrites with a highly branched structure and only one axon. The axon shows, especially near its end, fine branches that link to other

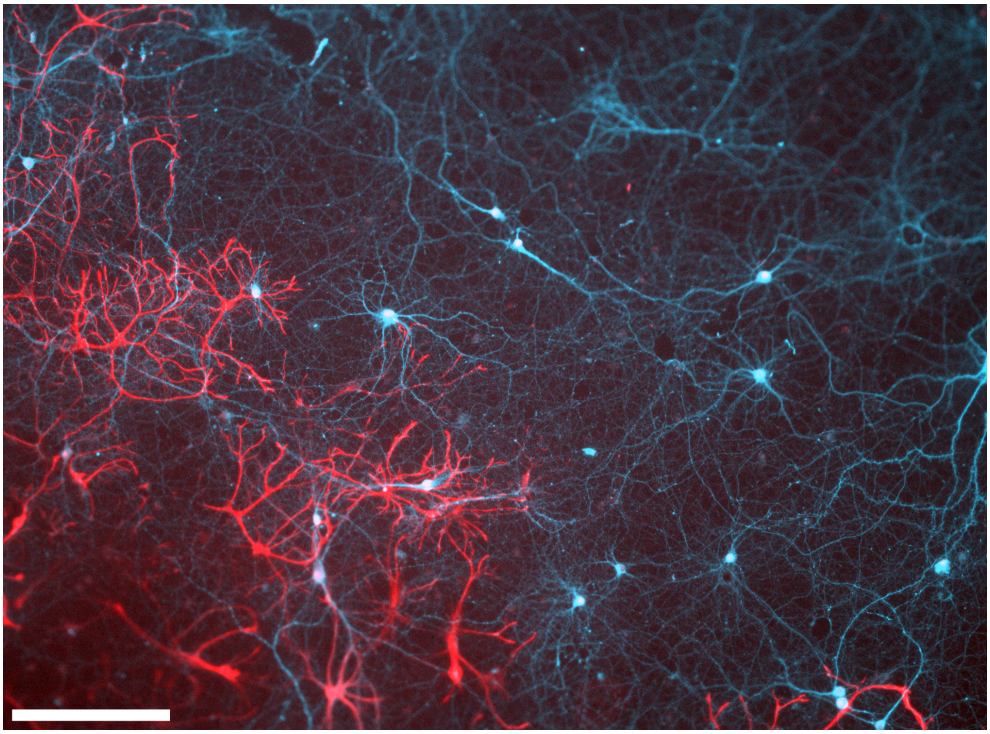

**Figure 2.1:** Dissociated neuronal and glial *in vitro* culture. Immunofluorescently labelled neuronal (blue) and glial cells (astrocytes, red). Scale bar 200 µm, 24 days in vitro (DIV).

neurons for signal transmission purposes. This link between two neurons is called synapse, consisting of a presynaptic terminal and a postsynapse.[79]

**Diversity of neuronal cells in the brain** The neuron, that was described in the previous paragraphs is a textbook neuron - a stereotyped neuron. In our brain we see many different types of neurons and they all vary in their functionality and appearance. Already in the 19th century scientists like Ramon y Cajal, Brodmann, Golgi and others, were interested in neurons and discovered different neuronal types. Utilizing sophisticated methods such as silver staining, these scientists were able to reveal different neuronal shapes.[79] Figure 2.3 displays neuronal shapes reported by several scientists. Figure 2.3.B shows a drawing adapted from Ramon y Cajal where neurons

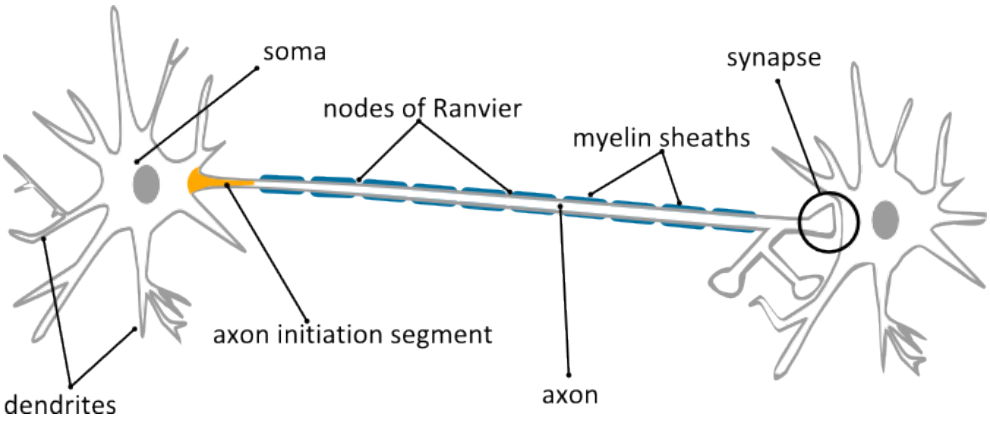


**Figure 2.2:** Morphology of a neuron. Dendrites receive the signal, which is further integrated and processed in the soma and propagated along the axon to the synapse and transmitted to the downstream neuron.

are classified upon the number of processes that are originating from their somata: ranging from no dendrite (unipolar), a single dendrite to extremely branched dendritic trees (bipolar); blank or branched axons; and other subtypes of neurons.[79,115,58]

**Neuronal Communication** Neurons communicate with each other via electrochemical events. The neuronal morphology with its specialised structures like dendrites, axons and synapses enable transmission of these events and thus neuronal communication. Electrical or chemical signals are received by the dendrites and propagated along the neuron as electrical signals.[79]

**Membrane Potential** To understand the signal propagation, we first need to take a closer look to the steady state of a neuronal cell - the resting membrane potential $V_{rest}$.
The cell membrane is a lipid bilayer and non-permeable to charged molecules. It blocks ion diffusion resulting in a charge separation along the membrane (Figure 2.4). The cytosol side of the neuronal membrane is slightly negative and the outer part is positive, respectively. The charging is mainly generated by different ions: sodium ion ($Na^+$), potassium ion ($K^+$), chloride ion ($Cl^-$)

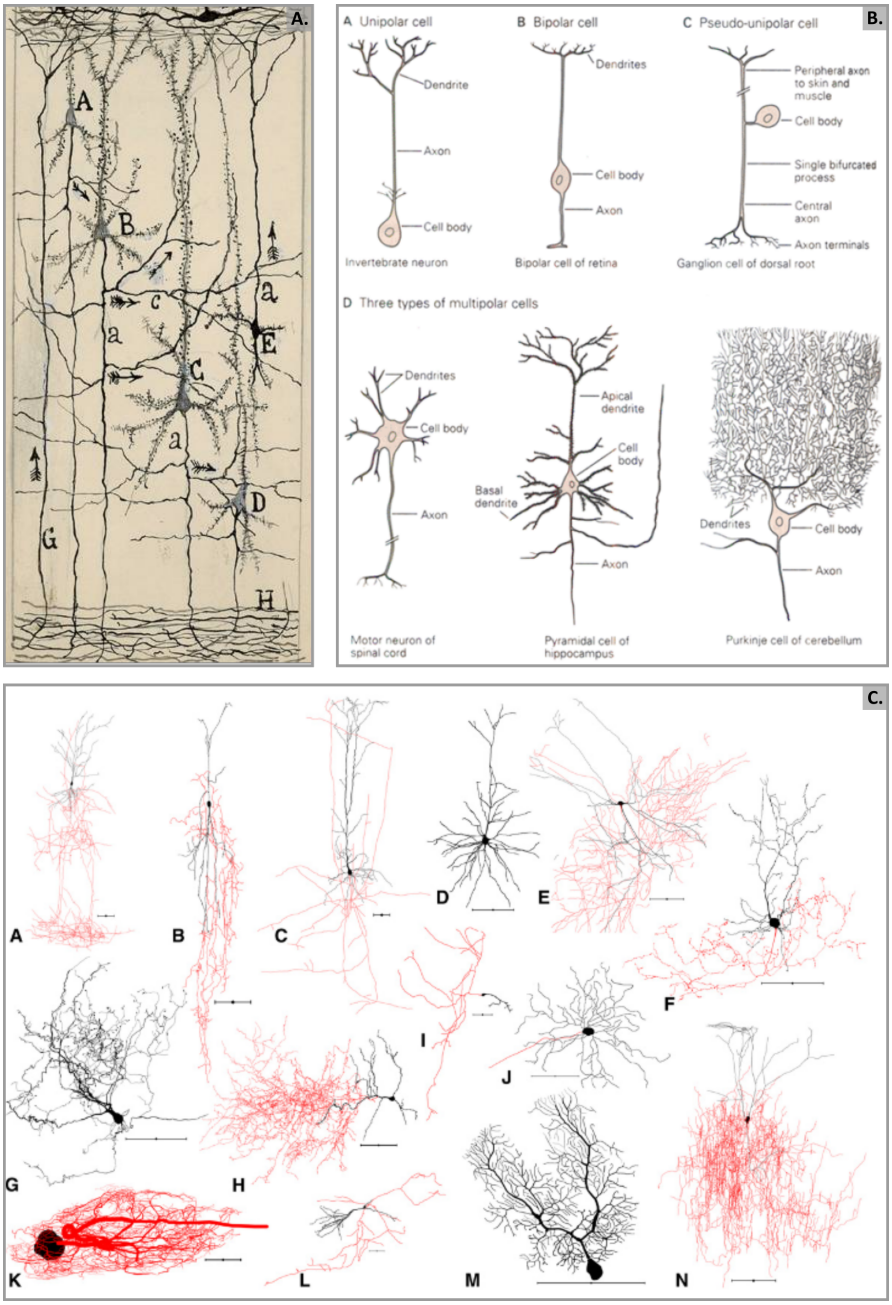


**Figure 2.3:** Diversity of neuronal shapes. A) Drawing of pyramidal cells of the cerebral motor cortex of a 15 days old child by Ramon y Cajal.[58] B) Neuronal cells can be classified depending on the number of processes originating from the soma. From Kandel et al..[79] C) Digitally reconstructed neurons from NeuroMorpho.Org. Scale bars 100 µm, somata and dendrites in black, axons in red. From Parekh and Ascoli.[115]

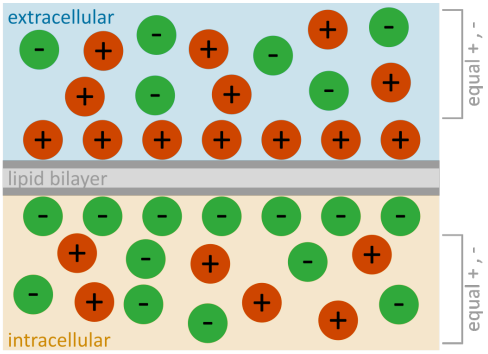


**Figure 2.4:** Charge separation at the cell membrane. The intracellular part of the cell membrane is slightly negatively charged compared to the outer part. Adapted and modified after Kandel et al.[79]

and negatively charged organic ion ($A^-$) in the cytosol. Table 2.1 shows the corresponding different ion concentrations at the inner ($[x]_i$) and outer part of the neuronal membrane ($[x]_o$).[79]

**Table 2.1:** Ion distributions across a cell membrane of a squid axon at $V_{rest}$.From Kandel et al.[79]

| Ion species | $[x]_i$ [mM] | $[x]_o$ [mM] | Nernst potential $E_x$ [mV] |
|---|---|---|---|
| $K^+$ | 400 | 20 | -75 |
| $Na^+$ | 50 | 440 | +55 |
| $Cl^-$ | 52 | 560 | -60 |
| $A^-$ (organic anions) | 385 | - | - |

Several ion channels are located in the neuronal membrane that enable ion flow into or out of the cell. There are two groups of ion channels: the leak and gated types. Leak channels are always open and do not change their state upon external factors. They are important for maintaining the resting potential. Different amounts of leaking channels contribute to different $Na^+$, $K^+$ and $Cl^-$ permeabilities of the cellular membrane. The second type of ion channels are gated channels. In contrast to leaking channels, gated channels are closed at resting state. Their opening is controlled by external influence

like membrane stretching, potential change or ligand binding.[79] The latter will be addressed in the following sections.

The membrane potential of neurons is calculated by subtraction of the extracellular from the intracellular potential:[79]

$$V_m = V_i - V_o \tag{2.1}$$

where:

$V_m$: membrane potential
$V_i$: intracellular potential
$V_o$: extracellular potential

Since $V_o$ is by definition 0 mV, the membrane potential is the intracellular membrane potential which is usually around $V_{rest}$ = -60 mV to -70 mV.[79]

Differences in ion distribution result in an electrical and chemical gradient leading to an ion flow. Nevertheless, the net ion flow is zero and thus, the resting potential $V_{rest}$ a steady state. Looking at every ion species independently ($Na^+$, $K^+$, $Cl^-$), one can define the equilibrium potential, the value at which the electrical driving force is equal to the chemical driving force. At this potential the $K^+$ inward movement balances the $K^+$ outward movement. The equilibrium potential for every ion species can be calculated using the Nernst equation:[79]

$$E_x = \frac{RT}{zF} ln \frac{[x]_o}{[x]_i} \tag{2.2}$$

where:

$E_x$: Nernst potential for an ion species $x$

$x$: ion species, e.g. $K^+$, $Na^+$

$R$: gas constant

$T$: temperature in Kelvin

$z$: valence of ion $x$

$F$: Faraday constant

$[x]_{o/i}$: ion concentration outside or inside a cell

Table 2.1 shows the calculated Nernst potentials for the main ions contributing to the resting potential at room temperature.[79]

To calculate the resting membrane potential, we need to consider all ion species that may cross the membrane at resting state. However, the Nernst equation only applies to the equilibrium state of one ion species. Also the different membrane permeabilities $P_x$ for different ion species need to be considered. The Goldman equation defines a relationship of all relevant permeabilities and can be used to calculate the resting potential $V_{rest}$:[79]

$$V_{rest} = \frac{RT}{F} ln(\frac{P_K[K^+]_o + P_{Na}[Na^+]_o + P_{Cl}[Cl^-]_o}{P_K[K^+]_i + P_{Na}[Na^+]_i + P_{Cl}[Cl^-]_i}) \tag{2.3}$$

where:

$V_{rest}$: resting potential

$R$: gas constant

$T$: temperature in Kelvin

$F$: Faraday constant

$[x]_{o/i}$: ion concentration outside or inside a cell of an ion $x$

$P_x$: permeability of the membrane to an ion species $x$

The number of open channels for an ion is proportional to its permeability.

Since there are mostly $K^+$ leakage channels in the neuronal membrane, the $V_{rest}$ is close to the $E_{K^+}$. The smaller proportion of $Na^+$ channels changes $V_{rest}$ to a slightly more positive value. $V_{rest}$ is neither accurately $E_{K^+}$ nor $E_{Na^+}$, resulting in a passive inward $Na^+$ and outward $K^+$ flow through the membrane.[79]
A transmembrane pumping enzyme is actively counteracting these fluxes: the $Na^+$-$K^+$-pump or $Na^+$-$K^+$-ATPase. This protein transports $Na^+$ out and $K^+$ into the cell, driven by adenosine triphosphate (ATP).[79,158]

**Action Potential** An action potential (AP) is the standard signal in the nervous system. Most stimuli, light, mechanical or chemical external cues are converted into the ubiquitous signal - the AP. This signal is a temporary, rapid change in the membrane potential caused by changes in the current flow through the neuronal cell membrane. In the last paragraph the fundamentals of the resting membrane potential and the transmembrane proteins involved in the maintenance of the $V_{rest}$ were lined out. Besides the passive leakage ion channels, several types of active, voltage-controlled channels are spanning the neuronal membrane.[79]
The typical shape of an AP is depicted in Figure 2.5. APs are generated at the axon hillock or AP initiation segment (AIS), located some micrometres away from the soma.[12] Incoming signals, received by dendrites and the cell soma, are integrated and propagate along the membrane as postsynaptic potential (PSP) (Figure 2.5.A). PSPs are changes in the membrane potential away from $V_{rest}$ (Figure 2.5.B) that trigger the opening of voltage-gated $Na^+$ channels. If the input signals depolarise the membrane to a certain voltage - the threshold potential $V_{thresh}$ - voltage-gated $Na^+$ channels (VGSC) open rapidly causing a fast influx of $Na^+$ into the cell. This results in a depolarisation of the membrane with an amplitude of approximately 100 mV (Figure 2.5.C, D). After this activated state the VGSC transition to an inactivated state where the channel is closed for a certain time, stopping the $Na^+$ flux into the neuron. At a voltage of around +30 mV voltage-gated $K^+$ channels (VGPC) open resulting in an efflux of $K^+$ ions and a repolarisation

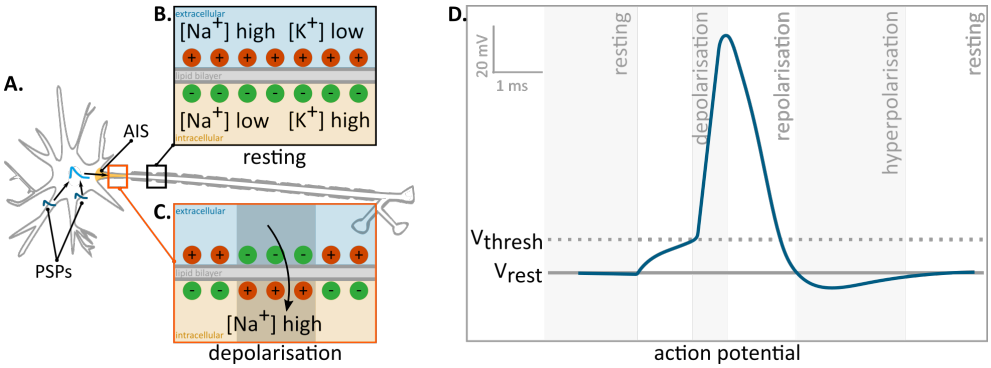


**Figure 2.5:** Anatomy of an AP. A) Neuron with its AIS. Postsynaptic potentials (PSPs, dark blue) are transmitted through the dendrites to the soma. B) The axon is still at resting potential with a high $Na^+$ concentration at the outer part of the membrane and a high $K^+$ concentration at the inner part. C) At the AIS, a region with a high density of voltage-gated channels, the AP is initiated. The intra- and extracellular ion distributions show a $Na^+$ influx into the axon. D) A typical AP with its different phases. After the membrane potential reaches a threshold potential $V_{thresh}$, opening of VGSC triggers a fast membrane depolarisation. Closing of these channels and opening of VGPC results in a re- and a hyperpolarisation. After that the membrane potential returns to resting membrane potential.

of the neuronal membrane. Due to the efflux of $K^+$ ions, the membrane reaches a lowered membrane potential than $V_{rest}$, a stage called hyperpolarisation. At this voltage VGPC also close and finally, the $Na^+$-$K^+$-pump restores the ion distribution to the initial values as described in Table 2.1.[79,12]

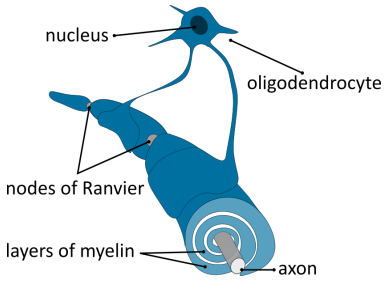


**Figure 2.6:** Myelinated axon. Adapted from Kandel et al.[79]

The AP is an all-or-none impulse, meaning that if the membrane potential is higher than $V_{thresh}$, an AP is generated. If it stay below that value, there is no AP. This impulse is conducted along the axon at propagation rates of 1 - 100 m/s. To increase the speed of the signal propagation, in vertebrate nervous system the axons are shielded by an insulation layer of myelin (Figure 2.2, Figure 2.6). This insulation layer is formed by glial cells - the oligodendrocytes in the central nervous system. Along the

myelinated axon regions enriched with ion channels, called nodes of Ranvier, interrupt the insulation layer regenerating the AP.[79,12]

**Synapse: Connecting neurons** Neurons are connected by synapses (Figure 2.2). Two classes of synapses are known: the chemical and the electrical synapse (Figure 2.7). At chemical synapses, the AP arriving at the presynapse is translated into a chemical signal at the synapse. The AP triggers the opening of voltage-gated calcium ion ($Ca^{2+}$) channels at the presynaptic terminal resulting in a $Ca^{2+}$ influx (Figure 2.7.a). The increasing concentration of $Ca^{2+}$ ions leads to the fusion of synaptic vesicles with the presynaptic membrane. Thus, neurotransmitters are released into the synaptic cleft. The neurotransmitters act as ligands for different channels or receptor proteins at the postsynaptic membrane. They trigger changes in membrane potential or initiate other signal cascades, like biochemical cascades or gene expression.[79,117]

On the other hand, at an electrical synapse the electrical signal is transmitted via a direct connection between two neurons (Figure 2.7.a). Due to gap junctions both cells are coupled and the electrical signal can pass from one cell to the other.[79,117]

Both types of synapses have their advantages. The electrical synapse enables a very fast signal propagation and provides the possibility for synchronisation. It also enables bidirectional and highly sensitive signal transmission including detection of subthreshold signalling. Therefore, it is mainly found in structures, where an almost delay-free or synchronised signal transmission is needed. Electrical synapses were found e.g. in the heart, retina, and escape networks (neuronal networks including sensory and motor neurons optimised for fast escape responses).[117] Electrical synapses are also present in many other brain regions, like the hippocampus or neocortex, and are believed to be widely spread in the nervous system.[28]

A chemical synapse however, enables different signal modi, like excitation, inhibition or amplification due to a variety of neurotransmitters and corresponding receptors. Additionally, the number of both - neurotransmitters

and receptors - can help modulate the signal amplification. For these modi the synapses require sophisticated molecular machineries to control and fine-tune the signal transmission.[117] Since most synapses in our brain are chemical synapses, this thesis will mostly consider these kinds of synapses.[91]

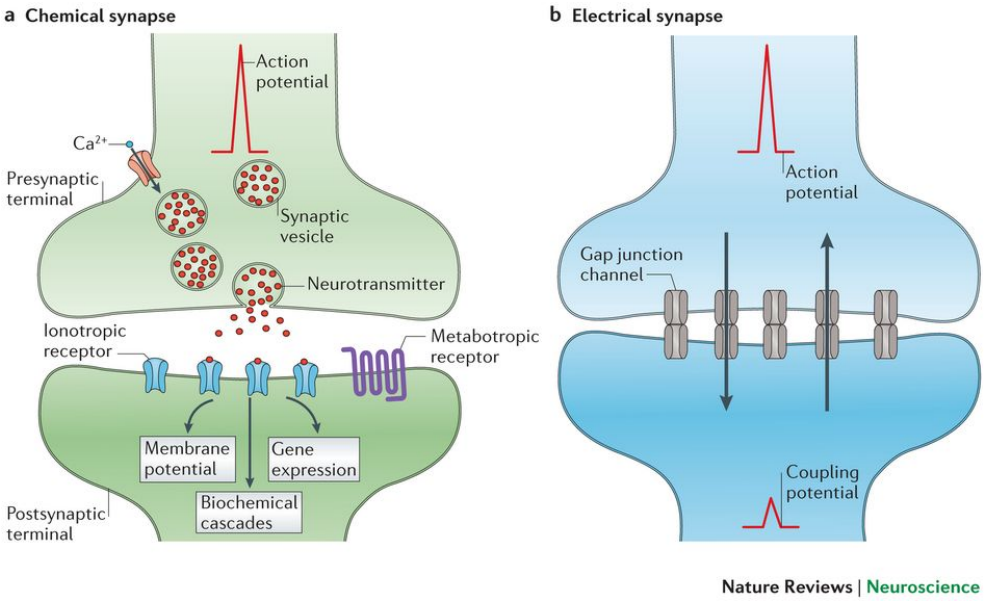


**Figure 2.7:** Chemical and electrical synapse. a) Chemical synapse. An AP reaches the presynaptic terminal which triggers opening of voltage-gated $Ca^{2+}$ channels and a $Ca^{2+}$ influx. $Ca^{2+}$ ions trigger vesicle fusion with the presynaptic membrane. Neurotransmitter are then released into the synaptic cleft and bind to specific receptors (ionotropic or metabotropic) in the postsynaptic membrane and trigger various cellular processes like membrane potential, biochemical cascades or gene expression. b) Electrical synapse. Pre- and postsynapse are directly linked by gap junction channels. APs are electrically transmitted to the subsequent cell resulting in a coupling potential. Figure from Pereda.[117]

**Synaptic signal transmission** Figure 2.8 displays the process of a signal transmission at a chemical synapse. An AP travels down the axon and reaches the presynaptic terminal. The depolarising membrane triggers opening of voltage-gated $Ca^{2+}$ channels that are present in the postsynaptic cellular membrane. $Ca^{2+}$ ions flow into the cytosol from the extracellular space

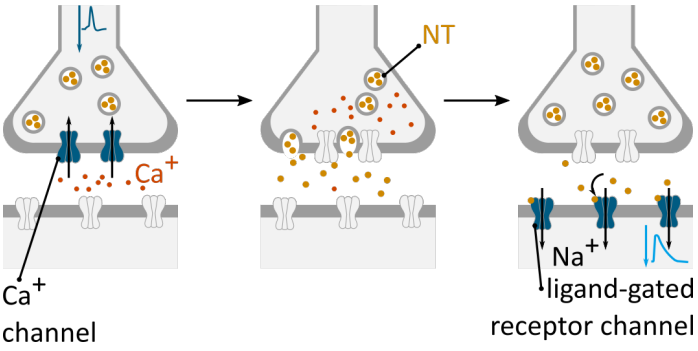


**Figure 2.8:** Synaptic transmission. Left: $Ca^{2+}$ influx into the cytosol from the extracellular space and internal $Ca^{2+}$ storages (like e.g. the endoplasmic reticulum, not depicted here) modified after Kandel et al.[79]

and from internal $Ca^{2+}$ storages, like the endoplasmic reticulum (Figure 2.8 left). The increasing $Ca^{2+}$ concentration triggers vesicles to fuse with the cell membrane of the presynapse and the neurotransmitters inside the vesicles are released into the synaptic cleft (Figure 2.8 middle). Neurotransmitters bind to ligand-gated receptor channels in the postsynaptic membrane resulting in a $Na^{+}$ influx and a depolarisation of the membrane (Figure 2.8 right). This potential is called excitatory postsynaptic potential (EPSP) and is displayed in the blue graph in the right panel of Figure 2.8. The EPSP is a graded potential, that is varying in amplitude.
Another type of ligand-gated channels, the $Cl^{-}$ channels, trigger $Cl^{-}$ influx resulting in an hyperpolarisation of the membrane. The hyperpolarisation decreases the membrane potential. Thus, a higher signal amplitude is necessary to reach the threshold potential. This potential is called inhibitory postsynaptic potential (IPSP).[79,117,91]

**Signal integration** As outlined before, the AP is a digital signal following the all-or-nothing principle. Thus, the neuronal signal is decoded in a frequency of APs. Typically a neuron has several synapses from other neurons at different locations. Synapses can be formed between all cellular substructures - axons, dendrites and soma. Incoming APs are translated into PSP in the postsynaptic neuron. Multiple PSPs at multiple synapses are integrated,

a property which is called summation. If an integrated potential reaching the initiation segment exceeds $V_{thresh}$, it can trigger an AP.[79]

### Glial cell

In the human brain there are 10 to 50 times more glial than neuronal cells. Their name derives from the Greek, and means glue. For a long time, glial cells were believed to be "only" a supporting and surrounding structure for the neurons. Nowadays glia is known to have multiple functions. One of these functions was already mentioned in Figure 2.6: production of the myelin sheath. Schwann cells in the peripheral and oligodendrocytes in the central nervous system wrap around axons to insulate them and enable a faster signal propagation. Glial cells can also separate and group populations of neurons to provide a structuring in the brain. They facilitate the uptake and release of several molecules, like neurotransmitters or growth factors. Moreover, glial cells play an important role in the brain's safety by participating in the blood-brain barrier and in the immune system.[79]

## 2.1.2 Neuronal development and polarisation

### Neuronal polarisation *in vivo*

Neuronal development and polarisation *in vivo* is a self-organised process driven by multiple interacting factors. Scientists were able to partly reveal some the complex processes but still many of them are undiscovered. It is known so far, that during the embryogenesis neuronal cells develop in a process called neurogenesis.

Timing is a very important factor in neurogenesis. In rodents, neurogenesis starts from embrionic day (E) 12 to 18 (E12 - E18) with the development of neuronal cells, followed by glial cell development (Figure 2.9). This subsequential timing indicates that neuronal connectivity is established first and then a matching of glial cell number and position follows. Both, neuronal and glial cells differentiate from multipotent precursor cells. Internal and ex-

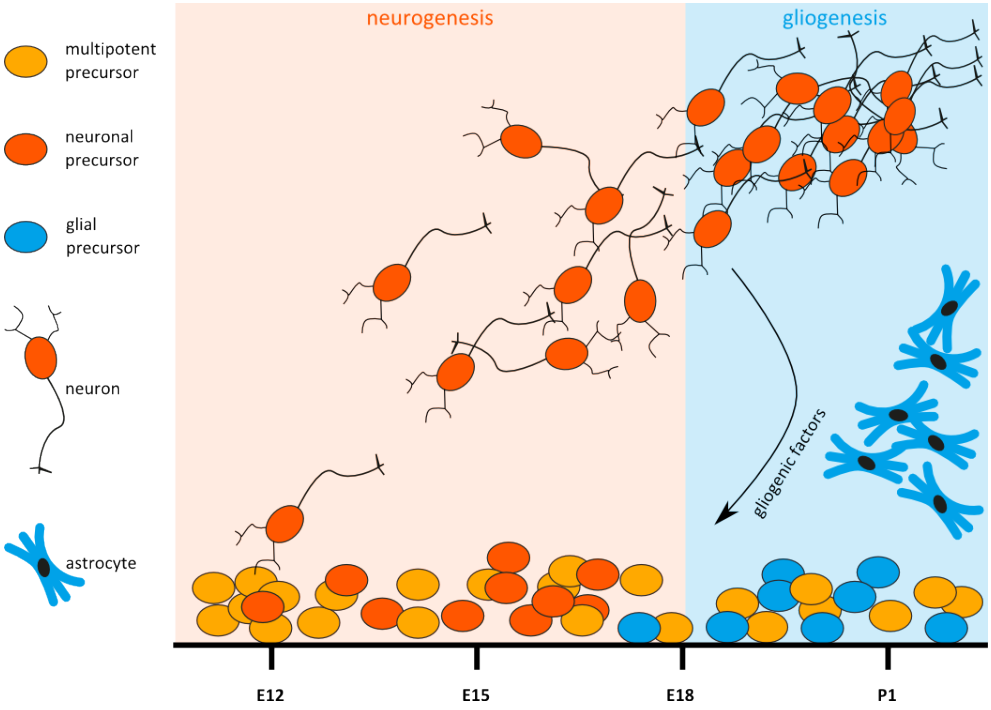


**Figure 2.9:** Timing of neurogenesis *in vivo*. In the developing rodent neocortex neurons are generated first from multipotent precursors from E12 to E18 (neurogenesis). Later, the newborn neurons secrete gliogenic factors that trigger glial cell generation (gliogenesis). Image adapted and modified from Miller and Gauthier.[98]

ternal factors induce the differentiation into either neuron or glia.[98] First, a machinery of signalling molecules promotes neurogenesis and suppresses glial cell development: Glial genes as *gfap* for example are methylated and thus inactive. At the same time proteins (e.g. neurogenic basic helix-loop-helix, bHLH) activate neurogenesis. Newly born neurons then secrete gliogenic factors like the cytokine CT-1, that together with other cues activate signalling pathways and transcription factors which triggers glial development after E18.[98,11]

The polarisation processes of neurons *in vivo* show a huge variety depending on the brain region. Cortical and hippocampal neurons are probably best studied so far. In these regions the neurons polarise during their differentiation.[109,140,57] In the cortex the neuronal organisation is established in

an inside-out process, where the latest-born neurons migrate to the outer cortex layer and thus being the most superficial.[98] The formation of polarisation differs between excitatory and inhibitory neuronal cells in the cortex development *in vivo*.

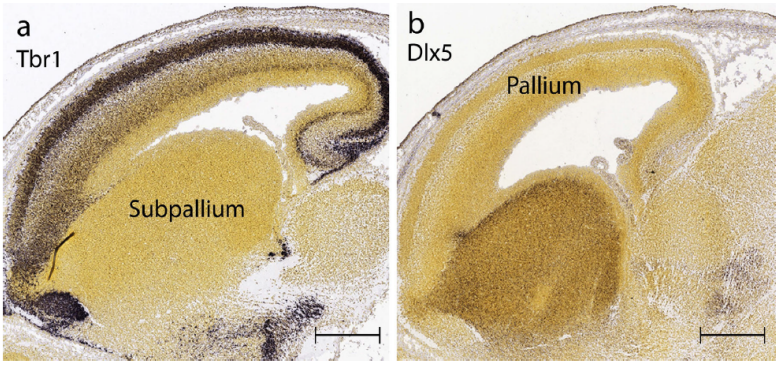


**Figure 2.10:** Neocortex during mouse neurogenesis (E15.5). Sagittal sections showing expression of (a) pallial marker Tbr1 and (b) subpallial marker Dlx5. Scale bar = 0.5 mm. Image from Watson and Puelles,[154] originally taken from Allen Institute for Brain Science.[6]

Excitatory cells, which comprise 70 - 80 % of cortical neurons in rodents, differentiate from radial glial cells of the cortical ventricular zone (VZ) in the pallium (Figure 2.10). These radial glial progenitors undergo asymmetric division which generates progenitor cells and intermediate progenitors. The intermediate progenitors further divide and generate neurons.[130] Newly born multipolar shaped neurons start migrating through the subvebtricular zone (SVZ) and intermediate zone (IZ) elongating and retracting short processes (Figure 2.11.A I). In the IZ one process suddenly elongates tangentially and becomes an axon (II). Another process, the leading process, elongates further (III) through the cortical plate (CP) towards the marginal zone (MZ), followed by a soma movement towards the leading process (IV). In the last step, the soma translocates to the final position.[130]

Inhibitory neurons originate from the subpallium, the ganglionic eminence (Figure 2.10), and migrate tangentially towards the MZ and further to the CP.[104] As depicted in Figure 2.11.B they show a multipolar shape until sud-

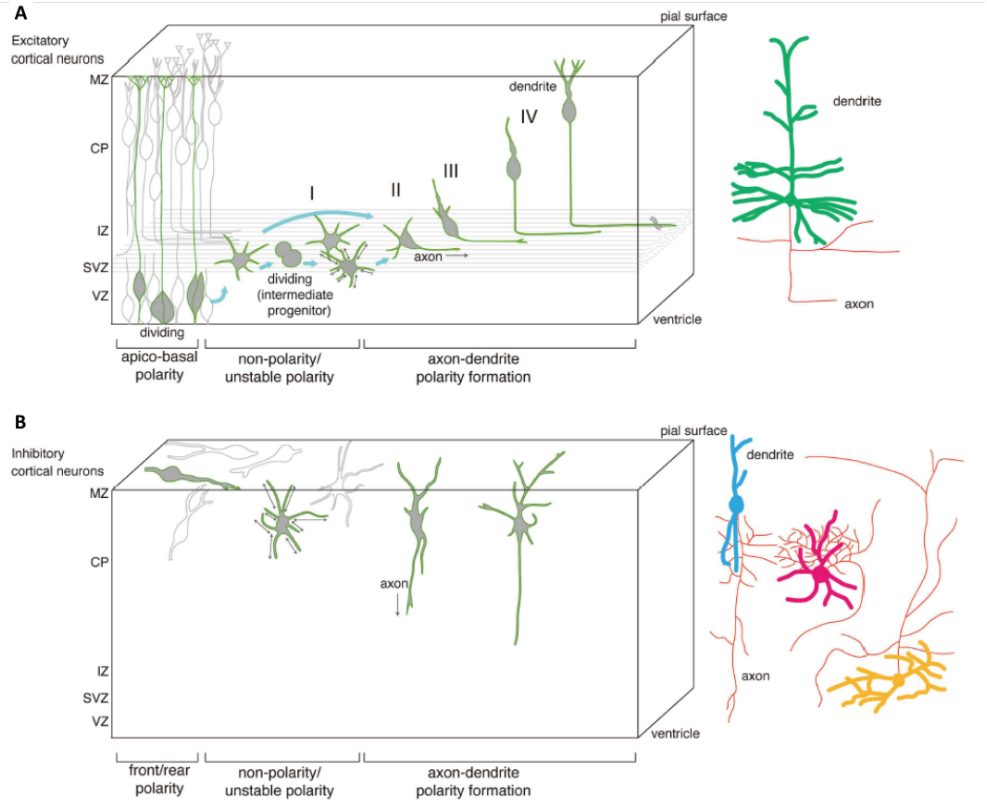


**Figure 2.11:** Neuronal polarisation in the cortex *in vivo*. A) Polarisation of excitatory neurons starts in the VZ. Here, young multipolar neurons repeatedly extend and retract their processes (I) until suddenly the symmetry breaks and one process elongates tangentially, becoming an axon (II). The dendrites transform into a pia-directed leading process (III) resulting in a bipolar shaped neuron that migrate towards the pia (IV). When the neuron reaches its final position, the neurites mature. B) Inhibitory neurons are generated in the subpallium and migrate towards the MZ within the cortex. Here, neurons appear bipolar with a leading and a trailing process. Neurons migrate toward the CP while development proceeds, transforming into multipolar cells that extend and retract their processes repeatedly. These cells show a low soma motility. Suddenly an axon extends towards the ventricle. After this symmetry break, axon and dendrites elongate and mature. Inhibitory cells are reported to be highly diverse in morphology and thus, the drawing depicts the formation of polarity for only one subtype of inhibitory neurons. The details are still under investigations. Image from Sakakibara and Hatanaka..[130]

denly the symmetry breaks and neurons exhibit a leading and trailing process. Contrary to the excitatory neurons, inhibitory neurons are reported to show a

lower soma motility. It is unknown so far, if all inhibitory neuronal subtypes undergo the same procedure during differentiation as described here.[130] Glial cell differentiation in rodents is starting from E18 and peaks at a neonatal stage.[130]

### Neuronal polarisation *in vitro*

The polarisation of neurons *in vitro* has been mostly studied in dissociated hippocampal neurons.[43,30,143] In contrast to the high complexity and diversity of neuronal polarisation and development *in vivo*, the polarisation process of cultured neurons happens in a less complex environment.

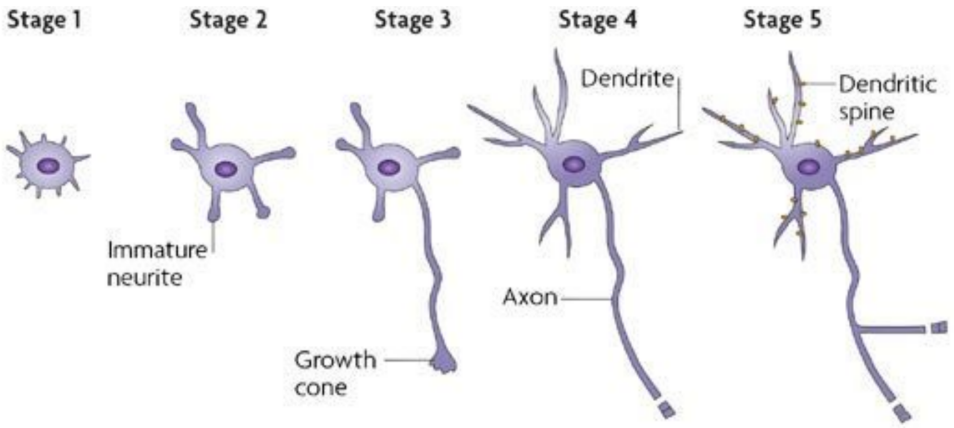


**Figure 2.12:** Neuronal polarisation *in vitro*. Stage 1: Neurons form short filopodia. Stage 2: Minor processes can be observed, that extend and retract repeatedly. Stage 3: After several hours one process elongates rapidly, transforming into an axon that is characterised by a growth cone at the tip. This stage is also called symmetry break. Stage 4: All neurons elongate further, Stage 5: and dendrite and axon maturation proceeds. Image from Arimura and Kaibuchi.[9]

After isolation, dissociation and plating, the polarisation process can be divided into five stages as depicted in Figure 2.12. During the dissociation and isolation of the tissue, neurons retract their processes and have a round shape. After plating cells adhere to the substrate within minutes and start to develop short filopodia within the first days in vitro (DIV) (DIV 0 - 0.5,

stage 1). In the second stage (DIV 1 - 2) the neurons exhibit minor immature neurites. In this stage the cells are still symmetrical and do not show any polarity. One of the immature neurites starts to elongate faster and at some point becomes the axon (stage 3, DIV 2 - 3), a process which is called "break of symmetry". From here on, the neuron is a polarised cell and the axon and dendrites mature and form synapses (stage 4, DIV 4 - 7). In the fifth stage (DIV 7 - 14) the connections are developing further, more synapses are formed, dendritic spines develop and the network is becoming electrically active.[43,130]

### 2.1.3 Organisation of the brain

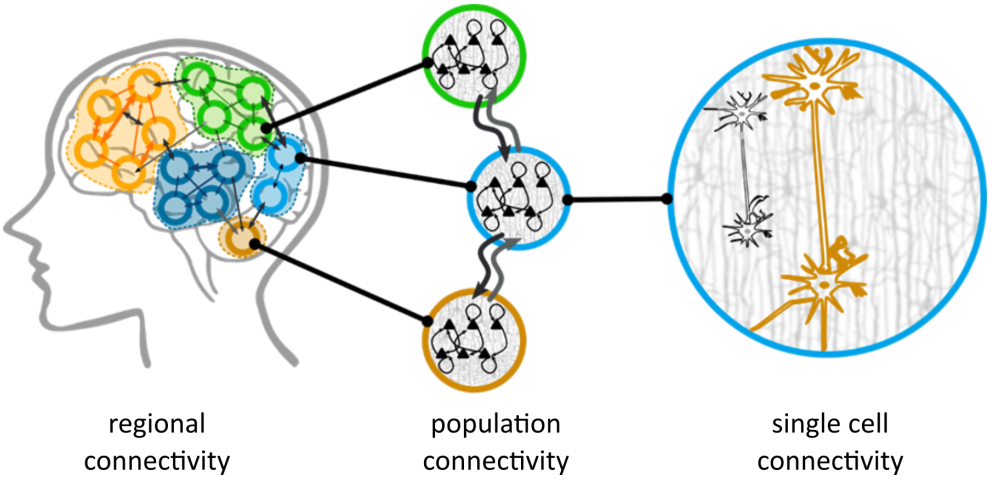


**Figure 2.13:** Brain connectivity. Different connectivity levels of the brain are depicted. Left: Groups of neurons are connected into regions. These regions are highly interconnected with other regions of the brain. Middle: Within one region groups of neurons show similar behaviour or morphology and are regarded as populations forming the populational level of connectivity. Right: Zooming in further, individual cells are organised and connected to other neurons. This is the level of single cell connectivity within the brain. Image adapted from Park and Friston.[116]

The polar and directional character of a neuron is the fundament for the brain and its hierarchical and modular architecture. Specificity of neuronal

cell types and their connections ends up in a self-organisation of functional neural circuits. Multiscale hierarchical organisation was observed on the anatomy as well as on the functional level. Connectivity patterns reach from individual neurons and their connections (single cell connectivity) to macrocolumns or nodes (population connectivity) to macroscopic connection of brain areas. Anatomical topology results in functional connectivity, where correlating activity patterns can be observed.[116] The hierarchy of modular organisation of the brain is depicted in Figure 2.13.

**Columns: Single cell to population connectivity level** Some examples of the different connectivity levels can be found in the topology of the cortex. The neocortex is a 3 mm thin, 45 by 45 cm sheet of neuronal tissue and has an area around 2'000 to 3'000 $cm^2$.[65,41,103] The number of neurons is estimated to around 25 billion.[66] The horizontal organisation of the human neuronal cortex contains six cortical layers, called laminae. The layers are groups of neurons interconnected horizontally and linked vertically to other cortical laminae.[103]

Mountcastle first published a concept of columnar organisation where 80 to 100 neurons are vertically linked. A schematic representation of such a minicolumn is depicted in Figure 2.14. Since the diameter of a minicolumn is around 50 µm, the structures can be regarded as a sort of single cell connectivity.[101] Minicolumns are believed to be the basic unit of the cortical information processing.[103,78] Researchers have different theories about the reason for this minicolumn architecture. One of them is that organisation in microcolumns minimize the wiring amount in the microcircuits.[65] Many minicolumns form a cortical (macro-) column by horizontal interconnectivity. The diameter of macrocolumns is around 500 µm.

Examples of columnar organisation in the brain are the ocular dominance (OD) columns and the orientation columns in the primary visual cortex (V1) or the barrel cortex in the somatosensory cortex of some rodents. OD stripes are anatomically and functionally different regions that respond either to stimuli from one eye or the other.[101] Neurons in orientation columns show

a difference in response depending on the orientation angle of the stimulus.[71,101] Barrel cortex represents the whisker region.

The hypothesis of a columnar organisation is discussed controversially among the neuroscience community. The linguistic shortcoming of the word "column", the broad usage of this term for anatomical, functional, micro- and macroscopic versions, the distribution, presence or absence of columns in different brain regions and even the whole concept of the column as a functional unit are contentious.[101] Nevertheless, the concept of columnar cortex organisation is currently the most widely used explanation for cortical signal processing even though it is not obligatory to the cortex. On the other side, the concept of modular organisation is not limited to the cortex but is also observed in subcortical areas, e.g. in the thalamus. Despite the imperfect naming, a column defines a basic unit of signal processing that is highly connected across columnar boundaries and embedded in higher order networks.[127]

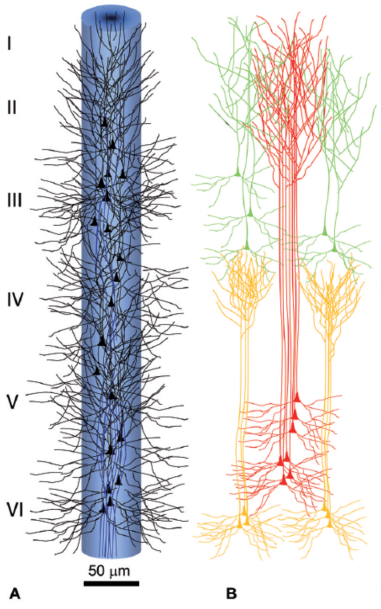


**Figure 2.14:** Minicolumn. A) Schematic representation of somata, proximal dendrites (black) and main axons (blue) of a minicolumn in cortical layer I - IV. B) Bundles of apical dendrites. From DeFelipe.[37]

**Regional Connectivity** Some well understood higher order networks are pathways within the brain (examples see Figure 2.15), like the nigrostriatal pathway. The nigrostriatal pathway is a connection of the substantia nigra pars compacta and the striatum. The striatum receives and integrates inputs from various brain regions including cortex, hippocampus, amygdala and the midbrain and orchestrates motor actions. Dopaminergic inputs from the midbrain play an important role in the Parkinson's disease and voluntary

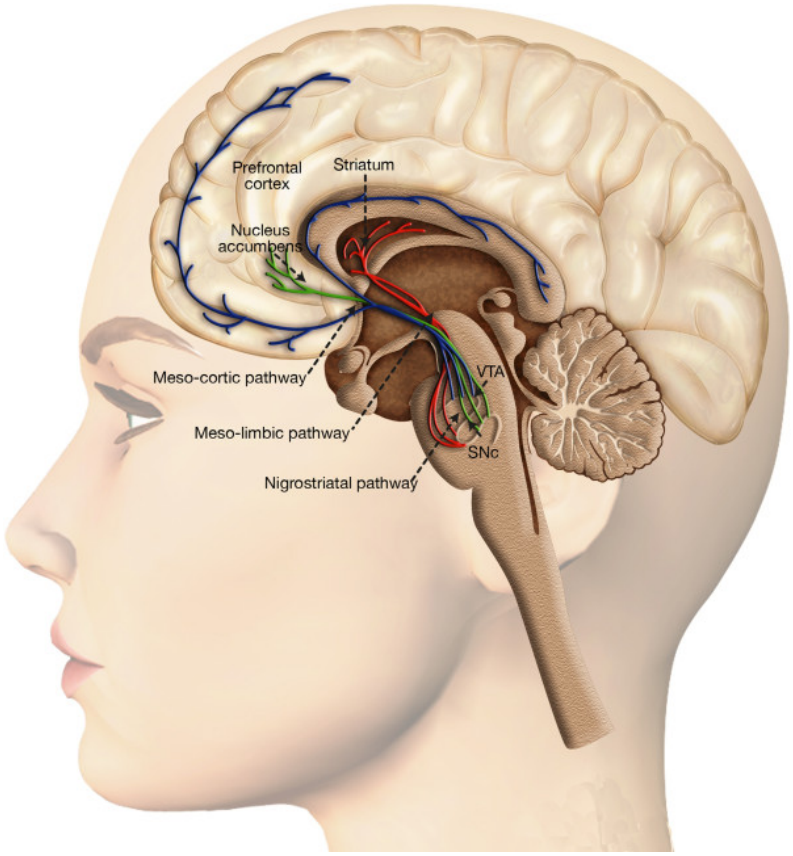


**Figure 2.15:** Brain pathways. The mesolimbic, mesocortic and nigrostriatal pathways are depicted. The nigrostriatal pathway is probably the best studied of dopaminergic brain pathways. The system is involved in the control of voluntary movement. Image from Arias-Carrión et al.[8]

movement. Other discovered pathways are the mesolimbic and mesocortical pathway that are involved in reward and motivation.[148,8]

These examples show how regional connectivity is linking different areas of the brain resulting a complex functional network. Some of these regions show obvious anatomical separation whether others can be only observed by analysing the functionality.

## 2.2 Creating connectivity levels *in vitro*

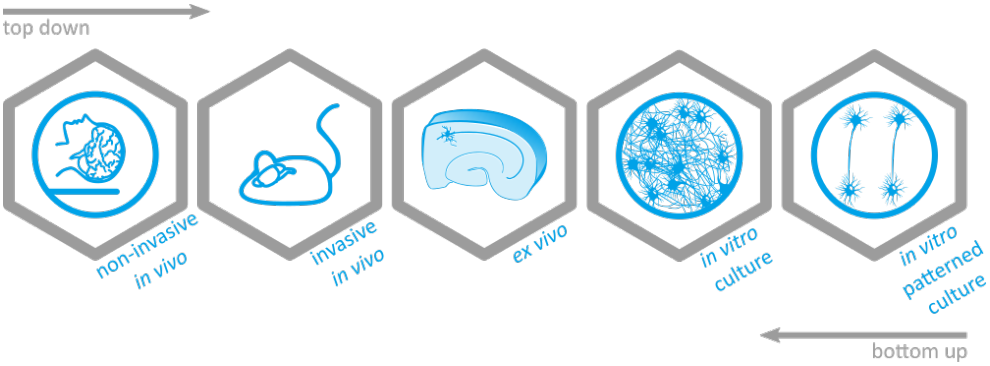


**Figure 2.16:** Analysing the brain at different levels.

Multiple approaches are used by scientists to reveal and understand the principles behind the complex brain architecture. These approaches can be categorised into different macro- and microscopic levels as depicted in Figure 2.16 With top down non-invasive approaches one can look at regional organisation within the human brain by functional magnetic resonance imaging (fMRI), positron emission tomography (PET), magnetoencelography (MEG) or electroencephalography (EEG).[110] These techniques reveal the macroscopic structural and functional areas and activity patterns but suffer from low resolution which is limited to regions.

A higher resolution can be achieved by invasive methods that are used in *in vivo* animal experiments. Many insights into the complex neuronal signal processing were gained from *in vivo* MEA recordings from cats, rats, mice or macaques.[110] Nevertheless, these methods show a population resolution. With computational approaches the recordings can be separated and clustered to obtain single-cell separation.

But, to analyse the neuronal characteristics on a true cellular level, *ex vivo* experiments have to be performed. This can be done by preparation of the brain regions of interest and analysing brain slices with optical or electrical methods. In brain slices we still have a system that approaches *in vivo* con-

nectivity, but is reduced in complexity by reduction of the neuronal population and connections.

If one wants to analyse cell to cell connectivity, the complexity of the analysed neuronal network has to be further reduced. This can be achieved by culturing dissociated neurons on flat surfaces. Even though this is a widely used approach, the random neuronal cultures lack the organisation and architecture of an *in vivo* environment.

To overcome this limitation a bottom-up approach can be used to create structured neuronal networks with specific connectivity or networks' characteristics. Networks with defined structure and connectivity can be created by various microengineering methods, most of them promoting growth of neuronal cells on specific areas while inhibiting it on other areas.[156] This approach exploits cellular sensitivity to geometrical and mechanical constraints from their environment.

Microfluidic devices can be used to create regional connectivity *in vitro*. Here, independent cell culture chambers separated by funnel-shaped channels enable engineering of neuronal networks with directional connectivity. By culturing different neuronal subtypes in each chamber, neuronal pathways can be reconstructed *in vitro*.[119,73]

For regional and populational connectivity, soft lithographic techniques like µCP, as well as photolithographic techniques like photo- or laser-patterning can be employed. They all create patterns of adhesive regions on the substrate. Photo-patterning employs UV illumination through a photomask to modify surface chemistry in a defined pattern. With this method, previously grafted polyethylene glycol (PEG) can be modified in order to induce binding of cell-adhesive proteins. Laser-patterning employs a focused laser beam to induce cross-linking of functional groups on a non-adhesive surface. The advantage of photo- and laser-patterning is the possibility of modulation: With varying parameters (e.g. exposure time), the density of the modification can be controlled. However, specialised equipment is needed and there is only a limited number of photo-sensitive chemicals suitable for cell culture.[7,145] µCP

is another technique that can be used for micropatterning. Here, a stamp is used to transfer patterns onto a substrate. In contrast to photo- and laser-patterning, specialised equipment is only needed in order to fabricate the template for the stamp. Afterwards all experimental steps can be performed in a regularly equipped cell culture laboratory. Additionally, µCP can be used to pattern many materials and chemicals. Because of these advantages this technique is of central focus of this thesis.

### 2.2.1 Microcontact printing

Photolithographic patterning methods developed for the microelectronic industry were first used for bio patterning in the late eighties.[64,84] Even though the biological use was successful, it was a rather expensive technique and its application was limited to photosensitive resists.[156] In the mid-nineties a method called soft lithography was developed in the research group of Whitesides et al. for preparing patterned gold substrates.[87] This method called microcontact printing is simple and inexpensive and enables patterning of different materials like proteins.[156]

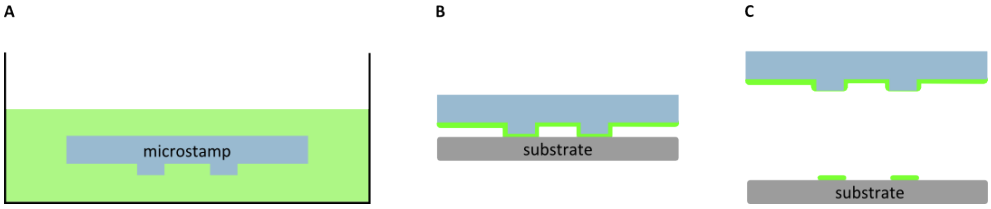


**Figure 2.17:** Schematics of microcontact printing. A) The microstamp is incubated in a cell-adhesive (protein) ink. B) The stamp is dried and placed on the substrate. C) The pattern is transferred onto the substrate.

The principle of µCP can be compared to stamping: An ink is transferred onto a surface via a topographically patterned stamp (Figure 2.17). This technique provides the possibility to easily shape and control the architecture of a neuronal culture *in vitro*. Depending on the design of the stamp multiple features of network connectivity can be engineered.

The choice of inking solution depends on the specific application. For culturing neurons a protein solution is used for inking the polymer microstamp. The proteins of choice should mimic components of the extracellular matrix surrounding the neuronal cells *in vivo*. Here, the contrast of the adherent and repellent surface is a very important factor.[112]
Polydimethylsiloxane (PDMS) is often used for moulding the microstamps because it is biocompatible and easy to handle. It is used in many different areas, like food industry, hair conditioners or biomedical industry. In addition, thermoplastics like Polyolefin plastomer (POP) are a widely used material for the stamps. Both, PDMS and POP are hydrophobic. To enable a protein transfer from the microstamp to the substrate it is important, that the binding energy of the protein to the substrate is favourable compared to that of the protein to the microstamp. Additionally, only the feature surface should be in close and homogeneous contact with the substrate. That ensures first, an homogeneous protein transfer from microstamp to the substrate and second, that only the desired protein pattern is transferred onto the substrate.[112]

### Patterning neuronal cultures by µCP

Since µCP was discovered for cell culture applications, some research groups analysed the influence of different shapes onto neuronal outgrowth and network architecture. In the following paragraphs some examples of this research will be lined out.

**Controlling single cell connectivity** By controlling single cell connectivity one can unravel complex connection patterns and get a deeper insight into neuronal signal propagation. Vogt et al. for example created a grid pattern to reduce the network's complexity and achieve cell separation. They showed that electrical activity persisted (see Figure 2.18 A).[150] Yamamoto et al. observed, that if you allow only one neurite to exceed a certain path length, this neurite is likely to become an axon (see Figure 2.18 C). After

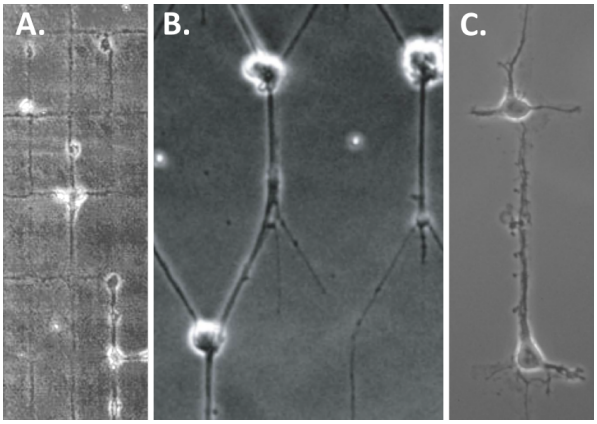


**Figure 2.18:** Selection of published single-cell networks. A) Grid networks presented by Vogt et al.[150] B) Polarisation controlled by angle between neurites. Image from Zhu et al.[167] C) Daisy-chained single cell patterns separated by a minor gap. Published by Yamamoto et al.[162]

2 DIV more than 70 % of the cultured neurons on pattern showed a polarity. This is similar to the percentage of polarized neurons on a homogeneously coated substrate at this stage.[163] Zhu et al. were able to achieve polarity by choosing an appropriate angle between the axonal and dendritic pattern lines (see Figure 2.18 B).[167] These selected publications show that neuronal structure can be influenced via specifically patterned substrates *in vitro*. Additionally, it demonstrates the potential of engineered neuronal networks by µCP to analyse single cell connectivity. With a sophisticated pattern design one can control different attributes of the neuronal polarity: soma and neurite position, polarity or number of neurites.

**Controlling populational connectivity** On population level, Feinerman et al., Albers et al. and others demonstrated, that triangular shapes can impact neuronal network directionality (see Figure 2.19).[51,4,60] Albers et al. were able to engineer a polarised network architecture. They have chosen different triangular shapes and demonstrated, that the geometry of the network impacts the direction of axon outgrowth and signal propagation. Thus, they engineered neuronal populations with controlled directionality.[4,3]
These examples show the power of µCP to design neuronal networks with specific structural characteristics. Analysis of such engineered, structured networks *in vitro* can give a deeper insight into the architecture and function of the brain.

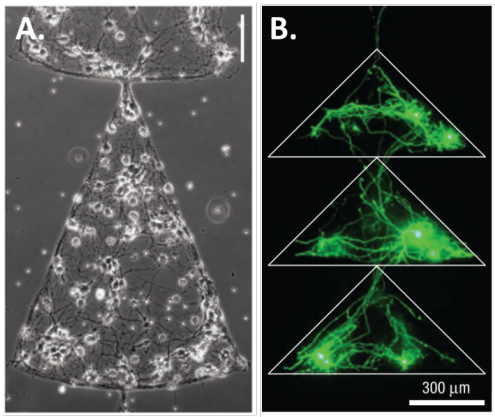


**Figure 2.19:** Selection of published patterned population networks. A) Neurons at DIV 14. Scale bar 100 µm. Image from Albers et al.[4] B) Image from Feinerman et al.[51]

## 2.3 Analysing neuronal networks

This section gives an overview of the methods used to analyse neuronal networks, focusing on the techniques used to obtain the results for this thesis. First, the immunofluorescence method is described - a powerful tool to characterise the structural and molecular composition of different cells. Calcium imaging is introduced afterwards as a widely used technique to analyse the functionality of neuronal networks. Last, methods to analyse electrical properties of neuronal networks are described.

### 2.3.1 Analysing neuronal morphology via immunofluorescence

Immunofluorescence (IF) is a widely used laboratory technique where antibodies are chemically conjugated to fluorescent molecules. These antibodies then bind directly or indirectly to cellular structures of interest, so called antigens. For the direct method the antibody for the antigen of interest is directly chemically conjugated to the fluorescent dye. The indirect method uses a primary unlabelled antibody for the antigen of interest and a secondary tagged antibody toward the primary antibody. Figure 2.20 schematically depicts the direct and indirect IF methods.

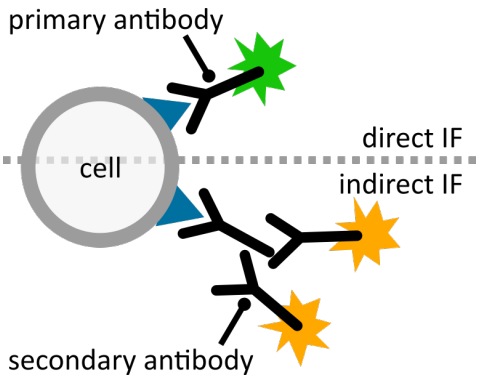


**Figure 2.20:** Immunofluorescence methods. Antigen of interest is represented in blue. The primary antibody binds directly to the antigen (top). The direct IF method uses a fluorescently tagged (green) primary antibody. The indirect IF method (bottom) uses an unlabelled primary antibody and a secondary antibody with a fluorescent tag (yellow). Figure adapted from Robinson et al..[126]

Because the direct IF method is linked to higher cost and less flexibility, most laboratories favour the indi-

rect IF method. Additionally, the indirect method offers signal amplification due to a higher amount of secondary antibodies binding to the primary antibodies.[126]

### Structural characterisation of neuronal subparts

Protein and cytoskeleton composition vary depending on the cellular structure.[79] To analyse cellular structures - as for example dendrites, axons and somata - one can define the antigens of interest and visualise them via IF. Several neuronal markers are used in the neuroscience community to label the substructures of interest. These can be neuron-specific cytoskeleton parts or associated proteins expressed only or abundant in neurons or their substructures.

One example is the microtubule-associated protein 2 (MAP2), a neuron-specific cytoskeleton protein that is involved in microtubule stabilisation and enriched in dendrites.[141,86] Another marker for neurons is βIII tubulin. This tubulin is expressed widely in neurons throughout early and late developmental stages and localized in every neuronal subpart. Tuj1 is an antibody towards this tubulin subclass.[97]

To label the axon, one can visualise a special type of intermediate filaments, the neurofilaments (NF). NF are distributed all over the neuron: they are present in dendrites, perikarya and in the axon. However, NF are abundant in the axon and its major cytoskeleton component. The heteropolymers consist of different subunits, namely NF light, medium and heavy - NFL, NFM and NFH respectively. Antibodies towards the high molecular weight neurofilament (NFH) can be used for visualisation.[34,15,165] In addition, antibodies towards the tau protein - a protein enriched in axons - can be used to visualise the axons.[86]

### Technical principles of IF labelling

Cells have to be prepared prior to labelling. The preparation starts with fixation that preserves the morphology and prevents degradation by cross-

linking. For that, agents like paraformaldehyde are utilized. Treatment with detergents alter the permeabilisation of the cellular membrane and allow antibodies to enter the cell. In the next step, non-specific sites are blocked by serum to increase antibody specificity. After that cells are incubated with antibody solutions for the actual labelling of the antigens of interest.[95]

### Fluorescence principles

After the neuronal cultures are prepared and labelled with specific antibodies they can be analysed via fluorescence light. The physical principles of fluorescence are briefly described in the following paragraph.
A molecule with fluorescent properties has a specific atomic structure. In a molecule, electrons are arranged around the nucleus with each electron having a certain predefined energetic level. When absorbing light, the electrons of

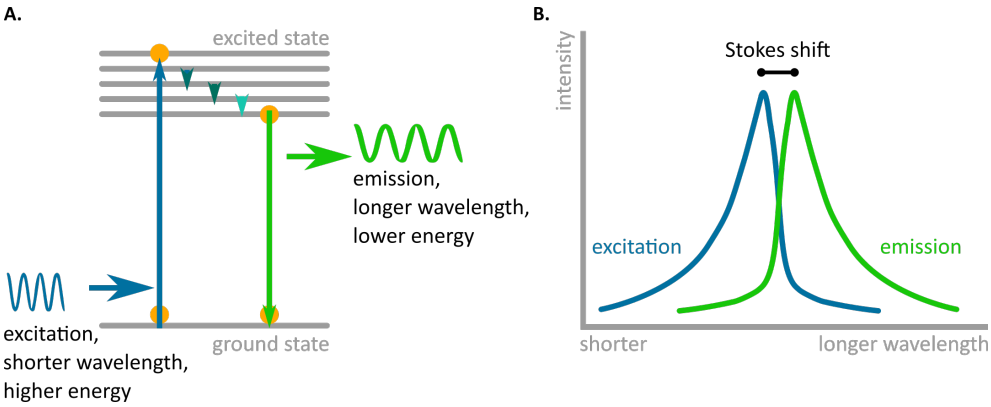


**Figure 2.21:** Principles of fluorescence. A) Jablonski diagram showing the different energy levels of the fluorophors' electrons excited via e.g. laser energy. After excitation with light of a specific wavelength the electron (yellow) changes to the unstable excited state (blue arrow). It changes back to ground state rapidly, emitting a photon with a longer wavelength due to its lower energy (green arrow). B) Schematics of an excitation and emission spectrum. The Stokes shift is the wavelength shift from excitation to emission wavelength.

fluorescent molecules change their energetic level to one with a higher energy. However, this excited state is less stable and of very short duration. The electron rapidly changes back to normal energy state emitting a fraction of

energy as heat. The remaining energy is emitted as a photon with a longer wavelength than the excitation light because of the lower energy amount (see Figure 2.21 A). This energy difference from excitation to emission is called "Stokes shift" and results in a wavelength shift (see Figure 2.21 B).[126]

### 2.3.2 Analysing neuronal activity with calcium imaging

Calcium ions play an important role as messenger molecules in various cellular signalling cascades, e.g. in regulation of cell cycle aspects or contraction of heart muscle cells.[113,46]

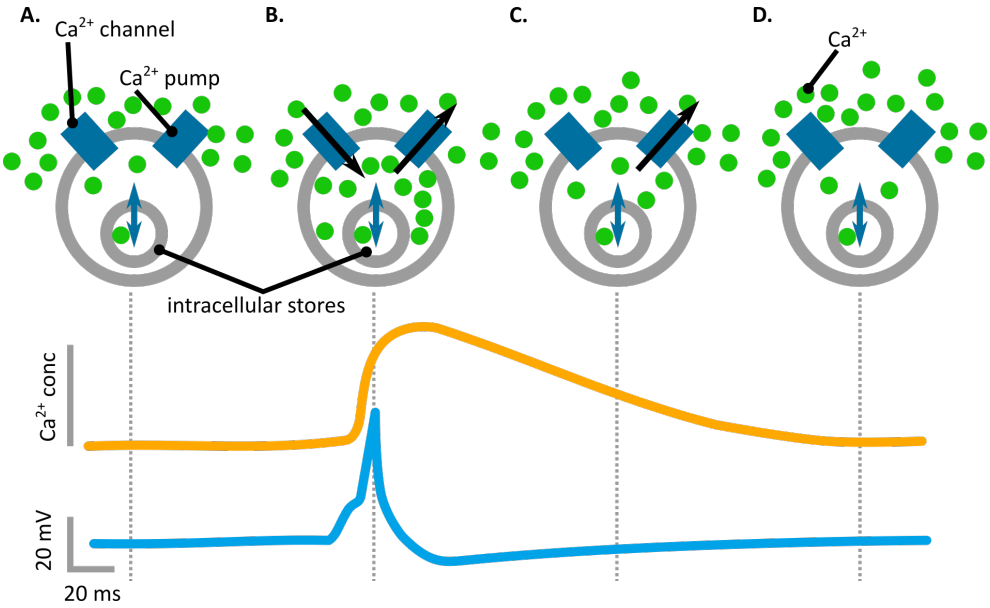


**Figure 2.22:** Calcium ions and neuronal activity. Top: Schematic image of a neuron and calcium channels, pumps and ions. Middle: Intracellular $Ca^{2+}$ concentration over time. Bottom: Corresponding AP and voltage over time. A) At rest the intracellular $Ca^{2+}$ concentration is lower compared to the extracellular space. B) Upon neuronal activity - an AP - internal $Ca^{2+}$ concentration rises because of ion influx into the cytosol through $Ca^{2+}$ channels. C) $Ca^{2+}$ pumps and the internal stores slowly restore the internal $Ca^{2+}$ concentration back to resting state. Image modified from Castanares et al..[25]

One function of ($Ca^{2+}$) ions was mentioned earlier in this chapter: $Ca^{2+}$ influx into the presynaptic terminal triggers neurotransmitter release. In mammal neurons the intracellular calcium concentration at rest is around 50 - 100 nM. Upon neuronal activity, $Ca^{2+}$ ions from the extracellular space or internal $Ca^{2+}$ storage organelles, like the endoplasmic reticulum (ER) or mitochondria, rise the concentration up to values of 10 to 100 times higher than the resting concentration (see Figure 2.22, AP in blue, intracellular $Ca^{2+}$ in yellow).[13,62] Additionally, multiple intracellular $Ca^{2+}$ binding proteins as e.g. parvalbumin act as buffers, also playing an important role in calcium signalling since only free $Ca^{2+}$ ions are active messenger molecules.[132]
This connection of neuronal signalling and the internal $Ca^{2+}$ concentration can be used as an indirect marker for neuronal activity (Figure 2.22). Thus, visualising $Ca^{2+}$ and improving methods became an early goal of various scientists.

## Calcium indicators

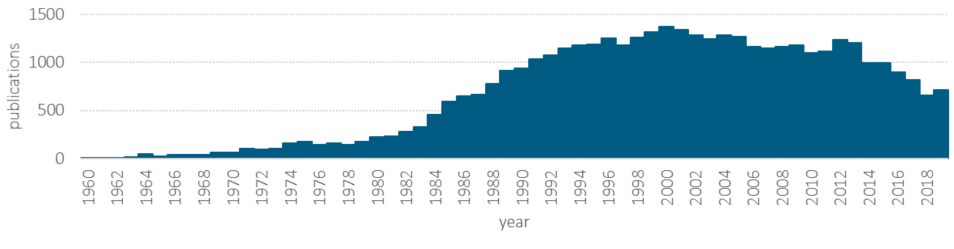


**Figure 2.23:** Publications on "calcium indicators" and "calcium sensors". From Pubmed, February 2019.

In the last decades, popularity of $Ca^{2+}$ sensors increased as can be seen by the increase in publications in Figure 2.23. One of the first reported $Ca^{2+}$ sensors was aequorin, a bioluminescent $Ca^{2+}$-binding protein.[62] In the 60ties, aequorin was firstly purified from the jellyfish *Aequorea* and injected directly into the cells. The technical challenging procedure paired with a relatively low signal-to-noise ratio (SNR) limited the usage of aequorin.[94] Another early

type of $Ca^{2+}$ indicator was arsenazo III, a synthetic compound that changes its absorbance spectrum upon changing intracellular $Ca^{2+}$ concentration.[21,62] These first indicators gave important insights into $Ca^{2+}$ dynamics in neuronal activity, but suffered from limited usability.[62]
The next leap of $Ca^{2+}$ indicators was published by Tsien in 1980, where an easier to use small-molecule indicator was described. They linked $Ca^{2+}$ chelators like BAPTA and EGTA to fluorescent chromophores. The result was a generation of highly calcium-selective indicators: fura-2, fluo-3, indo-1 and others.[149,63] The sensor was linked to acetoxymethylated esters, that enabled a non-invasive dye loading. Because of this feasibility some of the dyes became widely used in the neuroscience community.[94,62] Further development and research contributed to a large $Ca^{2+}$ dye family over the years with Oregon Green BAPTA, fluo-4 and other sensors with improved characteristics like binding affinity or SNR.
The introduction of genetically encoded calcium indicator (GECI) proteins like cameleon followed, with Foerster resonance energy transfer (FRET) based sensors consisting of two fluorophores. For these indicators, two fluorescent proteins were fused to the $Ca^{2+}$ binding domain consisting of calmodulin (CaM) and CaM-interacting peptide M13 from myosin light chain kinase.[99,118] From now on genetically targeted expression of $Ca^{2+}$ sensors to specific cell types offered even more opportunities for neuroscience. Other benefits like the non-invasive character of the GECIs enabled imaging over long and chronic time scales.[26] Further research led to improvements of sensors or introduction of single fluorophor GECIs like GCaMP.[105,118,26]

**GCaMP** One widely used single fluorophore GECI is GCaMP.[105]
GCaMP consists of the calcium-binding protein calmodulin (CaM) and CaM-interacting peptide M13 from myosin light chain kinase and a circularly permuted green fluorescent protein (cpGFP). Upon $Ca^{2+}$ binding to the CaM-M13 complex, the protein changes its conformation resulting in an increased brightness of the fluorophore.[26] The first GCaMP was introduced by Nakai et al. in 2001 (Figure 2.24a).[105] From here on several mutations have been

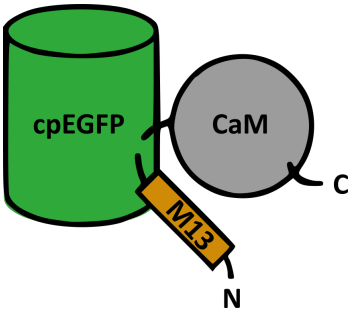


**(a)** GCaMP.

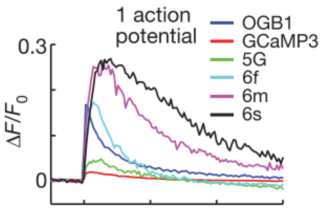


**(b)** Different calcium dyes and GECIs.

**Figure 2.24:** GCaMP6f. (a) GCaMP. Figure modified from Nakai et al..[105] (b) Comparison of different calcium dyes and GECIs. Figure from Chen et al.[26]

introduced at multiple sites to increase the SNR and improve the sensitivity and kinetics of the GCaMP indicators (GCaMP3, GCaMP5).

In 2013 a new family of GCaMP sensors was reported: GCaMP6. Chen et al. introduced various mutations and presented GCaMP6 sensors with faster kinetics as well as an improvement in the SNR (Figure 2.24b).[26] Mutations at the CaM-M13 interface aimed to improve calcium affinity, while mutations between the cpGFP and CaM increased sensitivity. As depicted in Figure 2.24b, the calcium transients recorded by GCaMP6f, 6s and 6m are characterised by different amplitudes and decay times. While GCaMP6s shows the greatest amplitude, GCaMP6f is characterised by the fastest rise and shortest decay time. The fast GCaMP6f is even able to detect single AP.[26]

Now the trend is moving further to develop red-shifted GCaMPs and other GECIs to perform in tissue imaging.[81]

### Gene delivery methods

Genetically encoded indicators can be genetically targeted to defined cells and even specific locations within cells. The SNR of a GECI highly depends on the expression level within the cell. An expression level too high might lead to an extreme buffering effect, interact within important cellular pathways and result in a cytotoxic effect. On the other hand, in cultures with a rather low

expression level higher laser power or longer exposure times are required for imaging, resulting in a phototoxic effect and reduced imaging speed. Thus, a balanced expression is beneficial for imaging neuronal cultures efficiently.[20] Viral and non-viral gene delivery methods are available to introduce DNA into cells. The non-viral - chemical and physical - methods usually take naked DNA and introduce it via physical forces (e.g. by using an electric field to alter the cell membrane's permeability) or chemical carrier compounds into the cell.[93,42] However, gene delivery efficiency of non-viral methods is low and stressful to primary cells.[42] Viral mediated gene delivery methods are reported to be beneficial because of their minimally invasive character. For viral gene delivery, the DNA of interest is packed into the genetic code of the virus, substituting some of the viral genome. Viruses like lentivirus, adenovirus, herpes herpes simplex virus (HSV), and adeno-associated virus (AAV) are widely used.[131] The use of different virus types has advantages and disadvantages. However, for gene delivery in neurons the advantages of the AAV outperform the other virus types. Adenovirus and HSV induce a high immune response and only allow transient expression and thus, are not suitable for an expression in non dividing cells such as neurons. Lentiviruses show a high risk of insertional mutagenesis. The AAV is known to be non pathogenic and to induce a low immune response. The virus infects dividing as well as non dividing cells such as neurons. Additionally, the gene expression is reported to persist for a longer time.[27] Therefore, AAV is a widely used method to insert genes into neurons.

**Adeno-associated virus - AAV** AAVs are very popular vehicles used to introduce foreign DNA. The small sized (25 nm), non-enveloped virus contains a single-stranded DNA (ssDNA) genome of approximately 5 kb and was discovered in 1965.[10] Figure 2.25 shows the model of an AAV2 capsid with its fivefold symmetry. The pore in the middle is believed to be the opening for DNA entry.[131,159] Different AAV serotypes were discovered so far with AAV2 being the best studied.[131] Differences in receptor binding affinity, cell entry and DNA uncoating influence tissue tropism *in vivo* between the

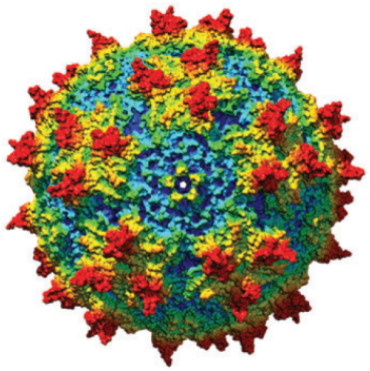

**Figure 2.25:** Model of an AAV2 capsid. The heat map colouring indicates the distance of the surface amino acids from the capsid centre with blue representing the nearest and red the farthest distance. Figure from Samulski and Muzyczka.[131]

serotypes.[70,131] Usage of recombinant adeno-associated viruses (rAAVs) in laboratories is considered feasible. One reason is, that the virus is stable to short heat, high pH and enzyme exposures. Another reason is the aspect of the rather safe handling: AAVs are unable to spread without the presence of helper viruses which provides a safety feature. Additionally, more than 70 % of humans are seropositive for at least one subtype of AAV, but no disease has been associated with the small virus yet.[24,23,131]

The wild-type viral DNA is flanked by inverted terminal repeats (ITRs) that serve as primer for second-strand synthesis.[36] Two open reading frames (ORF) - *rep* and *cap* - encode proteins for the viral life cycle and capsid proteins. Only the ITRs are necessary to produce a functioning rAAV vector and target genetic expression within a cell. Additionally the target vectors should include a promoter, an enhancer and splice signals to ensure a correct and efficient gene expression.[131]

Once the rAAVs are produced, cultures or cells can be transduced with the virus. The mechanism of cell entry and trafficking is relatively well understood: Virus particles bind to cellular surface receptors like integrin and to surface sugars on proteoglycans like galactose. This binding then promotes endosomal uptake. After infection virus particles accumulate close to the nucleus. Phospholipase activity and nuclear localisation signals allow the capsid to enter the nucleus and uncoat its DNA. The uncoating is followed by the synthesis of the second DNA strand. This part is reported to be the

rate-limiting step in AAV-mediated gene expression *in vivo*.[131] Researchers have shown that most likely the rAAV DNA persists in cells as episomes. Only a small fraction is integrated into the cellular DNA.[131]

### 2.3.3 Analysing neuronal activity with electrical recordings

Neurons and the conduction of signals within neurons was studied extensively in the 20th century. Discoveries of the electrical and chemical nature of signal transmission were made. Alan Hodgkin and Andrew Huxley made a huge contribution to the basic knowledge of the nature of an AP in the 1950ies. To come around the small size of neurons in the range of µm they studied the giant squid axon which has a diameter up to 1 mm. They utilized an innovative tool at that time, the voltage clamp. With setting the potential of a membrane they were able to investigate the contribution of different ions to the change in membrane potential during an AP. Their discoveries were rewarded with a Nobel Prize in Physiology or Medicine in 1963.[67,133]

In the late 1970ies and early 1980ies Erwin Neher and Bert Sakmann invented the patch clamp technique, a method that can be used to study the function of single ion channels from the smallest cells. An electrode inside a micropipette filled with electrolyte solution is brought to contact with a cell membrane and provides access to the inside of the cell. The close membrane contact leads to a sealing, the "gigaseal", which removes most of the background noise and thus, results in good electrical coupling and high resolution. The two German cell physiologists were awarded with the Nobel Prize in Physiology or Medicine for 1991.[108,142,79,133]

Ever since this Nobel-prized discovery, neuronal activity was analysed intracellularly with the patch clamp technique (see Figure 2.26a) by various groups. Researchers were able to reveal the underlying current and ion flows associated with the AP.

However, with patch clamp only few neurons can be analysed simultaneously. For some research questions the activity of multiple neurons in a network is

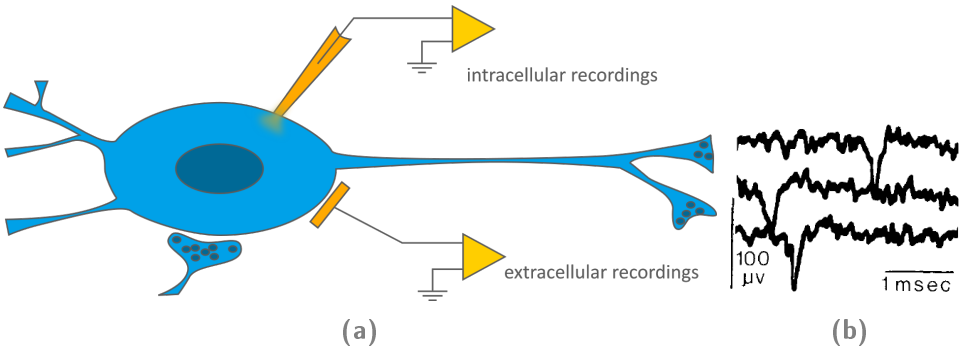


**Figure 2.26:** Electrical recording techniques. (a) Intracellular patch clamp method (top) and extracellular recording methods, like they are performed with MEAs (bottom). Image adapted and modified from Spira and Hai.[142] (b) First reported extracellular recordings of cultured neurons. Image from Pine.[120]

of central interest. Additionally, information about long term behaviour is desired. Thus, non-invasive methods are needed.

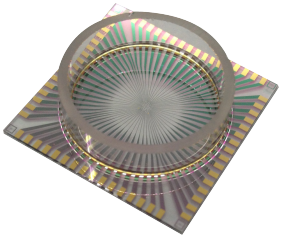

**Figure 2.27:** MEA.

The development of MEAs combined these requirements resulting in a powerful technique for neuroscience.[83] First extracellular electrical recordings of cultured cells were reported by Thomas et al. in 1972. Using a 30-electrode MEA the group was able to record APs from cultured chick heart cells.[146] The first successful extracellular recordings from neuronal cells were reported in 1980 by Pine (depicted in Figure 2.26). He cultured dissociated neurons on a array of 8 x 10 µm platinum black electrodes.[120]

MEAs are produced with standard photolithographic cleanroom technologies, details about the several fabrication steps are described in section 3.6. Figure 2.27 illustrates a substrate-integrated standard MEA used in the ICS-8 institute. MEAs provide the possibility to measure all electrodes, in our case up to 64 electrodes, simultaneously, and non-invasively, allowing a high spatial and temporal resolution of the network's electrical activity. Therefore, MEAs are the method of choice to record neuronal activity over a longer period. Cells grow directly on the electrodes and thus, are in close contact

with these. For cultured cells the extracellular electrical recording can be explained using the electrical circuit model in Figure 2.28.

The model has three components: the neuronal cell, the electrode and the cleft between neuron and electrode. The neuronal membrane is classified into a junctional membrane part that is in close contact with the electrode and a non-junctional part. The cleft at the interface of neuron and electrode is considered as a sealing resistance $R_{seal}$. An AP induces a current flow within the cleft that modulates the voltage over $R_{seal}$, changing the charge dispersal across the electrode. This change in charge can be recorded by the electrode.[142]

**Nanocavity MEAs:** Although MEAs show several positive aspects (e.g. the non-invasiveness, the possibility to perform simultaneous recordings with multiple electrodes, and the enabled high temporal- and spatial resolution),

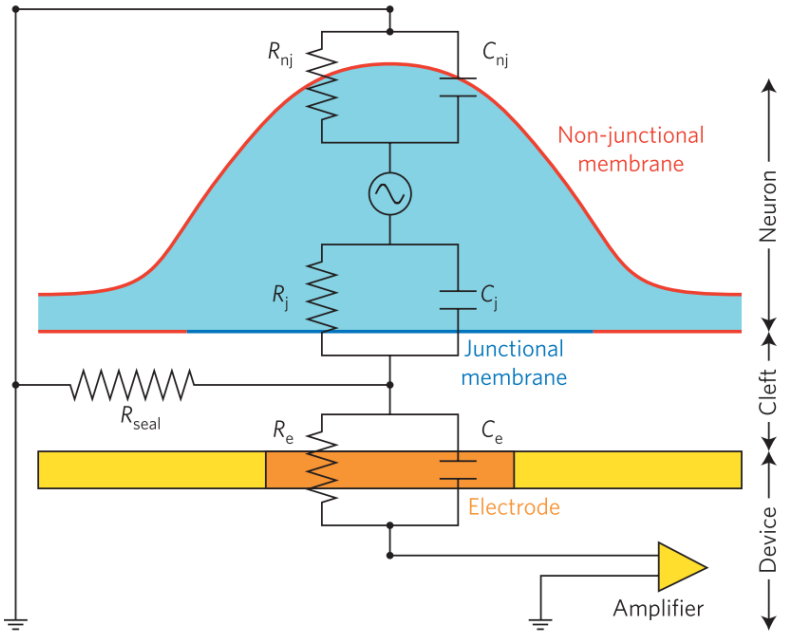


**Figure 2.28:** Schematics showing the electrical circuit model of a cell on a MEA. Image from Spira and Hai.[142]

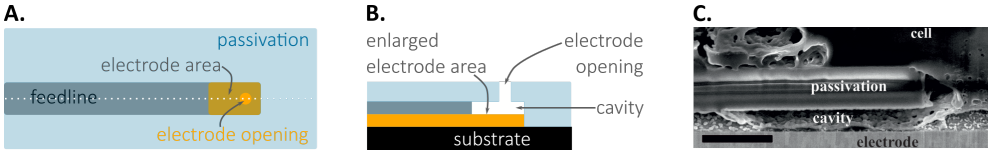


**Figure 2.29:** Nanocavity MEA. A) Schematical top view onto a nanocavity sensor with a small electrode opening and an enlarged electrode area underneath the passivation. Dashed white line indicates the cross section depicted in B. B) Schematics of a cross section of a nanocavity sensor. C) SEM picture of a cross section of a nanocavity sensor with a cell. The cell protrudes into the cleft between the electrode and passivation. Scale bar 1 µm. Image from Czeschik et al.[33]

one drawback of planar MEAs is their low SNR. This is due to the extracellular recording approach and the resulting relatively low sealing resistance between the cell and the electrode. To overcome this drawback a special type of MEA was designed in our institute - a MEA with a small cavity as depicted in Figure 2.29.

The nanocavity MEA (ncMEA) combines a small aperture with an enlarged electrode area and a nano sized cavity. Such ncMEAs allow recordings at a SNR far superior to the ratios observed in planar MEAs due to the increased electrode area. Additionally, cells were observed to protrude into the cleft between the sensor and the passivation (Figure 2.29.C) which result in a probably better sealing between cell and electrode.[69,32,33] Furthermore, the small electrode opening allows for single cell addressability.

# Chapter 3

# Materials and methods

The aim of this study was to develop engineered neuronal networks that mimic the cellular connectivity observed inside the brain and analyse the activity of these networks with electrical and optical methods. This thesis focuses in particular on the level of single cell and regional connectivity. Several methods are used in the neuroscience community to shape neuronal connectivity. These include microfluidic chambers, nano- or microtopographic substrates and micro patterned substrates.[96] Here, microcontact printing was chosen to create neuronal networks with specific connectivity. In case of the single cell networks the aim was to control soma position as well as to guide neuronal polarisation. To create population connectivity differently sized triangles were chosen to impact the neuronal population size and structural directionality. These different neuronal networks were then analysed with immunofluorescence to reveal the morphological properties of the neuronal network connectivity. Afterwards, neuronal activity was investigated using two powerful methods: Calcium imaging and extracellular electrical recordings. This chapter provides information about all methods used for the experiments of this thesis.

## 3.1 Sample preparation

To be able to investigate electrically active neuronal networks, culturing periods of several weeks are required. This necessitates substrates that remain stable over this period of time, the prevention of bacterial or fungal contamination, as well as stable protein coating to promote and maintain cellular adhesion. Additionally, the employed substrates should shape the structure of the neuronal networks. The preparation of such substrates is described in this section.

### 3.1.1 Microcontact printing

The technique of microcontact printing is used to shape neuronal networks in 2D. This method utilizes a structured microstamp to transfer cell-adhesive proteins onto a substrate. By choosing different stamp designs, it is possible to control several parameters of the neuronal connectivity on single cell and network level, such as soma position or neurite outgrowth.

#### Stamp design

By defining different geometrical patterns, various attributes of neuronal polarity can be controlled. In this study different pattern designs were analysed with respect to their ability to control the polarity of neuronal networks. Some were designed to create a directional connectivity on the single cell level, others for defining population connectivity. An additional aim was to bridge single cell connectivity and population connectivity, which enables the investigation of the effect of different population sizes onto network morphology and activity.

All stamp designs were adjusted to standard MEA layouts used in the institute.

### Influencing single cell connectivity

**Soma positioning with the Xgrid pattern** To control the soma position of neuronal cells in a network, nodes with a diameter of 12 µm and a spacing of 200 µm between the centres connected by 4 µm thin horizontal, vertical, and diagonal lines were used (Figure 3.1).

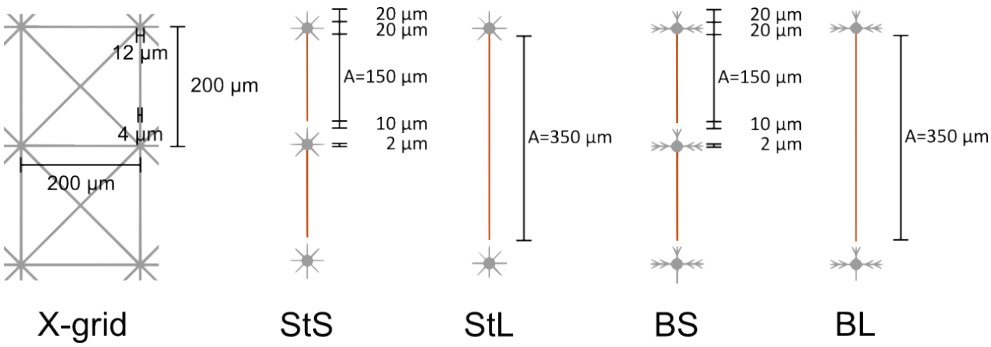


**Figure 3.1:** Stamp design and dimensions to create single cell connectivity. X Grid pattern suppose to control soma position on the nodes. Asymmetrical star patterns suppose to create a directionality in single cell connectivity. Shooting stars with a short (StS) and a long line (StL) and branched stars with short (BS) and long lines (BL) were designed to control a directional axon outgrowth along the A line in red.

**Neuronal polarisation with the star shaped pattern** As mentioned in chapter 2, neurite outgrowth commences immediately after adherence of the neuron to the substrate and after approximately 3 days in vitro (DIV) the neuron polarizes.

The pattern designs are depicted in Figure 3.1 and aim to influence neuronal polarisation. The pattern consists of a node with a diameter of 20 µm for the cell soma and 2 µm thin lines for the neurites. Here, the longer line is designed to promote neurite elongation and promote polarisation into an axon. Two different lengths were chosen: 150 µm (StS, BS) and 350 µm (StL, BL).

The other 7 shorter lines of the shooting star patterns (St) have a length of 20 µm.

In case of the branched patterns (BS and BL), additional lateral lines of 20 µm length are added to provide branching possibilities and promote dendritic development. These additional lateral lines are arranged at an angle of 45°to the main dendritic lines.

### Influencing population connectivity

In previous studies, Albers et al. analysed several triangular pattern designs and their influence on neuronal network directionality. It was shown that a triangular structure with concave sides and a straight bottom part (circles with a radius of r = 900 µm subtracted from a triangle with a height of h = 650 µm and a width of w = 550 µm) arranged in a daisy chain pattern introduced a preferred unidirectional morphology and functionality to these neuronal networks.[4,3] This observation motivated the structure design for population connectivity of this thesis, with the aim to analyse whether this effect is also present for smaller network sizes.

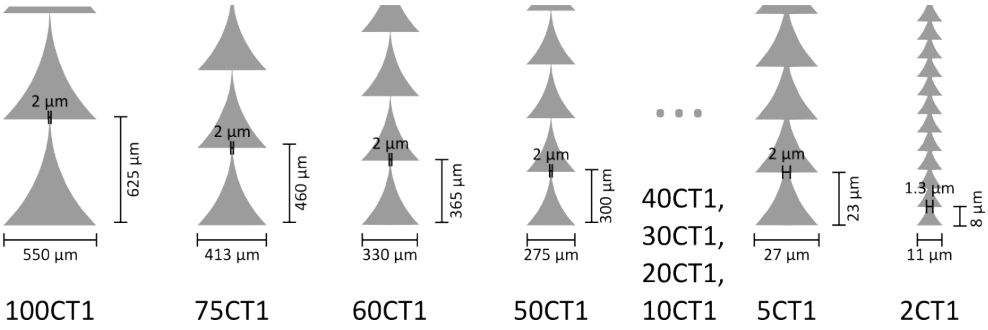


**Figure 3.2:** Stamp design and dimensions of the dsCT1 patterns. The original CT1 structure was adapted from Albers et al. and downscaled to several sizes.

Figure 3.2 and Table 3.1 summarise the dimensions of all dsCT1 structures used in this study. The original CT1 structure (Figure 3.2) was scaled (downscaled CT1, dsCT1) in several steps, in detail: 100 %, 75 %, 60 %, 50 %, 40 %, 30 %, 20 %, 10 %, 5 % and 2% (from here on referred to as 100CT1, 75CT1, ... 2CT1). To ensure a consistency in the gateway, the tip size touching the downstream triangle was set to 2 µm for the 100CT1 - 5CT1

**Table 3.1:** Dimensions of dsCT1 patterns.

| Structure | height [µm] | width [µm] | gateway [µm] |
|---|---|---|---|
| 100CT1 | 625 | 550 | 2 |
| 75CT1 | 460 | 415 | 2 |
| 60CT1 | 365 | 330 | 2 |
| 50CT1 | 300 | 275 | 2 |
| 40CT1 | 235 | 220 | 2 |
| 30CT1 | 170 | 165 | 2 |
| 20CT1 | 110 | 110 | 2 |
| 10CT1 | 52 | 55 | 2 |
| 5CT1 | 23 | 27 | 2 |
| 2CT1 | 8 | 11 | 1.4 |

and 1.3 µm for the 2CT1 structures.

**Mold production** The masters for the microstamps were fabricated in the Helmholtz Nanoelectronic Facility Jülich (HNF) following previously described protocols.[4,112]

The fabrication steps are schematically shown in Figure 3.3. Briefly, the designed structures were first written into a 5 inch dark-field chromium mask with an electron-beam writer (Visitec EBPG 5000plus HS, Vistec Electron Beam GmbH). A 1.4 µm thick layer of a positive photoresist (AZ® 5214E) was spin coated onto a 4 inch silicon wafer followed by a one minute pre-bake at 110 °C to remove any solvent residues (Figure 3.3.A, B). The resist was then illuminated with UV through the chromium mask (23 s, 75 mJ/cm$^2$, MA Suess), upon which exposed resist areas undergo a photochemical reaction becoming soluble to the developer (MIF 326, Michrochemicals) as depicted in Figure 3.3.C and D. Thus, in the next development step, the exposed areas are removed (Figure 3.3.E). The process is stopped with MilliQ water and the wafer is subsequently hard-baked at 130 °C for 5 min to remove the wa-

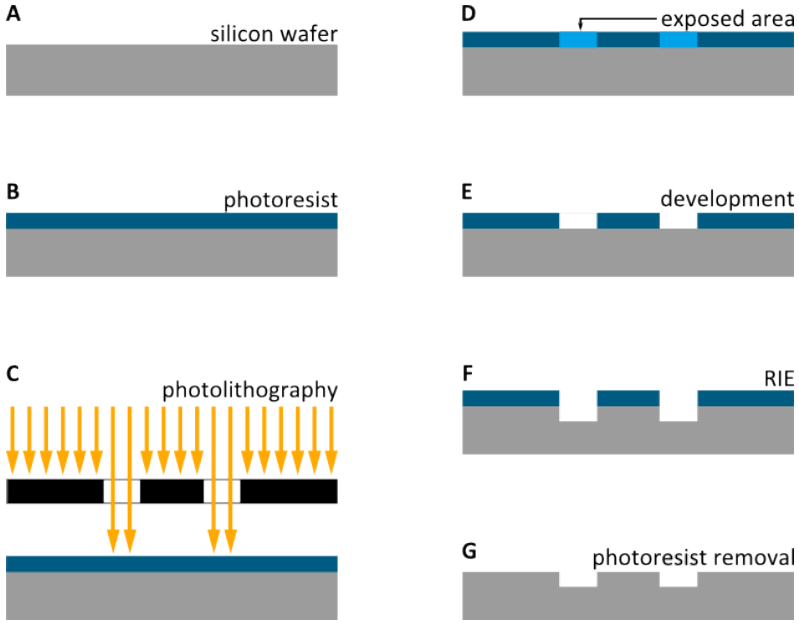


**Figure 3.3:** Mold fabrication. A. Silicon wafers are used as substrate for the mould fabrication. B. A positive photoresist is spin coated onto the wafer and C. the pattern is transferred into the resist via photolithography. D. Exposed areas undergo a photochemical reaction and become soluble and are thus removed in the development step (E). F. The structure features are etched into the Si via reactive ion etching followed by photoresist removal (G).

ter. In the final step depicted in Figure 3.3.F, the structures are etched 5 µm deep into the Si with $SF_6$ at -100 °C via reactive ion etching (RIE)(Oxford Instruments, Abingdon, U.K.). Afterwards, the resist was removed by acetone and isopropanol (Figure 3.3.G). Finally, the structured wafer was chemically modified by vapour deposition of 1H,1H,2H,2H-Perfluorooctyl-trichlorosilane (FOTCS, Alfa Aesar) in an argon atmosphere at 45 mbar for 1.5 hours for anti-sticking properties.

**Stamp production** Microstamps were fabricated of either polydimethylsiloxane (PDMS) or polyolefin plastomer (POP).
PDMS stamp fabrication is displayed in Figure 3.4.D to F. PDMS (Sylgard®184 Silicone Elastomer Kit, Dow Corning) is a two component siloxane which shows a high softness if used in the standard 1:10 ratio of curing

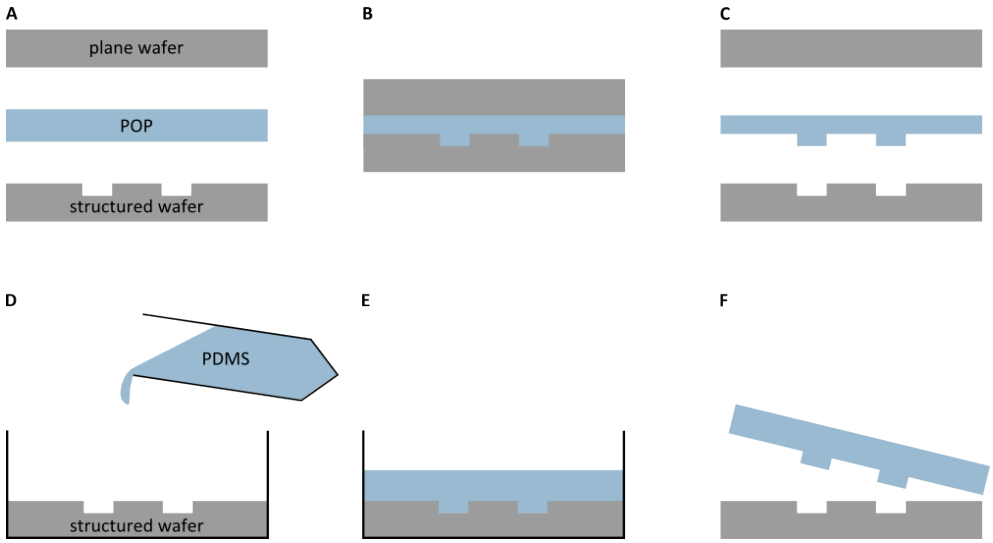


**Figure 3.4:** Casting of the microstamps. Different fabrication steps are required for Polydimethylsiloxane (PDMS, A-C) and Polyolefin plastomer stamps (POP, D-F). A) 1:10 PDMS (curing agent to siloxane) is poured onto the FOTCS-modified mould. After baking at 60 °C over night (B) the cross-linked PDMS block can be carefully removed from the wafer(C). D) For POP stamps a POP block is placed between a plane and the structured wafer, both FOTCS-modified. E) Moulding is performed under heat and pressure (90 °C, 60 psi). F) After cooling down the mould can be released from both wafers.

agent to siloxane.[31]

This softness results in a nice contact between stamp surface and structure but might also result in sagging effects (Figure 3.5.A and B) depending on the aspect ratio of the structure features to structure-free area. For PDMS stamps, a mixture of approximately 30 ml 1:10 curing agent to PDMS is poured onto the FOTCS-modified wafer and cured over night at 60 °C. The PDMS cast is then carefully removed from the mould. For PDMS stamps used in combination with microelectrode arrays, a glass coverslip was additionally glued onto the unstructured part of the stamp to ensure a plane surface.

In contrast, POP shows stiffer properties, therefore application of slight pressure is needed to ensure a sufficient contact between the stamp and the substrate. Sagging effects are rare and the protein transfer in general is more

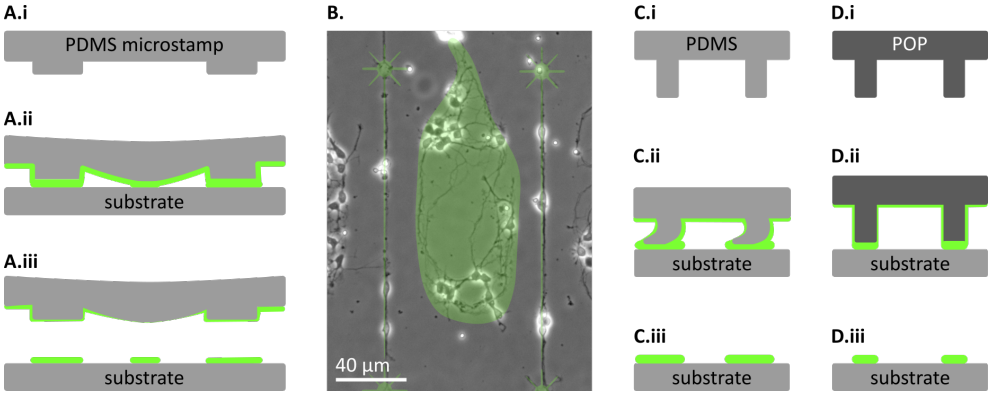


**Figure 3.5:** Possible deformations of PDMS microstructures. A) Schematics of a sagging effect. An unsuitable aspect ratio of the microstamp structures (A.i) can result in a sagging effect (A.ii) and an undesired protein transfer in the area between the structures (A.iii). B) Example photograph of a substrate with sagging effect. Neuronal cells at 3 DIV. C) Elastic PDMS stamps are prone to application errors, especially if the stamp exhibits very thin structure features. D) For some very thin stamp features, the stiffer POP stamps are more suitable and µCP results in a more accurate protein transfer.

accurate (see Figure 3.5.C and D).

POP stamp fabrication is schematically shown in Figure 3.4.A to C. POP stamps are fabricated by a hot embossing process. Briefly, a POP block (Affinity VP 8770G1 Polyolefin Plastomer, Dow, Michigan, USA) is placed between a structured and a plain silicon wafer, both modified with FOTCS for anti-sticking properties. The temperature is then increased to 90 °C and pressure is set to 60 psi for 5 min. After cooling down to 30 °C the POP cast can be removed from the wafers with isopropanol. Individual stamps are cut out resulting in 1 x 1 cm micro stamps.

### Patterning substrates

For this study, different substrates with different surface chemistries were used: substrates like coverslips, ibidi culture dishes with a glass bottom, and microelectrode arrays (MEAs) with a polyimide surface. Different substrates need different cleaning procedures and cell-adhesive coatings. Therefore,

the patterning protocols described in this section vary from substrate to substrate.
Prior to microcontact printing, substrates and stamps need to be cleaned to remove any organic or anorganic contaminants.

**Stamp cleaning** Micro stamps were cleaned in 70% ethanol (Merck) in an ultrasound bath for 15 min followed by rinsing with MilliQ water to remove ethanol residues.

**Substrate cleaning** Glass coverslips (VWR) with a diameter of 18 mm were cleaned in 70% ethanol in an ultrasonic bath for 15 min, rinsed with MilliQ water, dried with either nitrogen gas or at 60 °C in an oven and subsequently sterilised via UV irradiation for 1 h.
MEAs were first cleaned with 70% ethanol in ultrasonic bath for 5 min followed by a washing with MilliQ water and sterilisation with UV illumination for 1 h.

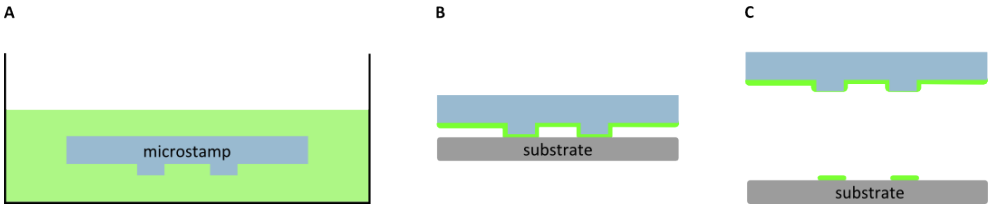


**Figure 3.6:** Microcontact Printing. A) Clean microstamps are inked in a protein solution (green) for 20 min on ice. B) Stamps are then dried with nitrogen gas and placed onto the substrates. PDMS stamps are left on the substrate for 20 min, POP stamps are pressed with a slight pressure onto the substrates for 2 min. C) Subsequently, the microstamps are removed and the patterned substrate is stored until cell seeding.

**Stamp inking and protein solutions** Cleaned stamps were dried with $N_2$, transferred into a protein solution, and incubated on ice for 20 min (see Figure 3.6.A). The different protein solutions employed for µCP on different substrates are summarized in Table 3.2.

**Table 3.2:** Protein solutions employed for µCP on different substrates in later stage of this thesis.

| Substrate | Mixture | Ratio |
|---|---|---|
| Glass coverslip | HBSS, PLL, ECM | 100:1:1 |
| Ibidi dish | HBSS, PLL, ECM | 100:1:1 |
| MEA with PI passivation | HBSS, PLL, ECM, gelatine | 100:1:1:2 |

For patterning glass substrates, a protein solution consisting of Poly-L-Lysine (Sigma-Aldrich, 1 mg/ml) and laminin (Sigma-Aldrich, 1-2 mg/ml) in Hank's Balanced Salt Solution (HBSS, Sigma-Aldrich) in a 1:0.5:100 ratio was used. During the studies the microcontact printing process showed some inhomogeneity in reproducibility, most likely due to different surface properties of different lots of coverslips. Therefore, the process was adapted multiple times. For later experiments, extracellular matrix protein (ECM) (ECM Gel from Engelbreth-Holm-Swarm murine sarcoma, Sigma-Aldrich, 1 - 2 mg/ml) was used instead of laminin to ensure a homogeneous protein transfer.
For MEA substrates with a polyimide a protein solution that is more sticky was employed for µCP. The protein solution used for pattering MEAs consisted of gelatine, PLL, and ECM in HBSS in a 2:1:1:100 ratio. For later experiments, a protein solution without gelatine was employed to reduce the distance between the electrodes and the cells.
To visualize the transferred protein pattern FITC-labelled PLL was used (PLL-FITC, Sigma-Aldrich) in the same concentration as the unlabelled PLL for some cultures.

**Protein transfer** After the inking step, stamps were dried with $N_2$ and placed onto the substrates as depicted in Figure 3.6.B. To ensure a tight contact between the POP stamp and the substrate and thus, a homogeneous protein transfer, slight pressure was applied with the finger onto the stamp for 2 min.

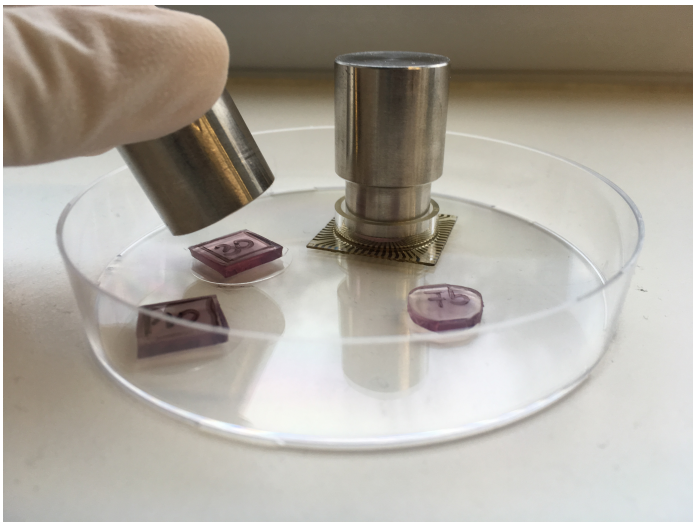

**Figure 3.7:** µCP with POP stamps and weights.

During the reported studies, an optimised protocol for microcontact printing including the usage of stainless steel weights (2 cm diameter, 3 cm height, 75 g) instead of applying pressure with a finger was implemented to ensure a better reproducibility. The microcontact printing procedure with weights is shown in the photograph in Figure 3.7.

PDMS stamps are placed onto the substrates, no additional pressure is needed to ensure a tight contact. Stamps are removed after 20 min.

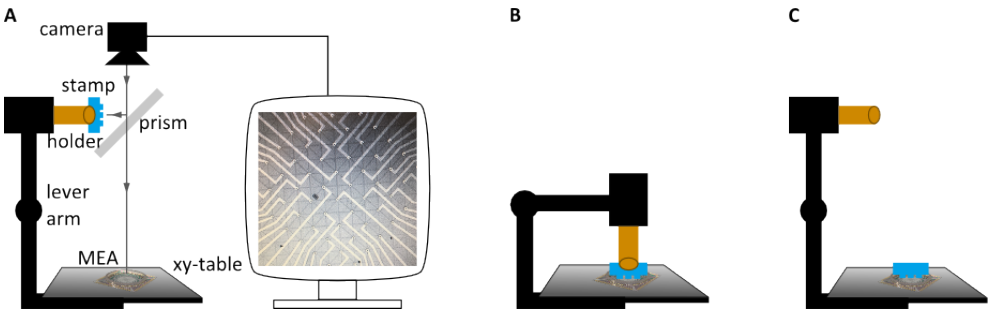


**Figure 3.8:** Aligned microcontact printing via fineplacer. A) The stamp is attached to the holder. Chip and stamp are aligned. B) The stamp is positioned on the MEA. C) The stamp is released. Adapted from Hofmann et al.[69]

**Aligned microcontact printing** Microcontact printing on MEAs is performed with a Fineplacer® lambda (Finetech) to ensure alignment of the protein pattern to the single electrode openings, resulting in a precise protein transfer along the MEA design (Figure 3.8).
The fineplacer is a device used to align two surfaces with respect to each other. The inked and dried microstamp is attached to the holder of the fineplacer via vacuum and the chip is placed onto the xy-table. The overlap of both planes is monitored on the screen and both, the chip and the stamp, are aligned via micrometer screws. Afterwards the stamp is positioned on the chip with the lever arm and, by releasing the vacuum, the stamp detaches from the holder and attaches to the chip.
Patterned substrates were stored at 4 °C for a maximum of 14 days until cell seeding.

### 3.1.2 Homogeneously coated substrates

Homogeneously coated substrates, either MEAs or coverslips, were used as controls (CTRL) to monitor the cell culture condition without any restrictions to the neurite outgrowth.
Glass coverslips (VWR) were either sterilised over an open flame or with 70% ethanol in an ultrasonic bath, rinsed with MilliQ water, and dried. Afterwards, coverslips were incubated in a 1:100 solution of PLL in HBSS (both Sigma-Aldrich) at room temperature for 1 h, washed with HBSS thrice, and stored at 4 °C until cell seeding.

## 3.2 Cell culture

For this thesis, primary embryonic rat cortical neurons were used to engineer structured neuronal networks. In order to obtain these cells, embryonic rat cortices had to be dissected and dissociated into single cells.

### 3.2.1 Preparation of neuronal cells

During the course of this thesis, the dissociation protocol was changed from a mechanical dissociation employed in the early stages of this body of work to a more gentle enzymatic dissociation procedure utilized in the later stage. Heads were obtained from E18 Wistar rat embryos of either sex and cortices were separated from the brain tissue in Hank's Balanced Salt Solution without calcium and magnesium ($HBSS^-$, Gibco).

**Mechanical dissociation protocol** Isolated cortices were transferred into 2 ml $HBSS^-$ and the tissue was first homogenized by trituration with a silanized glass pipette with a normal tip diameter followed by a pipette with a smaller tip diameter to ensure a homogeneous cell suspension. 4 ml HBSS with calcium and magnesium ($HBSS^+$) were added and after 3 minutes resting time the liquid separated into two phases. Glial cells bind to the calcium and magnesium ions and sink to the bottom while neuronal cells stay in the upper phase. The supernatant was centrifuged at 1100 rpm for two minutes at room temperature and the pellet was resuspended in 1 ml Neurobasal medium supplemented with 1% B-27 (Life Technologies), 5 mM L-glutamine (Invitrogen) and 50 µg/ml gentamycine (Sigma-Aldrich) (from here on referred to as NB). In the last step, the cells were counted and plated on the substrates.

**Enzymatic dissociation protocol** Isolated cortices were transferred into 0.05% Trypsin-EDTA (Invitrogen) and incubated for 10 minutes at 37 °C, 5% $CO^2$, and 95% humidity. During this time, the enzyme hydrolyses intercellular

protein bonds, gently separating the neurons. Cortices were then transferred into NB and washed with NB five times to remove any trypsin residues. In the last washing step, the tissue was gently triturated via an 1,000 µl Eppendorf pipette. The cell suspension was allowed to stand for one minute so that the residual tissue clumps can sink to the ground and afterwards, the supernatant was transferred into a fresh tube. Cells were counted and plated on the substrates. If the cells were not dissociated right away, cortices were stored in Hibernate® Media (Gibco) until preparation.

**Cell density** The pattern designs differ in their pattern area. Additionally, the sample area varied from substrate to substrate, e.g. 9.6 $cm^2$ for a 6 well plate and 3 $cm^2$ for a MEA. Thus, different cell densities were used for the different pattern designs as summarised in Table 3.3.

**Table 3.3:** Plated cell number for different pattern designs.

| Pattern design | pattern area [$mm^2$] | well area [$cm^2$] | medium volume [ml] | cell number |
|---|---|---|---|---|
| Xgrid | 9 | 9.6 | 2 | 100k |
| star structures | 2 - 3 | 9.6 | 2 | 100k |
| dsCT1 | 3 - 20 | 9.6 | 2 | 200k |
| homogeneous CTRLs | – | 9.6 | 2 | 200k |

**Culture maintenance** Cells were cultivated in an incubator at 37 °C, 5% $CO_2$, and 95% humidity. Half of the culture medium was exchanged every 3 - 4 days with fresh Neurobasal medium supplemented with 1% B-27 (Life Technologies), 0.5 mM GlutaMAX (Sigma-Aldrich) and 50 µg/ml gentamicin (Sigma-Aldrich). The culturing medium is referred to as "NB" in this chapter.

**Post-experimental MEA cleaning** After an experiment, the cells were enzymatically removed. The MEA surface was incubated with 0.05% Trypsin-

EDTA (Invitrogen) for at least 30 min at room temperature. Trypsin is removed and MEAs are cleaned subsequently with MilliQ water and ethanol via ultrasonication.

### 3.2.2 Immunostaining

For morphological analysis of the neuronal networks, cellular substructures were visualized with fluorescently labelled antibodies. Cells were fixed and analysed at different days in vitro (DIV). As described in chapter 2, neuronal polarisation takes place before DIV 3, therefore single cell networks were observed at DIV 3 - 4. This early stage facilitates an identification of the neurites belonging to one cell. Networks designed to guide populations of neurons were analysed at DIV 3 - 7, because neuronal connectivity is developed in later stages.[43]

**Fixation, permeabilisation and blocking of unspecific binding sites** First, samples were washed three times with prewarmed 1 x PBS (PBS) and afterwards fixed with 4% paraformaldehyde (Sigma-Aldrich) in PBS (4% PFA) for 10 minutes at room temperature. This was followed by three washing steps with PBS and permeabilisation with 0.3% Triton-X-100 (Sigma-Aldrich) in blocking buffer (PBS containing 1% bovine serum albumin (BSA, Gibco) and 2% heat-inactivated goat serum (Sigma-Aldrich)), for 10 minutes at room temperature. After three washing steps with PBS, unspecific binding sites were blocked with blocking buffer for either 1 h at room temperature or over night at 4 °C.

**Primary antibodies** Dendrites and neuronal somata were visualized via β-III-tubulin or microtubule-associated protein 2 (MAP2) antibodies at a 1:500 dilution for 2 hours at room temperature. For axon visualisation, either anti-tau (Tau) for earlier development stages (until DIV 4) or anti-neuro-filament-heavy (NFH) antibodies for more mature neurons (>DIV 4) were used as primary antibodies. Primary antibodies were diluted in blocking

buffer. Table 3.4 summarises the details of the antibodies used for these experiments.

**Table 3.4:** Primary antibodies used for morphological analysis of neuronal networks. Primary antibodies were diluted in BB. Samples were incubated in subsequent steps for 2.5 h.

| Target | 1st antibody, Anti- | Host | Manufacturer | Dilution |
|---|---|---|---|---|
| Dendrites | β3-tubulin | rabbit | Cell Signalling Technology | 1:500 |
| Dendrites | MAP-2 | rabbit | Merck Millipore | 1:300 |
| Axon | Tau-1 | mouse | Merck Millipore | 1:500 |
| Axon | Neurofilament heavy polypeptide antibody | chicken | Abcam | 1:400 |

Samples were incubated with the primary antibody solutions (one primary antibody per incubation step) in a wet and dark chamber at room temperature for 2.5 hours. Finally, samples were washed thrice with PBS.

**Secondary antibodies** After labelling the neuronal proteins with a primary antibody, an incubation with secondary, fluorescently labelled antibodies was performed for 1 h. All secondary antibodies were diluted in blocking buffer. Table 3.5 summarises the details of the antibodies used for these experiments.
DNA was stained with 4',6-diamidino-2-phenylindole (DAPI, 2.6 mg/ml, Life Technologies) at a 1:1,000 dilution for nucleus visualisation.
Simultaneous incubation of all necessary secondary antibodies was performed simultaneous in a wet and dark chamber at room temperature for 1 hour. Afterwards, coverslips were rinsed once with PBS and twice with MilliQ water. Stained samples were embedded in mounting medium (Dako) onto glass slides and finally dried at RT over night in a dark chamber.

**Table 3.5:** Secondary antibodies used for morphological analysis of neuronal networks. Antibodies were diluted in BB and samples were incubated for 1.5 h at R

| 2nd antibody | Manufacturer | Dilution |
|---|---|---|
| Alexa Fluor anti-mouse 350 | Invitrogen | 1:500 |
| Alexa Fluor anti-mouse 633 | Invitrogen | 1:500 |
| Alexa Fluor anti-chicken 488 | Invitrogen | 1:500 |
| Alexa Fluor anti-rabbit 546 | Invitrogen | 1:500 |

## 3.3 Quantification of somata and neurites

The location of somata and neurites on the patterns was evaluated and quantified.

**Image acquisition** Immunofluorescence images were acquired with a Zeiss Observer.Z1 equipped with a Colibri illumination system, a PCO edge 5.5 sCMOS camera with 2,560 x 2,160 pixels, and the Zeiss Zen 2012 Blue Edition software.

**Data analysis - Xgrid pattern** Images were analysed manually and somata were investigated with respect to their location on the single cell patterns. Results are presented in section 4.1.
Statistical analyses for hypothesis testing of soma location on pattern were performed in accordance to Corey et al.,[29] adjusted to my specific statistical questions: To test the null hypothesis $H_0$ that cellular somata distribute randomly on the pattern, probabilities were calculated under the assumption that a Bernoulli process described the probability of a cell soma located on the node of the pattern or anywhere on the pattern. If $N$ cells are considered as independent Bernoulli trials, the number of cell somata that is on the pattern is binomially distributed. This distribution is approximately normal for large $N$.

$$H_0 : p = p_0$$

The probability $p_0$ of a single soma being located on the node of the pattern equals the fractional area of the pattern occupied by the nodes.

$$p_0 = \frac{area_{node}}{area_{pattern}}$$

The overall pattern area was determined with the CleWin software. The node area was calculated by multiplying the single node area with the number of nodes in one Xgrid pattern.

The observed proportion of somata located on the nodes $\hat{p}$ is defined as the fraction of the somata located on the node of all cells on the pattern. The alternative hypothesis $H_1$ would state, that the distribution of somata is not random and that the probability of a soma being located on the node is higher than $p_0$.

$$H_1 : p > p_0$$

$H_0$ was tested with a one-sided Z-test.
Additionally, the ratio of intersection area to the overall pattern area was calculated by multiplication of the number of intersections and the single intersection area. The size of an intersection was defined as a cross consisting of two 12 µm long lines. Ratio of line area to overall pattern area was calculated by subtraction of the intersection and node area from the determined overall pattern area.
The soma adhesion area was determined by drawing a circle of 12 µm diameter around the pattern features node, intersection and line and calculating the surrounded pattern area.

**Data analysis - Star patterns** Soma position on the pattern was manually determined for morphological analysis of the star patterns in section 4.2. A null hypothesised random distribution of somata on the pattern was analysed as described in the previous paragraph. Though, the additional dendritic line area was excluded from the overall pattern area. Thus, only the vertical dimension was considered in the analysis.

**Table 3.6:** $H_0$: probabilities for soma on node for the different star patterns.

| Pattern | $p_0$ |
|---|---|
| StS | 0.51 |
| StL | 0.31 |
| BS | 0.51 |
| BL | 0.31 |

The null hypothesised values $p_0$ for the different patterns are presented in Table 3.6. $H_0$ was tested with a one-sided Z-test.
To quantify axon elongation direction, immunofluorescence images were analysed manually and cells were investigated with respect to direction of axon outgrowth.

$$\begin{aligned} H_0 &: p = p_0 \\ & \quad p_0 = 0.5 \\ H_1 &: p > p_0 \end{aligned}$$

A one-sided Z-test was used to test the $H_0$ that neurons elongate their axon randomly in the right or wrong direction. The alternative hypothesis $H_1$ would state, that the observed proportion of neurons elongating their axons into the right direction $\hat{p}$ is higher than $p_0$.
Differences between patterns were also tested with a Z-test. Here, $H_0$ would state, that there is no difference in soma position or axon elongation direction between the patterns:

$$\begin{aligned} H_0 &: p_1 = p_2 \\ & \quad p_1 - p_2 = 0 \\ H_1 &: p_1 - p_2 \neq 0 \end{aligned}$$

**Data analysis - dsCT1** Morphological characterisation of neurons on the dsCT1 patterns is presented in chapter 6. Quantification and data analysis was performed by Lanzrath and is described in detail in her Bachelor thesis.[89]

## 3.4 Live cell imaging

Analysis of neuronal cells on defined DIVs offers only snap shots at specific time points. Information about cellular development over time can be obtained by time lapse microscopy experiments, also referred to as live cell imaging. Here, live cell imaging is performed from DIV 0 - 3 to observe neuronal polarisation and development on the shooting star pattern (StS). Neurons were cultured in ibidi dishes with an embedded glass bottom.

**Image acquisition** Experiments were performed with a Zeiss Observer.Z1 equipped with a illumination system (Zeiss Colibri), a CMOS camera (PCO edge 5.5, 2,560 x 2,160 pixels), and a temperature and humidity control system (Picon). The Picon incubation chamber allows for temperature, $CO^2$, and humidity control and thus long-term observation of cultures at *in vitro* culturing conditions with a temperature of 37°C, 5% $CO^2$, and a humidity of 100 %. For imaging multiple positions, a motorised xy-table (Maerzhaeuser, Germany) was employed. An area of 6.16 mm x 7.72 mm was imaged with a pixel size of 0.650 µm x 0.650 µm per pixel. The focus was stabilised with a Zeiss Definite focus unit over time. At the beginning of the experiment a fluorescence image of the FITC labelled protein pattern was acquired with an exposure time of 500 ms at 100% light intensity of the 470 nm LED. To prevent cell damage due to light irradiation, light intensity and duration for phase contrast images were chosen as low as possible. Subsequent images were acquired with an exposure time of 50 ms at a voltage of 3.2 V every 30 min.

**Data analysis** Time lapse images were analysed with the "Manual Tracking" plug-in in Fiji (a distribution of ImageJ). Here, individual somata and neurite tip positions were marked manually in all images. Afterwards, neurite lengths were calculated as the distance from soma to neurite tip with a Matlab (MathWorks) script, where the longest neurite was considered as the axon.

# 3.5 Calcium imaging

## 3.5.1 Transduction

Neuronal activity can be monitored with intracellular calcium indicators which change their fluorescence properties upon calcium ion binding. Genetical introduction of such a calcium indicator provides several advantages to regular dye loading, e.g. the possibility of long-term recordings and neuron specificity (in detail described in chapter 2). In this study, the optogenetic sensor protein GCaMP was used to monitor spontaneous neuronal activity.

### Virus with GCaMP construct

**AAV9.Syn.GCaMP6f.WPRE.SV40** rAAVs were purchased from Penn Vector Core, Perelman School of Medicine, University of Pennsylvania.

pAAV.Syn.GCaMP6f.WPRE.SV40 was a gift from Douglas Kim & GENIE Project (Addgene plasmid 100837).[26] The main part of the construct is the codon for the GCaMP6f protein. Additional sequences are added around the main construct to ensure a correct gene expression and are described in the following paragraphs.

The whole construct was packed into an rAAV serotype 9 (AAV9), which is reported to induce neuronal transduction in the central nervous system of the rat, including cortical neurons.[75] Expression is controlled via a synapsin promoter (Syn), ensuring an expression only in neuronal cells.[75] The Woodchuck Hepatitis Virus Post-transcriptional Regulatory Element (WPRE) is added in order to enhance gene expression.[90,27] Additionally, the termination and polyadenylation signal SV40 was inserted. Polyadenylation is crucial for nuclear export, translation as well as mRNA stability. Thus, polyA signals boost gene expression by increasing the efficiency of transcript polyadenylation.[123]

#### Transduction

Transduction was performed at 7 - 10 DIV. First, the culture medium was completely exchanged with fresh neuronal medium and $3.82 \times 10^5$ gene copies per neuronal cell were added. After 3 - 4 days post transduction (DPT), the culture medium was again fully exchanged for fresh NB to remove viral particles. Afterwards, half of the culture medium was exchanged with fresh NB every 3 - 4 days.

### 3.5.2 Fluorescent image acquisition

Imaging was performed with a Zeiss Observer.Z1 equipped with a illumination system (Colibri), a CMOS camera (PCO edge 5.5, 2,560 x 2,160 pixels), and a temperature and humidity control system (Picon). To ensure natural cell conditions, imaging was performed at 37 °C, 95% humidity, and 5% $CO_2$. Samples were illuminated with an excitation wavelength of 470 nm (Zeiss Colibri Light Emitting Diode (LED)) and an intensity of 100% for 5, 10, or 20 ms depending on the fluorescence signal intensity of the recorded sample. As GCaMP6f shows a higher signal-to-noise ratio (SNR), 5 ms exposure time was sufficient and therefore images were acquired with a rate of 200 frames per second (fps). Fluorescence of the GCaMP was imaged using the 38 HE filter (excitation: BP 470/40, beam splitter: FT 495, emission: 525/50) and recording was performed with the Zeiss Zen 2012 Blue Edition software for 30 s to 5 min. A 4 x 4 binning was applied to reduce data size and increase acquisition speed, resulting in an actual pixel size of 2.6 µm/pixel, which is still sufficient for single cell and neurite resolution. Additionally, the active area of the camera sensor was reduced vertically to a size varying from 100 - 500 pixels.

#### Data analysis

The recordings resulted in 1 - 3 GB files. Image sequences were analysed offline with the Fiji (ImageJ distribution) software and custom-written Matlab

(R2019a, MathWorks) scripts.
First, circular regions of interest (ROIs) were manually set around the somata of the cell showing a fluorescence change over time. Therefore, the "ROI manager" of Fiji was employed which provides the mean pixel intensity per ROI per image.

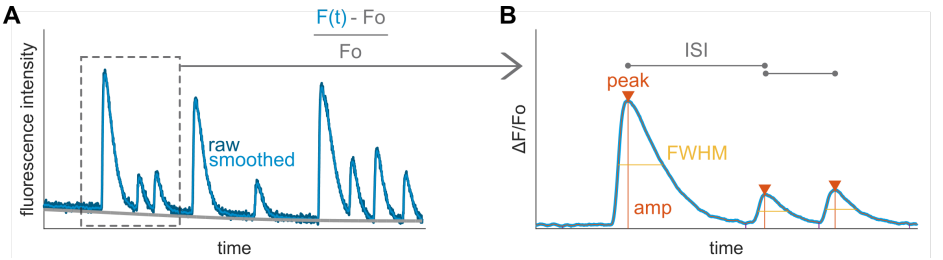


**Figure 3.9:** Processing procedure of calcium signals. A) Raw signal (dark blue) was smoothed via a moving average filter (light blue, F(t)). Baseline ($F_0$) was calculated by a moving minimum. B) $\Delta F/F_0$ was calculated. Peaks, amplitudes (amp), full width half maxima (FWHM) and interspike intervals (ISI) were identified.

Afterwards, the intensity data was analysed with a Matlab script and is schematically depicted in Figure 3.9.A. Here, the change in relative fluorescence intensity, $\Delta F/F_0$, was calculated from the raw fluorescence intensity F(t) as schematically depicted in Figure 3.9.A. For that, time traces were smoothed with the moving average function "movmean" over a sliding window of 125 ms. $F_0$ (Figure 3.9.A, grey) was obtained by processing the time trace with the moving minimum function "movmin" over a sliding window of 10 s followed by a zero-phase filtering with the "filtfilt" function for additional smoothing. $\Delta F$ was obtained from subtraction of F(t) from $F_0(t)$.
Individual transients of the time traces were detected with the "findpeaks" function. Here, individual time traces were reviewed and restriction parameters for the peak finding were adjusted manually to ensure a reliable data set. With this algorithm the transient parameters peak time (peak), amplitude (amp), and full-width at half maximum (FWHM) as displayed in Figure 3.9.B were obtained. The interval between two peaks (inter-spike interval, ISI) was calculated as the time between two adjacent peaks.

Transient parameters of different population networks (dsCT1) were examined by linear regression.
Interaction between two neurons in an imaged area was analysed by cross-correlation of their intensity sequences $\Delta F/F_0$.

## 3.6 Extracellular electrical recordings

### 3.6.1 MEA fabrication

Neuronal activity can also be analysed with microelectrode arrays (MEAs). Due to their non-invasive character, long-term monitoring of network activities can be performed. For this study, MEAs exhibiting a nanocavity underneath the passivation were used as described by Hofmann et al.,[69] from here on referred to as ncMEAs.

**MEA fabrication** MEAs were produced in an ISO 1 cleanroom. The fabrication steps are schematically depicted in Figure 3.10.
Borosilicate wafers with a diameter of 100 mm and a thickness of 500 µm (Schott) were used for the MEA fabrication. A standard photolithographic procedure was employed to transfer the 64 electrodes and corresponding feed lines pattern as depicted in Figure 3.10.C into the two layer photoresist consisting of Lor 3b (Microchem) and AZ nLof 2020 (MicroChemicals). After electron-beam evaporation (Pfeiffer PLS 570, Pfeiffer Vacuum) of a Ti, Au/Pt, and Cr (20 nm, 100 nm, 180 nm) stack and subsequent lift-off, the wafer was passivated with HD-8820 Aqueous Positive Polyimide (PI, MicroSystems™). Electrode openings and contact pads were transferred via photolithography into the photostructurable PI.
The wafer was diced into separate 24 x 24 mm chips (9 MEAs/wafer) and MEAs were cleaned consecutively with acetone and isopropanol under ultrasonication for 5 minutes and dried with $N_2$.

**Chromium etch** Back-etching of the sacrificial chromium layer is depicted in Figure 3.11. For that, 50 µl chromium etch solution on the basis of ceric ammonium nitrate and perchloric acid (Chrome Etch No. 1, MicroChemicals) was pipetted onto the electrode area. Etching was stopped with MilliQ water after 11 minutes. Afterwards, the chips were rinsed with fresh MilliQ water to remove any residual etching solution.

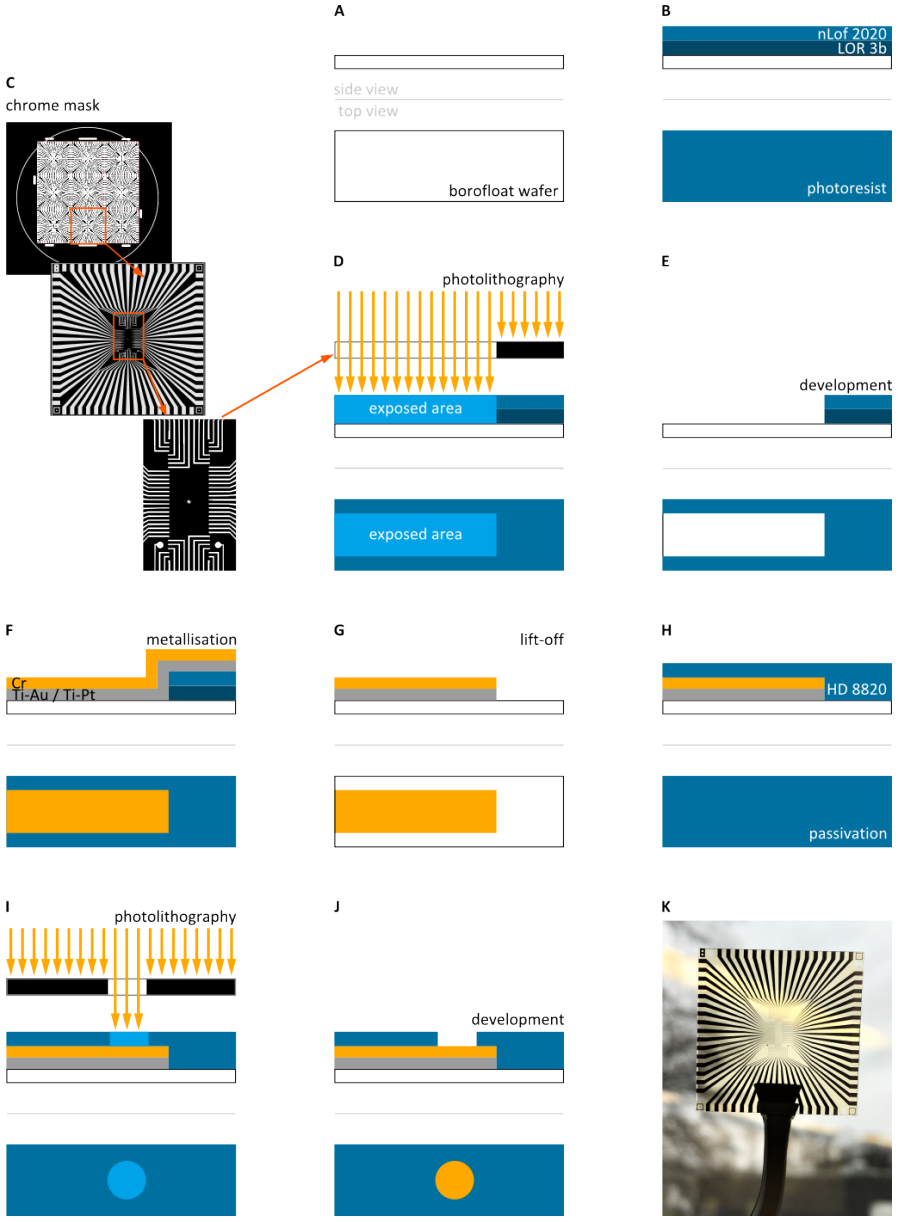


**Figure 3.10:** MEA fabrication. A) Borosilicate wafers were used as a substrate. B) A double layer of photoresist is spin-coated and after a pre-bake, the chrome mask is aligned onto the wafer (C). D) MEA features are transferred into the resist in the next photolithographic step. After development (E), metallisation if performed (F). Here, a stack of Ti, Au or Pt, and Cr is deposited (F) followed by removal of the photoresist (G). H) A layer of photostructurable passivation is applied and electrode openings and contact pads are transferred via photolithography (I). J) After development and a hard-bake step (J) the wafer is diced into individual chips (K). Adapted from Weidlich.[155]

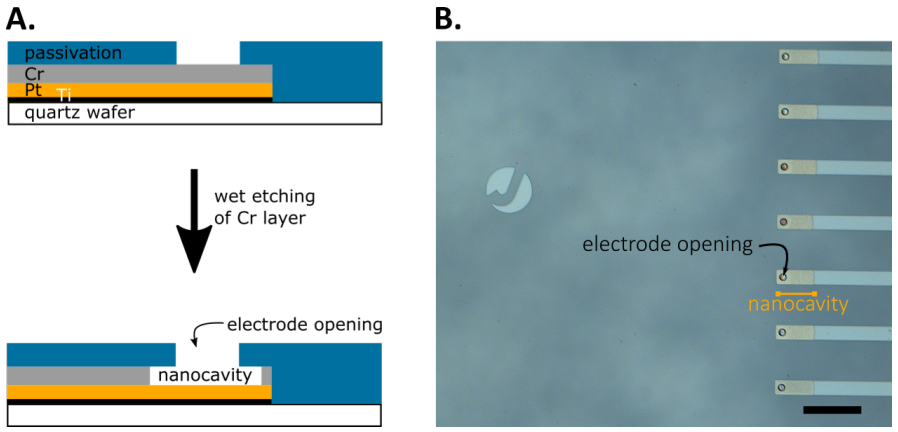


**Figure 3.11:** Chromium etch. A) Etching of the chromium sacrificial layer. B) ncMEA after etching. Back-etched area is marked with the yellow line. Scale bar 100 µm.

Glass rings with an outer diameter of 20 mm, a height of 5 mm and a wall thickness of 2 mm were glued onto the MEAs with PDMS (1:10 mixture of curing agent to siloxane, Sylgard 184, Dow Corning Corporation) and cured at 110 °C for 1 h.

### 3.6.2 Extracellular electrical recording system

Extracellular electrical recordings were performed with a setup developed in-house consisting of a pre-amplifier, a main amplifier, a multifunctional data acquisition device, and a recording software. The chip is inserted into the headstage or pre-amplifier, amplifying the electrical signal by a factor of 10 at an effective input impedance of 1 GΩ. The analog signal is transmitted to the main amplifier (BioMAS) providing further amplification (gain of 1, 10, or 100), coupling (AC- & DC-coupling), and high pass filter possibilities (0.01 to 72 Hz). The main amplifier operates with a low pass filter frequency of 3 kHz and allows a maximal output range of ± 10 V. Recordings reported in this thesis were acquired in the AC-coupling mode with a high-pass filter of 1 kHz and a gain of 100, resulting in an effective bandwidth of 1 - 3 kHz and a final amplification of 1,000.

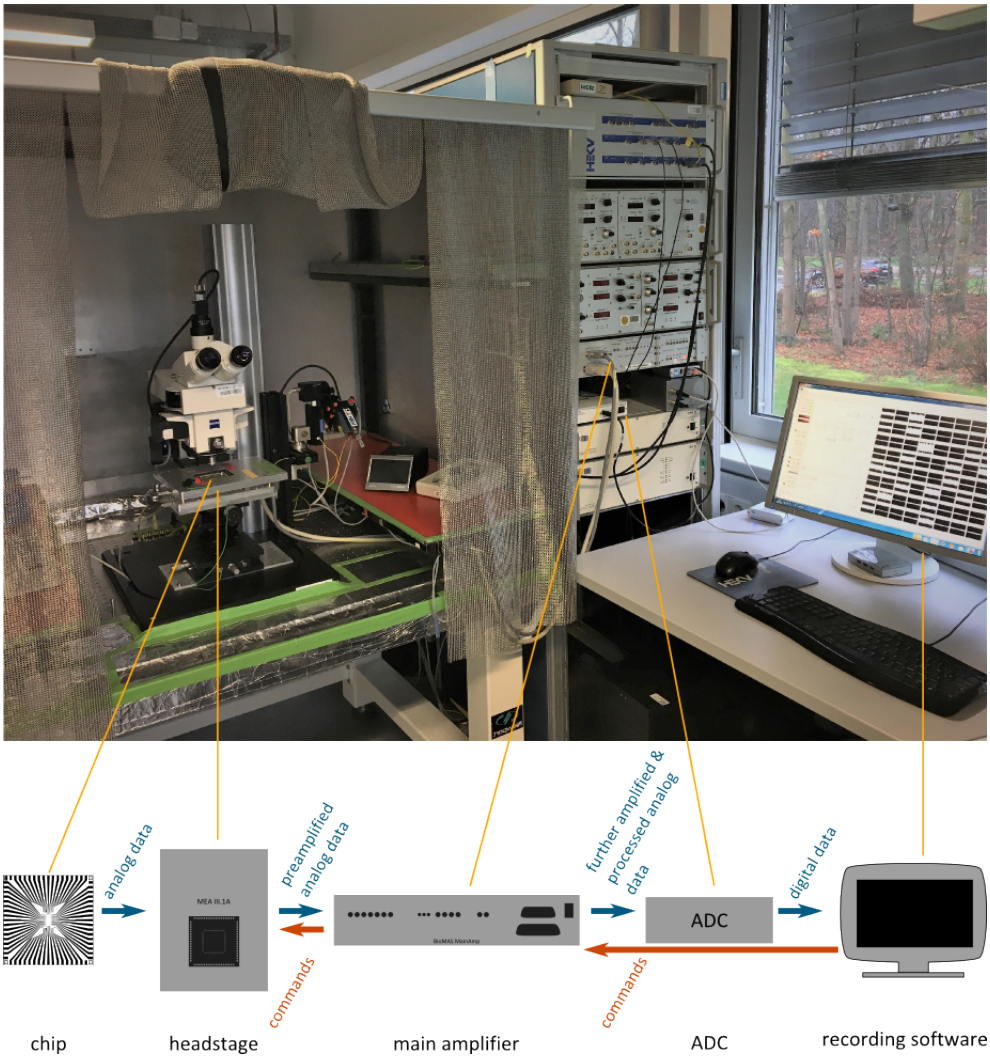


**Figure 3.12:** Electrophysiological recordings setup. Intra- and extracellular electrophysiological recordings can be performed with this setup. For this thesis, neuronal signal propagation was analysed with extracellular electrical recordings via MEAs. The headstage holds the chip and pre-amplifies the signal that is then transmitted to the main amplifier. The analog signal is converted into a digital one by the analog-to-digital-converter (ADC). The setup is operated via a software developed in-house.

The NI USB-6255 (National Instruments) allows simultaneous data acquisition of 64 channels with a sampling rate of 10 kHz and conversion of the analog into a digital signal with a 16-bit analog-to-digital converter (ADC).

A LabView software allows for real time signal displaying, data recording, and the control of the main amplifier. Voltage traces were recorded for 1 min and stored in a binary data file format.

**Data analysis** Data files were analysed offline with the BioMAS Analyzer software developed by Fabian Brings as well as an analysis script for peak detection developed by Johannes Lewen. Results are presented as raw, unfiltered data.

# Results

# Part I

# Single cell connectivity

The brain features a hierarchical architecture with multiple levels of organisation where on the microscale level individual neurons are specificly linked. However, random *in vitro* networks are characterised by a complex and unknown architecture and connectivity patterns. Thus, signal propagation analyses as well as individual neuron contribution are hard to investigate. Building custom *in vitro* microcircuits of defined architecture, polarity and connectivity on the level of single neurons provides the possibility to map individual connections, gain single cell adressability as well as influence the network complexity.

The control of neuronal structure has been largely investigated by means of micropatterned substrates, although other techniques like active cell entrapment,[48] laser guiding[121] or oriented carbon nanotube (CNT) substrates[49] proved to shape neurons and networks as well. An optimized design of the pattern geometry is necessary to control soma position, neuronal architecture and polarity. A versatility of patterns were designed to localise neuronal soma and confine their processes to dedicated substrate positions. Attempts toward interconnected architectures on single cell level included stripes, various geometrical shapes for soma placement[76] as well as different angles,[167,128] lengths[163] and thicknesses[55,147] for axon specification.

In this part, pattern designs with nodes and lines are chosen to control individual neurons within a neuronal network. The impact of the pattern design on the cell and network morphology is analysed in chapter 4. Active networks are required in order to investigate neuronal communication, thus, chapter 5 analyses the functionality of engineered single cell networks.

# Chapter 4

# Single cell networks: Controlling individual neurons

Approaches to control individual neurons by μCP target different cellular parts. All these approaches employ a contrast of adhesive patterns and non-adhesive surrounding. When seeding a cell suspension, cells sediment and attach to the surface. Cellular attachment is enhanced by adhesive proteins. Thus, cells poorly attached to the non-patterned surface are washed away in the washing step shortly after seeding. On microcontact printed substrates cells adhere and develop on the provided patterns. The pattern design plays a crucial role in the neuron's fate. Different shapes and structural properties of the neuronal soma, axons and dendrites can be utilised to control individual cell development.
In this chapter, the impact of grid and star geometries onto cellular and network morphology is analysed.

## 4.1 Soma positioning

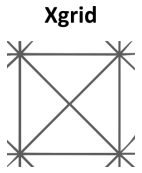


**Figure 4.1:** Xgrid pattern design.

The first attribute one can control in a defined neuronal network is the localisation of the soma. For some studies an increased accessibility of individual cells is intended. This is the case if one is interested in analysing individual cell behaviour without potential contamination by neighbouring neurons or in placing the somata onto specific locations like a sensor. Therefore the difference in shape between soma and neurites can be utilised. Somata appear as planar structures of some tens of µm while neurites are characterised by a thin and long shape. A combination of bigger nodes and thin lines is a common approach and was already reported in different publications, e.g. Corey et al.,[29] Nam et al.,[106] Tomba et al..[147] However, the efficiency of soma positioning or node occupation was poorly analysed. For the experiments presented in this section, a pattern with nodes and interconnecting lines was employed (see Figure 4.1). This pattern was first used in the institute by Hofmann with the aim to separate single cells and place the somata onto defined positions on a substrate.[68] It is referred to as the Xgrid pattern.

Dissociated neurons were grown on these Xgrid patterns and the network morphology with a focus on soma location was analysed via microscopy.

**Soma position** Neuronal cultures on the Xgrid pattern were evaluated on DIV 3 regarding their soma location on the pattern. The microscopic image in Figure 4.2 shows a representative culture. Some somata are located on the nodes (blue circle) as intended. But many neuronal somata are located either on the lines (bright yellow circle) of the pattern or the intersection of the diagonal lines (darker yellow circle).

A random distribution of neurons on the pattern ($H_0$) would show an effect of node area as a fraction of total area onto the soma distribution. This is not the case as 3.4 % of the pattern area are represented by nodes, while

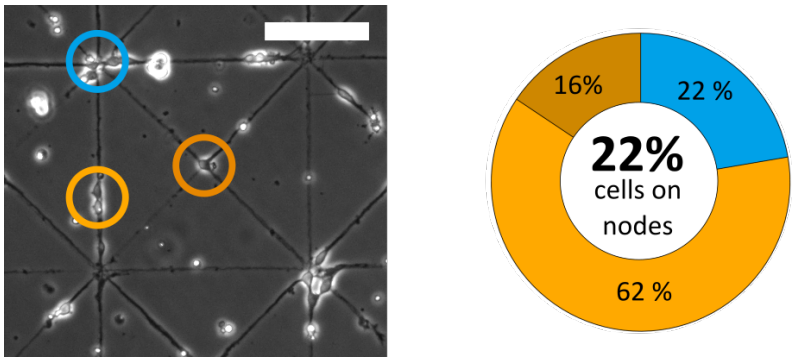


**Figure 4.2:** Soma positions on X-grid pattern. Somata on nodes are displayed in blue, somata on lines in light yellow and on intersections in dark yellow. Scale bar 100 µm. N = 269 cells.

22 % of the somata are located on the nodes (see Table 4.1). Thus, the null hypothesis is rejected ($p < 0.001$). Neuronal somata seem to preferably locate on the nodes. In addition, it is noticeable that there is a higher proportion of somata located on the intersections (16 %), than would be expected with a random distribution.

One hypothesis why somata preferably locate on the nodes, tested in Table 4.1.B, is that nodes provide a greater adhesion area for the natural flat somal shape. If this hypothesis were true, then the fraction of somata migrating to the node should reflect the adhesive area surrounding a node and as opposed to the local adhesive area available in the middle of a line or at an intersection. Therefore, the adhesion area of a soma can be considered

**Table 4.1:** Impact of the Xgrid pattern onto soma location.

| pattern feature | of somata | (A) % of pattern area | (B) somal contact area | (C) lines for neurite elongation |
|---|---|---|---|---|
| nodes | 22 % | 3.4 % | 113 µm$^2$ | 8 |
| lines | 62 % | 95.2 % | 48 µm$^2$ | 2 |
| intersections | 16 % | 1.4 % | 80 µm$^2$ | 4 |

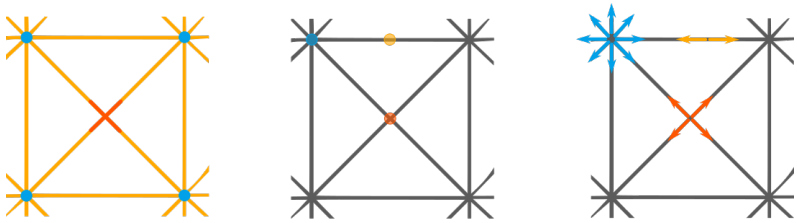


**Figure 4.3:** Pattern influence on soma adhesion. A) Ratio of node (blue), intersection (red), and line (yellow) area to the overall pattern area. B) Soma adhesion area. C) Number of lines surrounding the soma position.

simply as the area of a circle of 12 µm diameter. Nodes provide an adhesion area of 113 µm. A circle placed in the centre of an intersection has a pattern area of 80 µm and on a line a contact area of 48 µm (Table 4.1.B, Figure 4.3.B). However, the observed distribution of somata cannot be solely explained by the somal contact area either.

Moreover, the number of lines provided for neurite elongation could influence soma motility. Neurite elongation result in tension forces acting on the soma and might influence soma motility.[128] More lines might promote more neurites to elongate and thus, stabilise the soma position. The nodes are surrounded by 8 lines, intersections are characterised by 4 lines, and a position on a line only provides 2 lines for neurite elongation (see Table 4.1.C and Figure 4.3.C). Here also, the observed distribution of soma position cannot be solely explained by the number of lines.

In conclusion, 6.5 times more somata were observed on the nodes and 7 time more on the intersections than expected if the null hypothesis (random distribution on the pattern) were true. Soma position seems to be influenced by an interplay of multiple factors (Figure 4.3):

After cell seeding, cells sediment and are randomly distributed on the surface. Cells on pattern might develop stronger contacts to the surface than cells on non-patterned area. In the washing step some hours after cell seeding, cells off the pattern might be more likely removed from the culture. Remaining

cells migrate until they encounter adhesive cues by the pattern. Migration might continue on the pattern towards greater somal adhesion areas as the nodes (Figure 4.3.B). Encountering a greater adhesion area, migration might be inhibited and neurites might elongate along the lines surrounding the position. An effect that was already hypothesised by Corey et al.[29] More neurites spacing evenly on the planar surface might enhance the stabilisation of the current position due to counteracting tractive forces (Figure 4.3.C). Moreover, contact to other neurons may influence soma migration. In addition, the number of cells in culture as well as the DIV possibly play an important role in the ratio of neuronal somata located on the nodes. Further, the increased incidence of somata on the intersections might be influenced by an unprecise protein transfer. Excess ink on the stamps might have smudged the substrate, providing increased areas for somata to attach to.

**Node occupancy** For some applications it is aimed to place somata onto specific positions, like for example electrodes. It does not matter if cells are located at other positions, too. The Xgrid pattern is designed to place neuronal somata on the nodes that are matched to the standard MEA with the 8 x 8 electrode design in the institute.

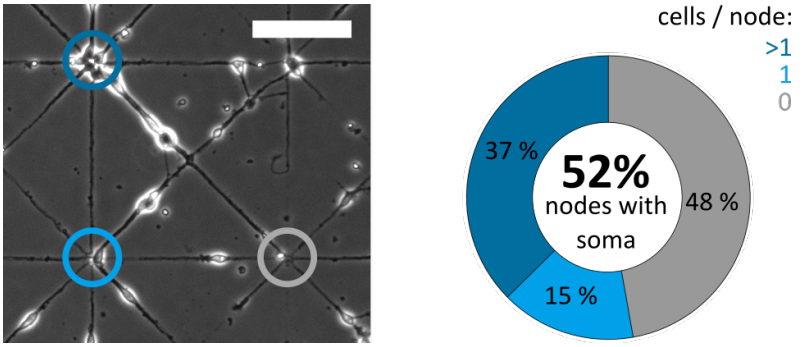


**Figure 4.4:** Nodes of Xgrid pattern with and without somata. Nodes with multiple somata are displayed in dark blue, nodes with one soma in light blue and nodes without somata in grey. Scale bar 100 µm. N = 266 nodes.

Therefore, in the next step the ratio of covered nodes was analysed. Figure 4.4 shows the share of nodes covered with multiple somata (dark blue

circle), single soma (light blue circle) and no soma (grey circle).
With the Xgrid pattern we can cover 52 % of the nodes with cells. Around 30 % of these nodes were covered by single somata, while the remaining nodes were occupied by more than one soma. Approximately half of the nodes are soma-free at DIV 3.

**Summary & discussion** The Xgrid geometry combines 4 µm thin lines with nodes of 12 µm diameter. The cells preferably grow on the protein pattern. At DIV3, 22 % of the neuronal somata were observed to be on the nodes, while the majority of the somata (78 %) was located on the lines. 16 % of those were located on the intersection of two lines. Concluding, the pattern geometry influences the soma position: 6.5 times more somata are located on the nodes than would be expected with a random distribution on pattern ($H_0$). The soma position might be influenced by an interplay of several factors, like e.g. the provided node area as a fraction of the overall pattern area. Additionally, factors influencing somal migration as the somal contact area or number of extruding neurites (influenced by pattern lines) might be important.
Looking at the node occupancy, half of the nodes (52 %) showed at least one soma attached to it. Around 70 % of these nodes were occupied by more than one soma.
For experiments where the aim is to place somata on sensors as for example on multi-electrode arrays (MEAs), this would mean that half of the electrodes are covered by somata. This is better than a random distribution, because we also achieve a reduction in network complexity and a better understanding of the network mapping. However, for future experiments a pattern design with thinner lines might be considered. This would increase the contrast between the node and line dimensions. In addition, it would increase the node fractional pattern area which might result in a decreased number of somata on the lines. A 2 µm line might force the soma into a inconvenient long shape with poor adhesion. Some somata with poor adhesion on the lines would be washed away in the washing step. The other somata might

migrate towards the nodes for a more convenient adhesion. At the same time, a decreased line thickness would decrease the area at the intersections and might also decrease the number of somata located here. However, due to neuron migration the distribution might vary at other DIVs and has to be investigated further in future experiments.

## 4.2 Neurite polarisation

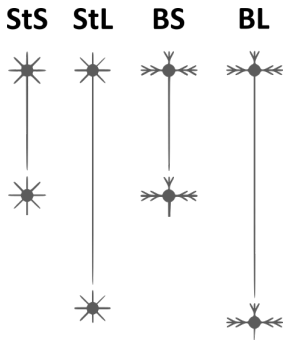


**Figure 4.5:** Star pattern designs. StS: Star Short, StL: Star Long, BS: Branched Short, BL: Branched Long.

The last section investigated the efficiency of soma positioning and node occupancy. This section employs the same geometric structures, nodes and lines, to control neurite specification. Yamamoto et al. showed that asymmetric patterns impact neurite specification. In brief, by designing a pattern with lines of different lengths only one neurite was allowed to elongate, while the others were restricted in growth.[163] This discoveries were inspiration for the pattern designs used in this section. Here, the aim was to analyse the impact of the line length onto axonal specification. Additionally, a changed design of the shorter lines was introduced and evaluated. In contrast to the approach of many other studies with single cell patterning, where only cells with somata on the nodes are included in analysis, the analyses presented in this thesis include all cells on the patterns. This holistic approach not only evaluates the pattern efficiency, but also the suitability of the pattern design as a tool to create a defined neuronal network with controlled single cell architectures.

The star shaped pattern designs (Figure 4.5) aims to connect neurons linearly and create directionality. A node of 20 µm diameter is designed to be occupied by the neuronal soma while the neurites should elongate along the lines. The long lines of 150 µm ("S" for shorter version) and 350 µm ("L" for longer version) aim to promote the elongation of one neurite to trigger a break of symmetry in neuronal polarisation. The branched geometry of the short lines of the "B" patterns aims to provide branching possibilities for future dendrites.

### 4.2.1 Neurons on Star patterns at DIV 3

To analyse the efficiency of geometrical control of the pattern design, neurons were cultivated on patterned coverslips and their morphology was analysed microscopically and immunocytochemically.

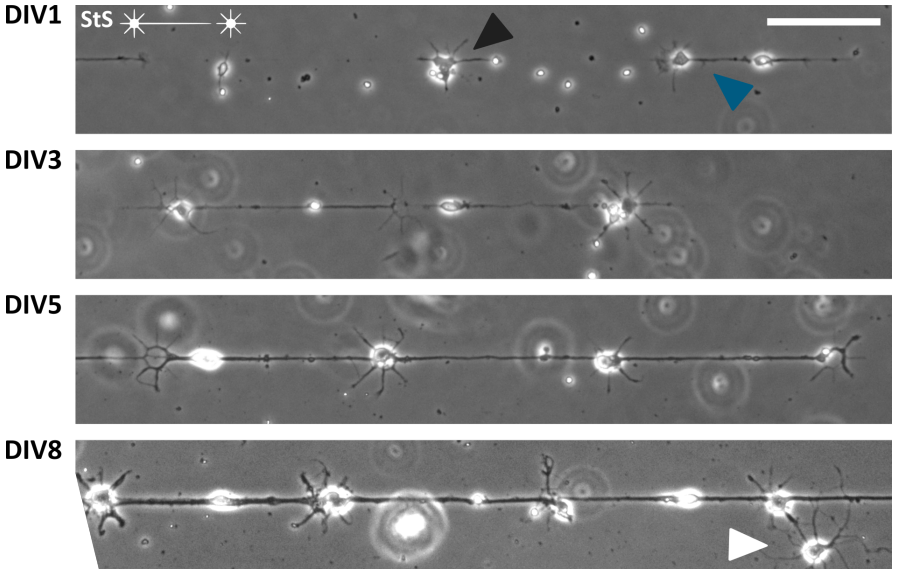


**Figure 4.6:** Phase contrast images of neurons on StS patterns at different DIVs. Neurons show different polarisation stages at DIV 1: unpolarised neuron (black arrow), polarised neuron (blue arrow). Cells at DIV 3 are mostly polarised and are still separated. Neurons at DIV 5 and DIV 8 form a linear network. Some cells are located on the non-patterned area (white arrow). Scale bar 100 µm.

**Culturing duration** Figure 4.6 shows neuronal cells growing on the StS pattern at different DIVs, namely DIV 1, DIV 3, DIV 5 and DIV 8. Neurons clearly follow the pattern on the substrate for DIV 1 - 5. At DIV 8 some neurites leave the patterned area and also some somata are located on non-patterned areas (white arrow).

Some neurons at DIV 1 already show a polarised neuronal appearance with some shorter neurites and one longer neurite (blue arrow). Many of them already have neurite lengths of at least 100 µm, while some other neurons only show neurites of similar lengths 24 hours after cell seeding (black arrow).

At DIV 3 most neurons show one neurite exceeding 100 µm length and single cells are still separated. A linear neuronal network with multiple neurites on the lines is visible at DIV 5 and even more noticeable at DIV 8.
According to Dotti et al. axonal outgrowth starts at DIV 1.5,[43] therefore the time point to analyse the direction of axon growth should be at a later DIV. Figure 4.6 supports this, since not all neurons at DIV 1 show a polarity yet. DIV 3, DIV 5 and DIV 8 neurons all show long neurites and can be considered being over the break of symmetry,[43] but neurons at later stages like DIV 5 and DIV 8 have even longer neurites and seem to be interconnected. This is making an assignment of individual neurites to the neurons they belong too difficult. Based on these observations, neuronal cultures were analysed at DIV 3 in the following experiments.

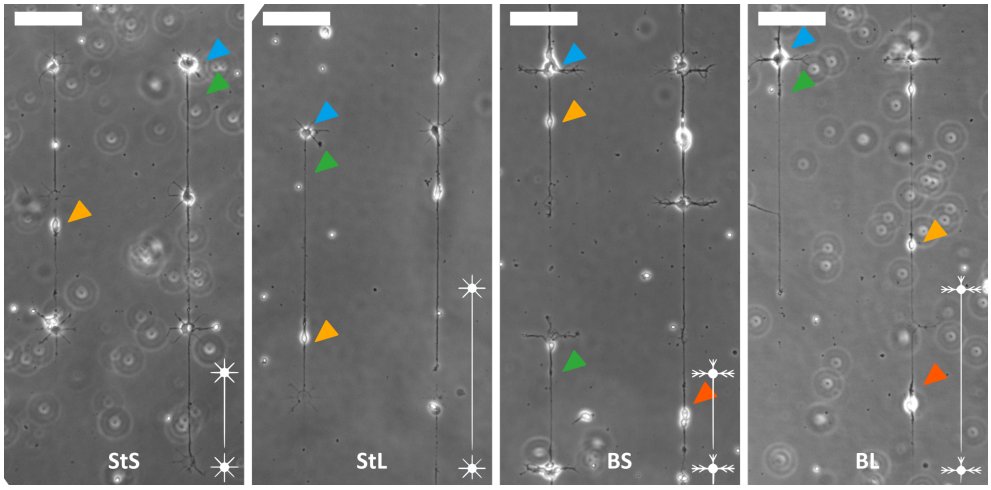


**Figure 4.7:** Phase contrast image of neurons at DIV3 on star patterns. Neuronal somata are located on nodes (blue arrows), but also on the lines of the pattern (yellow arrows). Outgrowth direction of the longest neurites is clear for some cells. Here, the longest neurites growing into the intended direction are marked with green arrows, while the ones elongating into the opposite direction are marked with an orange arrow. Scale bar 100 µm.

**Phase contrast observation** Figure 4.7 displays neurons growing on short and long shooting and branched star patterns at DIV 3 (StS, StL,

BS, BL; see Figure 4.5). Most neurons are located on the patterned area and exhibit shorter as well as elongated neurites. The soma position on all patterns vary, while some somata are located on the nodes (blue arrows), other neurons have their somata on the lines (yellow arrows). Looking at the longest neurites' outgrowth directions one can see neurites elongating in the preferred direction (which is along the long line of the pattern, green arrow) as well as into the opposite direction (orange arrows). In multiple publications the longest neurite is considered to be the axon of a neuron because of its fast elongation after the break of symmetry.[43,163,92] Taking this into account, neurons on all patterns show the axon outgrowth along the linear axis of the pattern. Neurons labelled with green arrows thus, extend their axons into the intended direction, while axons with orange labelled arrows grow into the wrong direction. Even though the longest neurite of some cells clearly can be seen (green and orange arrows), the identification of the axon outgrowth direction of many other cells is not possible in the phase contrast images of the cultures.
Short neurites are visible on the short lines of all star patterns and can be considered dendrites. They follow the geometry of the pattern for all pattern designs. On the StS and StL pattern, where linear lines are provided, they stay in a linear shape, while on the BS and BL substrates the dendrites follow the branching geometry of the pattern.

### Immunofluorescence analysis

The first observation of neuronal growth on the star patterns already showed some differences of soma position and axon elongation direction. Although the longest neurite is usually considered to be the axon,[43,163,92] an immunofluorescence analysis can give a clear statement about which neurite is the axon. Therefore, neuronal cultures were fixed and stained for neuronal and axonal marker proteins (beta-III-tubulin = Tuj1[151] for neurons and tau for axons[86]). Neurons are categorised depending on their soma position - soma on node or soma on line - and the axon outgrowth direction - right direction and wrong

direction. In sum around 4'500 neurons on all patterns were analysed: 1'811 on StS, 1'684 on StL, 370 on BS and 680 on BL substrates.

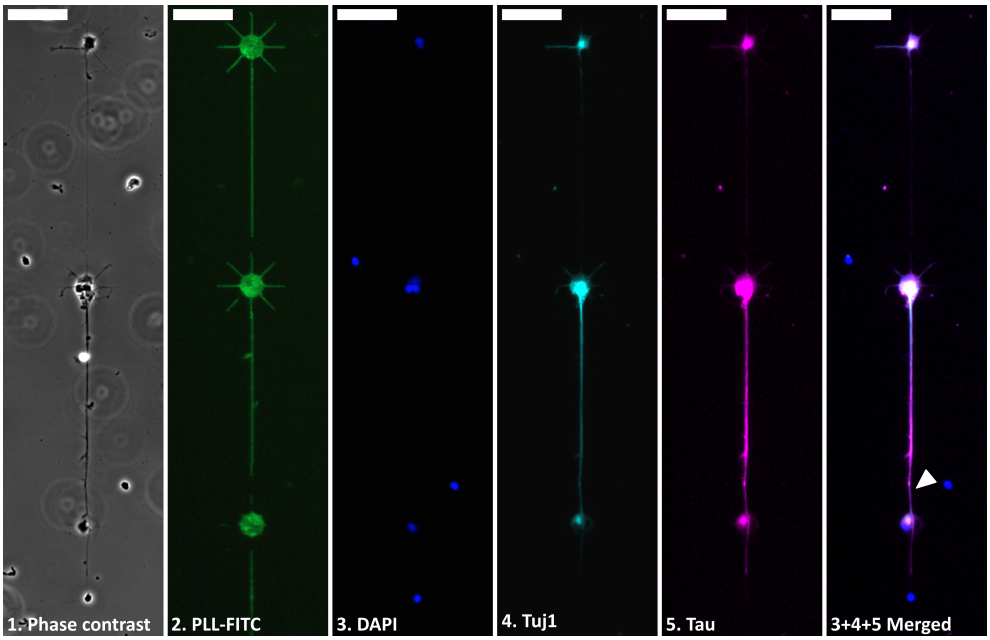


**Figure 4.8:** Immunofluorescence image of neurons growing the axon in the right direction on StS pattern. Cell somata are located on the nodes of the pattern while neurites (Tuj-1) follow the lines. Axon (tau, clearly visible in merged image) elongate along the long line of the pattern and is indicated with an arrow. Scale bar 50 µm.

**Axon outgrowth direction** Figure 4.8 and Figure 4.9 show neurons growing on StS patterns. The axon is clearly visible in the merged images, where an overlay of the DAPI, Tuj-1 and tau staining is presented. Axon outgrowth is marked with an arrow in the merged picture. While in Figure 4.8 the axon is elongating in the intended direction in Figure 4.9 it elongates into the opposite direction.

The quantification of axon growth direction is presented in Figure 4.10 and categorised into either right (along the long line, green colour in Figure 4.10) or wrong (opposite growing direction, orange in Figure 4.10).

On all patterns at least 60% of the neurons were elongating their axons into

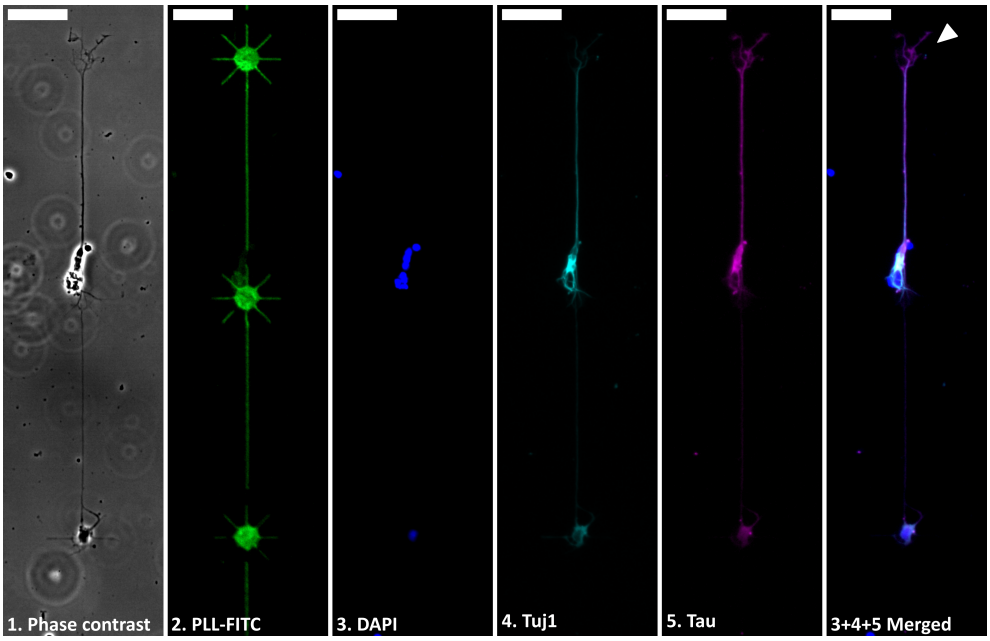


**Figure 4.9:** Immunofluorescence image of neurons growing the axon in the wrong direction on StS pattern. Cell somata are located on the nodes and some on the line of the pattern (see Phase contrast and DAPI pictures) while neurites (Tuj-1) follow the lines. Axon (tau, clearly visible in merged image) elongate into the unintended direction of the pattern and is indicated with an arrow. Scale bar 50 µm.

the intended direction. On the StS pattern 63% of the cells developed their axons along the long pattern line and 60% in case of the StL pattern. On the BS and BL patterns 65% of the neurons elongated their axon along the long line.

These results show, that all star shaped pattern used for this study influence the direction of axon outgrowth, thus shaping the connectivity of single cell neuronal networks and create a preferred structural directionality.

Comparing the long (StL, BL) with the short line patterns (StS, BS) only the short shooting star pattern (StS vs. StL) showed a 3% higher number of neurons elongating their axon into the intended direction. Comparing the shooting with the branched star design, the branched pattern showed a slightly higher number of neurons developing their axon into the right

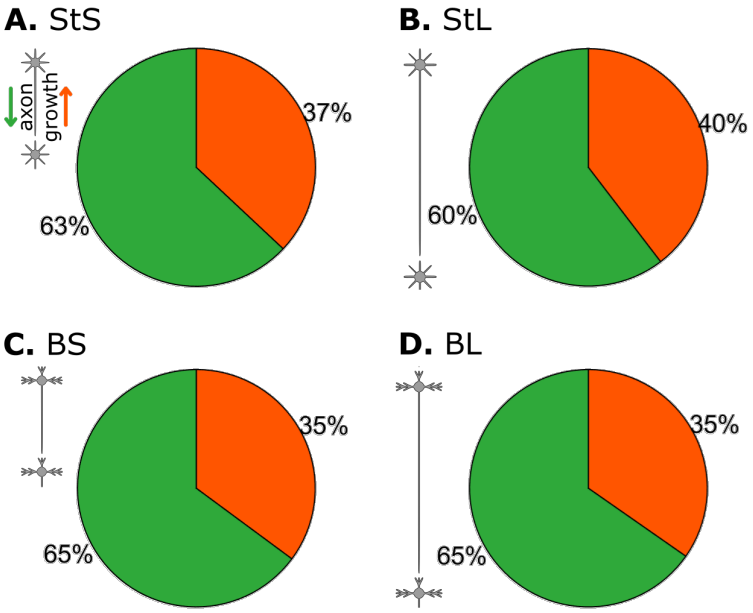


**Figure 4.10:** Quantification of axon outgrowth direction. Pie charts show percentages of neurons growing into the intended (green) or unintended (orange) direction on the different patterns. Number of cells counted: A) 1811; B)1684; C) 370; D) 680.

direction (+2% for BS and +5% for BL).

In general these results are comparable with other single cell pattern designs, that usually successfully control axon outgrowth direction for around 60%-80 % of neurons.[163,167,55] Even though it has to mentioned here, that for the quantification showed in Figure 4.10 all cells on the pattern were included. In contrast, some of the quantifications presented in literature only include neurons with somata located on the designed nodes and exclude all other cells on the patterns from their statistics. Yamamoto et al. even achieved a 78 % polarisation efficiency into the intended direction, however the individual pattern structures were stand-alone structures and not daisy chained as in the experiments presented here.[163] Stand-alone structures are often used to analyse cellular properties of single cells. Whether the aim of the daisy chained structures is to analyse the characteristics and behaviour of a single

cell within a network.

**Relation of soma position and axon outgrowth direction** Taking a deeper look into the phase contrast and immunofluorescence images, the soma position on the pattern and the axon outgrowth direction of this neuron seems to be related (see Figure 4.11).
Thus, the neurons were analysed first, according to their position on the pattern (node or line) and second, to their direction of axon elongation.

**Soma position** If neuronal somata were randomly distributed on the pattern ($H_0$), the probability of a soma being located on the node would equal the fractional pattern area occupied by the node. For the short pattern design (StS and BS) this would correspond to a probability of 51 % and for the long pattern (StL and BL) for 31 %. However, 65 % of neurons on both short pattern designs (StS and BS) have their soma located on the nodes, and 42 - 45 % of the somata were located on the nodes for the long pattern designs (see Figure 4.12). Thus, $H_0$ can be rejected ($p < 0.001$). This confirms the visual impression, that neuronal somata preferably locate on the nodes of the pattern.

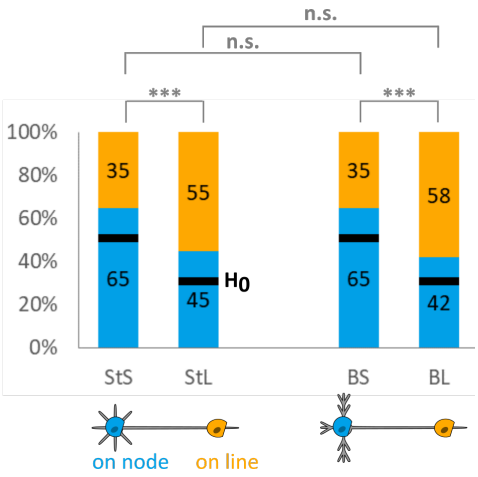


**Figure 4.12:** Soma position on the star patterns. Somata located on the node are represented in blue, somata on lines in yellow. $H_0$ marked with black lines. Significance level of $p < 0.001$ marked with "***", "n.s." indicates no significant difference ($p > 0.05$). Number of cells counted: A) 1811; B)1684; C) 370; D)680.

The compliance of somata to nodes is significantly stronger on the short than on the long patterns for both, the shooting star (StS, StL) and the branched star (BS,BL) pairs ($p < 0.001$). One explanation could be the higher ratio

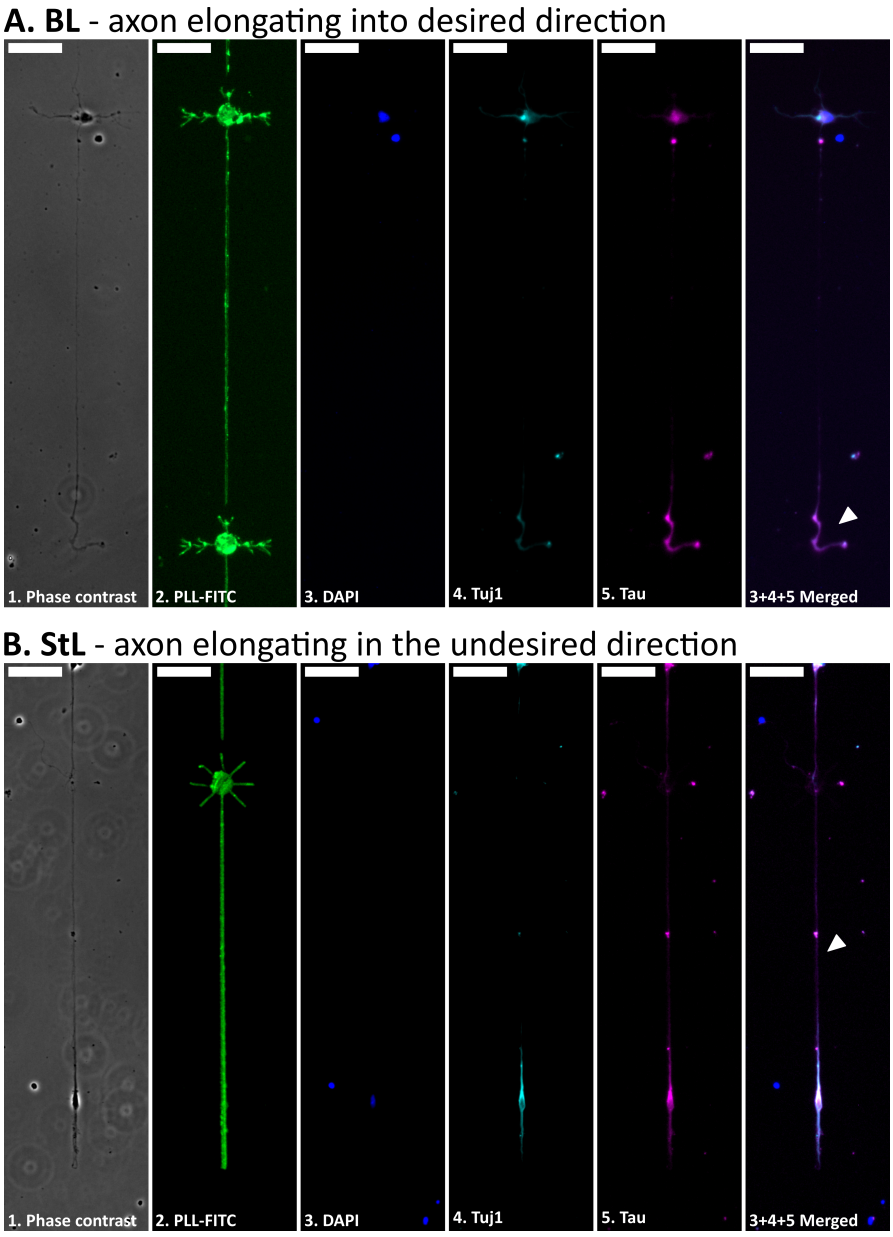


**Figure 4.11:** Neurons on BL and StL pattern with axons growing into the intended and opposite direction. A. Neuronal soma is located on the node and axon growing into the intended direction (marked with an arrow in the merged image). All neurites follow the pattern, even the short neurite branch along the pattern. B. Soma is located on the line (see phase contrast and DAPI picture) and axon is elongating along the line into the unintended direction (visible in merged image and marked with an arrow). Scale bar 50 µm.

of the node to line area for short structures. However, the fractional pattern area does not solely explain the soma position. As already assumed for the Xgrid pattern, both, the fractional pattern area as well as the pattern geometry might have an influence on the soma position. Concluding, short pattern designs are beneficial for soma positioning on the nodes.

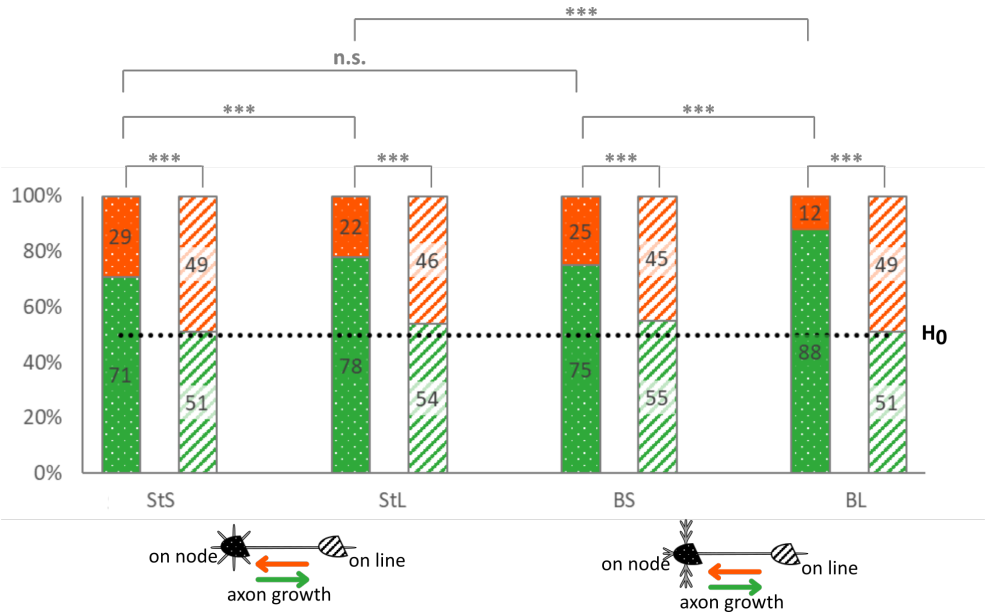


**Figure 4.13:** Axon elongation depending on soma position. Somata located on the node are represented by dots, somata on lines by lines. Axons growing into the right direction are shown in green, into the wrong direction with orange. $H_0$ is indicated with the dotted line. Significance level of $p < 0.001$ marked with "***", "n.s." indicates no significant difference ($p > 0.05$). Number of cells counted: A) 1811; B)1684; C) 370; D)680.

**Axon outgrowth direction** In the second step, the axon outgrowth direction depending on the soma position was analysed (see Figure 4.13). More than 70 % of neurons with their somata located on the nodes, elongated their axons into the intended direction (StS: 71 %, BS: 75 %, StL: 78 %, BL: 88 %). Thus, for neurons with their soma located on the node, the null hypothesis that axons elongate randomly into both directions can be rejected ($p < 0.001$). Here, the long pattern versions (StL, BL) show a significantly

stronger guiding effect than the short patterns (StS, BS) ($p < 0.001$). The branched star pattern shows the strongest guiding effect.
However, for neurons with their somata located on the line, only 45 % - 49 % of the axons are growing into the right direction, which corresponds to a random distribution.

**Soma distribution along the pattern and the related axon outgrowth direction** Up until now the soma location was categorised in either being on the node or on the line. However, the exact position on the line might be influencing the axon outgrowth direction. For that the direction of axon outgrowth of every individual neuron was analysed with respect to its soma position along the vertical axis of the pattern (supplementary immunofluorescent image in Figure 8.1 in chapter 8). The centre of the node is considered to be "0" and the distance of the nucleus' centre to the node's centre was measured.
The histograms in Figure 4.14 displays the counts of neuronal somata at different vertical pattern positions binned into 20 µm bins and categorised into the two different axon growth directions, right (green) and wrong (orange). All histograms show a high count number at the nodes (0 µm) and of these cells more than 70 % are elongating their axon into the right direction, which was already shown in Figure 4.13. The distribution of the soma position on the pattern lines is very broad and the portions of cells with axons growing into the right direction are decreasing with an increasing distance from the node.
This is even more obvious in Figure 4.15 (and in Figure 8.2 in chapter 8), where normalised data is displayed.
To further analyse the dependency of soma position distribution and axon outgrowth direction, the data is displayed separately in Figure 8.2 in chapter 8. The counts are normalised to the total number of counts in one graph and represented in percentage. The soma distribution along the both short patterns (StS and BS) is similar within both categories: axon growing into the right and wrong direction. Of all neurons with an axon growing into the

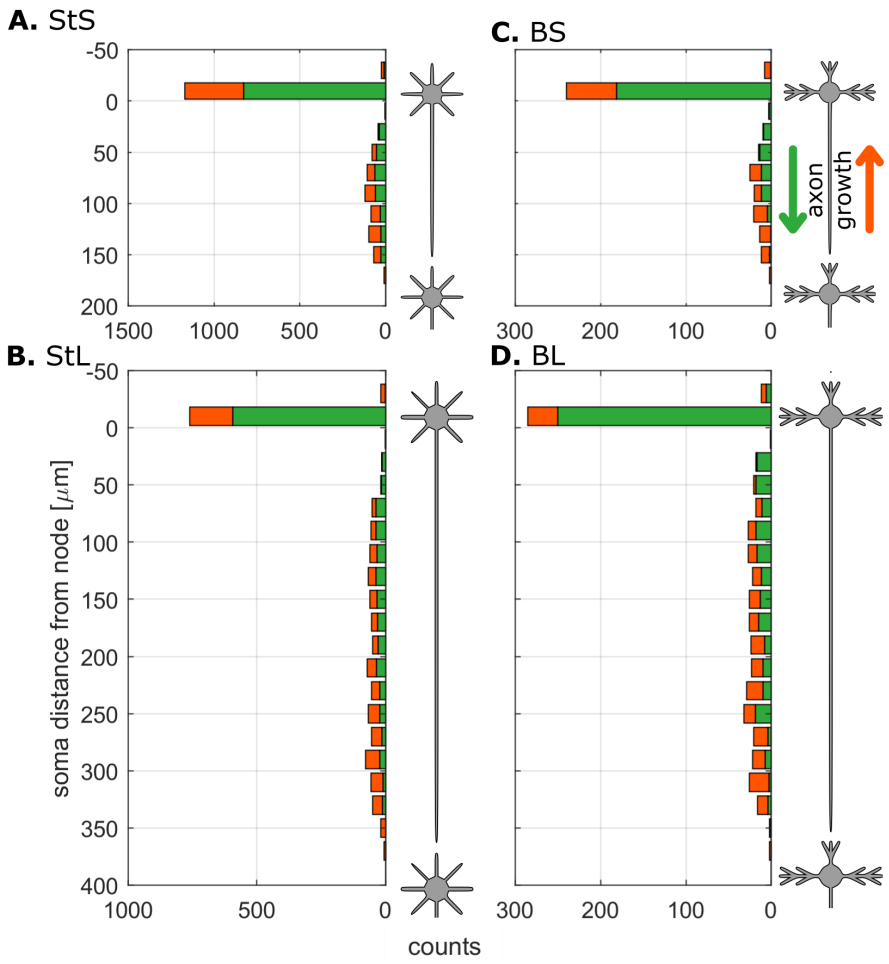


**Figure 4.14:** Soma position distribution on the pattern. Distance from the node is represented on the y-axis, cell counts on the x-axis. Counts of neurons elongating their axons into the intended (green) and unintended (orange) direction are stacked. Bin size: 20 µm. N: A) 1811; B) 1684; C) 370; D) 680 cells.

preferred direction around 75 % have their somata on the node (StS: 72 %, BS: 75 %). The other quarter of these neurons have their somata distributed along the lines with a maximum of 6 % around 80 µm away from the node's centre. In case of the cells elongating their axons into the wrong direction approximately 50 % of the somata are placed on the nodes. The distribution of the other half of the neurons is shifted towards higher distances from the node with a maximal number of cells around 130 µm.

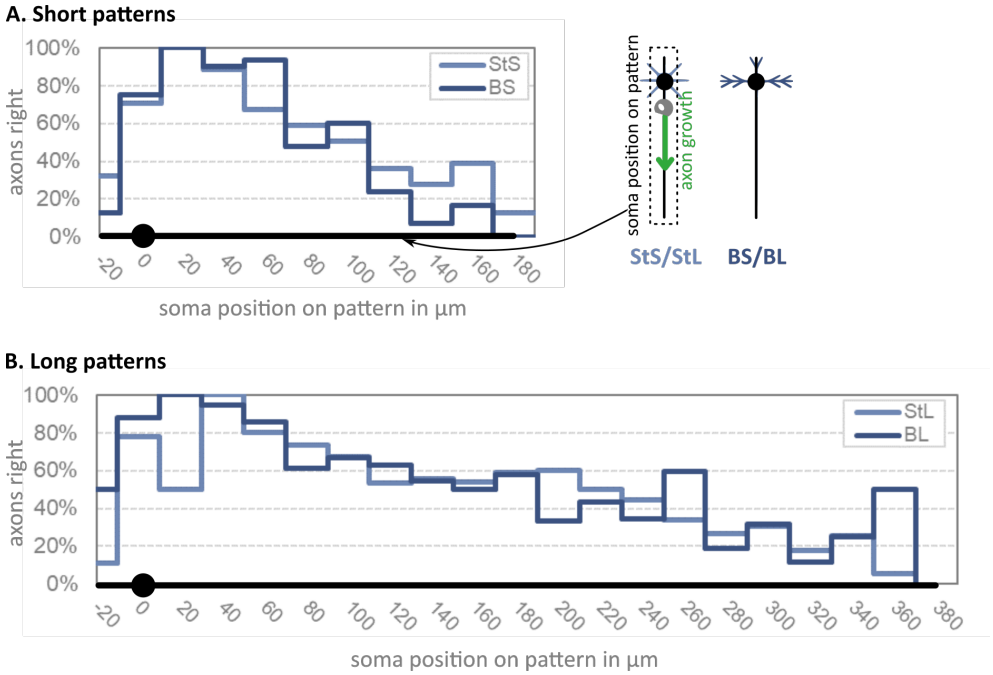


**Figure 4.15:** Share of axons growing into the right direction on the star patterns. Axons growing into the right direction in dependency of their soma position on the A) short star patterns (StS,BS) and B) long pattern versions (StL, BL). Bin size 20 µm.

The soma distributions along the long patterns (StL and BL) are also similar within both categories, but show differences compared to the distributions along the short patterns. For the cells elongating their axons into the right direction, approximately 60 % of the somata are placed on the nodes. The other neuronal somata are spread over the line, with only few percentage of somata per bin. In case of the neurons elongating their axons into the wrong direction, the number of cells with somata on the nodes is the lowest with only 18 % (BL) and 25 % (StL). This means, that the majority of the neurons with an axon into the wrong direction have their soma on the lines. Yamamoto et al. revealed some mechanisms of axon specification: the neurite allowed to elongate is becoming an axon. Neurites that are restricted to a certain length do not specify into axons. Additionally, if one neurite reaches a length that is 10 - 15 µm longer than the other neurites, it usually specifies

into an axon.[61,43] This could explain why the majority of the neurons with the somata on the lines far away from the nodes are developing their axon into the wrong direction.
Once the soma is placed on the node, the axon elongates mostly into the intended direction as shown in the previous results (Figure 4.13). One reason is that the conditions for axon specification are set beneficial: The short lines for the dendrites restrict the outgrowth of the neurites. The long line is long enough for the neurite to elongate fast and grow longer than the other neurites.[163,61,43] Additionally, since curved lines inhibit axon specification, the straight lines vice versa might promote axonal polarisation.[128]
Both, short and long pattern versions promote axon outgrowth into the intended direction if the soma is located on the node. The long pattern seems to be even more beneficial, even though polarisation occurs at a neurite length of approximately 50 µm.

### 4.2.2 Neuronal polarisation over time

The results described so far were snapshots at a certain DIV. We see a clear effect of the soma position along the vertical axis of the pattern onto the direction of axon elongation and the different distribution patterns (Figure 4.15). For further analyses, time lapse imaging experiments were performed to analyse how neurites elongate over time and whether the somata show movements.

**Neurite elongation over time** Time lapse imaging experiments were performed for a time period of 2 days and 6 hours. Experiments were performed with neurons cultured on the short shooting star patterns (StS). Exemplary neurons are depicted in Figure 8.3 and Figure 8.4 in chapter 8. Neurite growth for neurons with somata located on the nodes (as depicted in Figure 4.16) was analysed.
Figure 4.16 shows a neuron and the neurites at different time points (3.5 h, 12 h, 24 h, 36 h, 48 h and 53.5 h respectively). After 12 h in culture we see

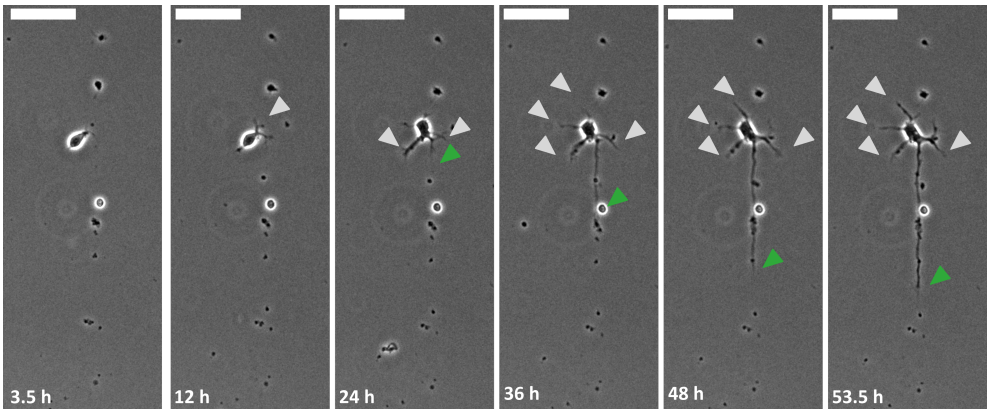


**Figure 4.16:** Neurite elongation over time on StS pattern. Neuronal soma is located on the node. First extruding neurites are visible after 12 h. After 36 h one neurite elongates fast and breaking the symmetry. This neurite is becoming the axon (marked in green). The other neurites are considered dendrites (grey). Scale bar 50 µm.

some first neurites growing out of the soma. After 36 h in culture we see 5 neurites, one of them is already longer and elongating further in the next hours while the other neurites stay roughly the same length. Thus, after 36 h we see a break in symmetry with one neurite (green) becoming the axon. All neurites grow along the pattern.

Figure 4.17 shows the neurite lengths over time for neurons elongating their axon into the right (A, B, green) and into the wrong direction (C, D, orange). The other neurites - the dendrites of the cells - are displayed in grey. The intense lines represent the average over all axons or neurites analysed for the specific graph. All graphs show an elongation pattern characterised by constant neurite outgrowth and retraction. The neurites (grey) reach a length of around 20 - 30 µm on average latest after 24 h but still do retract and elongate over the whole time. Axons elongating into the right direction (A, 11 cells) show varying elongation patterns over time. Some axons rapidly extend to 50 - 80 µm after 12 h while others stay at a length of around 25 µm until 48 h in culture. The lengths at 53.5 h vary from 92 to 143 µm with an average at $120 \pm 16$ µm. This corresponds to an average net axon growth rate of $54 \pm 7$ µm/day.

Axons elongating into the wrong direction also vary in their elongation patterns. Some are rapidly exceeding 50 µm length while others stay below that number for 2 days. The lengths at 53.5 h range from 117 - 324 µm with an average at $190 \pm 85$ µm. This corresponds to a net axon growth rate of $85 \pm 33$ µm/day.

This difference in average lengths of the axons growing into the right and wrong direction might be explained with the pattern architecture. While the axon growing into the right direction is most likely stopping elongation at the gap before the next shooting star, the axon growing into the wrong

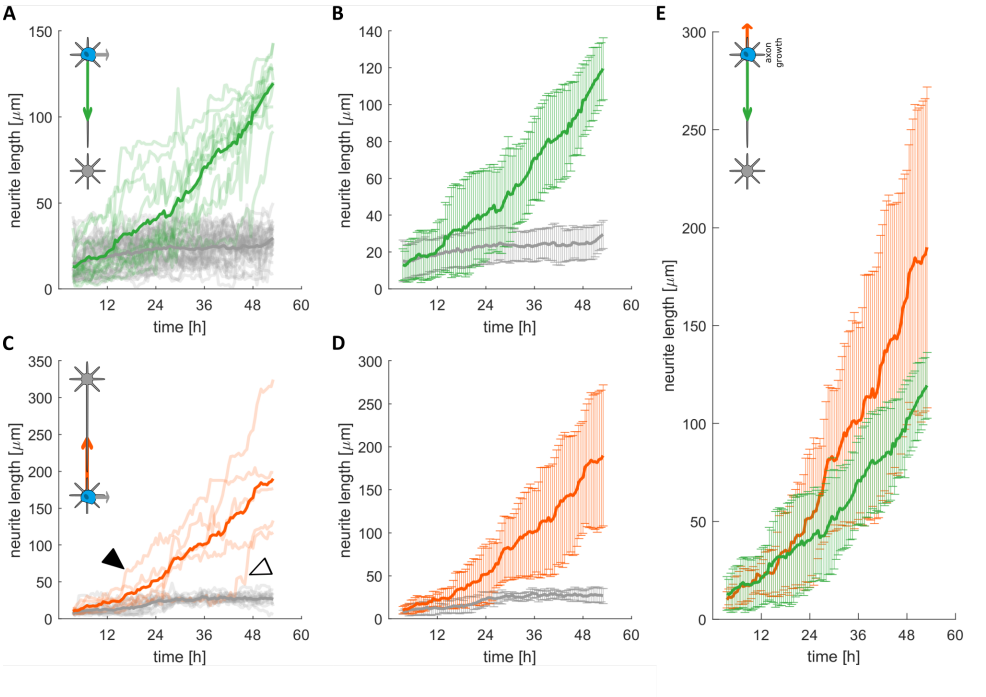


**Figure 4.17:** Neurite lengths over time for cell somata on nodes. A,B. 11 cells (47 neurites: 11 axons, 36 dendrites) with somata on node and longest neurite into the preferred direction were analysed for a time period from 3.5 h to 53.5 h after cell seeding. C,D. 5 cells (18 neurites: 5 axons, 13 dendrites) with somata on the node and the longest neurite elongating into the wrong direction were analysed. The longest neurite is displayed in shaded green (right direction) or orange (wrong direction), the other neurites are represented in shaded grey. The flashy graphs represent the average lengths of the corresponding neurites.

direction already overcame this gap for any reason in the first hours and thus, has in sum a longer line to elongate. It is not clear why some neurites can overcome a gap in the pattern quite fast (Figure 4.17.C, black arrow), while others remain short for almost two days and then suddenly jump over the gap and rapidly elongate (Figure 4.17.C, white arrow).


**Figure 4.18:** Inhomogeneities in the transferred protein patterns. Protein pattern is visualised via the FITC fluorophore that is covalently linked to the PLL. Orange arrows indicate a bad protein transfer that resulted in a blank area without protein. White arrows indicate smeared protein.

Inhomogeneities of the stamped proteins might be one potential reason. Figure 4.18 shows different issues that might occur with µCP: We see areas of low protein transfer (visualised with FITC) as marked with orange arrows. Moreover, if the stamp with the ink is not dried properly we see "smeared" pattern transfer as marked with white arrows. Even though the technique of µCP is a comparably simple method, application errors might happen and result in imperfect protein patterns on the substrates.

Another reason might be, that the other neurites already chose the short lines and the one in the vertical position feels the protein pattern over the gap with the finger-like projections (filopodia) in the growth cone. The growth cone undergoes highly dynamic changes during the constant extension and retention process. Especially the actin filaments within the growth cone are important in exploring the environment.[40] Still the question remains unclear,

why some neurites seem to feel the pattern after the gap earlier. However, the number of cells imaged for these thesis (N = 16) is too small to analyse whether the protrusion is random here. Moreover, the high standard deviation of the growth rate of cells elongating the axon into the wrong direction has to be considered.

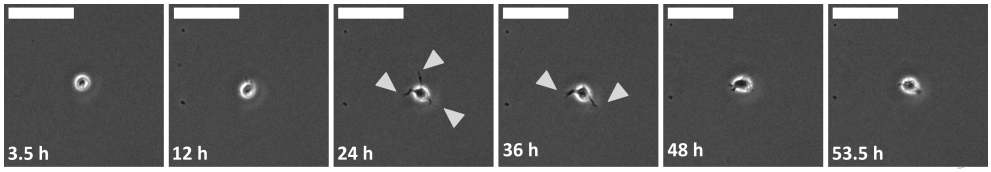


**Figure 4.19:** Neurite growth over time for one cell on unpatterned area. After 12 h we see short filopodia and after 24 h small processes that extend and retract over the following hours. Scale bar 50 µm.

Some neurons on uncoated and homogeneously coated area were analysed in order to compare the "restricted" neuronal growth with the "natural" growth. Figure 4.19 shows a neuron on an unpatterned surface. This neuron is showing some first filopodia after 12 h in culture. After 24 h we see three processes extending. These processes retract and extend over the following hours.

Figure 4.20.A and B show neurite elongation over time of neurons attached to a non-coated glass surface represented in a graph. Neurite lengths vary from some few µm to approximately 40 µm with an average of 10 µm. Also here a constant protrusion and repulsion is characterizing the elongation patterns. Interestingly, all of the neurites seem to have a similar length and non of them is exceeding or elongating faster than the others. Figure 4.20.C and D depict the neurite growth of neurons on a homogeneously coated area. Some neurites constantly elongate becoming the longest neurites (reaching approximately 86 - 156 µm with an average of $124 \pm 24$ µm) while others remain comparably short (10 - 50 µm with an average of 30 µm). This corresponds to a net axon elongation rate of $55 \pm 11$ µm/day on a homogeneously coated surface.

While the neurons on the unpatterned area stay unpolarised, the neurites

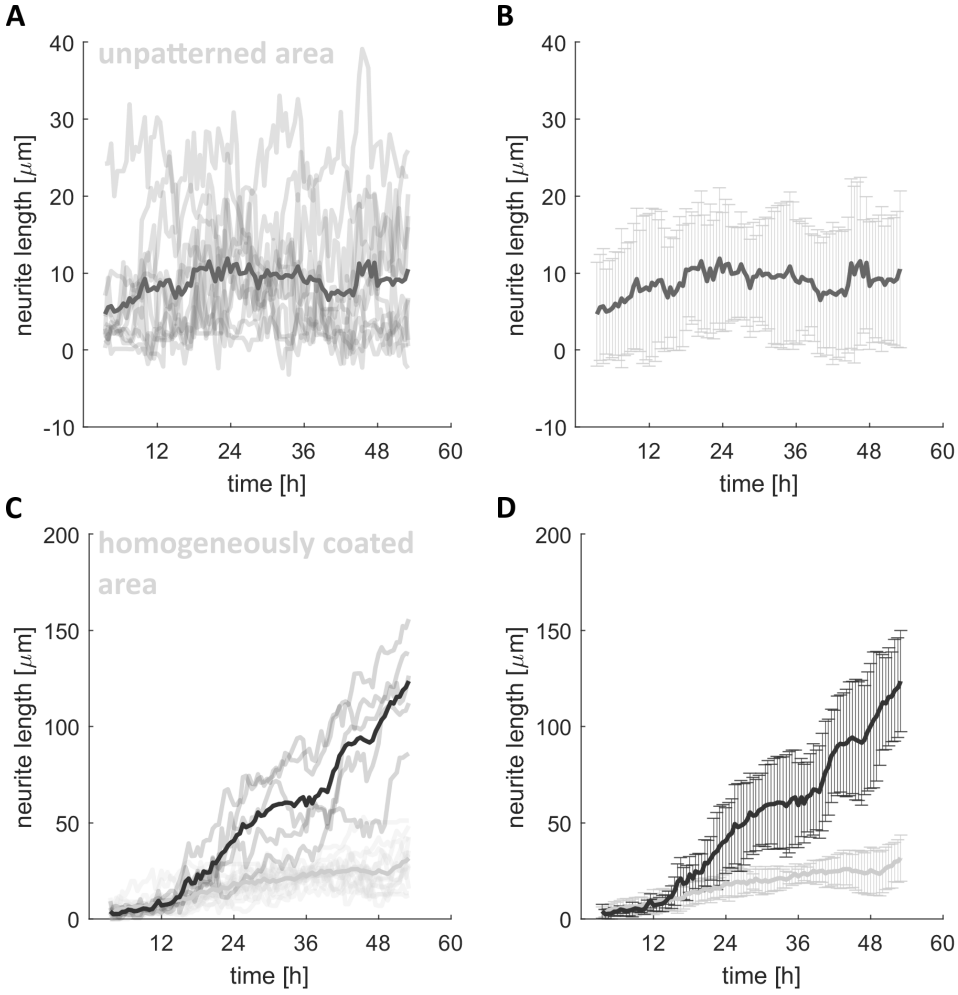


**Figure 4.20:** Neurite growth over time for cells on unpatterned and homogeneously patterned areas. A,B: 4 cells (11 neurites) on unpatterned substrate area. B,C: 5 cells (19 neurites: 5 axons, 14 dendrites) on homogeneously coated substrate areas. The flashy graphs represent the mean of the corresponding neurites.

on the homogeneously coated pattern all show a polarised appearance after 53 h. Uncoated bare glass surfaces are unattractive for neurons to grow, since they do not provide any molecules or groups to attach to as surfaces coated with proteins and peptides do. Thus, the extending neurites keep protruding and repulsing but do not receive any positive signals and remain short and unpolarised.[163,40]

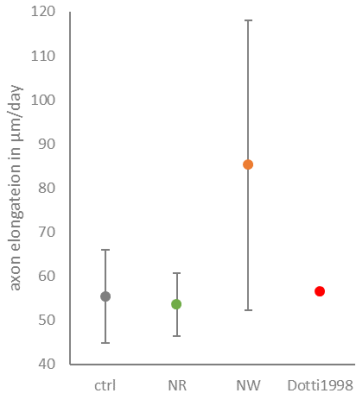


**Figure 4.21:** Comparison of axon elongation rates. Ctrl: homogeneously coated substrate. NR: Neuron located on the node of the StS pattern and elongating the axon in the right direction. NW: Neuron located on the node of the pattern and elongating into the wrong direction. Dotti1988 shows the corresponding calculated value according to Dotti et al.[43]

Comparing the axonal net elongation rate of neurons grown on homogeneously coated area and on patterned areas, we do not see a differences in the rates between the homogeneously coated (CTRL) and the NR (axon growing into the right direction) neurons (as summarised in Figure 4.21). Dotti et al. reported an axon elongation rate of hippocampal neurons of 40 µm for the first DIV and 70 µm for the following few days. This corresponds to an average rate for our observation period (0 - 53.5 h) of 57 µm/day which is consistent with the observed elongation rates for CTRL and NR. NW shows a higher rate, however with a high standard deviation.

**Soma movement over time** As already mentioned in the previous sections not all somata are located on the nodes of the pattern. While analysing the time lapse imaging experiments some somata attracted my attention, that were moving and changing their location along the pattern. Figure 4.22 shows neurons with somata located on the nodes (blue graphs and labelled with a "N") and or on the lines (yellow graphs and labelled with a "L"). Those graphs representing cells with the axon growing into the right direction are marked with a green arrow in the schematics in the upper left corner and labelled with an "R" while axons elongating into the wrong direction are marked with an orange arrow and an "W". Supplementary graphs with soma and neurite positions over time are presented in Figure 8.5 and Figure 8.6 in

chapter 8.

All somata are changing their location along the pattern over time. Looking at the NR plot, 3 somata stay on the nodes while the other 3 somata move upwards. The NW plot shows a reverse image: 3 somata stay roughly on the nodes while the other 3 move downwards. The maximal net movement is 21 µm. The LR plot shows 4 somata staying roughly at the same position at the end of the experiment as at the beginning. The two other somata move upwards, into the opposite direction as the axon growth. The LW plot depicts one soma keeping its position, 4 somata moving downwards and one soma moving upwards.

In sum 12 somata move into the opposite direction than the axon elongation, one moves into the same direction as the axon grows and 11 somata stay

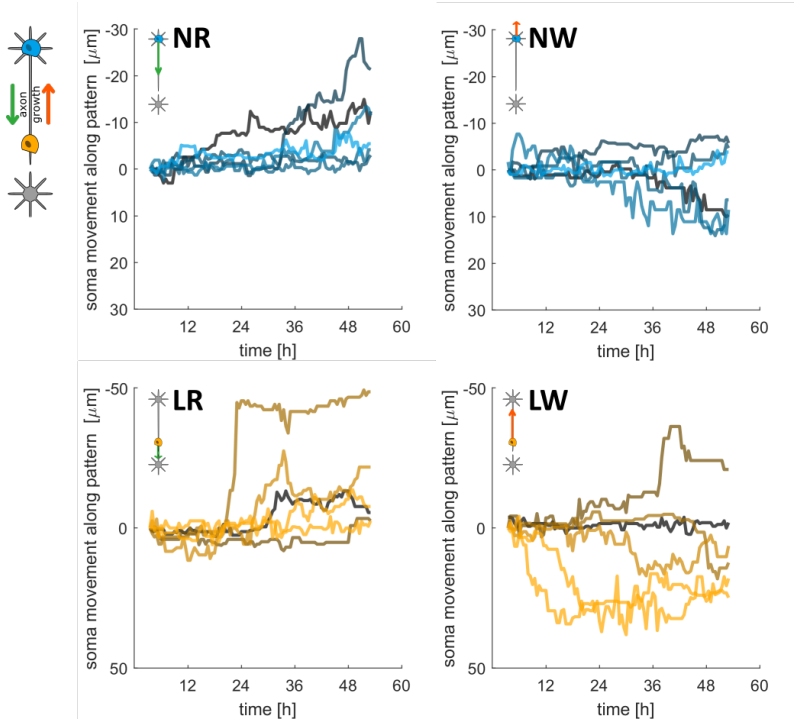


**Figure 4.22:** Soma movement over time. Blue represents somata on nodes (N) and yellow somata on lines (L). The outgrowth direction of the longest neurite is displayed in the top left corner of each plot: green for right (R) and orange for wrong (W). N = 6 cells per plot.

roughly at the same position.

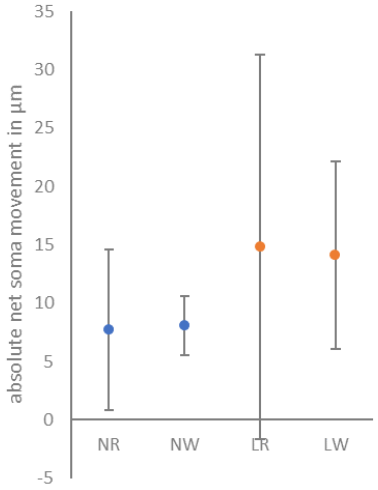


**Figure 4.23:** Mean net soma movement. Somata on the node are displayed in blue (NR, NW) and somata on the line in orange (LR, LW). Error bars mark standard deviation. N = 6 per mean value.

The absolute net soma movement was 2 - 21 µm, 5 - 12 µm, 3 - 49 µm and 2 - 25 µm for NR, NW, LR and LW respectively. An interesting observation is, that the maximal net movement of the somata located on the lines (49 µm) is bigger than the maximal net movement for the somata located on the nodes (21 µm). The mean net movement is depicted in Figure 4.23 and is $8 \pm 7$ µm, $8 \pm 3$ µm, $15 \pm 16$ µm and $14 \pm 8$ µm for NR, NW, LR and LW respectively.

One possible explanation for the difference in net soma movement is that the other neurites of the cells located on the nodes elongate in all possible directions due to the star shaped pattern. Thus, the other neurite might stabilise the soma by counteracting or inhibiting pulling forces.

A similar phenomenon - soma movement into the opposite direction than the axon elongation - was observed for excitatory neurons in the developing cortex. Here, newly born neurons elongate one process after a period of non-polarity, maturing into an axon. One other process becomes the dendrite and has a leading function: elongating towards the pia and followed by soma migration towards the leading process.[130] 70 - 80 % of cortical neurons in rodents are excitatory neurons. In the experiments only 50 % of the neurons showed a soma movement away from the axon elongation direction. This might have several reasons. First, the natural environment of neuronal polarisation is way more complex with multiple mechanical cues (high cell

density, extracellular matrix), chemical gradients and others. The orchestration of all factors influences the neuron development and polarisation. With the patterns we only influence the chemical cues - one single factor. Second, it has to be further analysed whether the cells moving their somata into the opposite direction than axon elongation are excitatory neurons. Third, the sample analysed for this section of the thesis was rather small ($N = 24$), so one has to be careful about the statistical power.

11 of 24 cells show a rather weak soma motility. It is reported in literature, that inhibitory cortical neurons show a low soma motility. Approximately 20 - 30 % of the cortical neurons is comprised of inhibitory neurons.[130] The observed share in the experiments reported here is higher (46 %). Again, the topography is only one of many parameters influencing neuronal polarisation and development *in vivo*.

Furthermore, only one out of 24 neurons (4 %) shows a soma motility toward the axon.

In summary, we observed soma movement either towards axon elongation (4 %), opposite the axon elongation (50 %) as well as no considerable net motility (46 %). Soma movement direction seems to be independent of the initial soma position on the pattern (node or line). Soma motility on the lines seems to be higher than on the nodes.

## 4.3 Summary and discussion

As demonstrated by the results in this chapter, neuronal polarisation is highly sensitive to external physical and especially topographical constraints. Thus, development of individual neurons can be controlled by using different pattern designs. In this chapter it was shown, that soma position as well as neurite elongation direction can be controlled with the chosen pattern geometries. Moreover, soma position influences the axon growth direction.

**Soma positioning** A pattern comprised of nodes and connecting lines was chosen to reduce the network complexity and control soma position. With the Xgrid pattern 6.5 times more somata (22 %) were located on the nodes than would be expected with a random distribution. Thus, the node pattern design characterised by a greater round area successfully influences the soma position on the pattern. However, also the intersections showed more somata than expected with a random distribution. This is indicating, that even two crossing lines are already enough to influence soma position. This observation supports the hypothesis, that a greater area for soma adhesion (somal contact area) attracts neuronal somata. Approximately 50 % of the nodes were covered with cells. For future experiments a pattern design with thinner lines might decrease the number of somata on the lines.

Soma position was also successfully controlled with the star patterns. Also here, more somata were located on the nodes than would be expected with a random distribution.

Various effects might influence soma position on pattern including the node pattern area as a fraction of the total pattern area. This hypothesis is supported by the fact, that the longer star pattern versions show a lower proportion of somata on nodes than the short versions. The Xgrid pattern has a lower fractional node area. On Xgrid an even lower number of somata on nodes was observed. However, the distribution cannot be solely explained by the fractional area. Moreover other factors as number of lines surrounding the

soma or somal contact area might influence soma position. This is consistent with the findings of Corey et al.[29] They reported an increasing compliance to nodes with increasing node diameter, with the highest compliance on a node of 20 µm diameter.
For future experiments a pattern design with thinner (as for the star patterns) and shorter lines (reduced fractional line area) might be beneficial for soma positioning. A potential future design is outlined in section 4.4.

**Soma motility** The analysis of the neurons on the star patterns revealed a movement of the somata along the pattern. Half of the neurons moved their soma into the opposite direction than the axon elongation, approximately 46 % roughly stayed at the same position and 4 % moved in the same direction as axon elongation. Net soma movement was increased for neuronal somata located on the lines compared to the net movement of the somata on the nodes. This observation supports the hypothesis, that additional lines for neurite elongation stabilise the soma position. Thus, the number of lines should be considered in the pattern design. Additionally, soma motility is influenced by intrinsic cell properties as the neuronal subtype.[130]

**Neurite polarisation** Asymmetric pattern designs as the star patterns successfully control neurite elongation direction. The star patterns are characterised by a node, multiple short lines and one long line. The guiding efficiency was observed to be highly dependent on the neuronal soma position on the pattern.
Neurons with their somata on the node of the pattern preferably elongated their axon into the right direction (up to 88 % of the cells) - along the long line of the star patterns. The effect was significantly bigger for the long than for the short patterns. Furthermore, the guiding efficiency of axonal growth direction was higher for the branched than for the shooting star pattern (see Figure 4.13). Thus, the highest guiding efficiency was observed for the long branched star pattern (BL) with 88 % of the neurons with somata on the nodes elongating their axons into the preferred direction.

In contrast, for neurons with somata located on the lines approximately half of the neurons elongate the axons into the right direction and the other half into the wrong direction. The farther the soma is away from the node, the higher is the share of cells elongating their axons into the wrong direction.
Cells undergo various structural changes during neuronal development *in vitro*. Several neurites start to elongate a few hours after seeding. On an homogeneously coated substrate one of them is suddenly growing faster, breaking the symmetry, and matures into an axon.[43] On our asymmetrical pattern only one neurite is allowed to grow long due to the pattern architecture. The shorter length of the dendritic lines restricts the outgrowth and inhibits axonal specification, thus promotes development into dendrites. The long axonal line is long enough and straight, thus promoting axonal specification.[43,61] The guiding effect of asymmetric patterns was also observed by Yamamoto et al.[163] The results presented here show, that soma positioning on the pattern is crucial for the later axon elongation direction. As mentioned in the previous paragraph, soma positioning is highly depending on the pattern geometry and its feature dimensions. Somata located on the nodes or close to the nodes preferably develop their axons into the intended direction. Moreover, longer lines for axons increase the guiding efficiency even further. However, some cells with their somata on the nodes (depending on the pattern 12 - 25 %) grow their axon into the wrong direction despite the gap in the protein pattern. Potential reasons might be inhomogeneities in the transferred micro patterns or intrinsic cellular properties as the extended outreach of the growth cone over the protein gap.

**Neurite elongation over time** For neurons with somata on the node and growing the axon into the right direction (NR) elongation rate was observed to be $54 \pm 7$ µm/day. This value is consistent with the rate of axon elongation on homogeneously patterned substrates ($55 \pm 11$ µm/day) and the reported rate of dissociated hippocampal neurons of 56 µm/day.[43]
The average elongation rate of neurons with somata on the node and growing their axon into the wrong direction (NW) is higher: $85 \pm 33$ µm/day. First,

we have to note the high, standard deviation as well as the low sample size analysed for all elongation rates ($N_{NR} = 11$; $N_{NW} = 5$; $N_{ctrl} = 5$). Also, the NR-neurons are restricted in axon growth at the end of the pattern (after 160 µm). For the NW-neurons, that overcame the gap either due to imperfect protein transfer or other intrinsic reasons, the protein path for the axon was slightly longer (around 200 µm). Only one out of 5 axons exceeded this length (see Figure 4.17), which is increasing the average value dramatically due to the low sample size. Here, further experiments are needed to get a reliable statistical statement.

In general, I would expect a higher axon elongation rate on patterned substrates with a straight line for the axon than on homogeneously coated substrates, because of the predefined growth path. Additionally, I would expect the break of symmetry earlier on asymmetrical patterns than on homogeneous surface, due to the predefined asymmetry. These hypothesis have to be tested in future experiments and are out of the scope of this thesis. A proposed next step could be the analysis of neurons growing on the patterns that were not analysed here (BS, StL and BL). After that a comparison of axon elongation rates between short and long patterns could give a deeper insight into the elongation dynamics and whether the designation of a neurite's faith becoming a dendrite or axon is influencing the break of symmetry or elongation rate.

## 4.4 Conclusion and outlook

Concluding, with the chosen pattern designs the soma positions as well as the axon elongation direction were successfully controlled. The pattern design and its features are crucial for an efficient network engineering. A combination of thin lines and bigger areas is able to impact soma position. Here, the fractional pattern area of nodes and lines is one important factor for a successful soma placement. Moreover, the number of lines surrounding the node might stabilise soma position and prevent soma motility. While a design with two lines might increase motility and can be utilised for experiments where soma movement is desired.

An asymmetric pattern design as the star patterns promotes axon elongation. Here, soma position on the pattern influences the elongation direction. Somata close to nodes develop their axons into the right direction. The longer pattern version has a higher guiding efficiency if the somata are placed on the nodes, however due to the lower node to line area ratio less cells are located on the nodes. Thus, both, the short and long pattern designs showed a similar axon guiding efficiency of 60 - 65 % if all cells on pattern are considered. Overall, the star pattern design can be used to create directional single cell networks. However, to increase the structural directionality an optimised design might be considered.

Therefore, different pattern modifications can be considered: The first add-on would be removing the two lower short lines on the star patterns. In theory this might result in an even higher number of axons specifying into the right direction, because highest mechanical tension is reported to promote axonal specification.[128] Although the branched star patterns showed a higher guiding efficiency than the shooting star patterns, a further optimisation of the short dendritic lines of the StS and StL patterns might be of interest. The short straight dendritic lines might be replaced by curved lines with a rather small diameter.[128] In order to improve soma positioning and thus, axon guiding efficiency, a line thickness of 1 µm might be considered, which

would increase the fractional soma area. Additionally, a polygonal shaped soma node might increase the guiding of neurites. Jang and Nam observed an induced neuritogenesis at the angles of polygonal shaped structures.[76]

Figure 4.24 shows an optimised pattern design that combines the mentioned attributes like line thickness, node geometry and structure length.

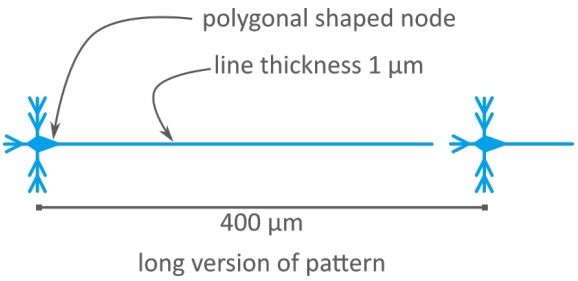


**Figure 4.24:** Sketch of an optimised pattern design for single cell connectivity. Attributes like polygonal shaped node, thinner lines and long version of the pattern might increase the control over neuronal substructure development even further.

In order to verify the observations and further analyse the hypotheses extensive time lapse experiments are necessary. These include additional time lapse experiments with StS cultures for statistical significance as well as experiments with the other three patterns (StL, BS and BL) to investigate the impact of the axonal line length and the dendritic line geometry and soma motility on the different pattern positions.

Concluding, this chapter examined the effects of pattern design onto neuronal development. The deeper understanding of the design features enables engineering suitable micro patterns and hereby create single cell neuronal networks with defined structural connectivity. This contributes to an improved usability of µCP in the neuroelectronics toolbox. Moreover, the findings of this research can be adapted when engineering neuronal networks in 3-D, for example by using microfluidic chambers.[54]

# Chapter 5

# Functionality of single cell networks

In the previous chapter we saw that neuronal growth and polarisation can be successfully controlled via single cell patterns as the Xgrid or star patterns. Single cell separation and directional polarisation enables investigation of individual neurons.

The object of this chapter is to analyse whether the cells within a single cell network show neuronal activity.

For that calcium imaging can be used, where intracellular $Ca^{2+}$ concentration is monitored over a time period. An increase in $Ca^{2+}$ concentration is associated with electrical events.[5] The advantages of this method are already discussed in chapter 2 and are mainly the high spatial resolution which enables imaging individual cells up to even individual neurites as well as the simplicity of this method. However, the temporal resolution of $Ca^{2+}$ imaging is lower compared to electrical methods. The velocity of electrical signal transmission in neurons is approximately 1 m/s.[72] In the following experiments an area with a width of 1.66 mm was imaged. A signal transmitted from the the outer left pixel to the outer right pixel would result in a transmission time of approximately 1.66 ms. Images were taken every 5 ms which is not sufficient to detect a delay on µm scale, and thus the directionality of the network. But other characteristics of the $Ca^{2+}$ transient such as am-

plitude, duration as well as the interval between two $Ca^{2+}$ events can be used to investigate the network's functionality. They all can give a deeper insight into the neuronal activity because they provide indirect information about the number of electrical spikes, bursts and activity pauses of neurons. Additionally, these measures indicate the neuron's electrical activity.[26,152]
Another way to investigate neuronal activity is using multi-electrode arrays (MEAs). Electrical measurements with MEAs provide a lower spatial resolution due to a limited number of sensors. However, a high temporal resolution enables detection of individual action potentials and thus, signal propagation directionality.

# 5.1 Xgrid patterns

## 5.1.1 Long term stability and activity

Single cell separation reduces the level of complexity and also limits the number of connections. Even though this is desired here, one has to analyse whether the reduction impacts the network activity, since neurons need a number of input signals above threshold for an output. Additionally, the total cell number is highly reduced in single cell patterned networks. The lower cell density might go together with some negative effects as reduced concentration of released growth and differentiation factors. A lower concentration could reduce the network's maturation speed and thus lead to unhealthy or non-active neuronal cultures.[53,14] To test the network's stability and activity, neuronal cultures on the Xgrid pattern were grown for at least 14 days. Networks were analysed via immunofluorescence, optical (Calcium imaging, GCaMP3-cyt) and electrical (MEA) measurements.

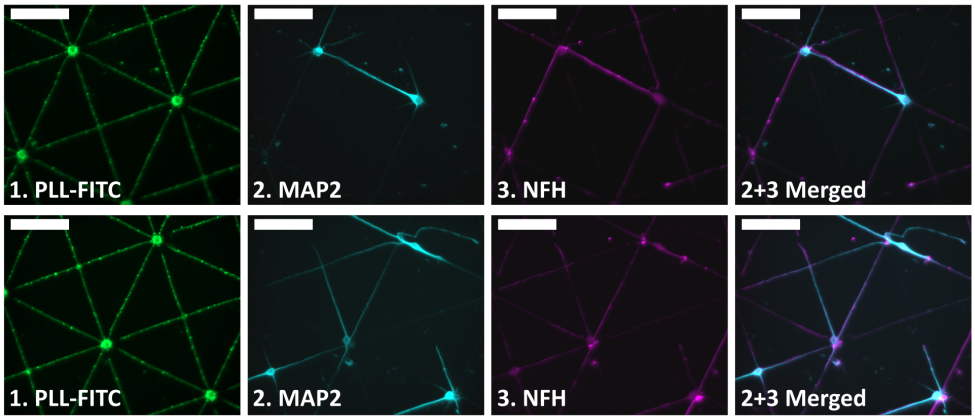


**Figure 5.1:** Immunofluorescence images of neurons on X-grid pattern. Two different areas are depicted. DIV 14. Scale bar 100 µm.

**Long-term stability** Figure 5.1 shows an immunofluorescently labelled neuronal Xgrid cultures at DIV 14. Neurites grow over distances of minimum

200 µm and are labelled MAP2- and NFH-positive indicating that the cells are mature and polarised.

## Network activity

**Xgrid networks and calcium imaging** A GCaMP sensor (GCaMP3-cyt) was genetically introduced into the cells to analyse neuronal activity.

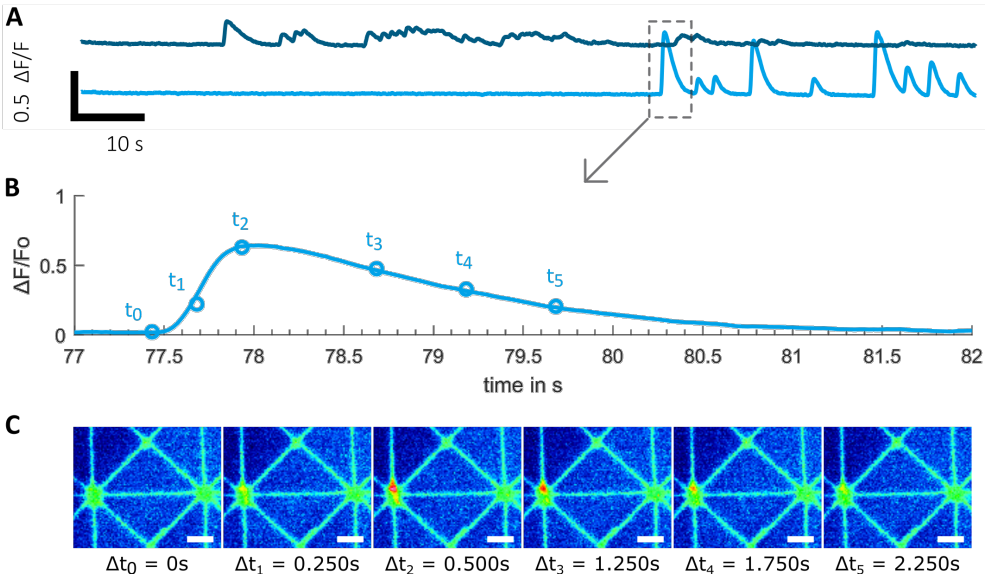


**Figure 5.2:** $Ca^{2+}$ signal of network on X-grid pattern. Ca sensor: GCaMP3-cyt. A. Fluorescence intensity over time of two ROIs. B. Zoom in of one transient. C. Microscopic images at different time points ($t_0$ - $t_5$ in plot B, $t_0$ is set to 0) displayed in a rainbow LUT. Protein pattern is FITC-labelled. Scale bar 50 µm.

In Figure 5.2.A presents intensity changes over time of two cells. One transient that is marked with a box is enlarged in B. The fluorescence pictures at the time points $t_0$ to $t_5$ are depicted below in C in false colours from blue to red with red as the highest intensity. The protein pattern was fluorescently labelled with FITC for visualisation purpose. Even though this helps to analyse whether the neurons are growing on the pattern, the background fluorescence pattern masks the fluorescence of the $Ca^{2+}$ sensor. Thus, only

sensor intensities higher than the pattern fluorescence intensity can be detected. Additionally, GCaMP3 is characterised by rather weak intensities compared to other $Ca^{2+}$ sensors as reported by Chen et al.[26] The combination of both, a higher background fluorescence due to the fluorescently labelled pattern and lower fluorescent intensities of the sensor result in a lower SNR and thus limits the number of active cells that are detectable. Nevertheless, the traces show multiple $Ca^{2+}$ transients with different amplitudes and durations, indicating active neuronal networks.

**Xgrid on MEA** Soma positioning and reduction of neuropil contamination is especially interesting for extracellular electrical recordings as often performed with MEAs.

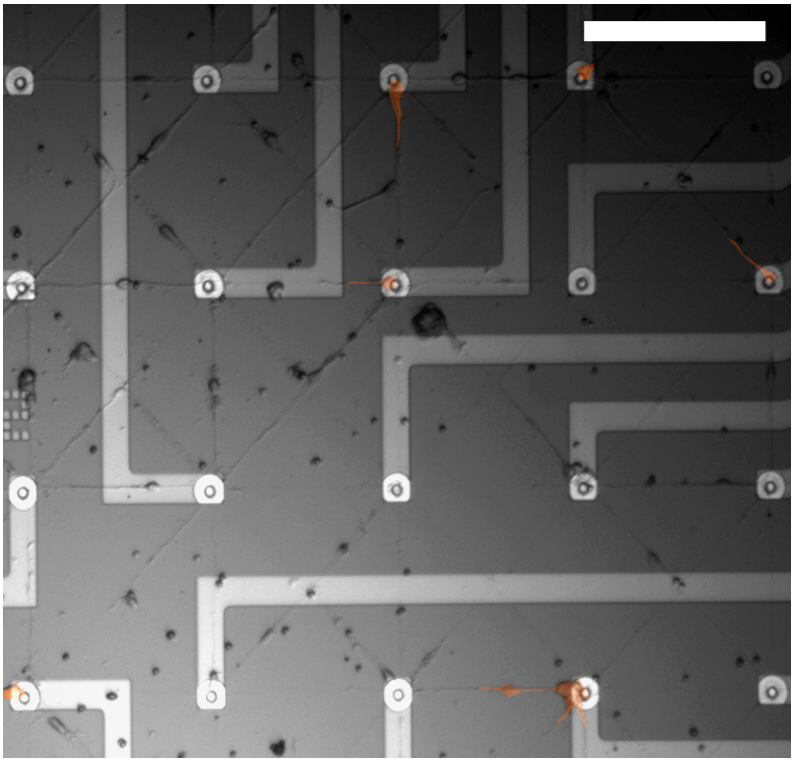

**Figure 5.3:** Xgrid pattern on MEA. Some exemplary cells are highlighted with light orange. DIV 14, Scale bar 200 µm.

Figure 5.3 shows neurons cultured on a Xgrid patterned MEA for 14 DIV. We

see a healthy looking culture with somata located on or close to the electrode openings, but also on the lines and intersections. Some exemplary cells are highlighted with orange for visualisation purpose. Overall, we see cells almost exclusively growing on the Xgrid pattern with defined architecture and reduced complexity.

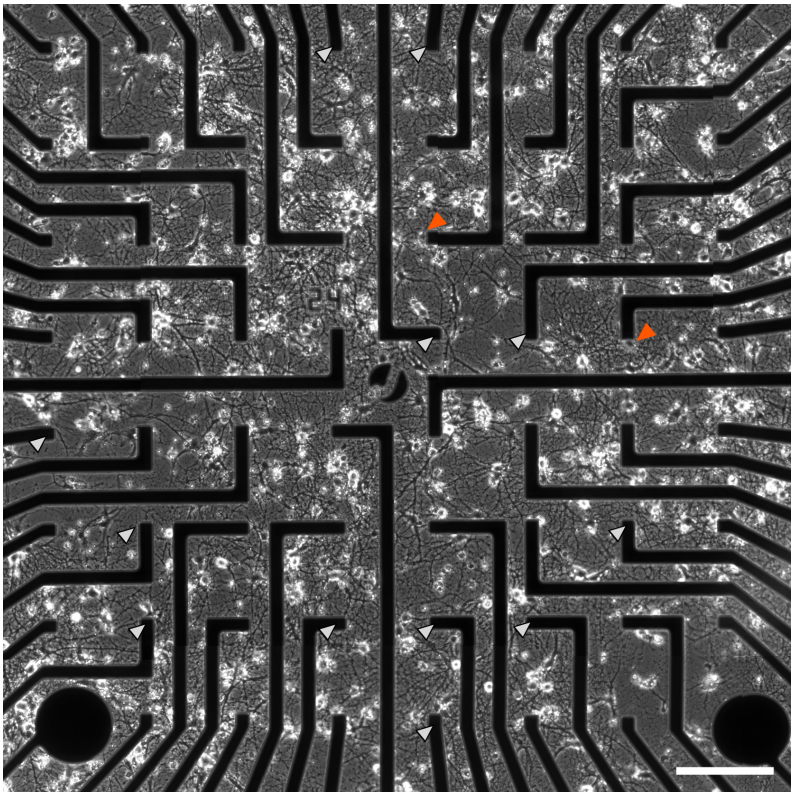

**Figure 5.4:** Homogeneous neuronal culture on MEA. Exemplary electrodes without neuronal somata are marked with a grey arrow while electrodes with somata close to but not onto an electrode are marked with an orange arrow. DIV = 30. Scale bar 200 µm.

For comparison an homogeneous neuronal culture is displayed in Figure 5.4. Here, we see many cells growing randomly. The image is taken at an inverse microscope setup thus, feed lines hide the actual electrode openings. Nevertheless, we can carefully estimate where we expect somata because of the network distribution. We see many electrodes without somata on them

as marked with a grey arrow. Some electrodes have somata close to the electrode openings but not on them (orange arrow). Additionally, we see a highly matured neurite network spanning the whole electrode area which might cause a signal contamination.

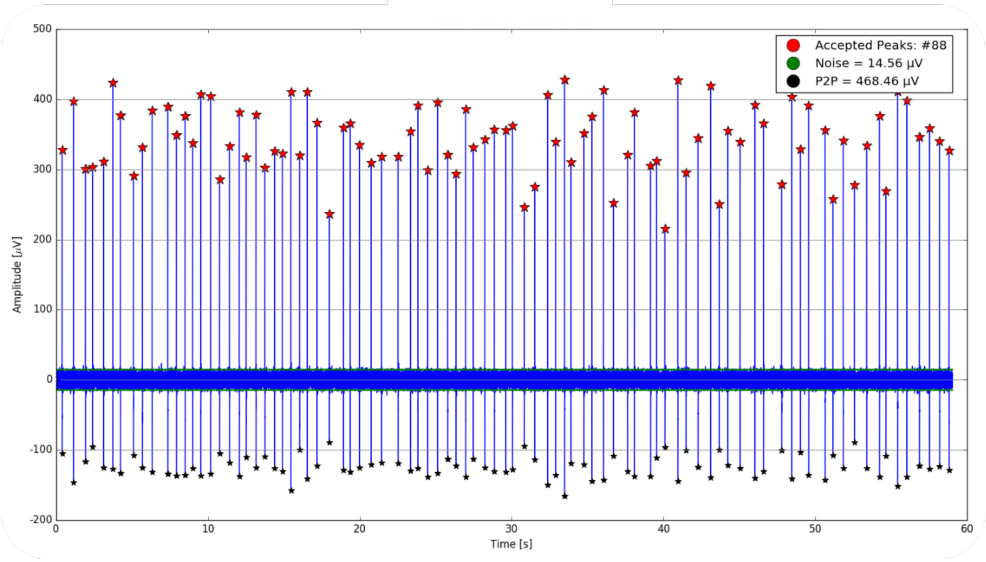


**Figure 5.5:** Exemplary MEA recording of neurons on Xgrid pattern. Experiments were performed in collaboration with Johannes Lewen, where I provided the patterned cultures on MEA and he performed the electrical recordings.

Electrical recordings with MEA of neuronal cultures growing on Xgrid pattern as presented in Figure 5.3 were performed in collaboration with Johannes Lewen. Figure 5.5 shows the time traces of one electrode with many peaks. The exemplary time trace shows a characteristic high signal to noise ratio (SNR) of 32 which is one major advantage of the nanocavity-MEAs.

### 5.1.2 Summary

Investigation of neuronal cultures grown on Xgrid pattern showed polarised and matured neuronal networks from DIV 14 onwards. Furthermore, we observed robust neuronal activity with $Ca^{2+}$ imaging as well as electrical recordings with MEAs. Despite the reduced complexity we have developed

an active neuronal networks with controlled geometry. These results are consistent with the literature, where groups were able to cultivate low density, electrically active neuronal cultures.[167,162]

However, only few cells showed a change in fluorescence. First, the fluorophore utilised to label the protein pattern should be of an other spectrum than the emission spectrum of the GECIS. Another possibility is to use an unlabelled protein solution. Moreover, GCaMP3 is characterised by a low SNR compared to other calcium sensors.[26]

## 5.2 Star patterns

As presented in the last section, the combination of the GCaMP3 sensor with a FITC-labelled protein pattern resulted in a masked GECI signal. Thus, for the following experiments an unlabelled protein solution (PLL without FITC) was utilised to transfer the star patterns onto the glass substrates. Additionally, the calcium sensor GCaMP6f was genetically introduced into the neuronal cultures. This sensor is characterised by a higher SNR compared to the GCaMP3 sensor and faster sensor dynamics.[26] Spontaneous neuronal activity was recorded via $Ca^{2+}$ imaging and individual $Ca^{2+}$ transients were analysed.

In sum 54 neurons growing on the star patterns were analysed at DIV 15 - 18. The fluorescence change over time of these cells is depicted in Figure 5.6. This picture shows the variety of transient durations, amplitudes and frequencies. A dot plot marking the peaks of the transients can be found in chapter 8.

Transient shapes show a fast rise and a slower decay as is reported for typical $Ca^{2+}$ transients.[26]

**Decay time** To analyse the decay time transients of cell 1 (bottom time trace in Figure 5.6) were selected. This cell was chosen because the amplitudes of the transients showed a low data dispersity ($IQR = 0.1\,\Delta F/F_0$). The median $\Delta F/F_0$ of cell 1 is 0.2, a value that is consistent with the reported $\Delta F/F_0$ magnitude for a single AP analysed via GCaMP6f.[26]

Figure 5.7 shows in grey a total of 92 transients extracted from the time trace. The amplitude of individual peaks was normalised and aligned in time. An average of all transients is displayed with the orange line. The average transient show a typical shape with a fast rising ($t < 0\,s$) and a slower decaying part ($t > 0\,s$). It is noticeable, that the peaks are not well separated, because the decaying and rising part are visible at the transient edges. Still the average transient data points ($t = [0, 0.2]$) could be used to

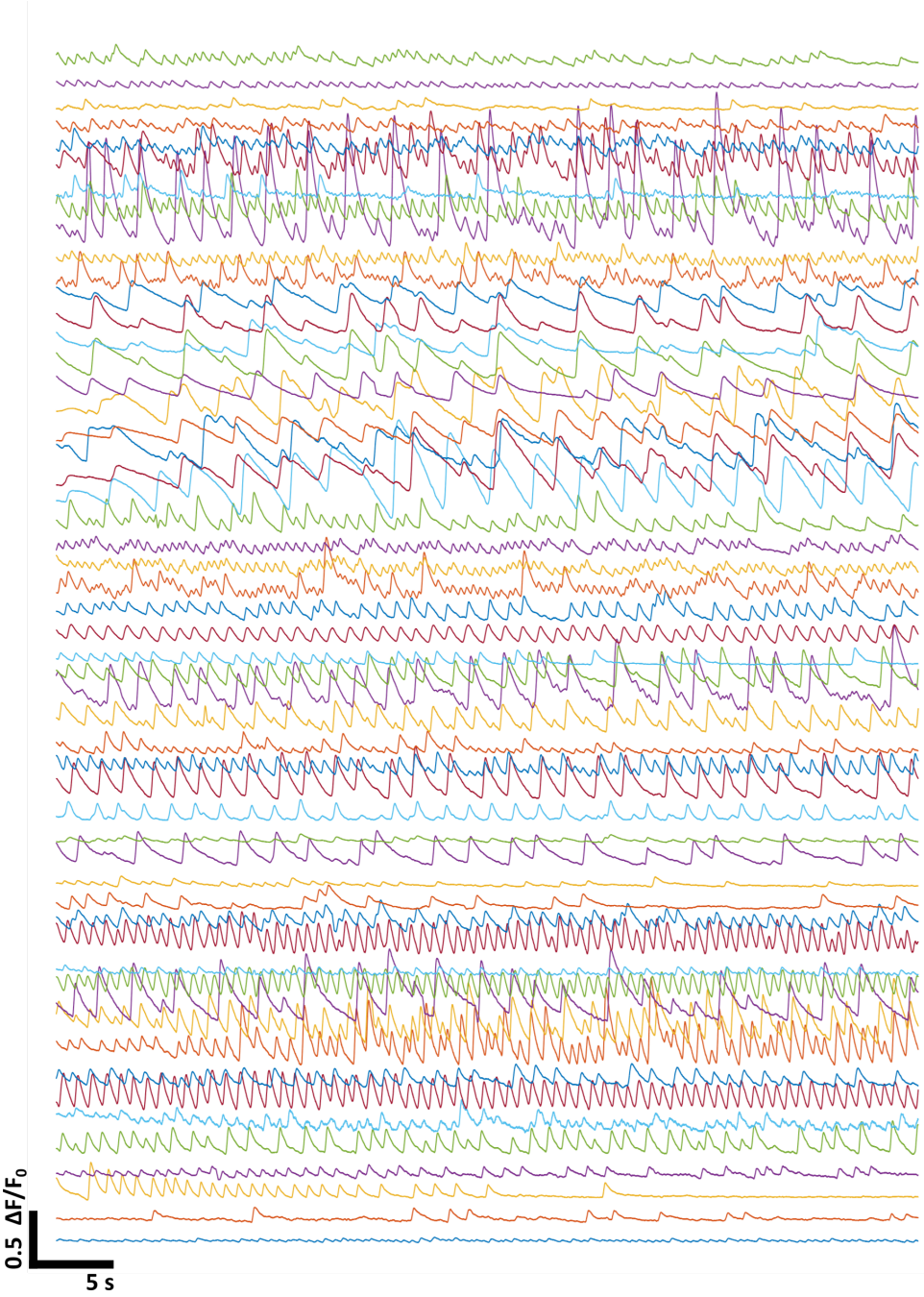


**Figure 5.6:** Calcium imaging time trace of neurons grown on star shaped patterns. ROIs were drawn around the neuronal somata. Imaging was performed at DIV 15 - 18 and DPT 8 - 11, N = 54 cells.

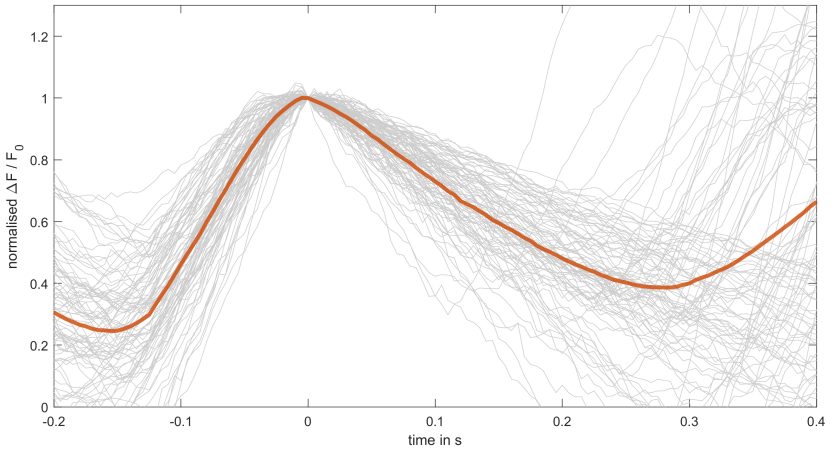


**Figure 5.7:** Average $Ca^{2+}$ transient. Peaks from cell 1 were extracted. For each transient, amplitude was normalised and aligned in time. Individual peaks (grey) were averaged (orange). N = 92 transients.

calculate the decay time constant, which is 3.8. This corresponds to a half decay time of $t_{1/2} = 0.183\,s$ and a mean lifetime $\tau = 0.264$. The exponential fit is depicted in Figure 8.7 in chapter 8. The $t_{1/2}$ value is consistent with the half decay time reported by Chen et al. for a single AP.[26]

**Spontaneous event amplitudes** The amplitude of a $Ca^{2+}$ transient is impacted by neuronal activity but also artefactual factors like differing sensor concentrations between cells. Thus, to analyse and compare the amplitude between different experiments the fluorescence change ($\Delta F$) is expressed relatively to its initial fluorescence ($F_0$): $\Delta F/F_0$.

Amplitudes of the different cells were analysed. The distributions of the magnitudes are depicted in Figure 5.8 in a box plot representation. The box indicates the 25th and 75th percentiles while whiskers indicate the most extreme data point not considered as outliers (that are represented as yellow dots). Orange lines display the medians. $\Delta F/F_0$ values vary from close to zero to 140 %. The distributions of individual cells show different data dispersities. While some cells show a small dispersity (interquartile range,

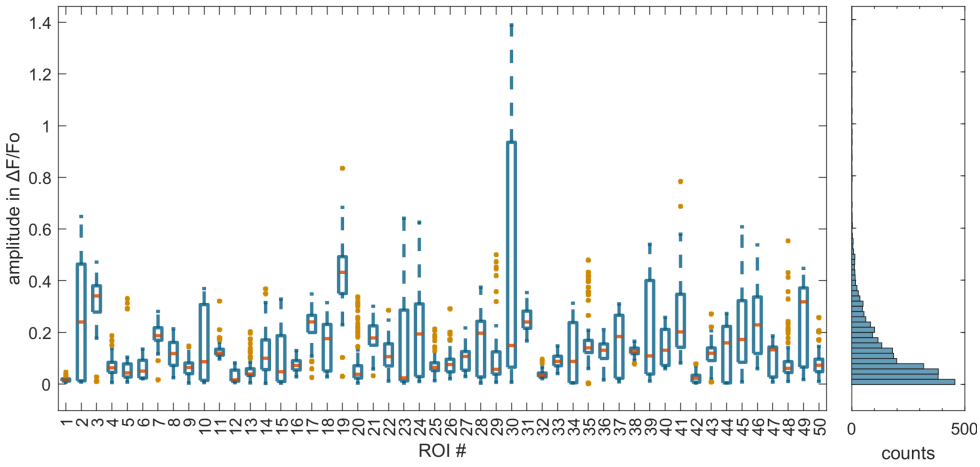


**Figure 5.8:** Amplitude distributions of cells on star patterns. Left: Box plots of amplitude distributions of individual cells. Orange lines indicate the median and box edges indicate the 25th and 75th percentile, respectively. Whiskers extend to the most extreme values not regarded as outliers. Outliers marked with yellow dots. Right: Histogram of all amplitudes. Bin size = 2 % $\Delta F/F_0$, N = 3,068 transients.

IQR) like cell 1, 11 or 32, some other cells show higher IQR like cell 2, 10, 30 and 39.

The histogram on the right side includes data points of all cells. We see a highly right-skewed distribution of amplitudes with most of the magnitudes being smaller than 37.8 % $\Delta F/F_0$ (maximum, IQR + 1.5 IQR). The median is 8 % $\Delta F/F_0$. The minimum (IQR - 1.5 IQR) is 0.2 % $\Delta F/F_0$.

The high positive skewness indicates, that most amplitudes have a small magnitude. Chen et al. reported a peak $\Delta F/F_0$ of around 0.1 for one single action potential and around 1 for 5 APs in a 250 ms bin. For 3 APs they reported a peak $\Delta F/F_0$ of around 0.5.[26] If we assume a similar relation for the results presented here, this would mean that almost all transients were evoked by less than 3 APs within 250 ms. Though some cells, like cell 30, show a broader dispersity with higher amplitude values which might correspond to even more APs.

A single AP resulting in a $Ca^{2+}$ transient detected by GCaMP6f is reported to have an amplitude of around 10 % $\Delta F/F_0$.[26] The median of all transient

amplitudes analysed here is 8 %. It is possible, that lower amplitudes correspond to sub-threshold potentials recorded either from the soma or from the neuropil that might surround somata. Another explanation for the small amplitude values might be that cell types show different relationships of their $\Delta F/F_0$ to number-of-AP as was described for inhibitory and excitatory neurons in layer 2/3 of the mouse visual cortex. Here, interneurons showed a lower $\Delta F/F_0$ response per AP.[88] In my experiments cultures most likely are comprised of all subtypes of cortical neurons including excitatory and inhibitory neurons. The different amplitude magnitudes might also correspond to specific neuronal subtypes.
In conclusion, the analysed cells grown on single cell patterns show a variety of calcium transient amplitudes. Because $Ca^{2+}$ amplitude is linked to the number of action potentials, these results indicate different activity patterns with varying number of of action potentials.[26,88]

**Spontaneous event durations** The duration of a calcium transient is dependent on neuronal activity as well as sensor characteristics. Upon electrical activity $Ca^{2+}$ channels open, resulting in an increase in intracellular $Ca^{2+}$ ion concentration.[5] $Ca^{2+}$ ion binding to the sensor is observed as an increase in fluorescence intensity, which is the rising part of a transient. After that $Ca^{2+}$ ions dissociate from the sensor. This process is highly dependent on the sensor properties. Intracellular ion concentration is restored by intrinsic cellular processes. These processes are represented in the decaying part of the transients. Thus, the duration of a recorded transient represents the period of the increased intracellular $Ca^{2+}$ concentration and is impacted by sensor kinetics and intrinsic $Ca^{2+}$ clearance mechanisms.[100,160,5]
Because determination of transient duration is difficult due to noisy and overlapping signals, the full width at half maximum (FWHM), sometimes also referred to as full width at half duration (FWHD) in literature, is a widely used measure.
FWHM can be used as a measure to compare durations of the transients. Due to the slower $Ca^{2+}$ signalling dynamics, high-frequent action potentials

would result in an increased intracellular $Ca^{2+}$ concentration for a longer time and consequently in a longer $Ca^{2+}$ transient without being able to resolve every single spike.[5,1]

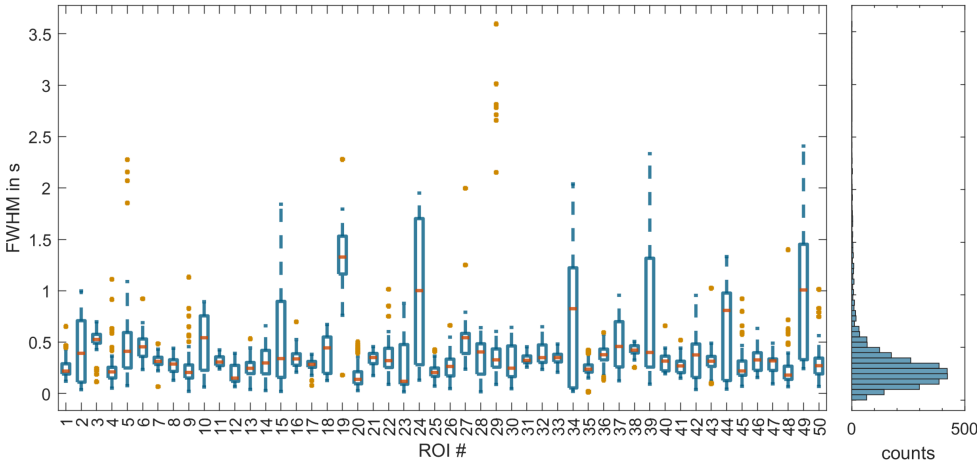


**Figure 5.9:** FWHM of calcium transients of neurons on single cell patterns. Left: Orange lines within the boxes indicate the median and box edges indicate the 25th and 75th percentile, respectively. Whiskers extend to the most extreme values not regarded as outliers. Outliers marked with yellow dots. Right: Histogram of all FWHM. Bin size = 50 ms, N = 3,068 transients.

Figure 5.9 shows the FWHM distributions of 50 individual cells in a box plot representation.

The box plot shows different data dispersities for the individual cells. While many cells show a rather low interquartile range (IQR), some cells exhibit a wider IQR such as cell 24, 34, 39 and 49. 84 % of the cells (42/50) show an IQR for the FWHM lower than 0.5 s. It is also noticeable, that most of the cells with a low data dispersity show low FWHM magnitudes (below or around 0.5 s). Only one cell with a low dispersity (cell 19) shows a higher FWHM median of 1.3 s.

The lower values of FWHM are also visible in the histogram on the right panel, which includes FWHM values of all cells. The distribution has a median FWHM of 0.277 s, the maximum not considered as outlier is 0.673 s. 6 % of the data are considered as outlier and are above the maximum value.

Even though $Ca^{2+}$ transient peaks are not able to resolve single APs of high frequent firing cells, an increased duration of the transient would indicate an increased spike rate.[88,26] As mentioned before, the transient duration is dependent on sensor properties as well as the duration of increased intracellular $Ca^{2+}$ concentration due to neuronal activity. For all experiments GCaMP6f was used, thus the main contributors to the changes in transient duration in the experiments are the intrinsic $Ca^{2+}$ clearance mechanisms and the number of action potentials in a certain time bin.
Concluding, we see different transient durations for the cells grown on single cell patterns. The FWHM of all transients shows a median FWHM of around 300 ms. For the average $Ca^{2+}$ transient of cell 1 the calculated FWHM is also 300 ms (see Figure 8.7 in chapter 8) which corresponds to a transient duration of approximately 1 s. This value is consistent with transient durations observed for one action potential with GCaMP6f.[26] Thus, most of the cells show transients that might represent only one to few APs.

**Inter-event interval** For analysis of neuronal activity the measure of inter-spike interval (ISI) is widely used. This interval is considered as the duration between two detected action potentials (spikes). The ISI conveys relevant information in neuronal signalling.[125]
In the analysis of calcium signals, the peaks might not represent individual action potentials, because the temporal resolution of $Ca^{2+}$ imaging is too low to detect e.g. high frequent APs. Thus, the interval between two $Ca^{2+}$ transient peaks does not represent the ISI known from electrical signals. Nevertheless, this peak-free period might indicate pauses in neuronal firing.[124] Hence, in the next step the intervals between two adjacent transient peaks were analysed. This inter-peak interval is referred to as inter-spike interval (ISI) in the following section.
Figure 5.10 shows the distributions of the ISIs of 50 neurons in a box plot representation. The individual cells show varying ISI distributions. Data dispersities vary from 70 ms to 2.64 s interquartile range (IQR). The average IQR is 650 ms. Most of the neurons show a lower ISI dispersity (IQR). 80 %

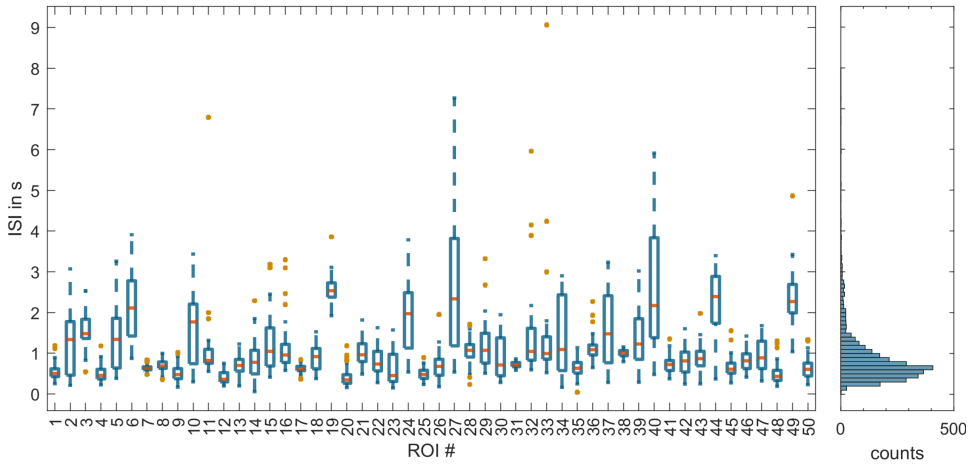


**Figure 5.10:** ISIs of cells on single cell patterns. Left: Orange lines within the boxes indicate the median and box edges indicate the 25th and 75th percentile, respectively. Whiskers extend to the most extreme values not regarded as outliers. Outliers marked with yellow dots. Right: Histogram of all ISIs. Bin size = 100 ms, N = 3,068 transients.

of the cells (40 cells) show ans IQR below 1 s. Only few cells, like e.g. neuron 10, 27 and 34 show short intervals as well as longer pauses up to several seconds. Most of the cells show activity traces with shorter pauses. 44 neurons (88 %) show a median ISI below 2 s, exceptions are e.g. cell 19 or 49.

In the right panel a histogram of all ISIs is displayed. Values not considered as outliers range from 40 ms to 1.76 s with a median ISI at 670 ms. Concluding, most of the neurons show a constant activity with only pauses of some tens of ms to 2 s.

According to literature a decaying part of calcium transients might represent time periods without any electrical activity. Spikeless activities of several seconds can occur.[26,39,102] Here we see cells with pauses of ms to some s indicating a varying patterns of neuronal activity.

Ideally, to get the activity pauses, the ISI has to be corrected for the rising time of the following calcium transient. The reported rising time for GCaMP6f transients for one action potential is around 50 ms. That means,

that the ISI times presented in Figure 5.10 have to be corrected for minimum 50 ms. Nevertheless one has to consider, that ISI might also mean, that no peaks were detected within a certain period which might be due to low SNR among various reasons.

### 5.2.1 Summary and discussion

To study whether the directional, low density networks presented in chapter 4 show neuronal activity, neurons were cultured on the single cell star patterns for minimum two weeks and the $Ca^{2+}$ sensor GCaMP6f was genetically introduced after 7 DIV. $Ca^{2+}$ imaging was performed at 15 - 18 DIV.
Multiple cells showed characteristic $Ca^{2+}$ transients, indicating that neurons are mature and show neuronal interactions and activity. 54 neurons were analysed more detailed. Multiple parameters of the $Ca^{2+}$ transient can be extracted to investigate neuronal activity. The focus of the analyses presented here is on transient amplitude, duration and the inter-peak interval. These measures can give deeper insights into changing numbers or frequency of action potential or pausing in neuronal activity.[26,152,124]
Each cell was imaged for 50 s and $Ca^{2+}$ transient parameters were analysed. The cells showed a variability in transient amplitudes ranging up to 140 % $\Delta F/F_0$, with different ranges for individual neurons. High variabilities in $Ca^{2+}$ amplitudes were already observed in dorsal root ganglion (DRG) neurons. These variabilities of amplitudes are believed to represent intrinsic differences in sensor expression between cells but also biological variation in the physiological properties of neurons.[152] The median amplitude was 8 % $\Delta F/F_0$. Chen et al. reported a 10 % $\Delta F/F_0$ transient amplitude for one action potential.[26] The transient represents an increased $Ca^{2+}$ concentration within the cell. Opening of low voltage gated calcium channels might also be triggered by subthreshold potentials. Thus, values far below the median $\Delta F/F_0$ might represent subthreshold activity. However, the neuronal cell body is mostly characterised by high-threshold calcium channels. Low transient amplitudes indicating subthreshold activity might originate from con-

tamination of the fluorescence signals from surrounding neurites.[5] In general, the amplitudes not considered as outliers showed values below 40 % $\Delta F/F_0$. Peak amplitudes of calcium transients show a dependency of the number of action potentials.[26] Thus, the results indicate that most of the transients recorded here represent single to few APs or a low frequency of APs.

The duration of transients was analysed and compared by the measure of full width at half maximum (FWHM). Most of the analysed transients were characterised by a FWHM below 1 s. The median FWHM is around 300 ms, which corresponds to a calculated transient duration of around 1 s. This agrees with the duration reported for one AP by Chen et al.[26] However, transients are characterised by a non-linear spike-to-fluorescence relationship.[5,152] This makes it difficult to estimate the number of AP that evoked the transient. Nevertheless, there is evidence, that transient amplitude is increasing with increased number of APs as well as increased AP frequency.[26,152] Additionally, a longer transient indicates an increased spike rate.[88] Hence, amplitude as well as FWHM distributions observed here indicate tonic spiking activity rather than bursting events.

GECI transients are a complex convolution of intrinsic physiologic properties, neuronal activity and sensor dynamics. Thus, intrinsic processes like diffusional or buffering properties of the ion within the cell influence the transients just like the properties of the indicator.[138] Differences in membrane excitability as well as $Ca^{2+}$ clearance mechanisms were observed between neuronal subtypes. Both determine amplitude and kinetics (duration) of $Ca^{2+}$ transients.[160,5] Therefore, one reason for the observed variability of amplitude and FWHM might be that different cortical subtypes were imaged, as also hypothesised in the morphological analyses (chapter 4).

A variability across cells was also observed for the inter-peak interval (here: ISI). Intervals of few ms to several s were observed with a median ISI of around 700 ms. The inter-event interval represents a peak-free period which indicates pauses in neuronal firing.[124] The variation in these peak-free periods between cells and for individual cells indicate non-repetitive, complex activity

patterns.

$Ca^{2+}$ imaging via genetical calcium indicators can provide valuable insights into neuronal activity. Analysing different parameters of the transient gives meaningful information onto electrical activity.

## 5.3 Conclusion and outlook

Understanding the brain's architecture and function requires an integrated systematic approach to study neuronal connectivity from macro- to microscale level. Evaluation of neuronal interaction as populations is as important as single neuron contribution and addressability. Engineering neuronal networks *in vitro* and recreating these different levels of connectivity is therefore a valuable tool to investigate neuronal behaviour in the different architecture levels. The star shaped patterns are suitable to engineer networks with separated individual neurons with a defined polarisation direction as presented in the last chapter. This chapter showed that the single cell networks show neuronal activity.

The networks grown on Xgrid and star patterns showed neuronal activity from 14 DIV onwards in electrical recordings via MEAs as well as calcium imaging. However, the SNR of the GCaMP3 sensor in a culture grown on FITC-labelled protein pattern is low.

Calcium signals from neurons cultured on star patterns were analysed more detailed. In summary, transient parameters as fluorescence amplitude, duration and inter-peak interval showed high variabilities between individual cells. This indicates a variability in neuronal activity that might result from differing neuronal subtypes and their intrinsic properties as well as from a variability of individual neuronal activity patterns.[88,26] Overall, we can conclude, that after more than two weeks *in vitro* we see active neuronal cells grown on the Xgrid and star shaped patterns. Further experiments would be necessary to explore the observed signals. First, it would be interesting to analyse the cell types in the networks via patch clamp and immunofluorescence to evaluate the differences between inhibitory and excitatory neurons or other cell types. Moreover, the low $\Delta F/F$ values should be analysed more detailed to understand whether they represent sub-threshold potentials or other intrinsic or artefactual signals. Nevertheless, the experiments presented here show, that a combination of the patterned networks with methods like calcium imaging

or electrical recordings, provides a powerful tool to analyse the contribution of individual neurons to neuronal activity with single cell addressability.
Despite the complex relationship of electrical activity and calcium transients, different parameters of the transient can give a deeper insight into the neuronal activity. Beyond the parameters analysed in this study, further transient parameters can provide more detailed information onto the cellular properties. Walters et al. analysed additional parameters like rise time and different periods of decay time to investigate calcium regulatory mechanisms as well as electrical activity of the large-diameter dorsal root ganglion (DRG) neurons, a specific neuronal subclass.[152] The combination of a designed single cell network with the method of calcium imaging can be used to further analyse differences in transient shapes in neuronal substructures as dendrites, axons and somata.
Furthermore, electrical activity can be estimated by deconvolution of $Ca^{2+}$ signals. It is a sophisticated approach because of the complex relationship of the $Ca^{2+}$ signal and the action potential.[102] The deeper understanding of the interaction of electrical signalling and the $Ca^{2+}$ transient could be integrated into deconvolution algorithms to provide more reliable spike train estimations.
Moreover, a combined analysis of single cell networks with calcium imaging and electrical recording tools like ncMEAs would provide a valuable tool for further experiments to extrapolate elementary functions of individual neurons and small circuits.
Both patterns presented here (Xgrid and star shaped patterns) are suitable for the MEA designs used in our institute. Cultured on MEA, experiments with electrical stimulation and simultaneous recording of calcium and electrical signals could be performed. This platform would provide a direct accessibility of single cells and complement *in vivo* studies towards a deeper understanding of the diverse functions of the brain architecture and circuits.

# Part II

# Population connectivity

On the mesoscale organisation level of the brain, groups of neurons are arranged into larger networks as observed in e.g. the cortical columns. These populations are characterised by certain common properties and show increased connectivity and directionality to other populations.[103]
The size is an important parameter of neuronal networks and was illuminated by studies of differently sized neuronal clusters.[136,157,164] However, experiments were performed with uniform networks, which have - despite many advantages - several limitations. Foremost, the topology of these uniform networks is unlike many *in vivo* circuits involved in information processing, which are characterised by a modular architecture. The markedly different organisation is also reflected in different repertoirs of activity patterns.[137] Thus, to increase the relevance of the uniform network model, it should be extended by structural features.
Specific pattern geometries can be utilised to recreate essential building blocks of these circuits *in vitro*. Approaches reported in literature include lines,[52] logical gates,[51] and diodes.[51,2] In case of diodes, small networks with unidirectional properties are created by triangular shaped patterns.[51,2,60]
This chapter aims to create networks with populations of different sizes and defined directionality and for that employs and adjusts the triangular shape from Albers.[2] Chapter 6 presents the characterisation of the structure of these different networks. Chapter 7 analyses the functionality of the population networks.

# Chapter 6

# Population networks: Controlling groups of neurons

In earlier studies Albers and Offenhäusser analysed the effect of a triangular shaped micro pattern on neuronal networks. They investigated different shapes and discovered, that a triangle with curved sides (curved triangle, CT) has the greatest effect on directionality control. The neuronal networks showed a directionality of signal propagation from the bottom to the tips of the triangles. They analysed two triangle sizes: 650 x 550µm and 500 x 430µm (height x width) with population sizes of 44 $\pm$ 18 and 29 $\pm$ 9 cells.[4,3] As a follow up on these results the question arose whether the effect of pattern geometry on directionality is linked to population size.

For that, the size of the curved triangular shaped pattern (CT) from Albers et al. was decreased in multiple steps. This chapter analyses the effect of the structure size of the dsCT1 structures onto the network's morphological characteristics, like cell number and structural connectivity.

First, neurons were cultured on the different dsCT1 patterns, with the number representing the percentage of the original CT1 size from Albers et al.[4] Figure 6.1 shows a representative phase contrast image of the different dsCT1 scales at DIV 5. Neurons show multiple neurites indicating interconnected networks. While on the 10CT1 structures neurons exhibit short neurites and fill the triangular form, on the 5CT1 and 2CT1 structures neurites elongate

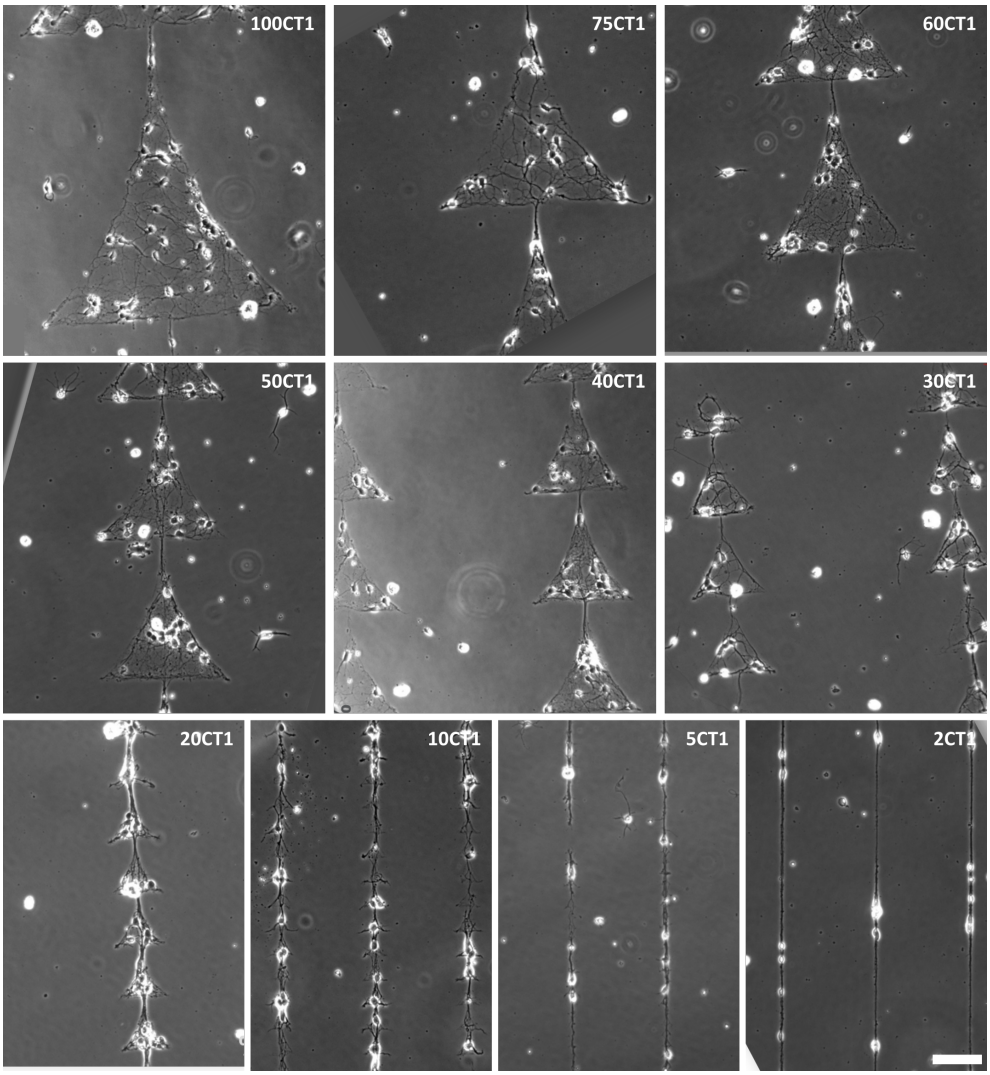


**Figure 6.1:** Phase contrast image of the downscaled CT networks. DIV 5, Scale bar 100 µm.

along one dimension resulting in networks with linearly connected cells. The somata on the 2CT1 structure show a round shape, which is typical for a bad cell attachment - suggesting, that the pattern size is too small for a neuron.

## 6.1 dsCT1 size and population cell number

To analyse the effect of triangle size on the population size, the cell number per triangle was quantified. Figure 6.2 shows the quantification of the cell number depending on the triangle size performed by Lanzrath in her Bachelor thesis project.[89] Cultures with (orange) and without co-culture (black) were analysed. The co-cultures were grown on the protein-coated well-plate area, surrounding the patterned cultures on the glass coverslips.

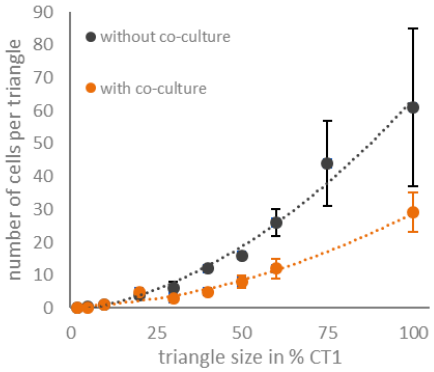


**Figure 6.2:** Average cell number within the different sized triangles and standard deviations. Data from Lanzrath.[89]

Cultures without co-culture show an almost doubled number of cells within a triangle compared to cultures with a co-culture. For the 75CT1 structure there is almost no difference between cultures with and without co-cultures. For both methods we quantified around 40 cells per triangle. For 100CT1 we see around 30 cells in the co-culture conditions and approximately 60 cells per triangle without co-culture. In the context of the overall observation, the value for 75CT1 with co-culture looks like an outlier. Especially when considering the lower value of 30 cells per triangle for the 100CT1 structure and the fitted graphs (dotted lines). In the small triangles (10CT1, 5CT1 and 2CT1) somata are separated, so that maximum one neuronal soma is placed in a triangle.

Figure 6.3 shows that the cell number is linearly proportional to the triangle area. The data point for the 75CT1 with co-culture was considered as an outlier and is not included for the fit. Cultured with co-culture

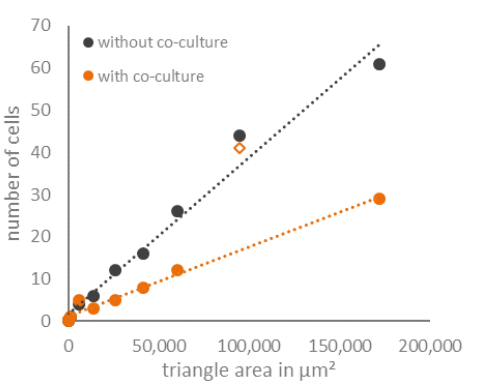


**Figure 6.3:** Average cell number over pattern area. Data from Lanzrath.[89]

180 cells/mm$^2$ were observed, while without co-culture the cell density increased to 380 cells/mm$^2$

In summary, with decreasing triangle area the number of cells within a triangle is also decreasing linearly. Using co-cultures is increasing the coated area and thus is limiting the cell number within the triangle even further.

## 6.2 dsCT1 size and structural connectivity

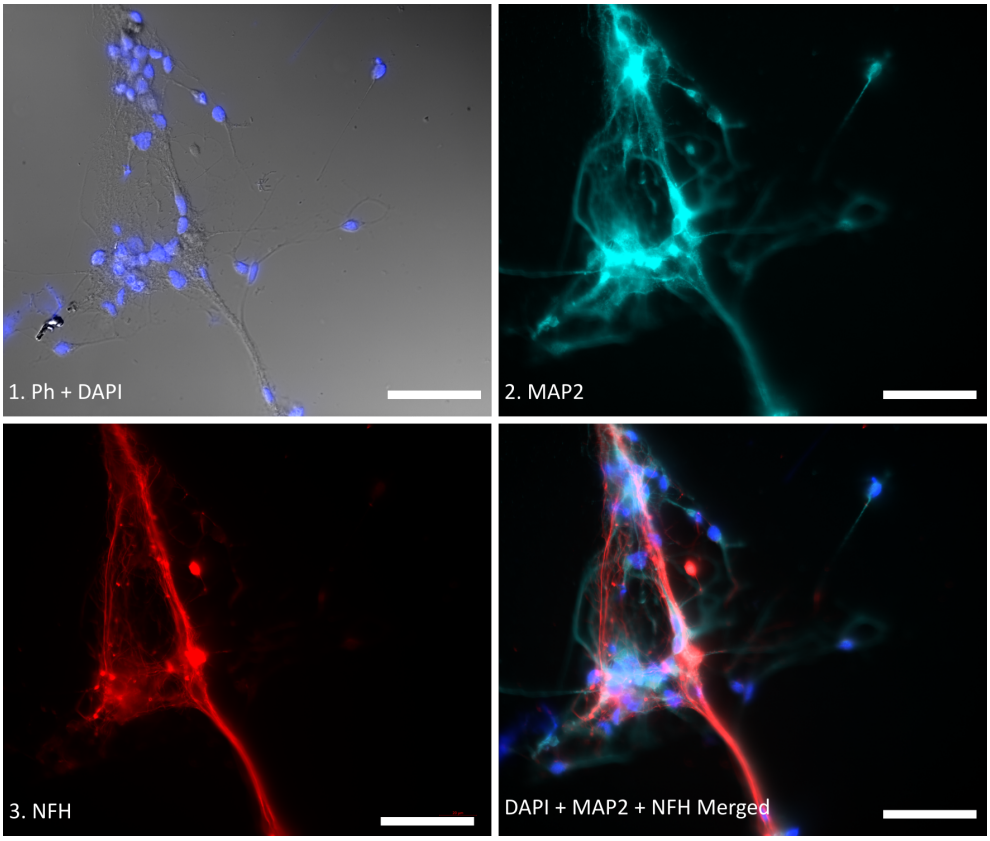


**Figure 6.4:** Immunofluorescent image of a culture grown on the 40CT1 pattern. Top left: This panel shows a phase contrast image merged with DAPI for nuclei staining. Top right: MAP2 staining for identification of dendrites and neuronal cells. Bottom left: Axons labelled with NFH. Axons form bundles. Bottom right: Overlay of DAPI (blue), MAP2 (cyan) and NFH (red). Scale bar 50 µm, DIV 10.

In the next step, the connections of the networks grown on the downscaled triangles were considered. For that neuronal substructures shaping neuronal connections, axons and dendrites, were investigated in detail. Cultures were immunofluorescently labelled utilizing the Tuj-1 or MAP2 and NFH-antibody. With that a classification into either dendrites or axons was possible. Figure 6.4 shows a culture grown on the 40CT1 pattern for 10 DIV. Nuclei (DAPI in blue, top left), neurons (MAP2 in cyan, top right) and axons (NFH

in red, bottom left) are fluorescently labelled. We see about 35 cells in the triangle with a developed network of neurites. The dendrites spread on the triangle area while the axons show bundles.

**Axon bundles** Networks growing an all dsCT structures showed long and branched neurites indicating well-established networks.

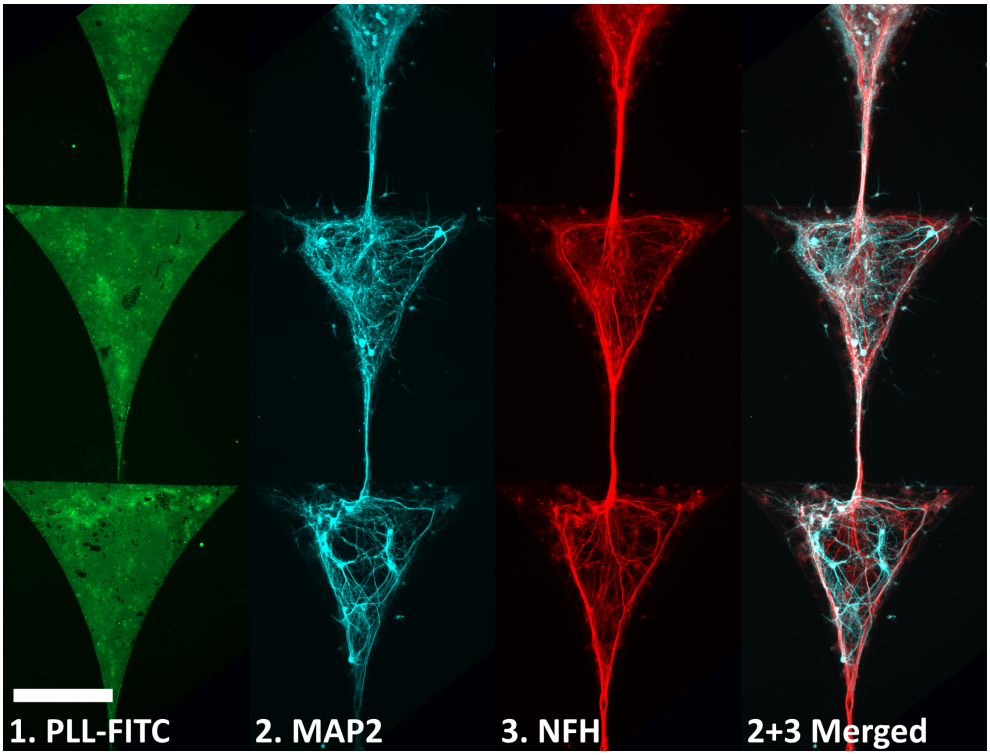


**Figure 6.5:** Immunofluorescent image of a culture grown on the 100CT1 pattern. The first panel shows the protein pattern with PLL-FITC. The second panel depicts dendrites immunofluorescently labelled with MAP2 and the third panel depicts axons labelled with NFH antibody. Axons form thick bundles at the tips of the triangles. The last panel shows an overlay of MAP2 and NFH. Scale bar 200 µm, DIV 21.

Figure 6.5 depicts an immunofluorescently labelled neuronal culture grown on the 100CT1 patterns. One prominent observation is that the axons form bundles at the edges of the triangles. The bundles are getting thicker especially at the tips of the triangles. Reaching the downstream triangle, bundles

diverge until they are funnelled back again at the tip of that triangle.

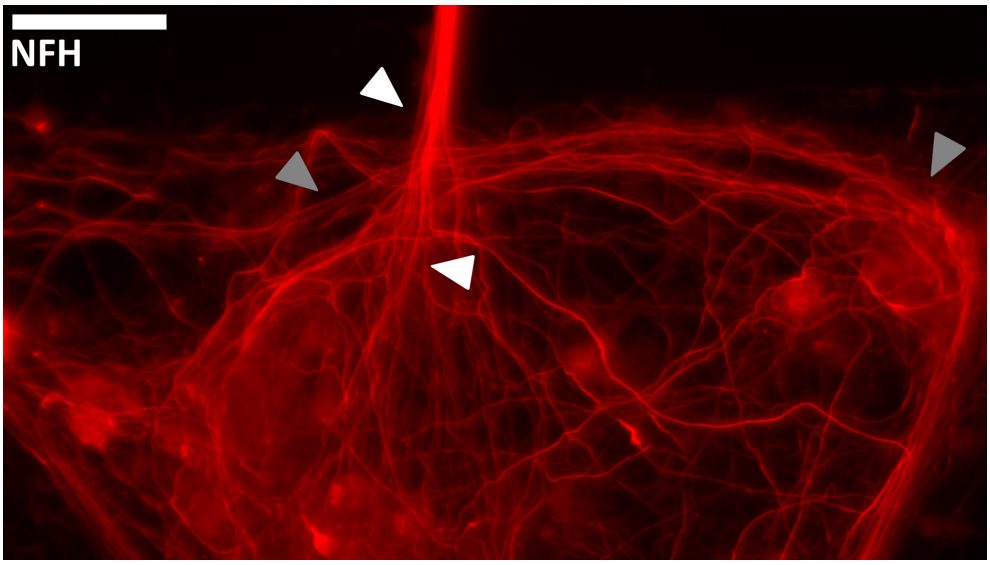


**Figure 6.6:** Axon bundling and diverging. Immunofluorescent image of a culture grown on a 100CT1 pattern. White arrows show bundles coming from the tip of one triangle diverging in the downstream triangle, while grey arrows are marking the axons making a turn at the other two tips at the side of the triangles and continuing along the edge of the same triangle - not entering the previous triangle. Axons are labelled with NFH. Scale bar 50 µm, DIV 21.

Figure 6.6 shows the axon bundling and diverging in detail. While the bundles coming from the tip of one triangle diverge in the downstream triangle (white arrows), the axons at the other two tips at the side of the triangles make a turn and continue along the edge of the same triangle (grey arrow) - without entering the previous triangle.

Another observation is that the neurite bundles are some µm away from the edge of the pattern. This effect of axon clustering at the edges of the triangles and also the distance of the bundles to the pattern edges were observed by Albers and Offenhäusser and others.[3,162] As visible in Figure 6.5, axons and dendrites seem to be pulled toward the triangle centre. Especially at the tips of the triangles, where the axonal bundle formation is most prominent, the contrast to non-bundled dendrites is clearly visible.

The effect of axon bundling or adherence during axon growth is known as

axonal fasciculation. Small groups of neurons form axonal pathways that have a guiding effect onto other neurons. Fasciculation is based on molecular interactions between proteins in the axonal membrane. These protein interactions can promote either fasciculation or defasciculation so that axons can also leave the bundles.[153] The understanding of the role of these pioneer fibres in the nervous system is still fragmentary, but it is assumed to have an impact on more targeted, shorter connections within brain areas due to limitation of the dispersion of individual axons. Additionally it is assumed, that fasciculation reduces the number of synapses needed for reliable signal transmission and thus leads to less complex networks.[82,35] Interestingly, the fasciculation observed in the experiments of this thesis (see Figure 6.5 and Figure 6.6) seems to be based on the mechanical forces evolving in the networks due to the triangular pattern. Axons entering a downstream triangle detach and disperse as shown in Figure 6.6. Alternating segments of axonal trajectories and "choice points", where axons detach from each other and change to other neuronal "highways" are also reported in literature.[144] In the triangular pattern the transition from one triangle to the downstream triangle may represent such a "choice point" where the axonal bundles are influenced by chemical cues of other axons or axon trajectories.
Concluding, the daisy-chained triangular patterns do not only provide neuronal networks with various population sizes, but also show fasciculation and defasciculation of axons. Thus, the networks grown on the dsCT patterns provide a to study the mechanical and molecular effects of the bundle formation.

**Quantification of axon outgrowth direction** The architecture of the neuronal networks cultured on dsCT1 patterns was analysed and quantified by Hannah Lanzrath in the framework of her Bachelor Thesis. She cultured neuronal cultures for 3 - 5 DIVs on the 2CT1, 5CT1, 10CT1 and 20CT1 structures and for 6 - 8 DIVs on the other, larger CT1 patterns. These DIVs were chosen to ensure a network that is polarised but still not too branched, to be able to distinguish individual neurites and their origin.[89]

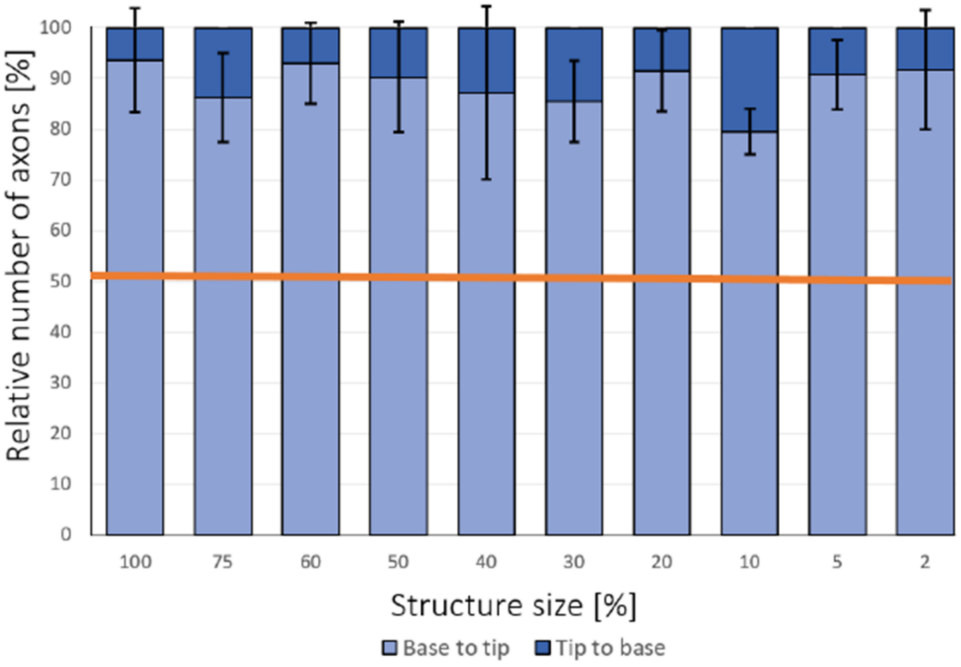


**Figure 6.7:** Quantification of axon outgrowth direction on dsCT1 patterns. Light blue represents the axons growing from bottom to tip (preferred direction) while the share of axons growing from tip to bottom (wrong direction) is represented in dark blue. Image from Lanzrath.[89]

Figure 6.7 shows, that all CT sizes guide 80 % to 93 % of the axons towards the tips of the triangles (which is the intended guidance direction). The 10CT1 structure shows with 80 % the lowest number of neurons growing into the preferred direction (base to tip). For the 20CT1 structure more than 90 % of the axons grow into the preferred direction. The 100CT1 structure shows with 93 % the highest share of axons elongating into the right direction. No clear effect of the structure size towards a reduction or increase of the share of the guided axons can be observed when evaluating the different dsCT1 sizes.

Triangular shapes were already used by scientists to guide neuronal and axonal outgrowth with different methods. Gladkov et al. designed a microfluidic culture chamber, where two larger chambers are linked by daisy-chained triangle tunnels. They observed a guiding effect of the axons along the triangles

similar to the observation described in this thesis. Axons were more likely to grow along the funnel shaped microchannels than in the opposite direction. They also showed that axon turning angles were small when elongating along the daisy-chained triangles.[60]

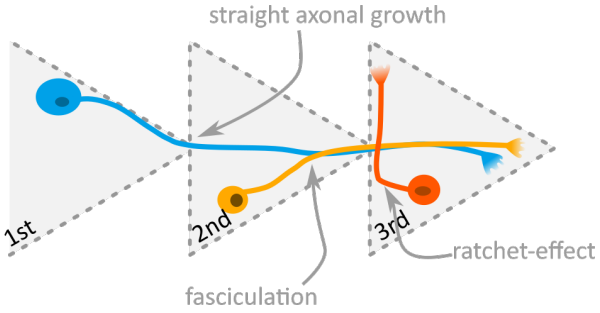


**Figure 6.8:** Guiding effects of triangular shaped patterns. The blue axon follows the pattern in the direction of the smallest turning angle in the 1st triangle. It enters the 2nd triangle and continues the axon growth with a low turning angle straight towards the 3rd triangle. The yellow axon adheres to the blue axon due to fasciculation effects and continues growth along this axon towards the 3rd triangle.

For smaller triangles the geometry might induce a directed polarisation as for the star shaped single cell patterns described in chapter 4. The triangular funnel geometry enable one neurite to elongate fast while another might be stuck in a corner at the triangle base. Thus, the pattern coordinates which neurite is becoming an axon.
In bigger triangles redirection of already polarised axons due to the"ratchet" geometry might predominate. Axonal redirection by triangles selectively permits elongation into one direction while preventing the passage into the previous triangle. Figure 6.8 shows a schematic image of neurons with axons on a CT pattern and the possible guiding effects by the bigger triangular patterns. The blue axon elongates and reaches the border of the pattern. Here, the growth cone might feel the contrast of the patterned to non-patterned area, continuing growth on the patterned surface. Once the axon is funnelled into the right direction due to the preference of elongation with lower turning angles as is displayed for the blue cell, the elongation might continue in an almost straight line along the daisy-chained triangles. A straight axonal

growth and an axonal resistance to bending was already observed earlier.[80] Due to the effect of axonal fasciculation,[153,82,35] the axon of the yellow cell might get attracted by the blue axon and thus also receive an additional guiding cue. The red neuron in the 3rd triangle initially elongates the axon towards the base of the triangle, turns at the edge of the pattern and continues to grow straight along the pattern edge. The pattern shape leads to a "ratchet-effect" preventing neurites to grow into the 2nd triangle. This effect was reported by Scott et al. for small triangular patterns.[134]

## 6.3 Summary and discussion

**Pattern area controls population cell number** The dimensions of the CT1 structures (and the protein area) is the determining factor of cell number per triangle. There is a linear dependency of triangular area to cells per triangle. For cultures with co-cultures the number of cells per triangle is about half the number of cultures without co-cultures.

A decreasing cell number per triangle means that there are also less cells within the triangular networks reducing the number of neurons within a population. The area of micro patterned surfaces was already used by various groups to extrinsically control the size of neuronal networks. Also here, a linear relationship was observed.[164,4,135,157,136]

**Triangular shape induces structural connectivity at all scales** All downscaled triangular structures show a strong guiding effect. 80 to 93 % of the neurons elongated their axons towards the tips of the triangles. This direction is the intended direction and was also observed by Albers and Offenhäusser.[3] No clear trend towards a decrease or increase of the share depending on the structure dimensions was visible.

Axons seemed to be funnelled along the edges of the triangles towards the downstream triangle. At triangle sides axonal bundles were very prominent. At the transition of the tip of one triangle to the base of the next triangle axons were elongating into the downstream triangle. Some axons were diverging while others remained in the bundles and showed a straight growth towards the next triangle. Thus, daisy-chained triangles are connected.

The other way around, axons growing at the edge of the base from the side tips, were continuing to grow along the triangular shape without entering the tip of the previous triangle.

Small as well as bigger triangle patterns showed a strong guiding effect. While for small triangles the geometry might induce directed polarisation by controlling which neurite becomes an axon, for bigger triangles the pattern

shape more likely redirects already polarised axons. This results in a funnelling effect towards the tips of the triangles and prevents passing into the previous triangle at the base of one triangle.
The guiding effect of triangles was already observed by other groups on micro-[134] as well as millimetre scale,[51] where around 70 % of the neurons were observed to elongate their axons into the forward direction.

## 6.4 Conclusion and outlook

The use of triangular sized patterns provides an easy to handle tool for the analysis of differently sized populations and structural directionality. Neuronal population size scale with the triangle area. Adjusting triangle area enables customisation of the population size and engineering of bottom-up replica of brain modules *in vitro*. The designed networks can be used to study fundamental effects of development and structure of microcircuits in a controlled and simplified environment, like axon elongation, fasciculation, and directionality, to name a few.
In the next step, the functional connectivity of the dsCT1 networks is analysed.

# Chapter 7

# Population networks: Size and functionality

Population size can be extrinsically controlled via triangle dimensions as proven in the previous chapter. All dsCT1 networks showed directional structural properties revealed by immunofluorescence. Moreover, the triangular geometry impacts structural connectivity from micro- to mm scale (up to 0.5 mm).

This chapter focuses on investigating whether population size impacts functional connectivity. Understanding how the network's functionality vary upon crossover from smallest populations (comprised of single neurons) over small to bigger populations may provide important insights needed to reveal the properties of neuronal network dynamics. Morphological analysis (chapter 6) showed, that neurons on small dsCT patterns as 10CT1 and 20CT1 are mostly linked into linear, one-dimensional networks, while bigger dsCT networks exhibit more complex two-dimensional network architectures. This changed network organisation and the number of interaction partners might influence functional dynamics. Changing as well as preserved neuronal dynamics were reported for differently sized neuronal networks in literature.[164,157,136] However, all studies focused on analysing randomly organised networks of defined sizes. Here, the aim is to investigate the functional dynamics of structured networks with different population sizes.

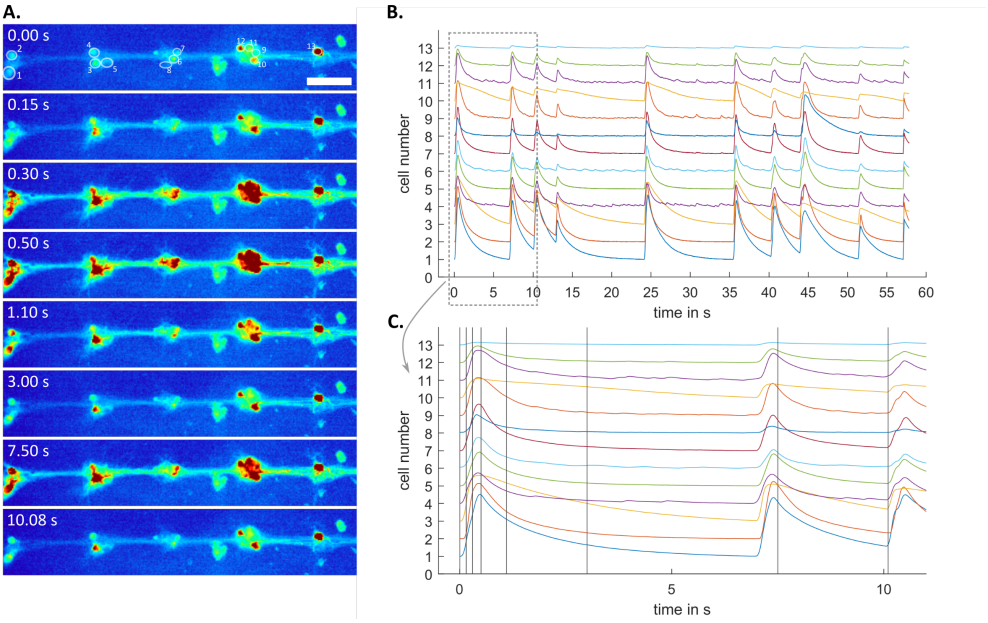


**Figure 7.1:** $Ca^{2+}$ imaging of a 30CT1 culture. Left: Fluorescent images at different time points of a $Ca^{2+}$ time trace. Fluorescence intensity depicted in a heat map LUT with blue representing the lowest and red the highest intensity. Scale bar 100 µm. Right: $\Delta F/F_0$ for 13 neurons. Bottom right: Time points from the left panel are indicated as vertical lines.

$Ca^{2+}$ imaging provides the advantage of observing every active cell in the imaged area. Figure 7.1 shows an exemplary $Ca^{2+}$ imaging time trace with the corresponding fluorescent images at 8 different time points (A). Figure 7.1 B displays the whole 60 s long time trace with 13 active cells. In C, the first 10 s are shown more detailed with the time points depicted in the left panel as horizontal lines. The neurons show multiple synchronous $Ca^{2+}$ transients with great amplitudes. Some transients with smaller amplitudes can be observed e.g. for cell 4, 7 and 11. The question arise whether the population size impacts the distribution of $Ca^{2+}$ transient parameters like the amplitude, duration or frequency. Another question is whether the synchrony observed in Figure 7.1 is preserved across networks of varying population size.

Besides optical methods, neuronal activity can also be analysed via electrical techniques. Here, the potential use of MEAs to investigate signal propagation

directionality of patterned cultures is evaluated at the end of this chapter.

## 7.1 Population size and transient parameters

**Table 7.1:** Number of analysed time series, regions of interest (ROIs) and transients.

| dsCT | time series | ROIs | transients |
|---|---|---|---|
| 10 | 27 | 196 | 10,520 |
| 20 | 11 | 155 | 5,319 |
| 30 | 26 | 407 | 17,868 |
| 40 | 8 | 94 | 5,428 |
| 50 | 8 | 153 | 6,851 |
| 60 | 8 | 127 | 7,107 |
| 75 | 11 | 240 | 6,407 |
| 100 | 8 | 130 | 5,403 |

This section analyses the influence of triangle size (and population size) onto $Ca^{2+}$ transients parameters. As already discussed in detail in chapter 5, transient amplitude, duration as well as pauses might give insight about neuronal dynamics. The signal parameters investigated here include amplitude, duration (full width at half maximum, FWHM) and inter-event intervals (inter-spike intervals, ISIs) of the $Ca^{2+}$ transients. Here, the approach was to quantify the entire distribution rather than focus on mean values, as only the entire distribution is believed to provide more accurate insights.[22]

In sum approximately 65,000 transients from 1,500 ROIs and more than 100 time series were analysed. Table 7.1 shows the number of analysed time series, ROIs and transients for each dsCT1 size.

2CT1 and 5CT1 structures were not evaluated for these experiments. Both sizes provide a very small attachment area to the linear networks growing on the substrates. This limited protein area made it difficult to culture networks

for a culture period of two to three weeks. Detaching networks were observed with increasing culturing time. Additionally, low-density networks are more difficult to maintain healthy over a longer culture period and thus, usually suffer from limited cell viability and network maturity.[53,14] For that reason, the 10CT1 structure was the smallest structure used for functional analysis. This size was observed to still provide an area big enough to maintain network attachment to the substrate, single-cell separation, and a healthy network.

**Spontaneous event amplitudes** The amplitude of the calcium transient is highly dependent on the calcium concentration within the cell during the signal. The intracellular concentration itself is dependent on the number of open calcium channels and thus, on the number or frequency of electrical signals reaching the cell.[102,161,5,26,1]

Transient amplitudes of all dsCT1 structures were quantified in order to analyse a potential effect of the triangle size. The amplitude of calcium transients is expressed in $\Delta F/F_0$, which shows the fluorescence intensity difference normalised by the background fluorescence of the individual cell. Figure 7.2 shows the amplitude distributions grouped by dsCT1 size in a box plot representation. The median is displayed with an orange line, boxes show the interquartile range (IQR) between the 25th (Q1) and 75th (Q3) percentile. Whiskers mark the minimum (Q1 - 1.5 IQR) and maximum (Q3 + 1.5 IQR) of the data. Corresponding histograms and box plot parameters are displayed in chapter 8 (Figure 8.8,Table 8.1).

The results show a variation of amplitude distributions for the different dsCT1 patterns, however similarities can be observed. One prominent similarity is the positive skewness observed for all dsCT1 sizes. Many parameters of neuronal activity are characterised by strongly skewed distributions with a heavy tail. These typically log-normal distributions are believed to be fundamental to structural as well as functional brain organisation. Examples include the firing rates or bursts of neuronal cells or the distribution of synaptic strength, that are reported to have a log-normal distribution.[22]

Beyond that, the data does not show any significant trends with changing

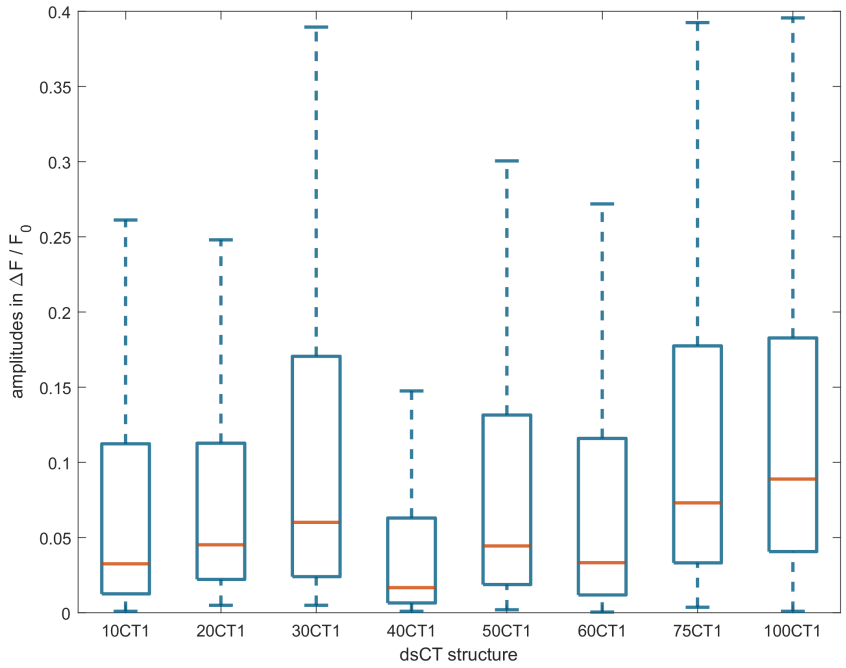


**Figure 7.2:** Box plots of amplitude distribution of different dsCT1 structures. Boxes indicate the interquartile range (IQR, 25th to 75th percentiles, Q1 to Q3), whiskers mark the minimum (Q1 - 1.5 IQR) and maximum (Q3 + 1.5 IQR). Median is represented with the orange line.

population size. A slight trend towards increasing 25th, 50th (median), 75th percentiles, and maxima can be observed, however without any significance ($p > 0.05$).

In conclusion, the amplitude distributions show a great variation and no significant dependence on the triangle size. A slight and non-significant trend towards greater amplitudes ($p = 0.1$ for medians) and broader amplitude distributions ($R_{IQR} = 0.5$; $p = 0.3$) with bigger triangle sizes was observed.

**Spontaneous event durations** FWHM can be used as a measure to compare durations of the transients. It was described in detail in paragraph 5.2 in chapter 5. Shortly, the width of a calcium transient is dependent on the

duration of the period with an increased intracellular calcium concentration. It represents the duration of the spike when $Ca^{2+}$ channels are activated and the intracellular $Ca^{2+}$ concentration is higher compared to resting state (base level).[100,5,1]

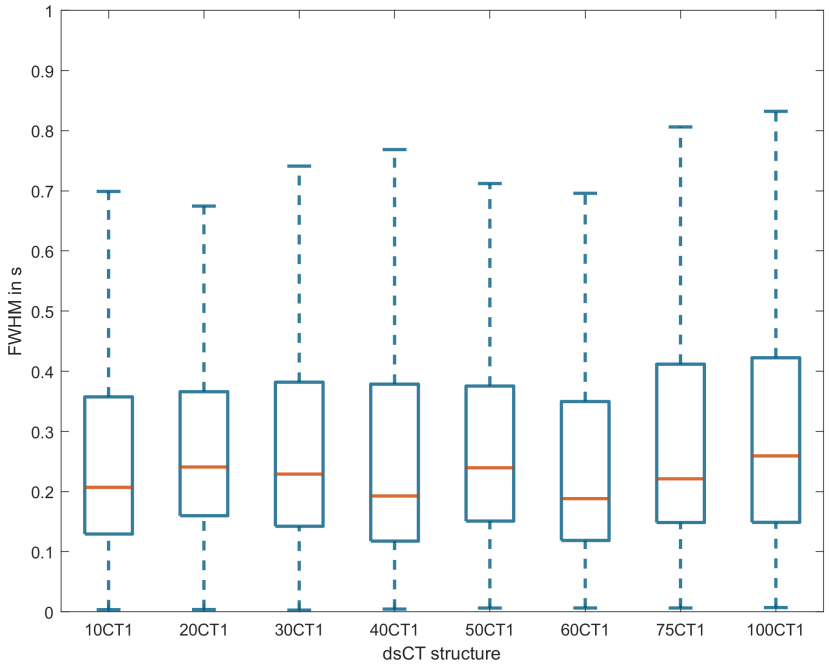


**Figure 7.3:** Box plots of FWHM distribution of different dsCT1 structures. Boxes indicate the interquartile range (IQR, 25th to 75th percentiles, Q1 to Q3), whiskers mark the minimum (Q1 - 1.5 IQR) and maximum (Q3 + 1.5 IQR). Median is represented with the orange line.

Figure 7.3 summarizes the FWHM distributions in a box plot representation. Corresponding histograms and box plot parameters are presented in chapter 8 (Figure 8.9, Table 8.2).

As for the amplitude distributions, we can observe a positive skewness. Furthermore, 50 % of the transients show a FWHM between 100 and 400 ms, which might correspond to a low number of APs.[26] Moreover, the FWHM distributions seem to be preserved across networks with different population

size.
Neither the minimum nor the 25th percentile or the median of the FWHM distributions show a trend with changing population size. However, the 75th quantile ($p = 0.08$) and the maxima (upper whisker, $p < 0.05$) increase with increasing population size. For maxima, this slight trend shows a slope of 16 ms/10% CT1. Despite this slight increase, the data dispersity for second half of data (median to maximum) does not show any significant increase.
As for amplitudes we see mostly preserved FWHM distributions across different population sizes indicating preserved functional dynamics.

**Analysis of the intervals between two signals** The inter-spike interval (ISI) is usually considered as the duration between two action potentials (spikes). It plays an important role in neuronal signalling and even determines the information conveyed by an action potential in some brain areas.[125] Even though a $Ca^{2+}$ imaging is not solely representing action potentials but is rather a complex combination of synaptic input, output and intrinsic cellular properties, it still can be used to monitor rate changes or pauses in spike firing.[124] This interval between two transient peaks can give insights onto neuronal activity, such as longer pauses within networks or a higher proportion of high-frequency activity.
Here, inter-spike intervals (ISI) correspond to the interval between two consecutive transients. The ISIs of the analysed time traces are displayed in a box plot representation in Figure 7.4 (histograms are displayed in Figure 8.10 in chapter 8). All distributions of the ISIs show a positively skewed shape and a high variability. The inter-event intervals range from some tens of ms to the second range. The distributions do not show any trends with changing population sizes.

**Summary and discussion** The stepwise downscaling of the daisy-chained triangular cultures results in networks with differently sized populations. In this section the functionality of the networks was analysed regarding two main questions: First, do all sized networks remain functional, showing neuronal

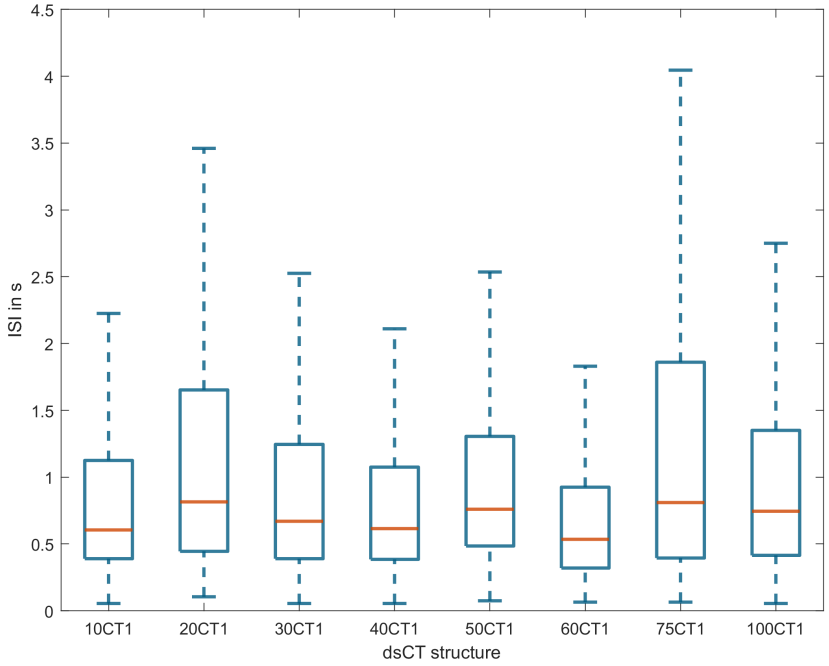


**Figure 7.4:** Box plots of ISI distributions of different dsCT1 structures. Boxes indicate the interquartile range (IQR, 25th to 75th percentiles, Q1 to Q3), whiskers mark the minimum (Q1 - 1.5 IQR) and maximum (Q3 + 1.5 IQR). Median is represented with the orange line.

activity and signalling. And second, do activity characteristics of smaller populations differ from the characteristics of bigger populations.

After three weeks in vitro, all neuronal networks exhibited noticeable spontaneous activity recorded by $Ca^{2+}$ imaging and thus, were functionally active.

Individual transients of neurons grown on the different patterns were analysed in detail to address the second research question. Different parameters of individual $Ca^{2+}$ transients were evaluated: transient amplitude and duration as well as the periods between two events.

Transient amplitude is influenced by multiple factors including neuronal activity and artefactual conditions. Intrinsic excitability due to cell type, sensor dynamics and intracellular indicator concentration as well as intracellular con-

ditions like pH or higher $Ca^{2+}$ concentration due to a bad health state of a cell or culture might change the indicator or cellular characteristics and thus, influence the fluorescence intensity. To faithfully analyse the characteristics of $Ca^{2+}$ transients, possible artefactual changes of fluorescence intensity must be considered carefully. Variations in fluorescence emission may reflect differences in intracellular indicator concentration rather than $Ca^{2+}$ concentration. A practical way to overcome the different indicator concentration is to express the fluorescence change relative to its initial fluorescence ($\Delta F/F_0$). This approach provides a method to compare recorded signals between different experiments, but does not compensate for other artefactual changes of fluorescence due to e.g. network's health status.[18] Additionally, different categories of synapses are characterised by differences in membrane excitability and $Ca^{2+}$ clearance mechanisms. Those differences might also impact the duration and amplitude of a $Ca^{2+}$ signals measured with GCaMP.[160] Thus, transient duration and amplitude might also depend on the neuronal subtype and their endogenous properties.[160,5] Furthermore, one has to keep in mind, that calcium signals do not represent exclusively action potentials. A subthreshold depolarization may also activate low voltage-gated calcium channels resulting in a detection of a calcium transient. Even though the spike-to-fluorescence relationship is not linear for genetically encoded calcium indicators and the transient properties are a complex convolution of intracellular properties, neuronal activity and sensor dynamics, the $Ca^{2+}$ signal is widely used to analyse neuronal networks and a correlation with neuronal activity was shown.[5,26,160]

Neuronal population size impacts the number of potential partners for cellular connections and thus, might influence the number of signal inputs. A change in functional properties towards increased neuronal activity or bursting might be anticipated. Studies with neuronal clusters of different sizes by Shein Idelson et al. revealed a scaling of network events (rate and duration of bursting events) with network size.[136] This shift in neuronal dynamics might be reflected in changed $Ca^{2+}$ transient distributions due to an increased calcium

entry resulting in a greater relative magnitude of amplitude and duration. The number of action potentials is reported to be positively correlated to the amplitude of $Ca^{2+}$ transients.[5] Thus, the amplitude might be used as a measure for changes in the firing rate of neurons. Increasing amplitudes with increasing dsCT1 structure size would indicate increasing firing rates of the networks with bigger population sizes. Moreover, a shift towards longer transients with a higher magnitude would indicate an increased occurrence of bursting events. However, the results of this section showed a scattered image and transient parameters seem to be independent of population size. Even though signal amplitudes as well as durations slightly increase with increasing population size, the trend is very vague and this hypothesis cannot be supported by a significant difference in the data. One shortcoming of the experiments might be the small size of the downscaling steps. For most structures there is no significant difference in cell number to the consecutive smaller or bigger population sizes as shown in chapter 6. A 20CT1 population might have the same cell number as a 40CT1 population. Moreover, the cell number might vary from triangle to triangle within one network which might also influence the overall activity. Alternatively, data might have been collected on the actual population size level rather than on the triangle size.

Also Wilson et al. compared differently sized neuronal clusters regarding their functionality. Similar to the results presented here, they observed preserved firing rates and neuronal dynamics across different neuronal cluster sizes. The authors hypothesised, that these stable dynamics are an important feature of neurons "to sustain meaningful dynamics while the number of its functional partners changes".[157] The change in the number of functional partners might occur in e.g. development, plasticity, and disease. One example is the lateral geniculate nucleus, where the axon inputs reduce from over 20 to a few during development. Another example is the ageing process. Here, despite the neuronal loss the activity levels remain comparable sustained.[157] In both publications analyses included network sizes ranging from some tens to 1'000 (Wilson et al.) or 1'000'000 (Shein Idelson et al.) cells. Their "small"

clusters had a similar dimension to the 100CT1 populations. In contrast to these reports, the actual network size is unknown for the dsCT1 networks and the focus was on creating networks with a defined structure comprised of subunits (populations). The neuronal populations are not isolated as the neuronal clusters analysed by Wilson et al. and Shein Idelson et al., but are interconnected and exhibit directional features as demonstrated by the morphological analysis in chapter 6.

The data analysed in this section showed highly varying and broad data dispersities. The distributions of the amplitudes and inter-event intervals showed highly varying statistical dispersions (minimum to maximum range) across the dsCT1 sizes. The variabilities of the event durations showed a broad data dispersity, albeit the values and magnitudes of the variance are preserved. Most studies reported in literature provide information about the calcium transients on few recorded events. Reported signal characteristics include average peak amplitudes with usually high standard deviations. This indicates, that the data of the measured parameters shows a widespread distribution.[160] Also Shein Idelson et al. observed a high variability in the firing patterns while analysing the collective activity of differently sized neuronal clusters.[136] The transients analysed in this chapter showed a similar picture. Cortical neurons are reported to have highly variable spiking responses even to repeated identical stimulation.[139,85] Additionally, different neuronal subtypes show a wide range of coding schemes and activity patterns, e.g. fast-spiking or regular-firing neurons.[59,74] Hence, this broad variability has to be kept in mind when analysing a low number of activity time traces or comparing different networks. Here, quantifications of entire distributions are more accurate, also because neuronal activity parameters are usually characterised by a skewness.[22]

In conclusion, an analysis of $Ca^{2+}$ transients of differently sized neuronal populations (1 - 40 neurons) within neuronal networks were presented in this section. Activity parameters were preserved over the dsCT sizes. No significant effects of the population size onto the statistical parameters were

observed. Non-significant trends towards increasing durations and amplitudes with increasing population size have to be considered carefully.

## 7.2 Population size and neuronal interaction

Cross-correlation is a common measure of functional neuron-neuron interactions in neuroscience.[107] Significant cross-correlations indicate direct synaptic connections between two neurons or common inputs to the neuron pairs.[114] Pairwise cross-correlations of the $Ca^{2+}$ imaging traces of different dsCT1 patterns could give a deeper insight into the functional connectivity. In this section examples of network correlations for some pattern sizes are described, namely 10CT1, 40CT1, and 75CT1. The other non-mentioned pattern sizes are presented in chapter 8 (see Figure 8.11, Figure 8.12, Figure 8.13, Figure 8.14, Figure 8.15).
The last paragraph provides a summarised analysis.

**10CT1** The 10CT1 structure is in most cases a linear series of neurons with usually one neuron per triangle. Figure 7.5 shows four different cross-correlation heat maps and the corresponding event traces. Triangles are separated by a white line between the cells (here all triangles have only one neuron per triangle). The cell number displayed in the correlation heat map and on the y-axis of the event plot is increasing in the direction of preferred axon outgrowth.
A highly active network with high-frequent event traces is presented in the top experiment, while the second experiment shows a rather low-frequent event time trace with some synchronous events (e.g. at 8 s, 16 s and 31 s). These few synchronous events occurring in all cell somata result in a high correlation in the whole recorded area. The third presented network shows synchronous events every 1 to 5 s in almost every ROI (neuronal soma) analysed. The correlation heat map indicates two highly correlating areas within the analysed region. The experiment displayed in the bottom shows a network with more frequent events. Most of the cells (all excluding cell 1 and 3) within the linear network show a high correlation of the $Ca^{2+}$ imaging

traces.

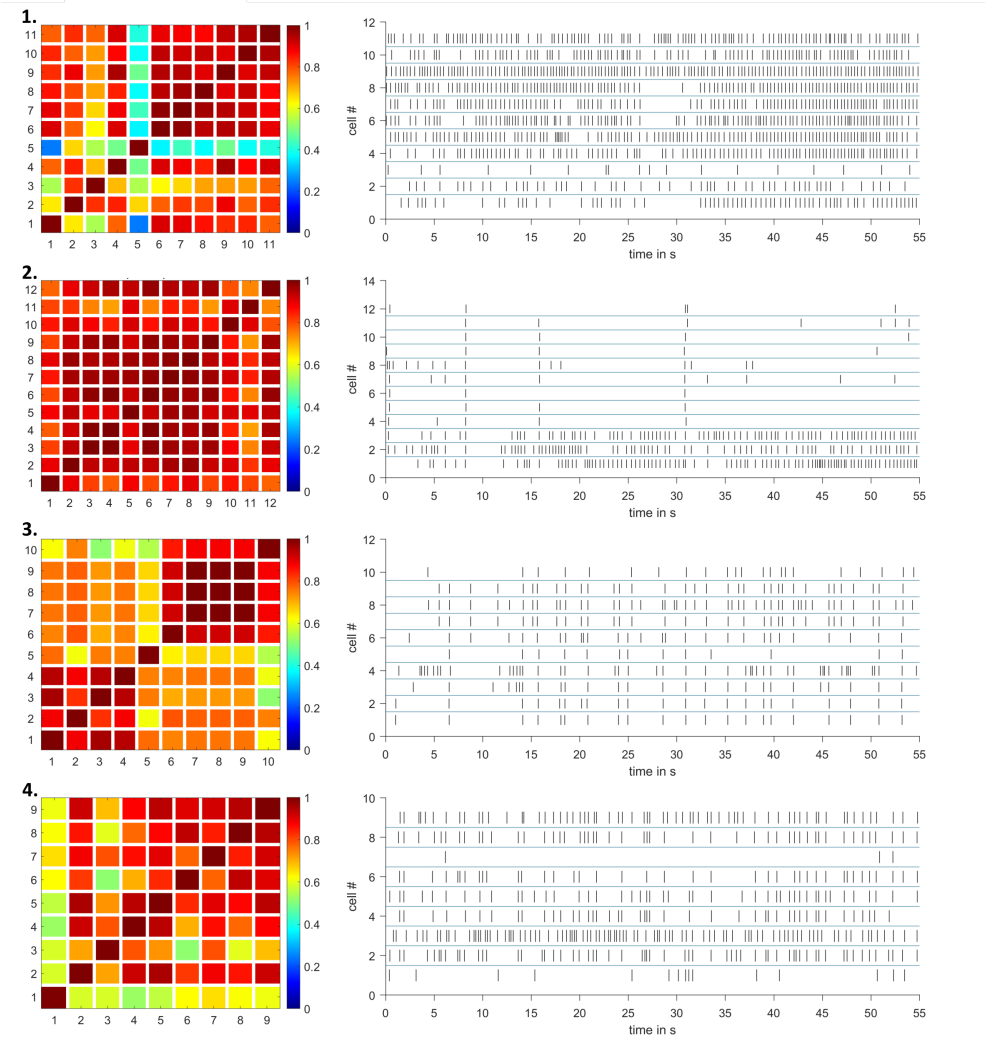


**Figure 7.5:** 10CT1: Correlation heat maps and corresponding activity raster plots of four exemplary experiments.

Overall these exemplary experiments show high neuron-neuron correlations within the observed regions of the networks. This indicates synaptic connections or even common synaptic inputs which is certainly conceivable if the spatial proximity and the structural connectivity observed in the previous chapter were considered.

**40CT1** For the 40CT1 structure around 5 cells per triangle were observed on average (see Figure 6.2 in chapter 6). Figure 7.6 shows exemplary experiments and their correlation heat maps and event traces. In these imaged areas we see one to five active neuronal somata per triangle (triangle separations are depicted as white lines in the heat maps and as blue lines in the event plots).

In the top experiment we see 17 cells spread over 7 triangles. Some of them show high-frequent events (cells 9, 12, 15) while others show fewer transients (cell 4, 5). The correlation coefficients differ between different cell pairs. Within one triangle we see highly correlated but also lower correlated activity traces as for example for the neurons 8 - 11. The correlations between cells of different triangles also show highly correlated cell pairs (cells 1, 3 and cells 6 - 9) as well as low correlated neuron pairs (cells 1 - 3 and cells 10 - 13). The second experiment shows only four triangles with 9 active cells with an overall high correlation. But also here we see lower correlated cell pairs like cell 2 with a very low correlation coefficient with every other neuron in the imaged area. The third experiment has a colder overall colour with some high as well as low correlated neuron pairs within each triangle and between different triangles. Also the event frequency varies between different cells and triangles. While the first two triangles (cells 1 - 2) show a rather low event frequency the last triangle is characterised by a high-frequent neuronal activity (neuron 6 - 10). In contrast to the third "colder" correlation map the heat map of the bottom experiment is characterised by a high ratio of highly correlated cell pairs. Looking at the event plot we see some synchronous events at 6 s, 12 s, 17 s, 22 s, 31 s and 36 s. These events might have a significant effect on the high correlation coefficients for the whole observed network area. Nevertheless, also cells showing less correlated activity patterns as for example cell 11 were observed.

In summary, the correlations of the cell pairs grown on the 40CT1 pattern show a more diverse image. We see areas and triangles with highly correlated cell pairs but also some with rather low correlations. This indicates a more

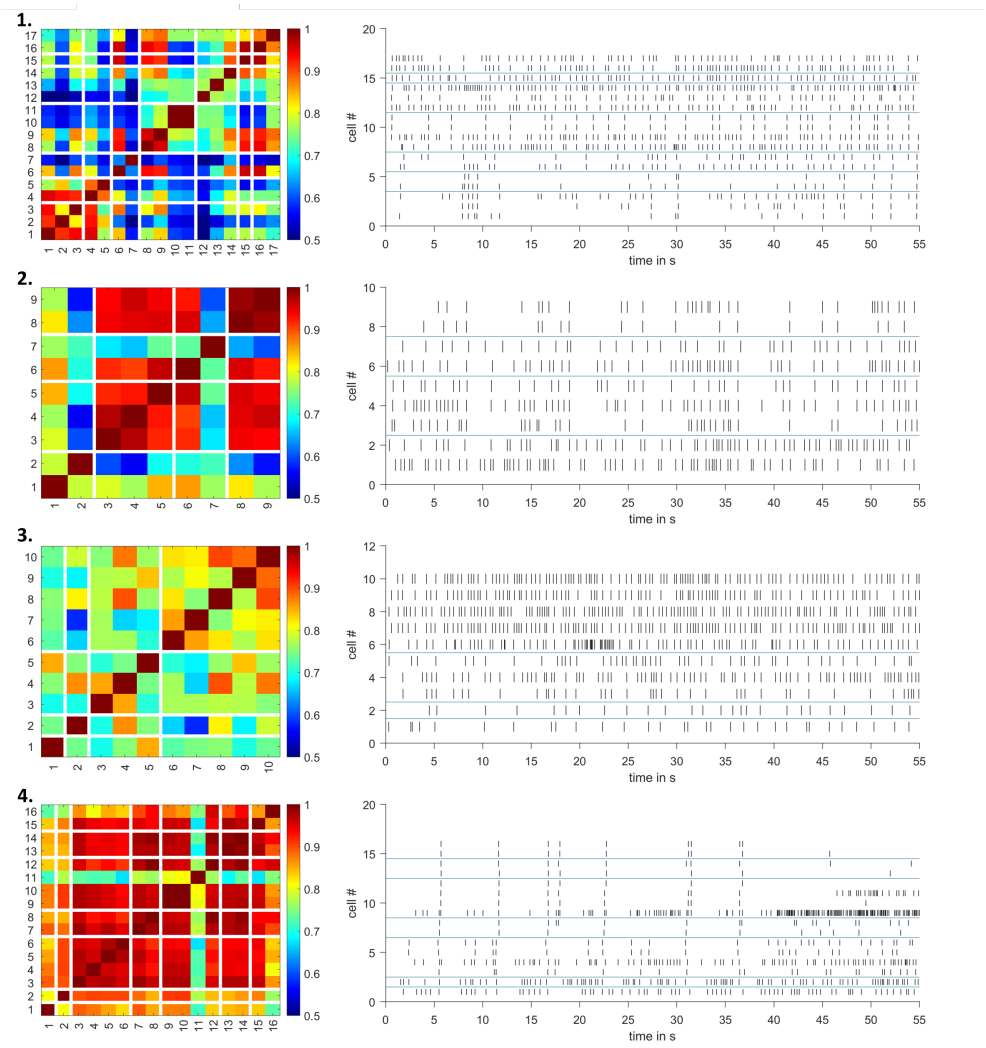


Figure 7.6: 40CT1: Correlation heat maps and corresponding activity raster plots.

complex connectivity pattern than for the 10CT1 structure with some cells being highly interconnected within one triangle, connections extending over triangles but also neurons that seem to be isolated or excluded from the population and network activity (e.g. cell 2 and 7 in the second experiment).

**75CT1** The cell number per triangle increased to approximately 20 neurons for the 75CT1 structure (see Figure 6.2 in chapter 6).

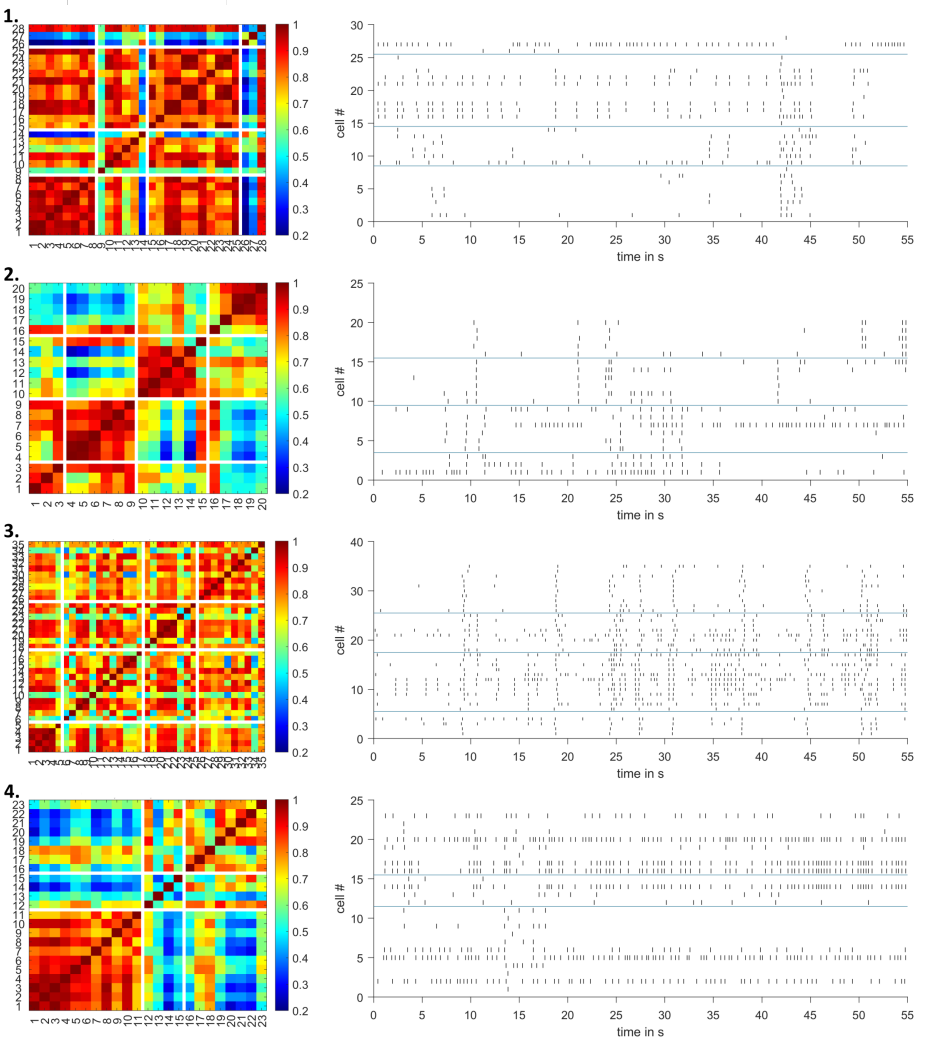


**Figure 7.7:** 75CT1: Correlation heat maps and corresponding box plots.

In the exemplary experiments displayed in Figure 7.7 we see triangles with 3 to more than 10 active neurons.

The top experiment shows a network with many highly correlated cell pairs within one triangle and between neighbouring triangles but also triangles not in direct vicinity. There are cells showing a high correlation with almost every other cell in the network (e.g. cell 1, 2, 3, 4) but also cells with low correlations to other neurons (cell 26 and 27). Overall the network shows a

rather low frequent activity with some neurons exhibiting only a few signals (less than 5 events within the 55 s of the imaging) like cell 5, 8, 25 or 28. Some events are occurring only within one triangle as for the time period between 20 s and 25 s for the triangle with cells 15 - 25. In contrast, other events seem to be transmitted along the whole network, occurring in every triangle (see time period between 40 s and 45 s).

Also the second experiment shows a low event frequency for most of the neurons. Compared to the heat map of the previous experiment we also see a high correlation within the triangles but a lower correlation between different triangles: The correlation between cell pairs of the neighbouring triangles is still moderate but is reduced for more distant triangles. In this experiment synchrony was mostly observed within cells of the same triangle. None of them were being transmitted along the whole imaged area.

The third experiment presented here shows 35 active cells in 4 triangles. We see a strong correlation between many cells across the whole region. In contrast to the previous experiment, triangle boundaries are not consistent with a similar colour code. The correlation magnitudes exhibit a higher variability within different triangles but also between different triangles. A closer look at the second triangle (cell 6 - 17) shows highly correlated neuron pairs (e.g. cell 16 and 6 or cell 16 and 12) but also neuron pairs with a lower correlation coefficient (cell 7 and 6, cell 7 and 10, cell 13 and 10). A similar distribution of the coefficients is present in all other triangle pairs. Nevertheless the complex network architecture, some time periods with events occurring in almost every cell of the observed area as for example at 8 s, 18 s or 38 s can be noted.

The bottom experiment shows 3 triangles with 23 active neurons. While the first triangle (cell 1 - 11) shows strong correlations between all cell pairs, the second triangle (neuron 12 - 15) has only one neuron pair with a moderate correlation. The last triangle shows diverse correlation values from lower (cell 18) to higher correlations (neuron 19). In contrast to the previous experiment the correlations between cell pairs of different triangles are much

lower.
To summarise, as already observed for the 40CT1 structure, the correlation patterns for the 75CT1 structures get more complex. We see experiments with high correlations for cell pairs inside triangles but decreasing or low correlation between different triangles. On the other hand, some other experiments show a more complex, not obvious pattern of correlations inside and between triangles.

**Mean correlations of different dsCT1** An examination of the calculated correlation matrices for the 8 different triangle sizes revealed a broad range of correlation patterns, from low correlation at all to high inter- and intra-triangular signal correlation. Every experiment shows a different, unique correlation pattern and thus, functional connectivity.
In order to analyse the effect of the triangle size onto the functional connectivity of the different neuronal networks the mean pairwise correlation inside the triangles (cell pairs within one triangle) and between different triangles (neuron pairs from different triangles) was calculated for each dsCT1 size. For this question rather the level of correlation than the direction is important. Therefore, the absolute correlations values were considered.
Figure 7.8 displays the absolute mean correlations between (blue circles) and inside (red triangles) the triangles of different dsCT1 sizes and the standard deviations.
It is noticeable that the average correlation inside the triangles is higher for every structure size than the mean correlation between triangles. The mean correlations inside the triangles ranges from 0.75 for 100CT1 to 0.9 for 20CT1. A trend towards a decreasing mean intra-triangular correlation with bigger dsCT1 sizes can be observed ($p = 0.1$). There is no mean correlation value for the 10CT1 structure because for this structure we observed maximum one cell per triangle and thus no cell pairs were present.
The mean correlation values between triangles range from 0.55 for 100CT1 to 0.75 for 10CT1. The value is highest for the 10CT1 structure and decreases further for the 20CT1, 30CT1, 40CT1 and 50CT1 structure to around 0.65

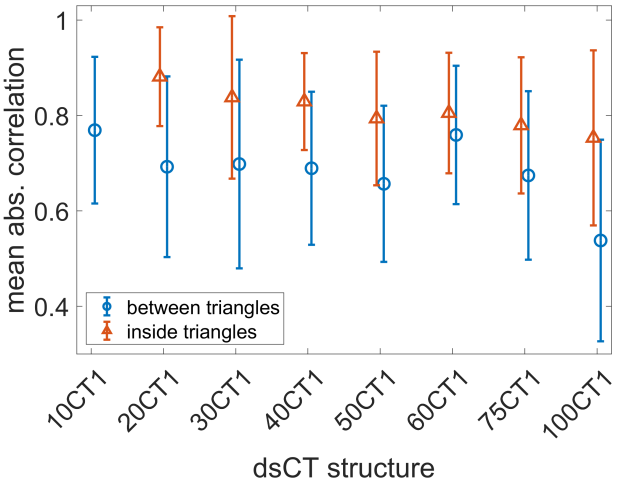


**Figure 7.8:** Mean absolute correlation inside (red triangles) and between triangles (blue circles) of different dsCT1 sizes and their standard deviations.

for the 50CT1 structure size. Correlation rises again for the following sizes (60CT1: 0.67, 75CT1: 0.7) structure and then reaches its minimum at around 0.55 for 100CT1. The overall trend is also towards decreasing mean inter-triangular correlation values with increasing structure size even though the variation of the values is higher than for the intra-triangular correlations. But here too, this negative trend is non-significant ($p = 0.1$).
We see high standard deviations for all mean correlations with values from 0.2 to 0.3. This reflects the broad range of different unique correlation patterns described in the previous paragraphs and observed with different experiments.

**Summary and discussion** Functional connections are a subset of structural connections. Neurons can be regarded as functionally linked, if they show an interdependence in their activities.[122]

**Networks with individual functional fingerprints** The neuron-neuron interactions within the different networks were analysed with pairwise cross-correlations. Each network showed its own functional fingerprint. A variety

of cellular activity patterns was observed in different experiments and for all triangle sizes ranging from very low to high-frequent cellular activity. Also the correlation patterns inside and between triangles were very different from experiment to experiment. Some experiments showed high correlations for the whole observed network area spanning all triangles. Other experiments showed a fraction of correlating cell pairs spread over the whole network while other cells seemed to be excluded from this activity. In some time traces correlations were limited to local areas, often observed within a triangle or some triangles in close vicinity while other recorded time lapse recordings showed almost no correlations. This broad variety of activity patterns are reflected in the high standard deviations of the mean absolute correlation magnitudes displayed in Figure 7.8. To summarise, every network has its own connectivity and activity fingerprint.

**Customising architectural complexity with dsCT size** The mean absolute correlations show some trends in inter- and intra-triangle connectivity depending on the population size.

First, the smaller the triangle size, the higher is the correlation inside but also between different triangles. For the small dsCT1 sizes (10CT1, 20CT1, 30CT1) only a few cells are within a triangle and also fewer neurons in the networks. These networks can be considered as one-dimensional networks with a linear neuron sequence. Bigger dsCT1 sizes are comprised of multiple neurons inside their triangles. An increasing number of neurons increases the architectural complexity of a network.[137] We are moving towards a two-dimensional neuronal network with more complex synaptic connections and thus, more complex activity patterns reducing the mean correlation between the cell pairs. One potential reason might be that synapses in networks with larger populations have a sparser paired connectivity and reduced unitary strengths compared to networks with smaller population sizes (and thus less provided potential partners).[157]

**Functional features of modular network organisation** Furthermore, the mean correlation within a triangle is higher than between different triangles, which was observed for all dsCT1 sizes. This might result from the proximity of the neurons within one triangle and thus, a higher chance of synaptic connectivity. Analyses of the previous chapter showed, that especially the dendrites seem to stay within the triangles and potentially form most of their synapses in the triangles. Also the axons are matured and branched within a triangle before funnelling in bundles towards the next triangle. A higher interconnection within the triangles was already anticipated after structural analysis and results of the cross-correlation analysis confirm this hypothesis. Thus, neurons inside a triangle can be considered as a highly-interconnected population. The weaker intra-populational and a high inter-populational connectivity are an essential feature of non-uniform, modular networks of many *in vivo* circuits involved in information processing.[137,103]

Synchrony of differently sized (20 to 400 neurons), uniform neuronal clusters was investigated by Yamamoto et al., among others. They observed an increasing synchrony with increasing network size.[164] In contrast to these results, reduced synchrony was observed with increased population size in this section. However, the research question as well as experimental conditions varied between the experiments. The networks in the experiments presented here are characterised by a clear structural feature in contrast to the random architecture investigated by Yamamoto et al.

Homogeneous and structured networks differ. Activity patterns of *in vitro* neuronal networks are highly dependent on the complexity of its geometry.[137] Uniform networks are more likely to show widely spread, synchronous bursting activity while structured networks usually tend to display non-repetitive activity patterns with local bursts and sparse spiking as depicted in Figure 7.9.[17] This increased repertoire of activity patterns indicates an additional level of hierarchy that is typical for *in vivo* circuits but is lacking in uniform networks.[137]

In contrast to the population size the actual network size is unknown in

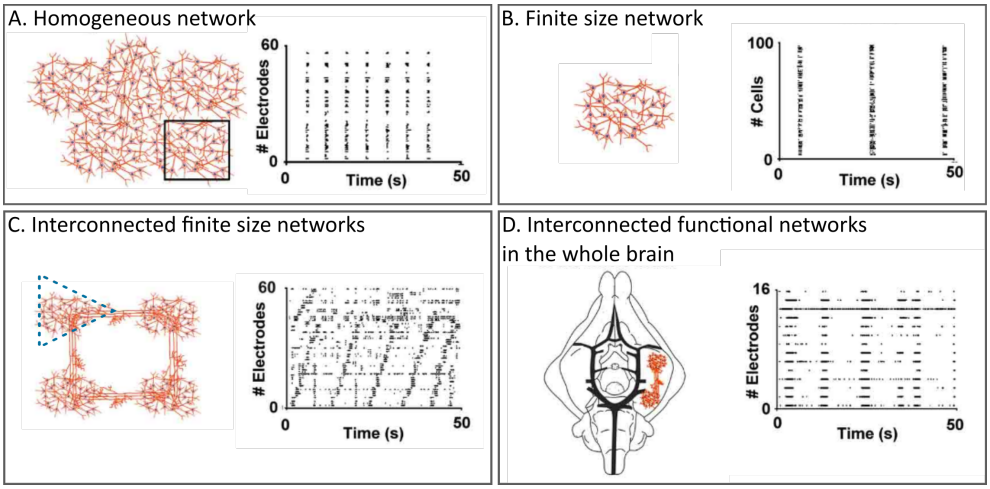


**Figure 7.9:** Network topologies and their activity patterns. Left panels show sketches of different network topologies and right panels display raster plots of typical electrophysiological activity patterns. A. Homogeneous network (1000 neurons) with widely spread, stereotype bursting patterns. B. A region of the homogeneous network (black box in A) can be described as a finite size network, showing bursting activity as observed in homogeneous networks. C. Interconnected finite size networks of about 100 neurons composed of smaller populations (framed with the dotted triangle) exhibiting more complex activity patterns. D. *In vivo* brain (guinea pig) consisting of interconnected functional networks with a high complexity of activity patterns that might be composed of a combination of the above mentioned topologies and activity patterns. Image modified from Bonifazi et al.[17]

our experiments. The focus was on implementing a modular architecture and customising the modules rather then on the size of the network itself. Studies by Yamamoto et al. correspond to the experimental setup depicted in panel B of Figure 7.9.[164] I analysed whether the number of neurons in a population within a bigger network impacts the synchrony in the activity patterns of the network. In Figure 7.9 this would correspond to the number of neurons in a population or node in the network topology displayed in panel C and framed with the dotted triangle.

Synchronous events as observed by Yamamoto et al. and Shein Idelson et al. in uniform neuronal clusters were also present in some experiments of this work and in earlier studies of Albers.[4,3,136,164] More specifically, they observed

activity patterns characterised by short intervals of intense firing followed by longer time windows of sporadic firing, similar to some activity patterns presented in this chapter (e.g. Figure 7.5.2/3 Figure 7.6.4, Figure 7.7.3). However, they are one form of activity patterns in the repertoire of our structural, modular networks.

Another difference between the reported studies is the culturing duration. While Yamamoto et al. measured activity after 10 DIV, dsCT networks were cultured until 21 to 22 DIV. Neuronal cultures are reported to undergo re-organization during development and maturation, and show developmentally dependent interactions. Young cultures exhibit a random topology while small-world topologies with highly interconnected nodes were observed from DIV 14 in *in vitro* cultures. Changing spontaneous activity patterns during maturation could drive a transformation in network's architecture.[44] Thus, culturing duration has to be carefully considered in the experimental design.

Summarising, a neuronal network's functional connectivity can be regarded as a subset of structural connectivity. Network topology plays a crucial role and impacts functional connectivity. Uniform *in vitro* networks show markedly different activity patterns to *in vivo* activity repertoires, foremost lacking localised activation. Thus, homogeneous network models should be extended by structural features to recreate the relevant *in vivo* organisation. The triangular geometry presented here can be utilised to engineer modular neuronal networks. The distinct populations are characterised by a high intra-populational connectivity and a weaker intra-populational connectivity, an essential feature of modular network architecture. An increased population size resulted in an increased architectural complexity revealed by a decreased synchrony.

Larger dsCT networks show a decreased synchrony indicating an architectural complexity with an extended repertoire of activity patterns.

## 7.3 Signal propagation directionality

The remaining question whether we see a directionality in signal propagation can be analysed via electrical recordings with MEAs. In contrast to the $Ca^{2+}$ imaging method, MEA recordings are characterised by a high temporal resolution, but a lower spatial resolution due to the limited number of electrodes for simultaneous recording (here 64 electrodes).

Electrical recordings of the dsCT1 networks might give a deeper insight into the signal propagation direction rather than a cell-to-cell interaction. For this thesis, some initial proof-of-concept experiments were performed with patterned dsCT1 cultures on lineMEAs.

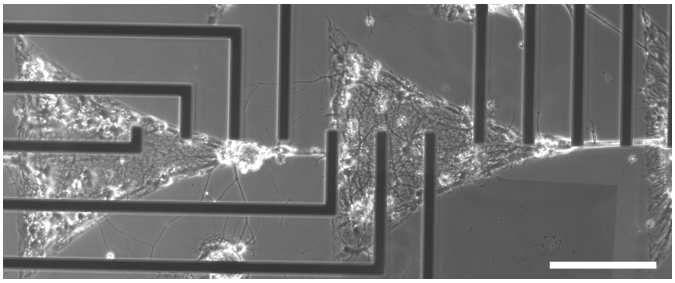

**Figure 7.10:** Good cell adherence on a MEA with silicon oxide surface. DIV 28. Scale bar 200 µm.

Initially, MEA substrates with a silicon oxide surface were used. Here, the patterning protocol was the same as for µCP on glass coverslips and cultures were stable over four weeks *in vitro*. One culture is depicted in Figure 7.10. However, changes in the fabrication process resulted in unstable passivation layers and thus, MEAs that could not be used for recordings.

After that, the protocol for MEA production was adapted in the institute including a change in surface material to polyimid (PI). Patterned PI-MEAs prepared with the µCP protocol for glass substrates resulted in cultures with cell clumps and detaching neuronal assemblies (Figure 7.11). The chance to record signals and analyse directionality with such cultures is very low.

Despite the unsatisfactory cell separation, electrical signals were recorded (Figure 7.12). Three channels showed multiple peaks, channel 2, 10 and 11.

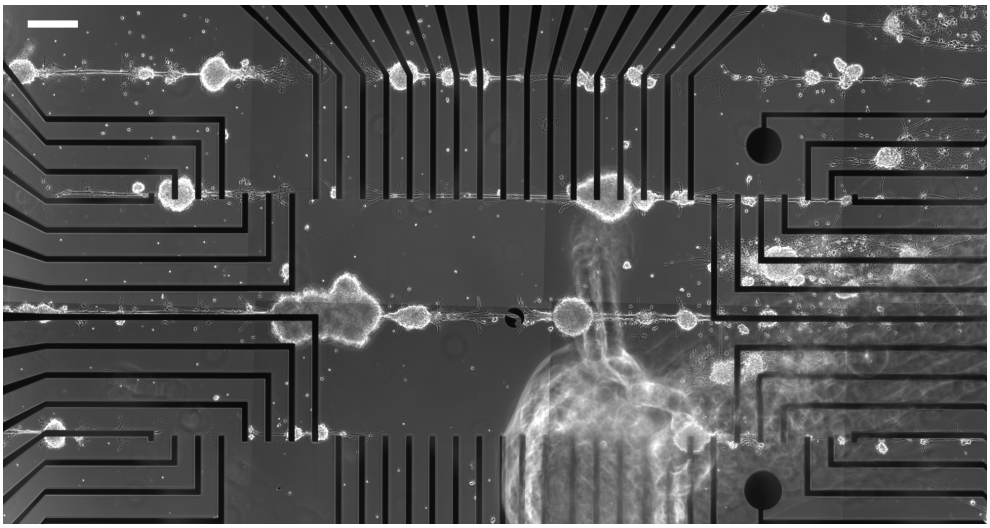

**Figure 7.11:** Detaching and clumped neuronal culture on MEA. Scale bar 200 µm.

Zooming into the time traces we can observe a delay between the signals with channel 10 showing a signal first, followed by channel 11 and then channel 2. For 23 signal pairs of channel 10 and channel 2 the signal was first observed in channel 10. Approximately 0.5 ms later the signal was also recorded in channel 2. Both channels are within one electrode line and the distance between them is 800 µm. If we consider the velocity of electrical signal transmission in neurons being around 1 m/s,[72] we would expect a signal delay of around 800 µs which is of the same order of magnitude as the observed delay of approximately 500 µs.

**Summary and discussion** The experiments proved, that directionality of the dsCT1 networks can be analysed via electrical recordings with MEAs. Despite some successful recordings with a few active channels, µCP protocol has to be optimised in order to obtain long-term stable cultures with single cell separation. Moreover, a higher number of channels with recorded activity and peaks is required.

To improve the stickiness on the surface, a mixture of ECM, PLL and gelatin was used for later experiments. However, protein composition and its inter-

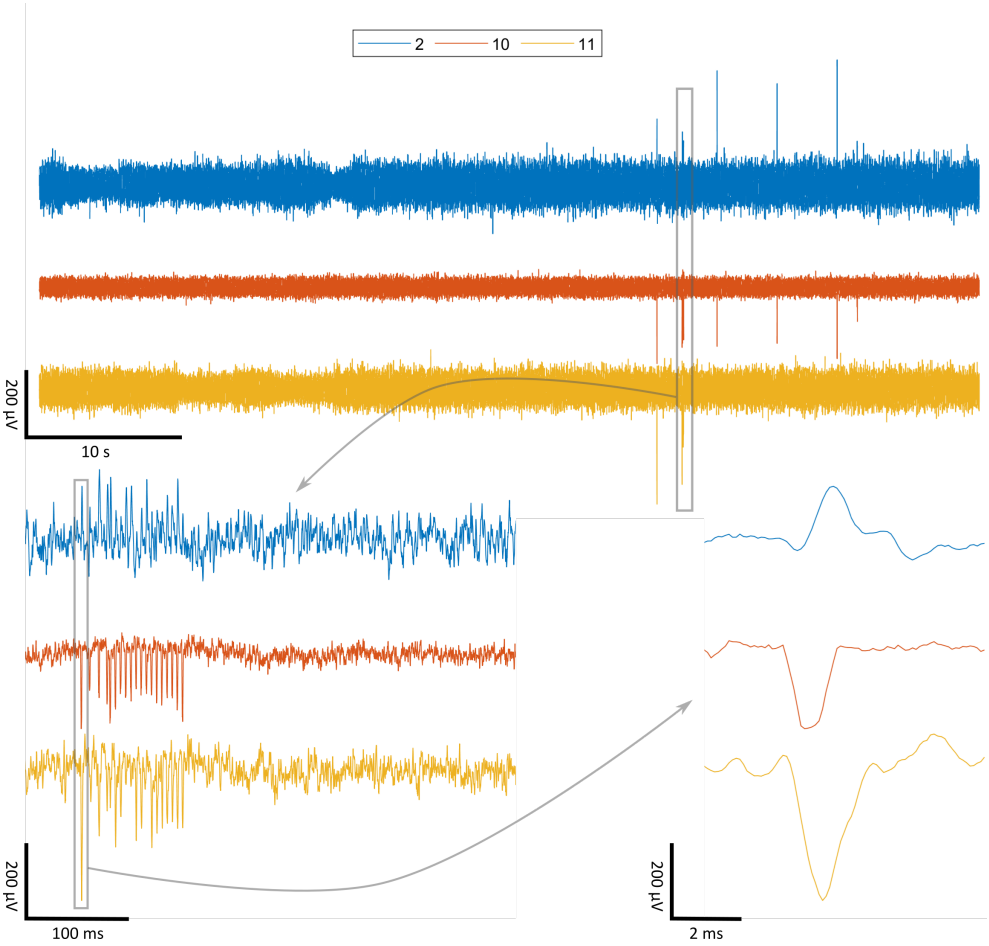


**Figure 7.12:** Electrical recordings from 30CT1 culture on MEA. 3 channels showed peaks, channel 2, 10 and 11. Zooming into the time trace we can see a potential delay between the signals.

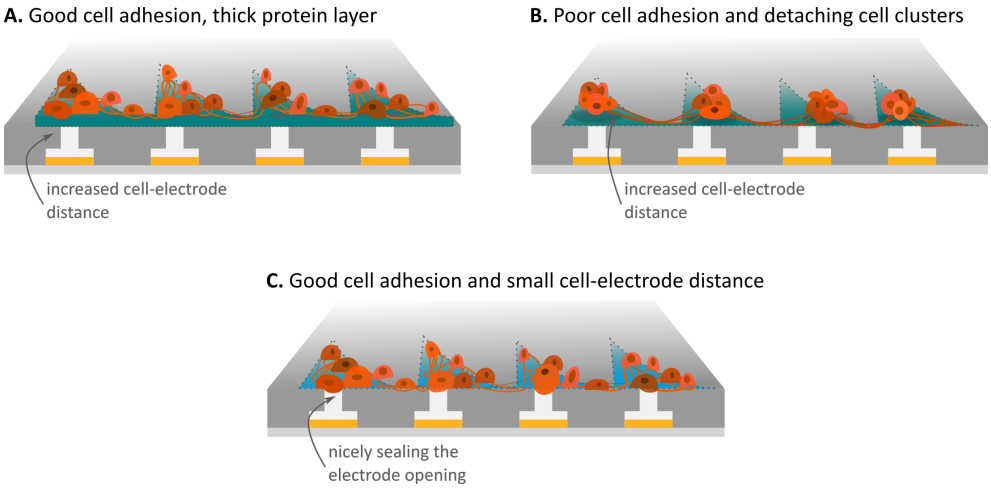


**Figure 7.13:** Cell adhesion on MEA. A. Good cell adhesion but a thick protein layer which increases cell-electrode distance and lowers the electrode's sensing abilities. B. Poor cell adhesion due to disadvantageous protein-surface interactions might result in detaching cell clusters. We lose single-cell resolution and increase cell-electrode distance. C. Good cell adhesion on a thin coating layer promotes a lower cell-electrode distance. Single cells nicely seal the electrode openings of the nanocavity-MEAs and further improve the electrode's sensing abilities.

action with the MEA surface plays an important role. Adhesive proteins have an impact onto the electrode's sensing ability by influencing the cell-electrode distance. While coatings like poly-lysines result in a cell-electrode distance of some tens nm, ECM proteins and gelatin result in several hundreds nm and might potentially prevent the electrode from sensing the electrical signals (as schematically shown in Figure 7.13 A).[16] This increased cell-electrode distance might result in a lower number of channels with recorded peaks. Indeed, recordings with active channels and signals were sparse after changing the protocol. A protein coating consisting of poly-lysine (and laminin) might be thinner, but was observed to result in an unstable protein layer on the PI surface of the MEA. The poor cell adhesion of long-term cultures (schematically shown in Figure 7.13 B) also lowers the chance for successful recordings. Moreover, we lose single-cell resolution due to cell clustering.
Here, we have to carefully balance a stable protein adhesion layer and the protein thickness in order to optimise electrical recordings because a good ad-

hesion to the substrate is crucial for the recording quality. A stable and thin adhesion layer (Figure 7.13 C) is necessary for successful recordings where cells can nicely seal the electrode openings of the nanocavity-MEAs reducing the cell-electrode distance as well as leakage of the extracellular potential. Additionally, single-cell resolution can be achieved. Therefore, some further protein compositions or surface coatings might be considered for future experiments to optimise long-term stability of neuronal cultures on dsCT1 patterns on MEAs like the usage of silanes to better bind poly-lysines.[16]
In summary, sparse neuronal activity was recorded from networks cultured on dsCT1 patterns. These recordings showed, that the lineMEA design in principle enables detection of signal transmission and delays within dsCT1 cultures. Further experiments are needed to optimise the patterning and cellular adhesion on the MEA surface as well as to gain deeper insights into the directional functionality.

## 7.4 Conclusion and outlook

Neuronal circuit properties are believed to be impacted by neuronal (e.g. subtype), synaptic (biochemical properties) and structural (specific coupling and connectivity) features.[45,137] Many studies focused on analysing the impact of structure onto function of *in vitro* neuronal networks. However, most examined networks were characterised by a uniformity.[157,136,164] Adequate *in vitro* models with specific structural features might be of a great help in order to gain a deeper understanding of *in vivo* neuronal circuitry.
Here, we present a system to incorporate the essential features of organisation and hierarchy into cultured neuronal networks. The dsCT structures provide an anatomical circuitry control over the population size and directionality of neuronal connections (chapter 6). Neuronal connectivity is characterised by the structural network architecture as well as by the strength and dynamics of the existing connections.[166,88] The dsCT networks showed a preserved neuronal activity independent of population size. However, the architectural complexity increased with population size as network architecture moves from 1D (small dsCT) to 2D (bigger dsCT). This increase of architectural complexity goes together with a decreased synchrony. Moreover, the networks showed functional features of a modular organisation characterised by a high intra-populational and a weaker inter-populational connectivity.[137]

### Perspectives towards future experiments

**Changing experimental conditions** Experimental conditions can be optimised in order to obtain even more healthy and stable cultures and thus, reliant results.
First, the neuronal density within the cultures can be increased. Neuronal cultures can be difficult to maintain over a long time period because chemical characteristics of protein patterns change the over time. Moreover, some neurons dissociate or even die over the culturing period of two to four weeks decreasing the cell number within a population. Additionally, not all neurons

show an activity in the $Ca^{2+}$ imaging traces. This leads to an overall lower number of active neuronal traces than planned. To overcome the decreased neuronal number, the plated cell concentration might be increased for further experiments.
Second, culturing duration has to be reconsidered because of reported reorganization of network properties during maturation. Small-world properties evolve after DIV 14 and mature, stable and organised networks are present from the age of DIV 28 to 35.[44] Thus, network's functional analysis should be performed from DIV 28 onwards.
Moreover, longer observation periods might increase information content. Here, neuronal network activity was analysed for a 60 s time period. However, networks can change their activity patterns from synchronised to unsynchronised states.[50] Additionally, synchronisation can occur at different time scales - from transient synchronisation between some populations to regularly synchronised activity over longer time scales.[44] Consequential, longer observation periods of one network area could give deeper insights into the temporal changes of network's activity patterns like the transition of asynchronous to synchronous activity state of small-size circuits with a few tens of neurons as in microcolumns or neuronal assemblies.[50] Moreover, long-term experiments could give a insight into the reorganisation of the functional activity of structured networks. For this purpose, activity of the same network areas have to be imaged at specific time points over weeks in culture.
In regard of analysing signal propagation direction with MEAs, surface modification and protein solution has to be further optimised to increase long-term culture stability. Here, a thin and stable adhesion layer would positively impact cell-electrode distance and thus the electrode's sensing abilities.

**Upscaled CT1 structures** The structure sizes chosen for these experiments resulted in populations of 1 to 40 neurons. This is a rather low analysed range if we consider network sizes in the brain that include many thousands of neurons and neuronal subpopulations of hundreds of cells. Shein Idelson et al. calculated that minimum 40 cells are needed to obtain networks with

collective dynamics.[136] Even though they analysed uniform networks, this observation might be included in the design of future experiments. Additional experiments with bigger populations (>40) might reveal interesting effects. With the experience gained here, I would suggest bigger steps of upscaling to a cell number of 500 neurons/population.
µCP surfaces were already used by different groups as systems to extrinsically control the network size and the area it occupies.[164,136,157] Their observed cell densities coincide with the cell density reported in the previous chapter. Thus, triangles with 1.5 - 2 mm dimensions are required to obtain neuronal populations comprised of 200 - 400 neurons/mm$^2$.

**Varying population sizes within a network** Another interesting question would be to combine different sizes of populations within a network architecture. Daisy-chained bigger and smaller triangles can be used to analyse effects of the population size onto signal input and output.

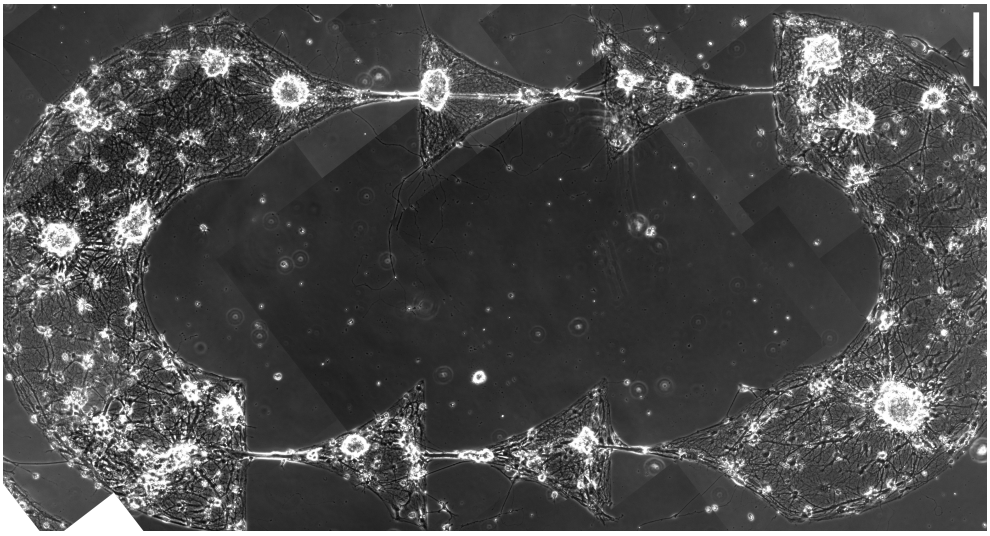

**Figure 7.14:** NeuroCAP structure from Albers for circular activity.[2] DIV 27, Scale bar 200 µm.

Moreover, one could think of a structure which promotes circular neuronal activity as designed by Jonas Albers (Figure 7.14).[2]

**Networks with defined network and populations size** Studies analysed the effect of size onto neuronal dynamics usually focused on the role of network size (e.g. Yamamoto et al.,[164] Shein Idelson et al.[136]). Studies by e.g. Yamamoto et al.[164] or Shein Idelson et al.[136] analysed uniform networks of different size that were lacking the modular or hierarchical architectural feature of *in vivo* circuits. In order to extend these models by the essential organisational feature, a defined number of daisy-chained triangles might be used. With that, modular, directional networks of defined network as well as population size can be engineered.

Summarising, the presented system provides many possibilities for future experiments that all can help to reveal a host of neuronal connectivity and functionality properties. *In vitro* systems extended by the essential feature of organisation and hierarchy are a powerful tool to bridge the gap between uniform *in vitro* models and *in vivo* circuits.

# Chapter 8

# General conclusion

Structure and function within the brain go hand in hand. Thus, structural organisation is an essential feature of the organ of mind.

With technical progress various novel methods were discovered for neuroscience including methods to extrinsically control the architectural properties of neuronal networks. Soft lithography, or μCP is one of these methods. Adhesive micro patterns on a substrate can be employed to impact individual neuronal and network features.[112]

The research work of this thesis focused on coordinating structure and size of deposited neuronal networks on single cell as well as population level. Extensive experiments have been performed with isolated rat cortical neurons growing on protein patterns with different geometries consisting of nodes, lines and triangles. The purpose was to explore the impact of pattern geometry features onto structure as well as function.

On the single cell level (Part I), the chosen pattern geometries consisting of lines and nodes influenced soma position and neuronal polarisation. Here, an interplay of multiple factors like node-to-line-area ratio, line lengths and number were found to impact neuronal development and polarisation. Moreover, soma positioning on the individual pattern is crucial for a high polarisation efficiency. With the presented single cell patterns, directed neuronal networks with individually addressable cells can be engineered. Those can contribute to unravel processes involved in neuronal development such as axon specifica-

tion and soma migration. Moreover, the networks showed long-term stability and neuronal activity which was analysed with MEA and calcium imaging. Combining defined networks with recording techniques provides a platform to study the impact of individual neuronal activity onto a network.

In the brain, we see different levels of hierarchy. Neuronal circuits involved in information processing are characterised by a modular architecture. Neurons contribute to collective dynamics in different populations.[137] Thus, analysis of population activity onto network dynamics is of great interest. Population connectivity was recreated by daisy chained triangles in the second part (Part II). Here, the aim was to add a level of hierarchy and engineer networks with differently sized modules as is observed for example in cortical columns in the brain. The designed patterns successfully controlled population sizes within the networks. Modules consisted of one to some tens of neurons and showed a directional structural connectivity. The networks were characterised by a stronger structural and functional intra-populational and a weaker intermodule connectivity, a feature that is typical for a modular network organisation[103,137] As population size increased, network architecture changed from 1D to 2D and resulted in a decreased synchrony indicating an increase of architectural complexity.

Being able to control the organisation of neuronal networks *in vitro* demonstrates the initial step toward engineering networks and investigate how structure effects function *in vivo*. This work presents patterns that can be employed to customise network architectures on single cell as well as population level and thus, recreate microcircuitry from the brain. The data presented here manifests that designed neuronal networks are a powerful platform to study fundamental motifs and units of neuronal organisation as well as neuronal activity dynamics. Unlike *in vivo* networks, deposited networks can be analysed in a controlled environment with a high susceptibility to manipulation. The outcome can then be transferred to the next, higher levels of organisation, and refine our understanding of the interplay of structure and function of the whole brain.

Combination of structured networks with other techniques as recording and stimulation methods offers a manifold toolbox. Various research questions investigating neuronal processes that need long term monitoring can be approached, such as network maturation or plasticity. Here, the possibilities are wide-ranging and some were presented in this work. These include establishing designed networks on MEAs that provides the possibility to non-invasively and simultaneously analyse electrical activity of multiple cells. Moreover, MEAs are suitable for electrical stimulation of individual neurons.[33,83] Besides electrical stimulation, stimulation via light provides spatio-temporal precise input.[77,38] Another powerful tool is the introduction of genetically encoded sensors (e.g. calcium sensors, voltage sensitive dyes) to optically monitor neuronal activity.[20] The suitability of calcium sensors to unravel functional connectivity was successfully demonstrated in this work. Developing and advancing bioelectronics tools contribute to a toolbox enabling highly controlled experiments. With that a host of experimental designs can be arranged to approach the interplay of neuronal cells. Individual cells can be addressed and their response as well as their neighbours' behaviour can be investigated and mapped precisely. Thus, providing the ability to perform long-term and non-invasive measurements of neurons within structured networks.

Future work using the outcomes of structured networks includes incorporation of the third dimension in order to meet the organised 3D architecture of the brain. Here, mechanisms discovered in 1D and 2D engineered neuronal networks provide essential information. First approaches towards 3D cultures with a defined architecture seem promising. With micro-chambers and fibre orientation techniques Odawara et al. were able to mimic the layered structure of the cerebral cortex on a chip.[111] So did Frimat et al. with a biogel scaffold.[56]

Customised neuronal 1D, 2D, and 3D networks provide robust experimental models for our understanding of fundamental neuroscience. Moreover, adequate *in vitro* models can dramatically reduce animal use for pharmacological studies. These systems provide the advantages of being more cost-effective,

robust and high-throughput. Additionally, customised structured networks can advance functional tissue engineering for transplantation and might be a promising approach for paralysed patients. Furthermore, engineered networks allow testing theories in simplified and pre-designed scenarios and thus are well suited for comparison with modelling results.

The pay-off from advancing neuroscience is expected to be huge. It will contribute to formulation of a viable theory of the brain's capabilities which might be one of the greatest intellectual challenges in mankind's history. Not only will a deeper understanding offer novel, real treatments of neurological diseases (instead of treating symptoms as it is nowadays) but also have tremendous applications for building intelligent machines inspired by the stunning organ of mind.

# List of Figures

# List of Tables

# Bibliography


[1] J. Akerboom et al. "Optimization of a GCaMP Calcium Indicator for Neural Activity Imaging". In: *Journal of Neuroscience* 32.40 (2012). DOI: 10.1523/JNEUROSCI.2601-12.2012.

[2] J. Albers. "Entwicklung axonaler Dioden zur Untersuchung des gerichteten Informationsflusses in neuronalen Strukturen". PhD thesis. RWTH Aachen University, 2016. DOI: 10.18154/RWTH-2016-11527.

[3] J. Albers and A. Offenhäusser. "Signal Propagation between Neuronal Populations Controlled by Micropatterning". In: *Frontiers in Bioengineering and Biotechnology* 4.June (2016). DOI: 10.3389/fbioe.2016.00046.

[4] J. Albers, K. Toma, and A. Offenhäusser. "Engineering connectivity by multiscale micropatterning of individual populations of neurons". In: *Biotechnology Journal* 10.2 (2015). DOI: 10.1002/biot.201400609.

[5] F. Ali and A. C. Kwan. "Interpreting in vivo calcium signals from neuronal cell bodies, axons, and dendrites: a review". In: *Neurophotonics* 7.01 (2019). DOI: 10.1117/1.NPh.7.1.011402.

[6] *Allen Institute for Brain Science*.

[7] S. Alom Ruiz and C. S. Chen. "Microcontact printing: A tool to pattern". In: *Soft Matter* 3.2 (2007). DOI: 10.1039/B613349E.

[8] O. Arias-Carrión et al. "Orquestic regulation of neurotransmitters on reward-seeking behavior". In: *International Archives of Medicine* 7.1 (2014). DOI: 10.1186/1755-7682-7-29.

[9] N. Arimura and K. Kaibuchi. "Neuronal polarity: from extracellular signals to intracellular mechanisms". In: *Nature Reviews Neuroscience* 8.3 (2007). DOI: 10.1038/nrn2056.

[10] R. W. Atchison, B. C. Casto, and W. M. Hammon. "Adenovirus-Associated Defective Virus Particles". In: *Science* 149.3685 (1965). DOI: 10.1126/science.149.3685.754.

[11] F. Barnabé-Heider et al. "Evidence that Embryonic Neurons Regulate the Onset of Cortical Gliogenesis via Cardiotrophin-1". In: *Neuron* 48.2 (2005). DOI: 10.1016/j.neuron.2005.08.037.

[12] B. P. Bean. "The action potential in mammalian central neurons." In: *Nature reviews. Neuroscience* 8.6 (2007). DOI: 10.1038/nrn2148.

[13] M. J. Berridge, P. Lipp, and M. D. Bootman. "The versatility and universality of calcium signalling". In: *Nature Reviews Molecular Cell Biology* 1.1 (2000). DOI: 10.1038/35036035. arXiv: 1502.05134.

[14] E. Biffi et al. "The Influence of Neuronal Density and Maturation on Network Activity of Hippocampal Cell Cultures: A Methodological Study". In: *PLoS ONE* 8.12 (2013). Ed. by G. F. Gilestro. DOI: 10.1371/journal.pone.0083899.

[15] A. Bignami and D. Dahl. "Axonal maturation in development—II. Immunofluorescence study of rat spinal cord and cerebellum with axon-specific neurofilament antibodies". In: *International Journal of Developmental Neuroscience* 5.1 (1987). DOI: 10.1016/0736-5748(87)90045-1.

[16] A. Blau. "Cell adhesion promotion strategies for signal transduction enhancement in microelectrode array in vitro electrophysiology: An introductory overview and critical discussion". In: *Current Opinion in Colloid & Interface Science* 18.5 (2013). DOI: 10.1016/j.cocis.2013.07.005.

[17] P. Bonifazi et al. "In vitro large-scale experimental and theoretical studies for the realization of bi-directional brain-prostheses". In: *Frontiers in Neural Circuits* 7.March (2013). DOI: 10.3389/fncir.2013.00040.

[18] M. D. Bootman et al. "Ca2+-Sensitive Fluorescent Dyes and Intracellular Ca2+ Imaging". In: *Cold Spring Harbor Protocols* 2013.2 (2013). DOI: 10.1101/pdb.top066050.

[19] K. Brodmann. *Vergleichende Lokalisationslehre der Großhirnrinde in ihren Prinzipien dargestellt auf Grund des Zellenbaues*. Leipzig: Barth, 1909.

[20] G. J. Broussard, R. Liang, and L. Tian. "Monitoring activity in neural circuits with genetically encoded indicators". In: *Frontiers in Molecular Neuroscience* 7 (2014). DOI: 10.3389/fnmol.2014.00097.

[21] J. Brown et al. "Rapid changes in intracellular free calcium concentration. Detection by metallochromic indicator dyes in squid giant axon". In: *Biophysical Journal* 15.11 (1975). DOI: 10.1016/S0006-3495(75)85891-7.

[22] G. Buzsáki and K. Mizuseki. "The log-dynamic brain: how skewed distributions affect network operations". In: *Nature Reviews Neuroscience* 15.4 (2014). DOI: 10.1038/nrn3687.

[23] R. Calcedo et al. "Worldwide Epidemiology of Neutralizing Antibodies to Adeno-Associated Viruses". In: *The Journal of Infectious Diseases* 199.3 (2009). DOI: 10.1086/595830.

[24] R. Calcedo et al. "Adeno-Associated Virus Antibody Profiles in Newborns, Children, and Adolescents". In: *Clinical and Vaccine Immunology* 18.9 (2011). DOI: 10.1128/CVI.05107-11.

[25] M. Castanares, G. J. Stuart, and V. Daria. "Holographic Functional Calcium Imaging of Neuronal Circuit Activity". In: *Advanced Optical Methods for Brain Imaging*. Singapore: Springer Singapore, 2019. DOI: 10.1007/978-981-10-9020-2_8.

[26] T.-W. Chen et al. "Ultrasensitive fluorescent proteins for imaging neuronal activity". In: *Nature* 499.7458 (2013). DOI: 10.1038/nature12354.

[27] J.-H. Choi et al. "Optimization of AAV expression cassettes to improve packaging capacity and transgene expression in neurons". In: *Molecular Brain* 7.1 (2014). DOI: 10.1186/1756-6606-7-17.

[28] B. W. Connors and M. A. Long. "Electrical Synapses in the Mammalian Brain". In: *Annual Review of Neuroscience* 27.1 (2004). DOI: 10.1146/annurev.neuro.26.041002.131128.

[29] J. M. Corey, B. C. Wheeler, and G. J. Brewer. "Compliance of hippocampal neurons to patterned substrate networks". In: *Journal of Neuroscience Research* 30.2 (1991). DOI: 10.1002/jnr.490300204.

[30] A. M. Craig and G. Banker. "Neuronal Polarity". In: *Annual Review of Neuroscience* 17.1 (1994). DOI: 10.1146/annurev.ne.17.030194.001411.

[31] G. Csucs et al. "Microcontact Printing of Macromolecules with Submicrometer Resolution by Means of Polyolefin Stamps". In: *Langmuir* 19.15 (2003). DOI: 10.1021/la0342823.

[32] A. Czeschik, A. Offenhäusser, and B. Wolfrum. "Fabrication of MEA-based nanocavity sensor arrays for extracellular recording of action potentials". In: *physica status solidi (a)* 211.6 (2014). DOI: 10.1002/pssa.201330365.

[33] A. Czeschik et al. "Nanostructured cavity devices for extracellular stimulation of HL-1 cells". In: *Nanoscale* 7.20 (2015). DOI: 10.1039/C5NR01690H.

[34] D. Dahl, E. E. Gardner, and C. J. Crosby. "Axonal maturaion in development—I. Characterization of monoclonal antibodies reacting with axon-specific neurofilament epitopes". In: *International Journal of Developmental Neuroscience* 5.1 (1987). DOI: 10.1016/0736-5748(87)90044-X.

[35] O. Davis et al. "Studying the role of axon fasciculation during development in a computational model of the Xenopus tadpole spinal cord". In: *Scientific Reports* 7.1 (2017). DOI: 10.1038/s41598-017-13804-3.

[36] S. Daya and K. I. Berns. "Gene Therapy Using Adeno-Associated Virus Vectors". In: *Clinical Microbiology Reviews* 21.4 (2008). DOI: 10.1128/CMR.00008-08.

[37] J. DeFelipe. "The anatomical problem posed by brain complexity and size: a potential solution". In: *Frontiers in Neuroanatomy* 9.August (2015). DOI: 10.3389/fnana.2015.00104.

[38] K. Deisseroth. "Optogenetics." In: *Nature methods* 8.1 (2011). DOI: 10.1038/nmeth.f.324.

[39] T. Deneux et al. "Accurate spike estimation from noisy calcium signals for ultrafast three-dimensional imaging of large neuronal populations in vivo". In: *Nature Communications* 7.1 (2016). DOI: 10.1038/ncomms12190.

[40] E. W. Dent, S. L. Gupton, and F. B. Gertler. "The Growth Cone Cytoskeleton in Axon Outgrowth and Guidance". In: *Cold Spring Harbor Perspectives in Biology* 3.3 (2011). DOI: 10.1101/cshperspect.a001800.

[41] C. J. Donahue et al. "Quantitative assessment of prefrontal cortex in humans relative to nonhuman primates". In: *Proceedings of the National Academy of Sciences* 115.22 (2018). DOI: 10.1073/pnas.1721653115.

[42] M. S. Al-Dosari and X. Gao. "Nonviral Gene Delivery: Principle, Limitations, and Recent Progress". In: *The AAPS Journal* 11.4 (2009). DOI: 10.1208/s12248-009-9143-y.

[43] C. G. Dotti, C. A. Sullivan, and G. A. Banker. "The establishment of polarity by hippocampal neurons in culture." In: *The Journal of neuroscience : the official journal of the Society for Neuroscience* 8.4 (1988).

[44] J. H. Downes et al. "Emergence of a Small-World Functional Network in Cultured Neurons". In: 8.5 (2012). DOI: 10.1371/journal.pcbi.1002522.

[45] R. Duarte and A. Morrison. "Leveraging heterogeneity for neural computation with fading memory in layer 2/3 cortical microcircuits". In: *PLOS Computational Biology* 15.4 (2019). Ed. by J. Ayers. DOI: 10.1371/journal.pcbi.1006781.

[46] A. F. Dulhunty. *Excitation-contraction coupling from the 1950s into the new millennium*. 2006. DOI: 10.1111/j.1440-1681.2006.04441.x.

[47] C. von Economo and G. Koskinas. *Die Cytoarchitektonik der Hirnrinde desErwachsenen Menschen. Textband und Atlas*. Wien und Berlin, 1925.

[48] J. Erickson et al. "Caged neuron MEA: A system for long-term investigation of cultured neural network connectivity". In: *Journal of Neuroscience Methods* (2008). DOI: 10.1016/j.jneumeth.2008.07.023.

[49] L. Fan et al. "Directional neurite outgrowth on superaligned carbon nanotube yarn patterned substrate". In: *Nano Letters* (2012). DOI: 10.1021/nl301428w.

[50] D. Fasoli, A. Cattani, and S. Panzeri. "Transitions between asynchronous and synchronous states: a theory of correlations in small neural circuits". In: *Journal of Computational Neuroscience* 44.1 (2018). DOI: 10.1007/s10827-017-0667-3.

[51] O. Feinerman, A. Rotem, and E. Moses. "Reliable neuronal logic devices from patterned hippocampal cultures". In: *Nature Physics* 4.12 (2008). DOI: 10.1038/nphys1099.

[52] O. Feinerman, M. Segal, and E. Moses. "Signal Propagation Along Unidimensional Neuronal Networks". In: *Journal of Neurophysiology* 94.5 (2005). DOI: 10.1152/jn.00264.2005.

[53] C. Forró et al. "Modular microstructure design to build neuronal networks of defined functional connectivity". In: *Biosensors and Bioelectronics* (2018). DOI: 10.1016/j.bios.2018.08.075.

[54] H. Francisco et al. "Regulation of axon guidance and extension by three- dimensional constraints". In: *Biomaterials* 28.23 (2007). DOI: 10.1016/j.biomaterials.2007.04.015.

[55] R. Fricke et al. "Axon guidance of rat cortical neurons by microcontact printed gradients". In: *Biomaterials* 32.8 (2011). DOI: 10.1016/j.biomaterials.2010.11.036.

[56] J.-P. Frimat et al. "Advances in 3D neuronal cell culture". In: *Journal of Vacuum Science & Technology B, Nanotechnology and Microelectronics: Materials, Processing, Measurement, and Phenomena* 33.6 (2015). DOI: 10.1116/1.4931636.

[57] Y. Funahashi et al. "Neuronal polarization in vivo: Growing in a complex environment". In: *Current Opinion in Neurobiology* 27 (2014). DOI: 10.1016/j.conb.2014.04.009.

[58] P. Garcia-Lopez. "The histological slides and drawings of Cajal". In: *Frontiers in Neuroanatomy* 4.March (2010). DOI: 10.3389/neuro.05.009.2010.

[59] W. Gerstner et al. "Neural codes: Firing rates and beyond". In: *Proceedings of the National Academy of Sciences of the United States of America* (1997). DOI: 10.1073/pnas.94.24.12740.

[60] A. Gladkov et al. "Design of Cultured Neuron Networks in vitro with Predefined Connectivity Using Asymmetric Microfluidic Channels". In: *Scientific Reports* 7.1 (2017). DOI: 10.1038/s41598-017-15506-2.

[61] K. Goslin. "Experimental observations on the development of polarity by hippocampal neurons in culture". In: *The Journal of Cell Biology* 108.4 (1989). DOI: 10.1083/jcb.108.4.1507.

[62] C. Grienberger and A. Konnerth. "Imaging Calcium in Neurons". In: *Neuron* 73.5 (2012). DOI: 10.1016/j.neuron.2012.02.011.

[63] G. Grynkiewicz, M. Poenie, and R. Y. Tsien. "A new generation of Ca2+ indicators with greatly improved fluorescence properties." In: *The Journal of biological chemistry* 260.6 (1985).

[64] J. A. Hammarback et al. "Guidance of Neurite Outgrowth by Pathways of Substratum-Adsorbed Laminin". In: *Journal Of Cell Biology* 220 (1985).

[65] J. Hawkins, S. Ahmad, and Y. Cui. "Why Does the Neocortex Have Columns, A Theory of Learning the Structure of the World". In: *bioRxiv* (2017). DOI: 10.1101/162263.

[66] S. Herculano-Houzel. "The human brain in numbers: a linearly scaled-up primate brain". In: *Frontiers in Human Neuroscience* 3.November (2009). DOI: 10.3389/neuro.09.031.2009.

[67] A. L. Hodgkin and A. F. Huxley. "The components of membrane conductance in the giant axon of Loligo". In: *The Journal of Physiology* 116.4 (1952). DOI: 10.1113/jphysiol.1952.sp004718.

[68] B. Hofmann. "Communicating with electrogenic cells". PhD thesis. RWTH Aachen University, 2009.

[69] B. Hofmann et al. "Nanocavity electrode array for recording from electrogenic cells". In: *Lab on a Chip* 11.6 (2011). DOI: 10.1039/c0lc00582g.

[70] R. Holehonnur et al. "Adeno-associated viral serotypes produce differing titers and differentially transduce neurons within the rat basal and lateral amygdala". In: *BMC Neuroscience* 15.1 (2014). DOI: 10.1186/1471-2202-15-28.

[71] D. H. Hubel and T. N. Wiesel. "Sequence regularity and geometry of orientation columns in the monkey striate cortex". In: *Journal of Comparative Neurology* (1974). DOI: 10.1002/cne.901580304.

[72] J. B. Hursh. "Conduction velocity and diameter of nerve fibers". In: *American Journal of Physiology-Legacy Content* 127.1 (1939). DOI: 10.1152/ajplegacy.1939.127.1.131.

[73] A. Iannielli et al. "Reconstitution of the Human Nigro-striatal Pathway on-a-Chip Reveals OPA1-Dependent Mitochondrial Defects and Loss of Dopaminergic Synapses". In: *Cell Reports* 29.13 (2019). DOI: 10.1016/j.celrep.2019.11.111.

[74] N. Insel and C. A. Barnes. "Differential Activation of Fast-Spiking and Regular-Firing Neuron Populations During Movement and Reward in the Dorsal Medial Frontal Cortex". In: September (2015). DOI: 10.1093/cercor/bhu062.

[75] K. L. Jackson et al. "Better Targeting, Better Efficiency for Wide-Scale Neuronal Transduction with the Synapsin Promoter and AAV-PHP.B". In: *Frontiers in Molecular Neuroscience* 9.November (2016). DOI: 10.3389/fnmol.2016.00154.

[76] M. J. Jang and Y. Nam. "Geometric effect of cell adhesive polygonal micropatterns on neuritogenesis and axon guidance". In: *Journal of Neural Engineering* 9.4 (2012). DOI: 10.1088/1741-2560/9/4/046019.

[77] L. Jin. "Optical control of primary rat cortical neural activity in vitro". PhD Thesis. RWTH Aachen University, 2016.

[78] E. G. Jones. "Microcolumns in the cerebral cortex". In: *Proceedings of the National Academy of Sciences* 97.10 (2000). DOI: 10.1073/pnas.97.10.5019.

[79] E. R. Kandel, J. H. Schwartz, and T. M. Jessell. *Principles of neural science*. New York, NY: McGraw-Hill Medical, 2000.

[80] M. Katz. "How straight do axons grow?" In: *The Journal of Neuroscience* 5.3 (1985). DOI: 10.1523/JNEUROSCI.05-03-00589.1985.

[81] S. Kerruth et al. "The kinetic mechanisms of fast-decay red-fluorescent genetically encoded calcium indicators". In: *Journal of Biological Chemistry* (2019). DOI: 10.1074/jbc.RA118.004543.

[82] J. S. Kim, M. Kaiser, and M. Kaiser. "From Caenorhabditis elegans to the human connectome : a specific modular organization increases metabolic , functional and developmental efficiency". In: (2014).

[83] R. Kim et al. "Recent trends in microelectrode array technology for in vitro neural interface platform". In: *Biomedical Engineering Letters* 4.2 (2014). DOI: 10.1007/s13534-014-0130-6.

[84] D. Kleinfeld. "Controlled Substrates". In: *The Jounral of Neuroscience* (1988).

[85] A. Kohn et al. "Correlations and Neuronal Population Information". In: *Annual Review of Neuroscience* 39.1 (2016). DOI: 10.1146/annurev-neuro-070815-013851.

[86] K. S. Kosik and E. a. Finch. "MAP2 and tau segregate into dendritic and axonal domains after the elaboration of morphologically distinct neurites: an immunocytochemical study of cultured rat cerebrum." In: *The Journal of neuroscience : the official journal of the Society for Neuroscience* 7.10 (1987).

[87] A. Kumar, H. A. Biebuyck, and G. M. Whitesides. "Patterning Self-Assembled Monolayers: Applications in Materials Science". In: *Langmuir* 10.5 (1994). DOI: 10.1021/la00017a030.

[88] A. C. Kwan and Y. Dan. "Dissection of Cortical Microcircuits by Single-Neuron Stimulation In Vivo". In: (2012). DOI: 10.1016/j.cub.2012.06.007.

[89] H. Lanzrath. "Morphological Characterisation of Neuronal Networks". Bachelor's Thesis. RWTH Aachen University, 2017.

[90] Y. B. Lee et al. "Optimizing regulatable gene expression using adenoviral vectors". In: *Experimental Physiology* 90.1 (2005). DOI: 10.1113/expphysiol.2004.028209.

[91] H. Lodish et al. "Molecular Cell Biology". In: *Molecular Cell Biology*. 4th ed. New York, NY: W H Freeman, 2000. Chap. Section 21.

[92] W. Lu et al. "Initial Neurite Outgrowth in Drosophila Neurons Is Driven by Kinesin-Powered Microtubule Sliding". In: *Current Biology* 23.11 (2013). DOI: 10.1016/j.cub.2013.04.050. arXiv: NIHMS150003.

[93] Y. Lu. "Recombinant Adeno-Associated Virus As Delivery Vector for Gene Therapy—A Review". In: *Stem Cells and Development* 13.1 (2004). DOI: 10.1089/154732804773099335.

[94] X. Luo and J. A. Hill. "Ca2+ in the cleft: Fast and fluorescent". In: *Circulation Research* 115.3 (2014). DOI: 10.1161/CIRCRESAHA.114.304487.

[95] B. Maity, D. Sheff, and R. A. Fisher. "Immunostaining". In: *Methods in Cell Biology*. Vol. 113. Elsevier Inc., 2013. Chap. 5. DOI: 10.1016/B978-0-12-407239-8.00005-7. arXiv: arXiv:1011.1669v3.

[96] A. Martinez-Rivas et al. "Methods of micropatterning and manipulation of cells for biomedical applications". In: *Micromachines* 8.12 (2017). DOI: 10.3390/mi8120347.

[97] J. Menezes and M. Luskin. "Expression of neuron-specific tubulin defines a novel population in the proliferative layers of the developing telencephalon". In: *The Journal of Neuroscience* 14.9 (1994). DOI: 10.1523/JNEUROSCI.14-09-05399.1994.

[98] F. D. Miller and A. S. Gauthier. "Timing Is Everything: Making Neurons versus Glia in the Developing Cortex". In: *Neuron* 54.3 (2007). DOI: 10.1016/j.neuron.2007.04.019.

[99] A. Miyawaki et al. "Fluorescent indicators for Ca2+ based on green fluorescent proteins and calmodulin". In: *Nature* (1997). DOI: 10.1038/42264.

[100] M. Moein et al. "Systems biology CaSiAn : a Calcium Signaling Analyzer tool". In: 34.April (2018). DOI: 10.1093/bioinformatics/bty281.

[101] Z. Molnár. "Cortical Columns". In: *Neural Circuit Development and Function in the Brain*. Vol. 3. Elsevier, 2013. DOI: 10.1016/B978-0-12-397267-5.00137-0.

[102] L. Moreaux. "Estimating firing rates from calcium signals in locust projection neurons in vivo". In: *Frontiers in Neural Circuits* 1.November (2008). DOI: 10.3389/neuro.04.002.2007.

[103] V. Mountcastle. "The columnar organization of the neocortex". In: *Brain* 120.4 (1997). DOI: 10.1093/brain/120.4.701.

[104] B. Nadarajah and J. G. Parnavelas. "Modes of neuronal migration in the developing cerebral cortex". In: *Nature Reviews Neuroscience* 3.6 (2002). DOI: 10.1038/nrn845.

[105] J. Nakai, M. Ohkura, and K. Imoto. "A high signal-to-noise Ca2+ probe composed of a single green fluorescent protein". In: *Nature Biotechnology* 19.2 (2001). DOI: 10.1038/84397.

[106] Y. Nam, D. W. Branch, and B. C. Wheeler. "Epoxy-silane linking of biomolecules is simple and effective for patterning neuronal cultures". In: *Biosensors and Bioelectronics* 22.5 (2006). DOI: 10.1016/j.bios.2006.01.027.

[107] N. S. Narayanan and M. Laubach. "Methods for studying functional interactions among neuronal populations". In: *Methods in Molecular Biology* (2009). DOI: 10.1007/978-1-59745-543-5_7.

[108] E. Neher and B. Sakmann. "Single-channel currents recorded from membrane of denervated frog muscle fibres". In: *Nature* (1976). DOI: 10.1038/260799a0.

[109] S. C. Noctor et al. "Cortical neurons arise in symmetric and asymmetric division zones and migrate through specific phases". In: *Nature Neuroscience* 7.2 (2004). DOI: 10.1038/nn1172.

[110] M. E. J. Obien et al. "Revealing neuronal function through microelectrode array recordings". In: *Frontiers in Neuroscience* 8.January (2015). DOI: 10.3389/fnins.2014.00423.

[111] A. Odawara, M. Gotoh, and I. Suzuki. "A three-dimensional neuronal culture technique that controls the direction of neurite elongation and the position of soma to mimic the layered structure of the brain". In: *RSC Advances* 3.45 (2013). DOI: 10.1039/c3ra44757j.

[112] A. Offenhäusser et al. "Microcontact printing of proteins for neuronal cell guidance". In: *Soft Matter* 3.3 (2007). DOI: 10.1039/B607615G.

[113] S. Orrenius, B. Zhivotovsky, and P. Nicotera. "Regulation of cell death: the calcium–apoptosis link". In: *Nature Reviews Molecular Cell Biology* 4.7 (2003). DOI: 10.1038/nrm1150. arXiv: arXiv:1011.1669v3.

[114] S. Ostojic, N. Brunel, and V. Hakim. "How connectivity, background activity, and synaptic properties shape the cross-correlation between spike trains". In: *Journal of Neuroscience* 29.33 (2009). DOI: 10.1523/JNEUROSCI.1275-09.2009.

[115] R. Parekh and G. A. Ascoli. "Neuronal Morphology Goes Digital: A Research Hub for Cellular and System Neuroscience". In: *Neuron* 77.6 (2013). DOI: 10.1016/j.neuron.2013.03.008. arXiv: NIHMS150003.

[116] H.-J. Park and K. Friston. "Structural and Functional Brain Networks: From Connections to Cognition". In: *Science* 342.6158 (2013). Ed. by S. Mack. DOI: 10.1126/science.1238411. arXiv: 1612.02741.

[117] A. E. Pereda. "Electrical synapses and their functional interactions with chemical synapses". In: *Nature Reviews Neuroscience* 15.4 (2014). DOI: 10.1038/nrn3708. arXiv: NIHMS150003.

[118] V. Pérez Koldenkova and T. Nagai. "Genetically encoded Ca2+ indicators: Properties and evaluation". In: *Biochimica et Biophysica Acta (BBA) - Molecular Cell Research* 1833.7 (2013). DOI: 10.1016/j.bbamcr.2013.01.011. arXiv: 1605.08705.

[119] J.-M. Peyrin et al. "Axon diodes for the reconstruction of oriented neuronal networks in microfluidic chambers". In: *Lab on a Chip* 11.21 (2011). DOI: 10.1039/c1lc20014c.

[120] J. Pine. "Recording action potentials from cultured neurons with extracellular microcircuit electrodes". In: *Journal of Neuroscience Methods* 2.1 (1980). DOI: 10.1016/0165-0270(80)90042-4.

[121] R. K. Pirlo et al. "Microfabrication, surface modification, and laser guidance techniques to create a neuron biochip". In: *Optoelectronics Letters* (2008). DOI: 10.1007/s11801-008-8059-6.

[122] D. Poli, V. P. Pastore, and P. Massobrio. "Functional connectivity in in vitro neuronal assemblies". In: 9.October (2015). DOI: 10.3389/fncir.2015.00057.

[123] S. K. Powell, R. Rivera-Soto, and S. J. Gray. "Viral expression cassette elements to enhance transgene target specificity and expression in gene therapy". In: *Discovery Medicine* 19.102 (2015).

[124] J. E. Ramirez et al. "Calcium Imaging Reveals Coordinated Simple Spike Pauses in Populations of Cerebellar Purkinje Cells". In: *CellReports* 17.12 (2016). DOI: 10.1016/j.celrep.2016.11.075.

[125] D. S. Reich et al. "Interspike Intervals , Receptive Fields , and Information Encoding in Primary Visual Cortex". In: 20.5 (2000).

[126] J. P. Robinson, J. Sturgis, and G. L. Kumar. "Immunofluorescence". In: *Education Guide - Immunohistochemical Staining Methods*. Ed. by G. L. Kumar and L. Rudbeck. 5th ed. Carpinteria, California: Dako North America, 2009. Chap. 10.

[127] K. S. Rockland. "Five points on columns". In: *Frontiers in Neuroanatomy* 4.June (2010). DOI: 10.3389/fnana.2010.00022.

[128] S. Roth et al. "How Morphological Constraints Affect Axonal Polarity in Mouse Neurons". In: *PLoS ONE* 7.3 (2012). Ed. by M. Giugliano. DOI: 10.1371/journal.pone.0033623.

[129] O. Sacks. *The Man Who Mistook His Wife for a Hat and Other Clinical Tales*. Gerald Duckworth, 1985.

[130] A. Sakakibara and Y. Hatanaka. "Neuronal polarization in the developing cerebral cortex". In: *Frontiers in Neuroscience* 9.APR (2015). DOI: 10.3389/fnins.2015.00116.

[131] R. J. Samulski and N. Muzyczka. "AAV-Mediated Gene Therapy for Research and Therapeutic Purposes". In: *Annual Review of Virology* 1.1 (2014). DOI: 10.1146/annurev-virology-031413-085355.

[132] B. Schwaller. "Cytosolic Ca2+ Buffers". In: *Cold Spring Harbor Perspectives in Biology* 2.11 (2010). DOI: 10.1101/cshperspect.a004051.

[133] C. J. Schwiening. "A brief historical perspective: Hodgkin and Huxley". In: *The Journal of Physiology* 590.11 (2012). DOI: 10.1113/jphysiol.2012.230458.

[134] M. a. Scott, Z. D. Wissner-Gross, and M. F. Yanik. "Ultra-rapid laser protein micropatterning: screening for directed polarization of single neurons". In: *Lab on a Chip* 12.12 (2012). DOI: 10.1039/c2lc21105j.

[135] R. Segev et al. "Long Term Behavior of Lithographically Prepared In Vitro Neuronal Networks". In: *Physical Review Letters* 88.11 (2002). DOI: 10.1103/PhysRevLett.88.118102.

[136] M. Shein Idelson, E. Ben-Jacob, and Y. Hanein. "Innate Synchronous Oscillations in Freely-Organized Small Neuronal Circuits". In: *PLoS ONE* 5.12 (2010). Ed. by O. Sporns. DOI: 10.1371/journal.pone.0014443.

[137] M. Shein Idelson, E. Ben-Jacob, and Y. Hanein. "Engineered neuronal circuits: A new platform for studying the role of modular topology". In: *Frontiers in Neuroengineering* 4.SEPTEMBER (2011). DOI: 10.3389/fneng.2011.00010.

[138] D. Smetters, A. Majewska, and R. Yuste. "Detecting Action Potentials in Neuronal Populations with Calcium Imaging". In: *Methods* 18.2 (1999). DOI: 10.1006/meth.1999.0774.

[139] A. C. Snyder, M. J. Morais, and M. A. Smith. "Variance in population firing rate as a measure of slow time-scale correlation". In: 7.December (2013). DOI: 10.3389/fncom.2013.00176.

[140] D. J. Solecki et al. "Neuronal polarity in CNS development". In: *Genes & Development* 20.19 (2006). DOI: 10.1101/gad.1462506.

[141] M. H. Soltani et al. "Microtubule-Associated Protein 2, a Marker of Neuronal Differentiation, Induces Mitotic Defects, Inhibits Growth of Melanoma Cells, and Predicts Metastatic Potential of Cutaneous Melanoma". In: *The American Journal of Pathology* 166.6 (2005). DOI: 10.1016/S0002-9440(10)62493-5.

[142] M. E. Spira and A. Hai. "Multi-electrode array technologies for neuroscience and cardiology." In: *Nature nanotechnology* 8.2 (2013). DOI: 10.1038/nnano.2012.265.

[143] T. Takano et al. "Neuronal polarization". In: *Development* 142.12 (2015). DOI: 10.1242/dev.114454.

[144] M. Tessier-Lavigne and C. S. Goodman. "The Molecular Biology of Axon Guidance". In: *Science* 274.5290 (1996). DOI: 10.1126/science.274.5290.1123.

[145] M. Thery. "Micropatterning as a tool to decipher cell morphogenesis and functions". In: *Journal of Cell Science* 123.24 (2010). DOI: 10.1242/jcs.075150.

[146] C. A. J. Thomas et al. "A miniature microelectrode array to monitor the bioelectric activity of cultured cells". In: *Experimental Cell Research* 74.1 (1972). DOI: 10.1016/0014-4827(72)90481-8.

[147] C. Tomba et al. "Geometrical Determinants of Neuronal Actin Waves". In: *Frontiers in Cellular Neuroscience* 11.March (2017). DOI: 10.3389/fncel.2017.00086.

[148] N. X. Tritsch, J. B. Ding, and B. L. Sabatini. "Dopaminergic neurons inhibit striatal output through non-canonical release of GABA". In: *Nature* 490.7419 (2012). DOI: 10.1038/nature11466.

[149] R. Y. Tsien. "New Calcium Indicators and Buffers with High Selectivity Against Magnesium and Protons: Design, Synthesis, and Properties of Prototype Structures". In: *Biochemistry* (1980). DOI: 10.1021/bi00552a018.

[150] A. Vogt, G. Brewer, and A. Offenhäusser. "Connectivity Patterns in Neuronal Networks of Experimentally Defined Geometry". In: *Tissue Engineering* 11.11-12 (2005). DOI: 10.1089/ten.2005.11.1757.

[151] O. von Bohlen und Halbach. "Immunohistological markers for staging neurogenesis in adult hippocampus". In: *Cell and Tissue Research* 329.3 (2007). DOI: 10.1007/s00441-007-0432-4.

[152] M. C. Walters et al. "Calcium Imaging of Parvalbumin Neurons in the Dorsal Root Ganglia". In: *eneuro* 6.4 (2019). DOI: 10.1523/ENEURO.0349-18.2019.

[153] L. Wang and T. Marquardt. "What axons tell each other: axon–axon signaling in nerve and circuit assembly". In: *Current Opinion in Neurobiology* 23.6 (2013). DOI: 10.1016/j.conb.2013.08.004.

[154] C. Watson and L. Puelles. "Developmental gene expression in the mouse clarifies the organization of the claustrum and related endopiriform nuclei". In: *Journal of Comparative Neurology* 525.6 (2017). DOI: 10.1002/cne.24034.

[155] S. D. Weidlich. "Nanoscale 3D structures towards improved cell-chip coupling on microelectrode arrays". PhD thesis. RWTH Aachen University, 2017.

[156] G. M. Whitesides et al. "Soft Lithography in Biology and Biochemistry". In: *Annual Review of Biomedical Engineering* 3.1 (2001). DOI: 10.1146/annurev.bioeng.3.1.335.

[157] N. R. Wilson et al. "Synaptic reorganization in scaled networks of controlled size". In: *Journal of Neuroscience* 27.50 (2007). DOI: 10.1523/JNEUROSCI.3863-07.2007.

[158] S. H. Wright. "Generation of resting membrane potential". In: *AJP: Advances in Physiology Education* 28.4 (2004). DOI: 10.1152/advan.00029.2004.

[159] Q. Xie et al. "The atomic structure of adeno-associated virus (AAV-2), a vector for human gene therapy". In: *Proceedings of the National Academy of Sciences* 99.16 (2002). DOI: 10.1073/pnas.162250899.

[160] X. Xing and C. F. Wu. "Unraveling synaptic GCaMP signals: Differential excitability and clearance mechanisms underlying distinct Ca2+ dynamics in tonic and phasic excitatory, and aminergic modulatory motor terminals in drosophila". In: *eNeuro* 5.1 (2018). DOI: 10.1523/ENEURO.0362-17.2018.

[161] E. Yaksi and R. W. Friedrich. "Reconstruction of firing rate changes across neuronal populations by temporally deconvolved Ca2+ imaging". In: *Nature Methods* 3.5 (2006). DOI: 10.1038/nmeth874.

[162] H. Yamamoto et al. "Unidirectional signal propagation in primary neurons micropatterned at a single-cell resolution". In: *Applied Physics Letters* 109.4 (2016). DOI: 10.1063/1.4959836.

[163] H. Yamamoto et al. "Differential neurite outgrowth is required for axon specification by cultured hippocampal neurons". In: *Journal of Neurochemistry* 123.6 (2012). DOI: 10.1111/jnc.12001.

[164] H. Yamamoto et al. "Size-dependent regulation of synchronized activity in living neuronal networks". In: *Physical Review E* 94.1 (2016). DOI: 10.1103/PhysRevE.94.012407.

[165] A. Yuan et al. "Neurofilaments at a glance". In: *Journal of Cell Science* 125.14 (2012). DOI: 10.1242/jcs.104729.

[166] C. Zhou and A. E. Motter. "Universality in the Synchronization of Weighted Random Networks". In: 034101.January (2006). DOI: 10.1103/PhysRevLett.96.034101.

[167] G. Zhu et al. "Effects of Morphology Constraint on Electrophysiological Properties of Cortical Neurons". In: *Scientific Reports* 6.1 (2016). DOI: 10.1038/srep23086.

# Own Publications

## Conference posters & talks

**Poster:** I. Tihaa, J. Albers, A. Offenhäusser. "Neuronal guiding: Designing In Vitro Networks On MEA". At: *MEA Meeting 2016 | 10th International Meeting on Substrate-Integrated Electrode Arrays, Reutlingen, Germany* (2016). doi: 10.3389/conf.fnins.2016.93.00080

**Poster:** I. Tihaa, S. Belaidi, N. Gruteser, A. Günther, A. Baumann, F. Müller, A. Offenhäusser. "Genetically encoded sensors and actuators: From cellular to cell-free application". At: *1st International Conference on Molecular Interaction Engineering (MIE), Karlsruhe, Germany* (2016)

**Talk:** I. Tihaa, J. Lewen, A. Offenhäusser. "Single cell activity: MEA recordings from engineered networks". At: *INM-ICS Retreat 2017, Jülich, Germany* (2017)

## Other talks

**Talk:** I. Tihaa. "Patterning: Structuring of Surfaces". At: *Int. Workshop on Bioelectronics, Hirschegg, Austria* (2016)

**Talk:** I. Tihaa. "Optical Stimulation". At: *Int. Workshop on Bioelectronics - New Challenges Outlook, Hirschegg, Austria* (2018)

# Acknowledgements/ Danksagung

An dieser Stelle möchte ich mich bei allen Menschen bedanken, die mich in dieser intensiven Zeit begleitet und zu dieser Arbeit beigetragen haben.
**Prof. Andreas Offenhäusser**, danke für die Betreuung, die Möglichkeit an diesem einzigartigen, interdisziplinären Institut zu forschen und für stetige Anregungen, Motivation und das Vertrauen in so vielen Situationen. **Prof. Marc Spehr** danke ich für sein zweites Gutachten.
Ein großer Dank gilt auch meinen Kollegen für Diskussionen, Zusammenarbeit, Ratschläge und Motivation. **Tina Breuer** danke ich für die Neuronen und SoooVieles im Biolabor, die gute Laune, Professionalität und Pragmatismus. **Michael Prömpers** - Danke für die Mikroprozessierung der Stempel, die lösungsorientierte Herangehensweise und die Pläuderchen. **Marko Banzet** möchte ich die Herstellung der MEAs danken. **Susanne Bippus** - Danke für die Unterstützung bei allen organisatorischen Fragen! **Dr. Vanessa Maybeck** möchte ich an dieser Stelle für ihr Engagement, den unvorstellbar enormen Wissensfundus und die anschaulichen Sicherheitsunterweisungen danken. **Dr. Jonas Albers** danke ich für die Vorarbeit und Einarbeitung, sowie zahlreiche Diskussionen. **Dr. Dirk Mayer** - für den **KAFFEE**, die Glovebox und sämtliche Diskussionen. **Prof. Bernhard Wolfrum** - danke für Gespräche, deinen Enthusiasmus und dein Engagement als Mafiaboss/Citizen/...
**Hannah Lanzrath** danke ich für ihre engagierte Arbeit an den Populationsnetzwerken im Rahmen ihres Bachelorprojekts, insb. für die Immunostainings und Quantifikationen. **Fabian Brings** - für die Arbeit am BioMAS Analyzer und die Fähigkeit komplexe Sachverhalte so simpel zu erklären - danke auch für die Geduld

und die Zeit. **Johannes Lewen** möchte ich für seine Arbeit an Teilen des BioMAS Analyzer und die Zusammenarbeit an den single cell networks on MEA danken. **Timm Hondrich** und **Dominik Brinkmann** - für Ideen und Diskussionen und die weitere Arbeit an strukturierten Netzwerken.
Thanks to my office mates **Sung-Eun** and **Kaitry** for the perfect mixture of concentration and fun. Sung-Eun - thank you for our chats and Korean lessons. Kaitry - danke, dass unser Büro manchmal so laut wurde! Es war mir eine Freude mit dir zu lachen, Nerf gun sessions zu halten, zu reisen, zu tanzen, zu laufen uvm.
**Silke**, **Sabrina**, **Andreea** und **Bastian** danke ich für die lange Zeit im Labor, die intensiven Gespräche und den Spaß und **Anna** für das Mentoring zu Beginn meines PhDs. Danke an **Frano** für die Zusammenarbeit am Imager, den Nachschub an vollen Festplatten, die Reisen, Feiern und die gute Zeit. Moreover, I would like to thank my fellow (PhD) students **Mathis**, **Pegah**, **Niko**, **Corinna**, **Chris**, **Lei**, **Lena**, **Nouran**, **Stella**, **Erfan**, **Dmitry**, **Lei**, the ones I mentioned above, and to the ones I forgot to mention for professional and private discussions, help, motivation, RTB time, hiking, party time - in sum: for the great atmosphere!
Den Kollegen des Graduiertenkollegs **BioSoft** und insb. **Dr. Thorsten Auth** als Organisator danke ich für die vielseitige fachliche und außerfachliche Weiterbildung. **Oli**, **Maddalena**, **Clara**, **Andreea**, **Sabrina** and many more - thanks for the fun!
Den Kollegen von der Unternehmenskommunikation und -entwicklung, insb. **Christina Hallen**, **Thomas Bierschenk** und **Henning Eggert** möchte ich für die Möglichkeit danken, das Forschungszentrum bei Besucherführungen, Karriereevents und anderen Veranstaltungen repräsentieren zu dürfen. Ob auf dem Campus, dem Rursee oder woanders - es war mir eine Freude, die Wissenschaft des FZJ nach außen kommunizieren zu dürfen.
Meiner Familie, insbesondere meiner **Mama**, möchte ich für die Förderung, Unterstützung und Vertrauen danken. **Sebastian**, danke für deine Neugierde, dein Interesse an meiner Arbeit, die Diskussionen, das Lektorieren, das Motivieren, deine Unterstützung und dein Verständnis. Danke an meine fachfremden Freunde **Lea, Tere, Wiena, Malte** für die motivierenden Worte wann immer sie nötig waren.

# Supplementary material

## 8.1 Single cell connectivity

### 8.1.1 Star patterns

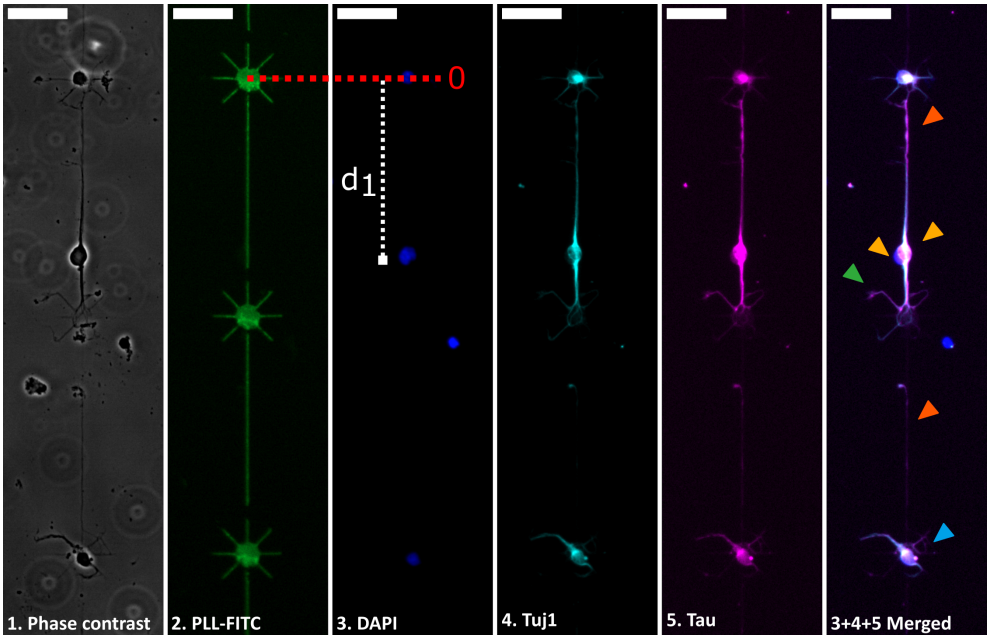


**Figure 8.1:** Representative image showing neurons of different categories. Neuronal somata are located either on the nodes (blue arrow) or on the line (yellow arrows) and elongate their axons into the desired (green arrow) or opposite (orange arrow) direction. The exact soma position on the pattern is measured as a distance ($d_1$) from the node's centre (marked as "0" in red). Scale bar 50 µm.

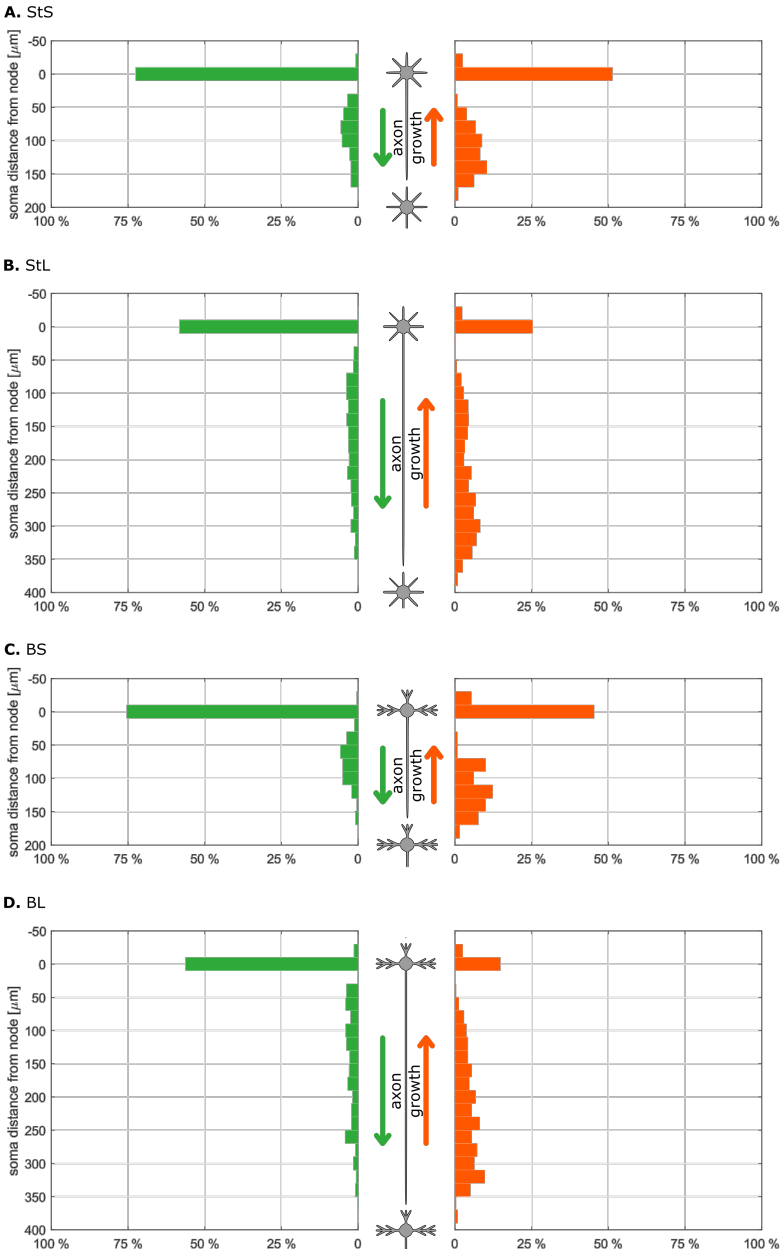


**Figure 8.2:** Soma position distribution on the pattern and their axon outgrowth direction. Distance from the node is represented on the y-axis, relative values of counts on the x-axis. Neurons elongating their axon in the desired direction are displayed in green, into the opposite direction in orange. Bin size: 20 µm. N (right, wrong): A) 1141, 670; B) 1017, 667; C) 240, 130; D) 444, 236 cells.

Figure 8.2 shows the relative numbers of soma position distribution along the star patterns and their axon outgrowth direction. Supplementary representation for Figure 4.14.

**Time lapse imaging of neurons on star pattern.** Exemplary neurons chosen to depict the different categories of neuron growth on the StS pattern as supplementary material for subsection 4.2.2 "N" describes neurons with their somata located on the nodes while "L" with their somata on the lines. "R" categorises the axon elongation into the right direction, namely along the long line, while "W" marks the axon elongation into the wrong direction.

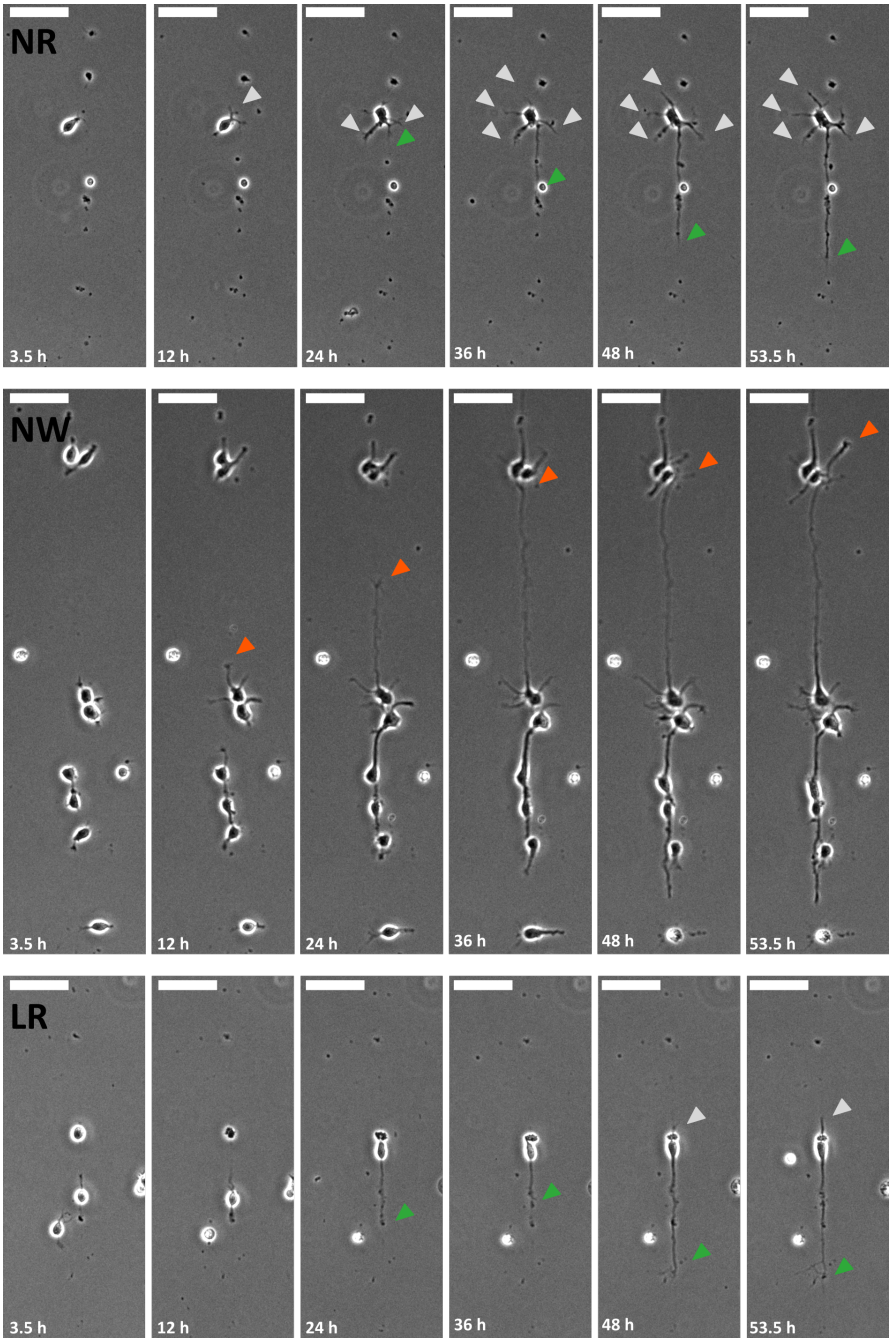


**Figure 8.3:** Time lapse imaging of neurons on StS - 1. "N": soma located on the node; "L": soma located on line; "R": axon elongation into the right direction; "W": axon elongation into the wrong direction. Scale bar 50 µm.

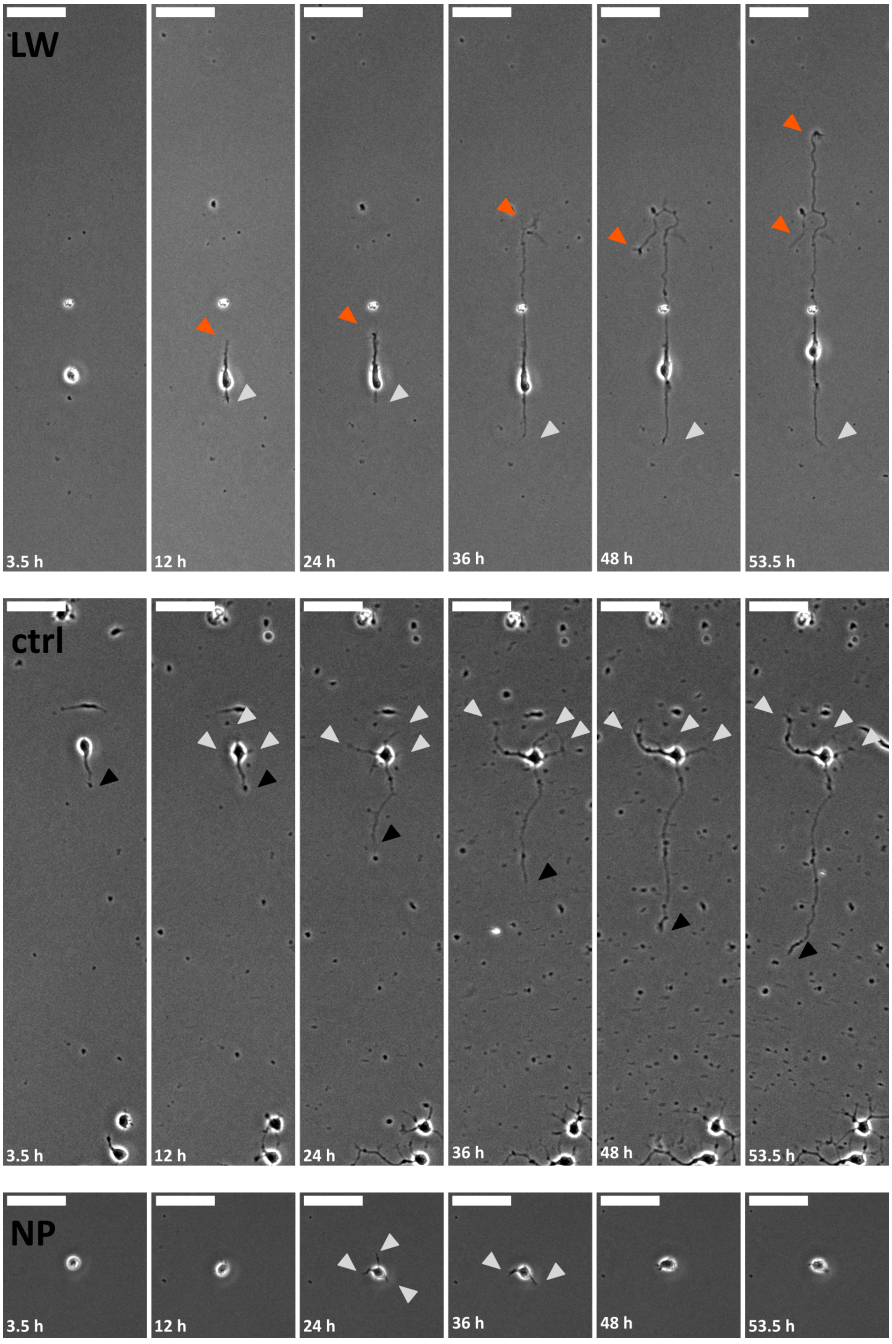


**Figure 8.4:** Time lapse imaging of neurons on StS - 2."N": soma located on the node; "L": soma located on line; "R": axon elongation into the right direction; "W": axon elongation into the wrong direction. Scale bar 50 µm.

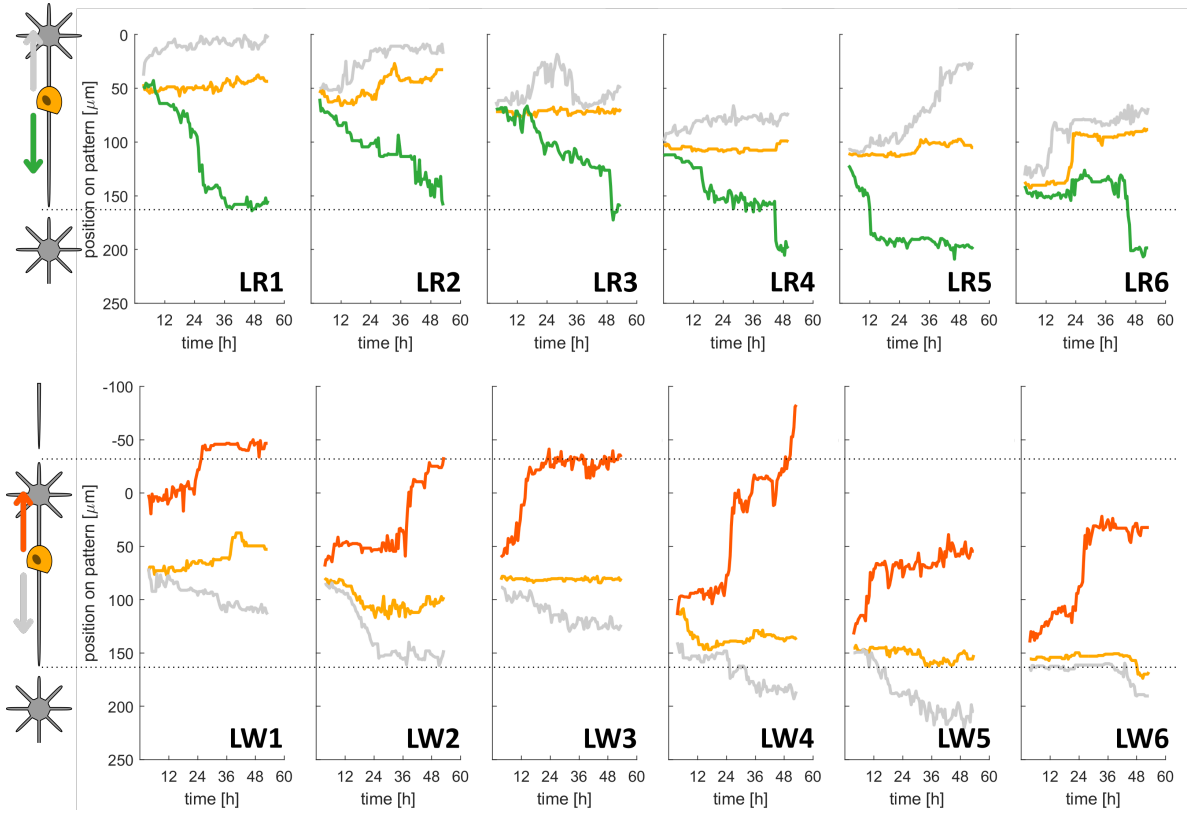


**Figure 8.5:** Neurite elongation and soma position of neurons with somata on the line on pattern over time. Top panel with LR1-3 shows neurons with somata on the line (orange) and axon elongation into the right direction (axon tip in green). Bottom panel shows neurons with somata on the line and axon elongation into the wrong direction (axon tip in red). The second neurite (= dendrite) is depicted in grey.

Figure 8.5 shows the positions of the axon and neurite tip and the somata of the individual cells (LW & LR). The dashed horizontal lines spanning all plots represent the top and bottom edge of the patterns.

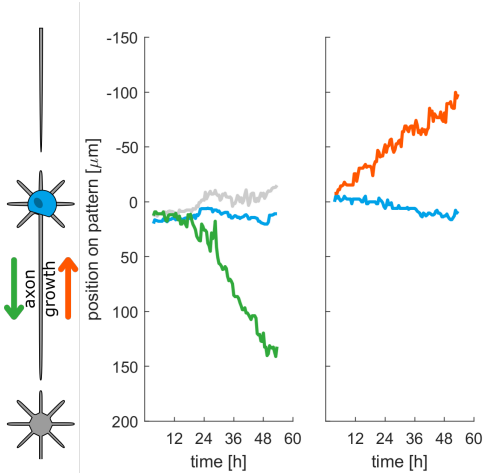


**Figure 8.6:** Somata on nodes - soma movement over time. Soma position represented by blue line, shorter neurite position in grey and longest neurite position in green or orange.

**Average calcium transient** Figure 8.7 shows the average of over 90 calcium transients from a neuron on a star pattern. The rising part of the transient is represented with black dots while the decaying part is shown in orange. The orange line depicts an exponential fitted function.

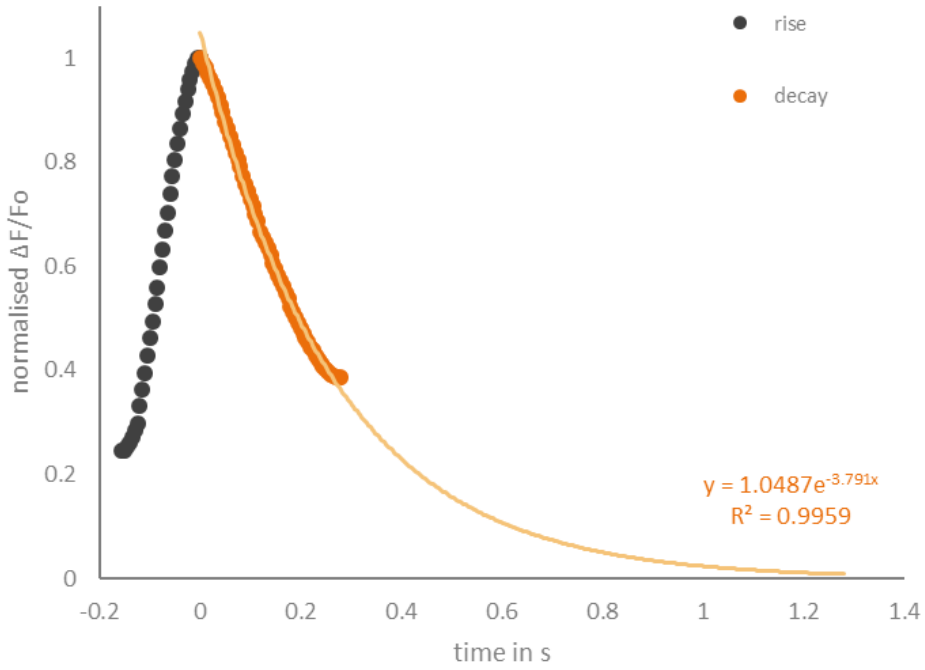


**Figure 8.7:** Average calcium transient and its decay time. Exponential decay function (orange line) fitted to the average decay data points (orange dots). N = 92 transients.

## 8.2 Population connectivity

### 8.2.1 Calcium transient parameters

The following tables and figures show supplementary information for the boxplots presented in Figure 7.2, Figure 7.3 and Figure 7.4.

**Table 8.1:** Boxplot characteristics of the calcium transient amplitude. Supplementary information for the boxplots presented in Figure 7.2. pctl = percentile. In % ΔF/F.

| dsCT | Q1 - 1.5 IQR | 25th pctl | median | 75th pctl | Q3 + 1.5 IQR |
|---|---|---|---|---|---|
| 10 | 0.1 | 1.3 | 3.3 | 11.2 | 26.1 |
| 20 | 0.5 | 2.2 | 4.5 | 11.3 | 24.8 |
| 30 | 0.5 | 2.4 | 6.0 | 17.1 | 39.0 |
| 40 | 0.1 | 0.7 | 1.7 | 6.3 | 14.8 |
| 50 | 0.2 | 1.9 | 4.5 | 13.2 | 30.1 |
| 60 | 0.05 | 1.2 | 3.3 | 11.6 | 27.2 |
| 75 | 0.37 | 3.3 | 7.3 | 17.8 | 39.3 |
| 100 | 0.1 | 4.1 | 8.9 | 18.3 | 39.6 |

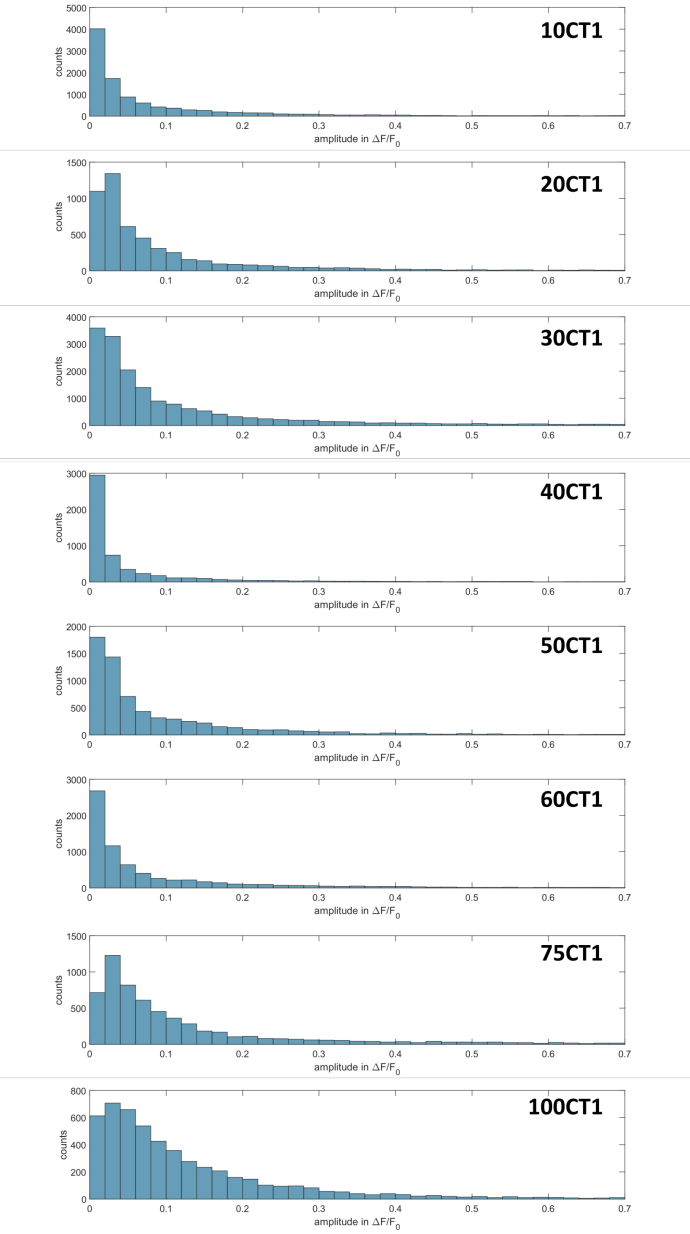


**Figure 8.8:** Histograms of the distribution of amplitudes of different dsCT1 structures. Supplementary figure for Figure 7.2. Bin size 2 % $\Delta F/F_0$.

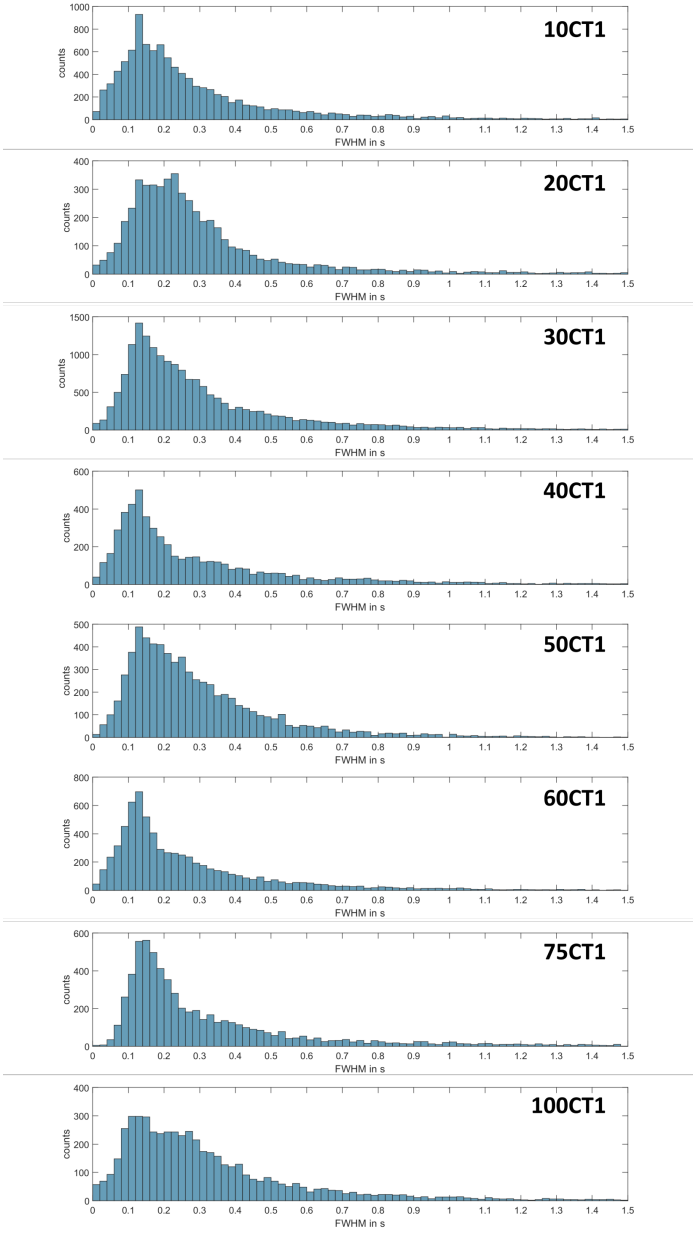


**Figure 8.9:** Histograms of the distribution of FWHM of different dsCT1 structures. Bin size 20 ms.

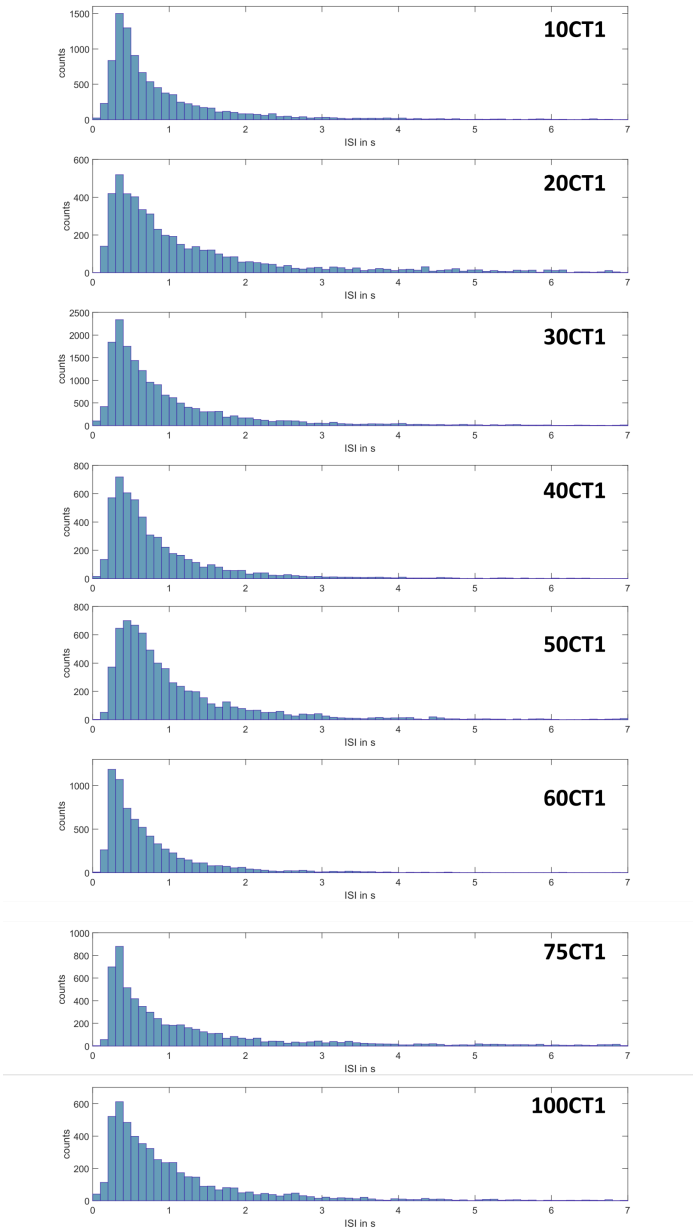


**Figure 8.10:** Histograms of the distribution of ISI of different dsCT1 structures. Bin size 20 ms.

**Table 8.2:** Boxplot characteristics of the FWHM. Supplementary information for the boxplots presented in Figure 7.3. pctl = percentile. In s.

| dsCT | Q1 - 1.5 IQR | 25th pctl | median | 75th pctl | Q3 + 1.5 IQR |
|---|---|---|---|---|---|
| 10 | 0.004 | 0.129 | 0.207 | 0.357 | 0.699 |
| 20 | 0.004 | 0.160 | 0.241 | 0.366 | 0.675 |
| 30 | 0.003 | 0.142 | 0.229 | 0.382 | 0.741 |
| 40 | 0.005 | 0.118 | 0.193 | 0.379 | 0.769 |
| 50 | 0.006 | 0.151 | 0.240 | 0.375 | 0.712 |
| 60 | 0.006 | 0.119 | 0.188 | 0.350 | 0.670 |
| 75 | 0.006 | 0.149 | 0.221 | 0.412 | 0.806 |
| 100 | 0.007 | 0.149 | 0.259 | 0.422 | 0.832 |

## 8.3 Cross-correlations in and between populations

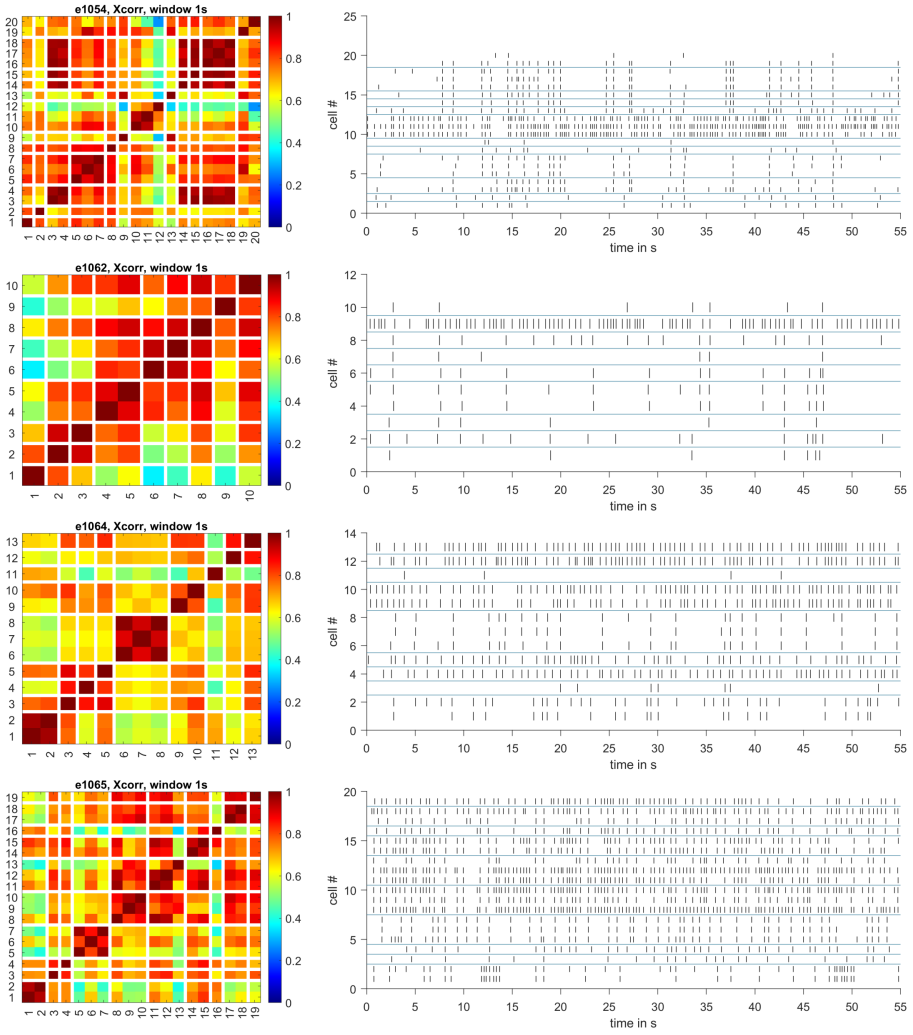


Figure 8.11: 20CT1: Correlation heatmaps and corresponding boxplots.

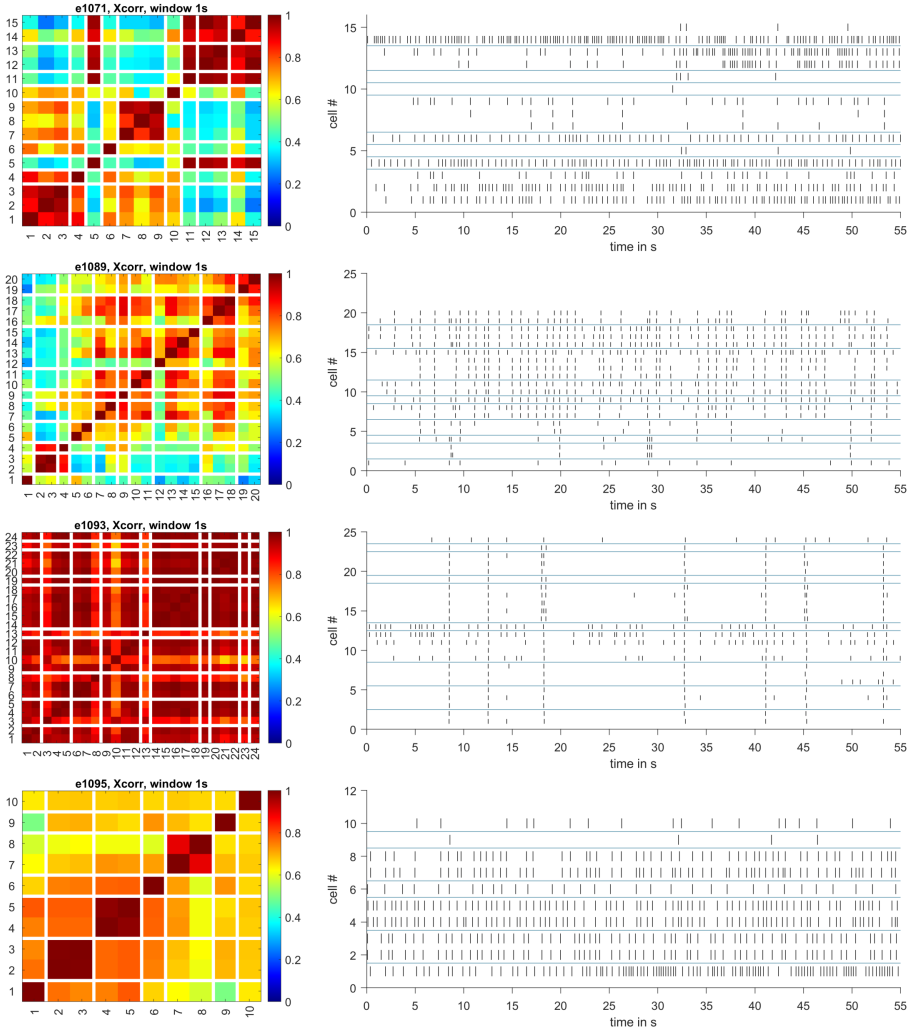


Figure 8.12: 30CT1: Correlation heatmaps and corresponding boxplots.

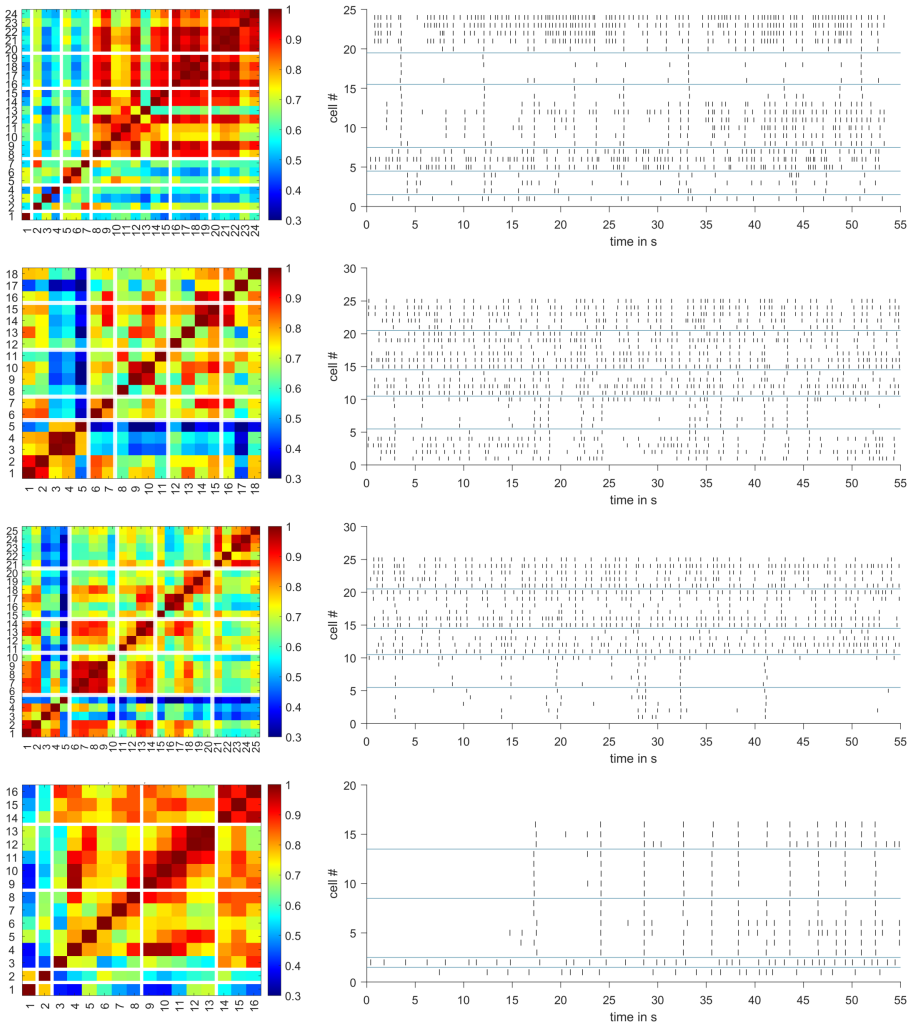


Figure 8.13: 50CT1: Correlation heatmaps and corresponding boxplots.

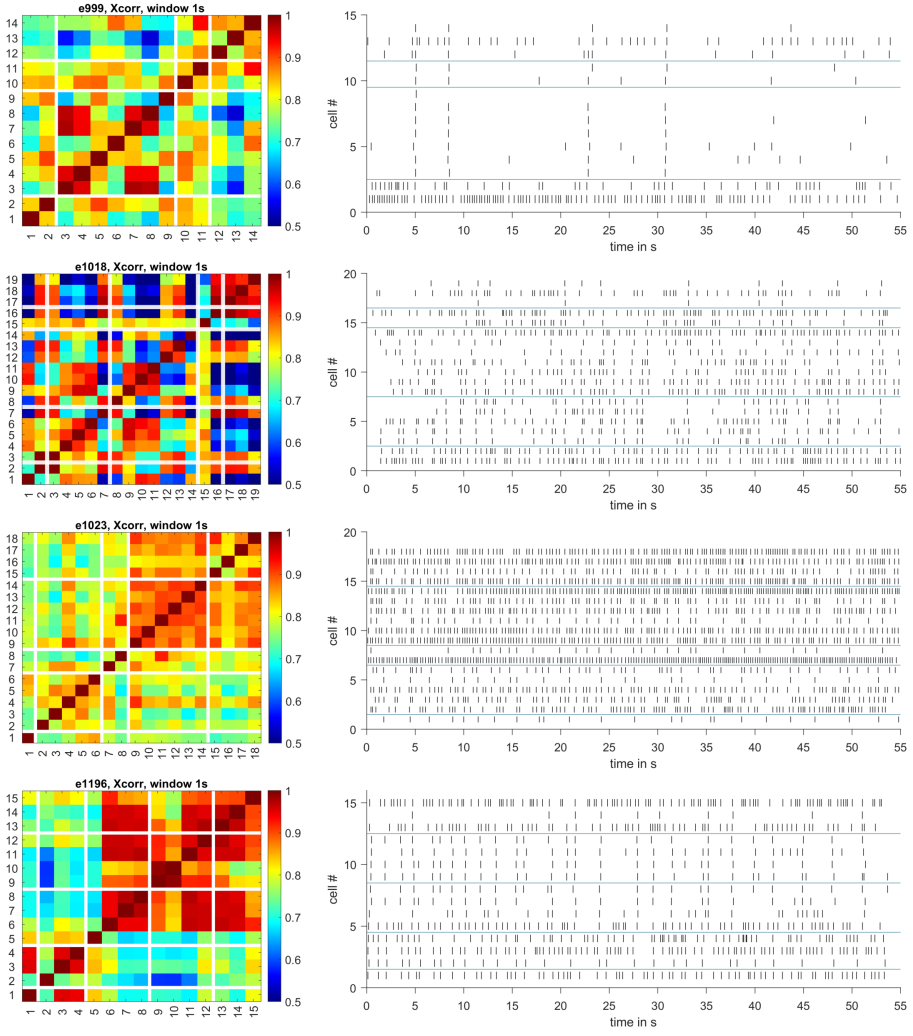


Figure 8.14: 60CT1: Correlation heatmaps and corresponding boxplots.

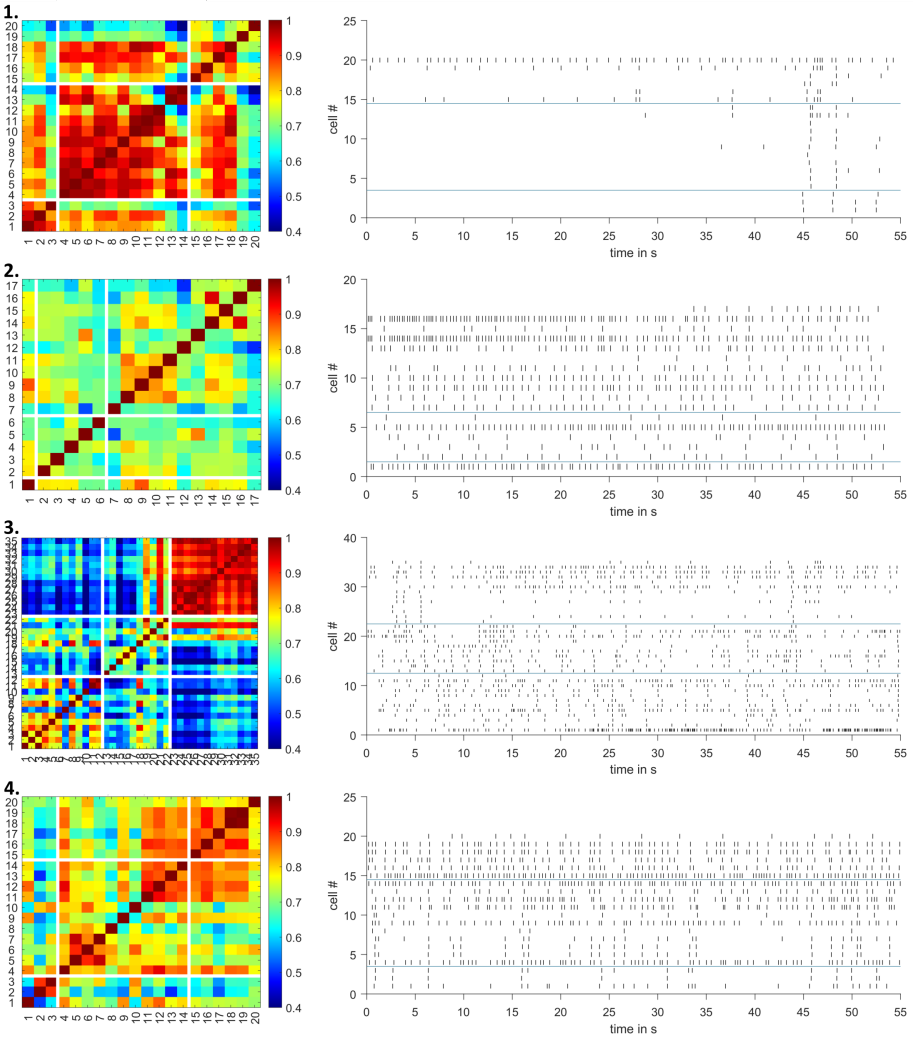


Figure 8.15: 100CT1: Correlation heatmaps and corresponding boxplots.

Band / Volume 64
**Quantitative investigation of group III-nitride interfaces by a combination of scanning tunneling microscopy and off-axis electron holography**
Y. Wang (2021), 102 pp
ISBN: 978-3-95806-534-5

Band / Volume 65
**Scalable Control Electronics for a Spin Based Quantum Computer**
L. Geck (2021), xiv, 114, xv-xxxiii
ISBN: 978-3-95806-540-6

Band / Volume 66
**DNA-capped silver nanoparticles for stochastic nanoparticle impact electrochemistry**
L. Nörbel (2021), VI, 142 pp
ISBN: 978-3-95806-541-3

Band / Volume 67
**Development, characterization, and application of intraretinal implants**
V. Rincón Montes (2021), XII, 173 pp
ISBN: 978-3-95806-553-6

Band / Volume 68
**Optogenetic and electrical investigation of network dynamics in patterned neuronal cultures**
T. J. J. Hondrich (2021), x, 177 pp
ISBN: 978-3-95806-555-0

Band / Volume 69
**Disentangling parallel conduction channels by charge transport measurements on surfaces with a multi-tip scanning tunneling microscope**
S. Just (2021), xii, 225 pp
ISBN: 978-3-95806-574-1

Band / Volume 70
**Nanoscale four-point charge transport measurements in topological insulator thin films**
A. Leis (2021), ix, 153 pp
ISBN: 978-3-95806-580-2

Band / Volume 71
**Investigating the Interaction between π-Conjugated Organic Molecules and Metal Surfaces with Photoemission Tomography**
X. Yang (2021), xviii, 173 pp
ISBN: 978-3-95806-584-0

Band / Volume 72
**Three-Dimensional Polymeric Topographies for Neural Interfaces**
F. Milos (2021), 133 pp
ISBN: 978-3-95806-586-4

Band / Volume 73
**Development, characterization, and application of compliant intracortical implants**
K. Srikantharajah (2021), xiv, 155, xv-xvii pp
ISBN: 978-3-95806-587-1

Band / Volume 74
**Modelling, implementation and characterization of a Bias-DAC in CMOS as a building block for scalable cryogenic control electronics for future quantum computers**
P. N. Vliex (2021), xiv, 107, xv-xxviii pp
ISBN: 978-3-95806-588-8

Band / Volume 75
**Development of Electrochemical Aptasensors for the Highly Sensitive, Selective, and Discriminatory Detection of Malaria Biomarkers**
G. Figueroa Miranda (2021), XI, 135 pp
ISBN: 978-3-95806-589-5

Band / Volume 76
**Nanostraw- Nanocavity MEAs as a new tool for long-term and high sensitive recording of neuronal signals**
P. Shokoohimehr (2021), xi, 136 pp
ISBN: 978-3-95806-593-2

Band / Volume 77
**Surface plasmon-enhanced molecular switching for optoelectronic applications**
B. Lenyk (2021), x, 129 pp
ISBN: 978-3-95806-595-6

Band / Volume 78
**Engineering neuronal networks in vitro: From single cells to population connectivity**
I. Tihaa (2021), viii, 242 pp
ISBN: 978-3-95806-597-0

Information
Band / Volume 78
ISBN 978-3-95806-597-0

Mitglied der Helmholtz-Gemeinschaft

JÜLICH
Forschungszentrum